NUCLEAR MAGNETIC RESONANCE SPECTROSCOPY AND ULTRASOUND

SUNIL UNKA PATEL

Doctor of Philosophy

THE UNIVERSITY OF ASTON IN BIRMINGHAM

March 1989

THE UNIVERSITY OF ASTON IN BIRMINGHAM

NUCLEAR MAGNETIC RESONANCE SPECTROSCOPY AND ULTRASOUND

SUNIL UNKA PATEL
DOCTOR OF PHILOSOPHY
1989

SUMMARY

The work described in this thesis is directed to the examination of the hypothesis that ultrasound may be used to perturb molecular motion in the liquid phase. These changes can then be detected by nuclear magnetic resonance (NMR) in spin-lattice and spin-spin relaxation times. The objective being to develop a method capable of reducing the pulsed NMR acquisition times of slowly relaxing nuclei.

The thesis describes the theoretical principles underlying both NMR spectroscopy and ultrasonics with particular attention being paid to factors that impinge on testing the above hypothesis.

Apparatus has been constructed to enable ultrasound at frequencies between 1 and 10 mega-hertz with a variable power up to $100W/cm^{-2}$ to be introduced in the NMR sample. A broadband high frequency generator is used to drive PZT piezo-electric transducer via various transducer to liquid coupling arrangements.

A commercial instrument of 20 kilo-hertz has also been employed to test the above hypothesis and also to demonstrate the usefulness of ultrasound in sonochemistry. The latter objective being, detection of radical formation in monomer and polymer ultrasonic degradation.

The principle features of the results obtained are: Ultrasonic perturbation of T_1 is far smaller for pure liquids than is for mixtures. The effects appear to be greater on protons (^1H) than on carbon-13 nuclei (^{13}C) relaxation times. The observed effect of ultrasonics is not due to temperature changes in the sample. As the power applied to the transducer is progressively increased T_1 decreases to a minimum and then increases. The T_1's of the same nuclei in different functional groups are influenced to different extents by ultrasound.

Studies of the ^{14}N resonances from an equimolar mixture of N,N-dimethyl-formamide and deuterated chloroform with ultrasonic frequencies at 1.115, 6, 6.42 and 10 MHz show that as the frequency is increased the NMR signal to noise ratio decreases to zero at the Larmor frequency of 6.42 MHz and then again rises. This reveals the surprising indication that an effect corresponding to nuclear acoustic saturation in the liquid may be observable. Ultrasonic irradiation of acidified ammonium chloride solution at and around 6.42 MHz appears to cause distinctive changes in the proton-nitrogen J coupling resonance at 89.56 MHz.

Ultrasonic irradiation of N,N-dimethylacetamide at 20 KHz using the lowest stable power revealed the onset of coalescence in the proton spectrum. The corresponding effect achieved by direct heating required a temperature rise of approximately 30^oC. The effects of low frequency (20 KHz) on relaxation times appear to be nil. Detection of radical formation proved difficult but is still regarded as the principle route for monomer and polymer degredation.

The initial hypothesis is considered proven with the results showing significant changes in the mega-hertz region and none at 20 KHz.

KEY WORDS: Nuclear Magnetic Resonance, Spin-Lattice Relaxation, Spin-Spin Relaxation, Ultrasonic, Sonochemistry

ACKNOWLEDGEMENTS

The research described in this thesis started in earnest and with an inspiration to that described by WH Bragg. To quote "A good research student is like a fire which needs but the match to start it. It is a discipline to put the text-book to one side and to get out further knowledge by one's own effort. It teaches the student how to value evidence; how to read with discretion, since he must weigh what others have done before he uses the previous knowledge as a foundation for his own advances. He learns to meet disappointment, to realise how little he can do in a day, and that weeks or months may go by without obvious progress. It is strange to discover that he must spend so much time on small things, that he must wait a week before he has succeeded in stopping a small leak, or go himself to buy some trivial thing, or spend weary hours in the adjustment of an instrument which in the end he learns to put straight in a moment. There is so much little work to be done before the good observations come; it may be that weeks are spent in preparation and five minutes in making the actual measurement. It is all very humiliating; and the blunders one makes are very foolish; and the one redeeming feature is that in its apparent perversity it is like every other piece of real work".

Writing a thesis, at any level of any size is never a single handed effort. In the background lie invaluable contributions from a host of people who have directed their efforts to the constant achievement of this goal.

I would like to express my sincere gratitude to my supervisor, Dr J Homer, for his invaluable assistance and encouragement throughout the course of this work.

I am grateful to many members of the department for all their personal and practical help. In particular, I would like to thank the following persons:

Dr JA Archer-Hall for his keen interest, enthusiasm and valuable assistance in building various ultrasonic apparatus.

Mr R Wheeler and Mr JM Duggins for their timely assistance and for the provision of the engineering facilities.

Dr M Wadhwa for the highly appreciated and much needed perpetual moral support and encouragement, and for the many useful discussions.

Mr JK Roberts for the use of computer programs and stimulating discussions.

Miss MA Choudhari, Dr MS Mohammadi and Dr PS Varma for their personal help and encouragement.

Sincere appreciation and gratitude is extended to Miss T Knight for her extreme patience and careful typing of this manuscript.

Department of Chemical Engineering & Applied Chemistry for the provision of the University Research Studentship.

BTG for the provision of equipment funds.

Last but not least, I am indebted to my parents and close relatives, for their love, tolerance and endless encouragement and further financial support without which this work would have been impossible.

Dedicated, with love

to my mother, father and brother.

PREFACE

Nuclear magnetic resonance spectroscopy (NMR) has, over the last ten years developed into a major spectroscopic technique. In doing so, it has assisted chemistry, organic chemistry in particular, in its rapid development. The applications of high resolution NMR in chemistry are enormous and are growing at an almost exponential rate.

In recent years NMR has undergone a revolutionary change with the addition of the pulsed excitation - Fourier transform technique to the earlier continuous wave approach. Advances in electronic technology creating the availability of computers, and the development of techniques in solid state electronics have made commercial pulsed spectrometers feasible.

This thesis and the research discussed within it are orientated towards designing and introducing a new technique rather than its applications.

In 1984, experimental work was initiated to investigate the hypotheses that ultrasonic perturbation of molecular dynamics in the liquid phase could be detected by changes in NMR spin-lattice and spin-spin relaxation times, T_1 and T_2 respectively. Although the work resulted in the creation of a novel method of investigating molecular dynamics, the original intention was to develop a technique that could significantly reduce the relaxation times. For nuclei with naturally long relaxation times, this would enable a reduction in the pulsed acquisition time of their NMR spectra.

In addition to the above work, attention is also paid to a revived interest in sonochemistry and its importance in the field of organic synthesis.

This thesis, in addition to the work performed, is intended to serve as a review of NMR spectroscopy as well as of ultrasound and discuss the interrelationship of these for the successful demonstration of the proposed new technique. For readers who are familiar with NMR as well as ultrasound, it may well be suitable for them to start reading from Chapter Six onwards.

The first four chapters introduce nuclear magnetic resonance. They discuss in depth the theory of magnetic resonance, continuous wave and pulsed Fourier transform methods, spin-lattice and spin-spin relaxation times with particular attention to nuclear dipolar-dipolar relaxation and the various mathematical models to represent this, and other relaxation mechanisms which affect spin-lattice relaxation times.

Chapter Five discusses the structure of liquids and mechanisms for the absorption of sound in liquid.

Chapter Six is divided into two sections. The first half discusses and examines two important and entirely separate techniques using sound waves. These two techniques are known as nuclear acoustic resonance and acoustic cavitation. In the second half, it aims to combine the first five chapters including the first part of this chapter and discuss the original hypothesis on which this research was based. In addition to this discussion it provides briefly an insight into the type of technical equipment necessary to perform the necessary experiments.

Chapter Seven discusses the instrumentation and experimental methods used, the apparatus designed, built and in some cases adapted to perform experiments involving measurement of the effects of ultrasonic perturbation of molecular dynamics in the liquid phase via detecting changes in NMR spin-lattice or spin-spin relaxation times, and experiments involving sonochemical reactions.

Chapter Eight concludes with the presentation of the results and discussion of the observation made from the experiments performed. It also discusses future work that needs to be performed for a further understanding of the ultrasonic perturbation of molecular dynamics in the liquid phase.

LIST OF CONTENTS

LIST OF TABLES

LIST OF FIGURES

CHAPTER ONE

INTRODUCTION TO NUCLEAR MAGNETIC RESONANCE SPECTROSCOPY

NOMENCLATURE

P	Spin Angular Momentum
I	Nuclear spin
μ	Magnetic moment
γ	Nuclear Magnetiogyric gyric ratio
B_o	Static magnetic field
ω_o	Larmor Angular Frequency
ν_o	Larmor precession frequency
B_1	Applied magnetic field
r.f.	Radiofrequency field
m	Nuclear quantum number
N_α	Number of participants (spins) in the lower level
N_β	Number of participants (spins) in the higher level
T_1	Spin-lattice relaxation times
T_2	Spin-spin relaxation times
M	Nuclear spin magnetisation
P	Simulated spin transition probability
w	Spin relaxation probability
$g(\nu)$	Lineshape function
Z	Saturation constant
M_o	Equilibrium magnetisation
θ	Pulse angle
δ	Chemical shift
σ	Shielding factor
$\hbar$	Plancks constant
T	Temperature (K)

INTRODUCTION TO NUCLEAR MAGNETIC RESONANCE SPECTROSCOPY

1.0 Historical

Nuclear magnetic resonance (NMR) spectroscopy involves the study of the magnetic properties of nuclei. The fact that nuclei have magnetic properties was first discovered through the study of optical spectroscopy. With the use of spectrographs of high resolving power so called hyperfine splitting was observed in these spectra. The study of the hyperfine structure led Pauli[1] in 1924 to suggest that the fine structure resulted from the interaction between the magnetic moments of nuclei with the magnetic moments of electrons in the atoms. Analysis of the hyperfine structure permitted the determination of the angular momentum and the magnetic moments of many nuclei.

Earlier in 1921 Stern and Gerlach[2] had demonstrated in their molecular beam experiments that the measurable values of the magnetic moment are discrete in nature and when an atom is placed in a magnetic field this corresponds to a space quantisation of the nucleus.

The demonstration of the principles of nuclear magnetic resonance was first demonstrated successfully by Ramsay[3] and co-workers. Their work involved the use of a molecular beam which was passed through two oppositely inclined magnetic fields of similar gradients. The molecules were thus diffused and then brought back to focus on a detector. A uniform magnetic field and a coil energised by a radiofrequency (r.f.) signal having its oscillating magnetic component at right angles to the main field were positioned between the first two fields. Whenever the frequency of the oscillating field was equal to that required to induce transitions between nuclear energy levels a reduction in density of the molecules reaching the detectors was observed.

The first nuclear magnetic resonance (NMR) signals were observed independently by two groups of physicists in 1945; Purcell, Torrey and Pound[4] at

Harvard University observed a signal from the protons in paraffin wax, and Bloch, Hansen and Packard[5] at Stanford University detected a signal from the protons of water. Bloch and Purcell were jointly awarded the Nobel Prize for physics in 1952 for this discovery. In 1949 and 1950, a number of investigators noted that nuclei of the same species absorbed energy at different frequencies and so the phenomenon of the chemical shift was discovered.

Since that time the development of NMR techniques has been rapid. The first commercial high-resolution continuous wave (CW) proton NMR Spectrometer was produced in 1953 and such spectrometers have been an integral part of every research and teaching laboratory for many years.

The problems associated with nuclei of lower sensitivity, in natural abundance compared with protons, were not satisfactorily overcome until the introduction of commercial Fourier transform (FT) spectrometers around 1970. Now, however, both CW and FT spectrometers are an essential part of any modern laboratory and with these techniques NMR signals of almost all nuclei with a magnetic moment can be detected routinely.

1.1 Magnetic Properties of Nuclei

Many atomic nuclei behave as if they are spinning. In fact, any atomic nucleus which possesses either odd mass or odd atomic number, or both, has a finite spin angular momentum P and a magnetic moment μ. Nuclei which have both an even atomic mass and atomic number possesses no angular momentum. Examples of such nuclei are, ^{12}C, ^{16}O and ^{32}S. These nuclei, as will be revealed, cannot experience magnetic resonance under any circumstances.

The total spin angular momentum of any isolated particle cannot have any arbitrary magnitude but may only take certain discrete values. The spin angular momentum is said to be quantized and its magnitude, P, can be specified in terms of a spin quantum number, I, by means of equation 1.0. The value of spin I is a

multiple of one-half.

$$P = \hbar [I (I + 1)]^{1/2} \qquad .....1.0$$

Amongst the most common nuclei which possess spin are:

$I = 1/2$ ^{1}H, ^{3}H, ^{13}C, ^{15}N, ^{19}F, ^{31}P, ^{29}Si

$I = 1$ $^{2}H(D)$, ^{14}N

$I > 1$ ^{10}B, ^{11}B, ^{17}O, ^{23}Na, ^{27}Al, ^{35}Cl, ^{59}Co

Nuclei which have a spin greater or equal to one ($I \geq 1$) do not have a spherical distribution of nuclear charge. As a result they possess an electric quadrupole moment Q, in addition to their magnetic moment. The quadrupole moment interacts with electric field gradients at the nucleus and this can produce a very efficient mechanism for relaxing the nucler spins. The mechanisms by which the quadrupole moments cause the nuclear spins to relax efficiently and its effects on the NMR lineshape will be discussed in detail in a later chapter.

1.2 Classical Description of Nuclear Magnetic Resonance

When a nucleus is placed in a magnetic field, B_0, the interaction of the nuclear magnetic moment, μ, with B_0 produces a torque L, acting on μ which tends to tip it towards B_0. However, since the nucleus is spinning, instead of tipping μ parallel to B_0, the torque causes μ to precess about the magnetic field B_0 at an angle θ with B_0.

Mathematically the torque L can be represented as:

$$L = \mu \cdot B_0 \qquad .....1.1$$

From classical mechanics[6], the rotational torque generated is equal to the rate of change of spin angular momentum P. This is represented as:

$$\frac{dP}{dt} = L \qquad \text{..... 1.2}$$

Equation 1.2 can be reexpressed using equation 1.1.

$$\frac{dP}{dt} = \mu \cdot B_o \qquad \text{....1.3}$$

Qualitatively, the magnetic moment is colinear with the angular moment vector and is expressed as:

$$\mu = \gamma P. \qquad \text{..... 1.4}$$

Because the nucleus is spinning the resultant motion does not change the angle θ but rather causes the magnetic moment to precess around the magnetic field B_o. Combining equation 1.4 and 1.3 , the rate of change of magnetic moment, μ, can be expressed as:

$$\frac{d\mu}{dt} = \gamma \cdot \frac{dP}{dt} = \gamma . \mu \cdot B_o \qquad \text{..... 1.5}$$

The precession of the magnetic momentum is represented by an angular velocity ω_o. This is expressed as:

$$\frac{d\mu}{dt} = \omega_o \cdot \mu \qquad \text{..... 1.6}$$

Comparison of equation 1.5 and 1.6 gives:

$$\omega_o = -\gamma B_o \qquad \text{..... 1.7}$$

The minus sign denotes the direction of precession of the magnetic moment around the field B_o.

Thus, the nuclear moment precesses about B_o with a frequency ν_o:

$$\nu_o = \frac{|\omega_o|}{2\pi} = \frac{\gamma}{2\pi} B_o \qquad \text{..... 1.8}$$

ν_o is known as the Larmor precession frequency and is directly proportional to B_o.

The Larmor frequency ν_o, varies from one nucleus to another. For a simple nucleus of spin one-half, this precessional behaviour may be represented diagramatically using a Cartezian axis that is taken to be the direction of the applied field B_o, as shown in Figure 1.1.

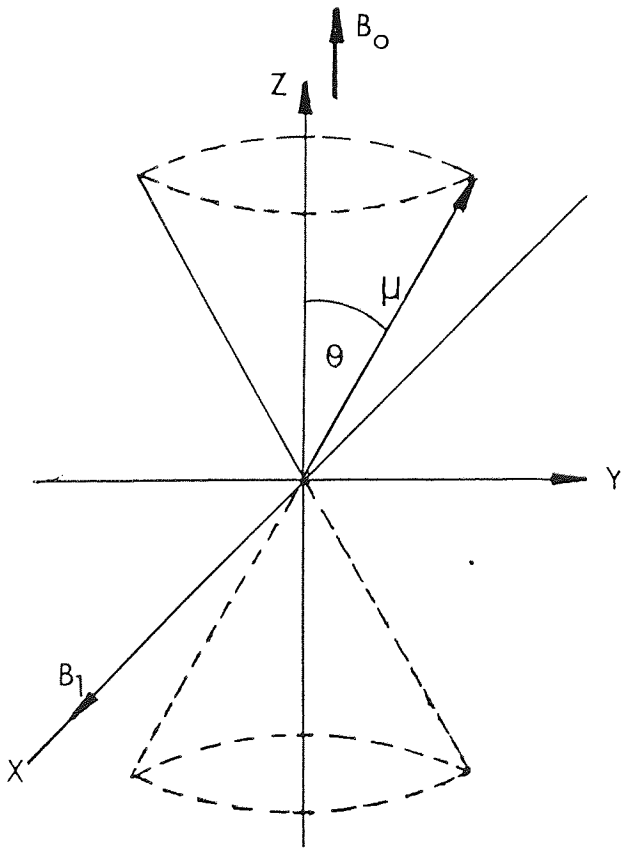

Figure 1.1: Diagramatic representation of Larmor precession for a single nuclear magnetic moment

1.3 Quantum Descripton

The energy of the interaction between a magnetic field, B_o, and the magnetic moment, μ, may be represented in terms of the Hamiltonian operator :

$$\hat{H} = -\mu \cdot B_o \qquad \text{..... 1.9}$$

The magnetic moment of the nuclei can be defined as:

$$\mu = \gamma \hbar I \qquad \text{..... 1.10}$$

I is interpreted as an operator and more commonly referred to as the nuclear spin quantum number.

Substitution of equation 1.10 into equation 1.9 gives:

$$\hat{H} = -\gamma \hbar I \cdot B_o \qquad \text{..... 1.11}$$

From the general properties of spin angular momentum in quantum mechanics[7,8] it has been shown that the solution of this Hamiltonian gives energy levels which can be represented as:

$$E_m = -\gamma \hbar m B_o \qquad \text{..... 1.12}$$

where m represents the nuclear magnetic quantum number.

When placed in a magnetic field, the number of allowed spin states which any nuclear spin may adopt is determined by its nuclear quantum number m. There are 2I + 1 allowed spin states which range with integral differences from +I to -I ($\equiv$ m). The individual spin states fit into the sequence; -I, (-I+1), ..., (I-1), I. In the absence of the magnetic field, all the spin states of a given nucleus are of equivalent energy, that is, they are degenerate. Thus given a collection of nuclei, all of the spin states should be populated with similar numbers occupying each of the allowed states.

NMR arises from transition of spins between different energy levels. These transitions are induced by the absorption of energy from an applied electromagnetic field. Consider the following: when a nucleus of total spin I is

placed in a magnetic field B_o, acting along the z axis, the stationary-state wave functions may be labelled by m, the component of I in the z direction. If, in addition, one has an oscillating magnetic field in the x direction, with amplitude B_{xo} $= 2B_1$ and frequency $\omega = 2\pi \nu$, then the presence of this field can be treated by adding to the Hamiltonian a term describing the interaction between the spin system and the applied radio-frequency field B_1 such that:

$$\mathcal{H} = 2 \mu_x B_1 \cos 2\pi \nu t \qquad \text{..... 1.13}$$

From transition probability theory, it has been shown[9] that this may give rise to a transition between two states m and m' corresponding to absorption or emission of radiation. The probability for such a transition is:

$$P_{m\,m'} = \gamma^2 B_1^2 \, | (m' | I_x | m)|^2 \, \delta (\nu_{m\,m'} - \nu) \qquad \text{..... 1.14}$$

where δ is the Dirac function, $(m' | I_x | m)$ is the quantum-mechanical matrix element of I_x between states m and m', and $\nu_{m\,m'}$ is the frequency corresponding to the energy gap between these states, that is:

$$h \nu_{m\,m'} = \frac{| m - m' |}{I} \mu B_o \qquad \text{..... 1.15}$$

It has been shown[10] that the matrix element $(m' | I_x | m)$ vanishes unless $m' = m \pm 1$. This determines the transition selection rule that only transitions in which the quantum number m is changed by $\pm$ 1 can occur. That is, $h \nu_{m\,m'} = \pm \mu B_o / I$.

Equation (1.14) predicts that absorption only occurs if the frequency ν coincides

exactly with the natural frequency $\nu_{m\,m'}$.

A detailed description of the effects of the application of an applied electromagnetic field will be discussed in chapter two.

1.4 The Population of Spin States

In nuclear magnetic resonance spectroscopy, the application of a radio frequency field B_1 to a sample, which is under the influence of an external magnetic field B_o leads, at resonance, to a net absorption of radiation even though the probabilities of absorption and emission are equal. This is due to the fact that there are a greater number of spins in the ground state than in the excited state. Hence, this leads to a greater number of spins being excited from the lower state to an upper state than vice versa. In view of this fact, the intensity of the absorption signal will depend on the difference in population between these two states. For most normal states in equilibrium at absolute temperature, there is a Boltzmann distribution between the number of participants N_β in the higher level and N_α in the lower level of the two energy states. The relative population as expressed in a Boltzmann distribution form is:

$$\frac{N_\beta}{N_\alpha} = \exp\left(-\frac{\Delta E}{kT}\right) \qquad \text{..... 1.16}$$

and

$$\Delta E = \frac{\mu B_o}{I} \qquad \text{..... 1.17}$$

where N_β and N_α are the number of spins in the upper state and lower state, respectively and k is the Boltzmann constant.

For example, hydrogen nuclei in a field of one Tesla have an excess population in the lower state of approximately 7×10^{-6} spins. The observation of NMR depends upon the net absorption of energy by this small excess population.

1.5 Magnetic Relaxation

If a physical system is perturbed from its equilibrium condition and the perturbing influence is removed, the system will return to its original equilibrium condition. However, this does not happen instantaneously, but takes a finite time to readjust to the changed conditions. The system is said to undergo relaxation and this usually occurs exponentially with time. In the case of NMR there are two mechanisms by which the nuclear spins can relax once excited. These are spin-lattice and spin-spin relaxations. They are also alternatively referred to as longitudinal and transverse relaxation respectively. These two relaxation mechanisms do not influence the population difference between the energy states.

Spin-lattice relaxation represents the exchange of energy between the spin-system and the lattice. The time taken by the nuclear spins to relax by this mechanism is represented by T_1. Spin-spin relaxation concerns the exchange of energy amongst the spins themselves. The time taken by the nuclear spins to relax by this mechanism is represented by T_2. These two processes will now be outlined briefly.

1.6 Spin-Lattice Relaxation

Nuclear spin transitions are induced by the application of a radiofrequency field B_1 perpendicular to the static field B_o. This radiofrequency field is applied at the Larmor precessional frequency of the magnetic moments. This perturbs the thermal equilibrium of the spin states such that a net number of nuclear spins are promoted to higher energy levels. In other words, the net energy of the

spin system has increased. In order to return to thermal equilibrium this excess energy has to be dissipated. This is brought about by energy exchange between the spin system and the lattice. The term lattice is used as a general term for the nuclear environment. The nuclear spins cannot exchange their magnetic energy with their surroundings by direct mechanical couplings but only indirectly by magnetic dipolar or electrical quadrupolar interactions. For example, for nuclear of spin one-half, the only interactions with the lattice are magnetic in origin. Transfer of energy from the spins to the lattice requires that there bea magnetic field at the nucleus fluctuating at the Larmor precession frequency in order to induce an NMR transition. This field originates from the magnetic dipoles in the lattice which is in thermal agitation, and since the frequency spectrum of these motions is very wide, the component actually in tune with the Larmor frequency is very weak. This is why NMR spin-lattice relaxation is a relatively slow process.

Another way of visualising spin-lattice relaxation involves the macroscopic (spin) magnetisation M. In the absence of an external field, the nuclear spins are randomly directed and there is no net magnetisation. When placed in a static field, the nuclear spins eventually line up, some parallel to the field, some anti-parallel, with a slight predominance of the former. The vector sum of the individual magnetic moments μ is known as the magnetisation M, which consequently points along the field axis. This polarisation does not take place instantaneously when the sample is placed in the field but with a finite time constant. The magnetisation builds up exponentially with a time constant equal to the spin-lattice relaxation time T_1. Likewise, if the spin system has been subjected to a strong saturating r.f. field, the return towards thermal equilibrium t kes place with a time constant T_1.

1.7 Spin-Spin Relaxation Times

In the absence of a r.f. field B_1 and in the presence of an external field B_o, the nuclear spins precess around the B_o field with their motional phases at random. Consequently there is no magnetisation perpendicular to the main field. If a r.f. field B_1 is now applied at resonance to the precessing spins, the individual magnetic moments of the spins become polarised along the axis of this rotation and a net transverse magnetisation is generated. This transverse magnetisation does not persist indefinitely. When the r.f. field is removed it decays to zero because of energy exchange amongst the nuclear spins themselves. This exchange of energy is brought about in the following manner: if one nucleus undergoes a transition from one spin state to another then the local magnetic field changes at the correct frequency to induce a transition in a second nucleus. If at this point in time a second nucleus of the same type and of opposite spin state is close by then the two nuclei can in effect exchange energy.

As the nuclear spins exchange energy there is a spread of Larmor frequencies across the sample. As a consequence of this, the spins dephase with a time constant given by T_2. In a perfectly homogeneous field, the slow passage width of the resonance line is inversely proportional to T_2. However, the magnetic field is never perfectly homogeneous. This is due to the presence of transverse gradients across the sample which means that the transverse magnetisation decays faster than predicted by T_2^*. For the effective transverse relaxation time T_2 the inequality $T_2^* < T_2$ holds. The full equilibrium magnetisation along the magnetic field axis can only build up after the transverse magnetisation has decayed to zero. From this it further holds that $T_2 \leq T_1$. In general, T_2 is regarded as the time in which phase coherence between spins in the xy plane is lost.

1.8 Saturation and Relaxation Effects

The interaction between the nuclear spin system and the lattice is responsible for the possibility of maintaining an absorption signal. If no such interaction occurs, the number of nuclei in the upper level (ß) would become equal to that in the lower level (α) as absorption of the incoming radiation raises their energy. If such an equality was produced no further absorption would take place. Similarly, if the power of the incoming radiation is high, it may drive the nuclei up to the higher level at a faster rate than the spin-lattice relaxation interaction can restore thermal equilibrium. In this case the absorption intensity will gradually decrease and the line will become broader.

Consider a nuclei with spin one-half in an applied magnetic field having two energy levels $|\alpha|$ and $|ß|$. Let n represent the population difference before a radiofrequency field is applied. If now the r.f. field is switched on, the rate of change of n can be expressed as:

$$\frac{dn}{dt} = \left(\frac{dn}{dt}\right)_{r.f.} + \left(\frac{dn}{dt}\right)_{SL} \qquad \ldots\ldots 1.18$$

where $\left(\frac{dn}{dt}\right)_{r.f.}$ represents the rate of change due to r.f. field pertubation.

Figure 1.2 shows the effects of the electromagnetic radiation and the spin lattice relaxation.

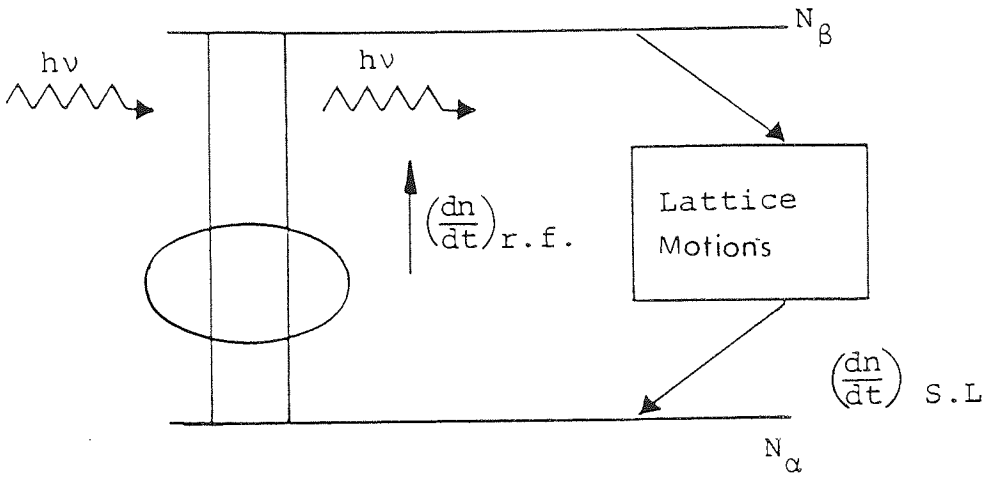

Figure 1.2: Saturation of resonance condition. The effects of electromagnetic radiation and spin-lattice interaction are indicated schematically in the diagram.

If P represents the stimulated transition probability and is such that

$P=P_{\alpha\beta}=P_{\beta\alpha}$, then the rate of change of population of the $|\alpha|$ state due to the radiation

can be expressed as:

$$\frac{dN_\alpha}{dt} = N_\beta P_{\beta\alpha} - N_\alpha P_{\alpha\beta} \quad \text{..... 1.19}$$

Therefore

$$\frac{dN_\alpha}{dt} = P(N_\beta - N_\alpha) \quad \text{..... 1.20}$$

Then

$$\left(\frac{dn}{dt}\right)_{r.f} = -2Pn \quad \text{..... 1.21}$$

where $n = N_\alpha - N_\beta$

The term $\left(\frac{dn}{dt}\right)_{S.L}$ in equation (1.18) originates in the lattice. The lattice is at thermal equilibrium which means that the probabilities of spontaneous spin transitions up and down are not equal as they were for r.f. induced transitions. If one denotes $w_{\alpha\beta}$ and $w_{\beta\alpha}$ as the upward and downward relaxation probability then:

$$\frac{dN_\alpha}{dt} = N_\beta w_{\beta\alpha} - N_\alpha w_{\alpha\beta} \quad \ldots\ldots 1.22$$

At thermal equilibrium $dN_\alpha/dt = 0$ and this implies that $N_\beta^o/N_\alpha^o = \frac{w_{\alpha\beta}}{w_{\beta\alpha}}$. This follows the Boltzmann law. Thus the population difference n is:

$$\left(\frac{dn}{dt}\right)_{S.L} = \frac{-(n - n_o)}{T_1} \quad \ldots\ldots 1.23$$

$$\text{with } T_1^{-1} = w_{\alpha\beta} + w_{\beta\alpha} \quad \ldots\ldots 1.24$$

T_1 is the spin-lattice relaxation time. It is a measure of the time it takes for energy to be transferred to other degrees of freedom. Equation 1.18 can be rewritten as:

$$\frac{dn}{dt} = -2Pn - \frac{n - n_o}{T_1} \quad \ldots\ldots 1.25$$

Thus at equilibrium equation 1.25 becomes:

$$n = \frac{n_o}{1 + 2PT_1} \quad \ldots\ldots 1.26$$

For protons, the probability P, per unit time per spin of transition being induced is: [10]

$$P = {}^1/_4 \gamma^2 B^2 g(\nu) \quad \text{..... 1.27}$$

where g (ν) is the lineshape function.

A second relaxation time, T_2, (spin-spin), is defined as :

$$T_2 = 1/2\ g(\nu)_{max} \quad \text{..... 1.28}$$

This relaxation results from interaction amongst spins themselves.

The ratio n/n_o is known as the saturation factor Z. When g(ν) is a maximum Z is minimum. That is:

$$Z_o = [1 + \gamma^2 B_1^2 T_1 T_2]^{-1} \quad \text{..... 1.29}$$

The saturation effects produced by large values of T_1 and B_1 will not only reduce the actual power absorption but also alter the line shape, showing its effects in the centre before the wings, and thus increasing the apparent width of the absorption line. This explains why it is so important to apply a low r.f. field B_1 in order to avoid saturation as much as possible.

1.9 Principles of Continuous Wave Nuclear Magnetic Resonance

There are two principal methods by which absorption of energy from an applied field, B_1, will cause nuclear magnetic resonance: These are continuous wave nuclear magnetic resonance and the pulse Fourier transform magnetic resonance.

In continuous wave nuclear magnetic resonance there are two approaches to obtaining resonance. These are called frequency sweep and field sweep. In frequency sweep the field B_o is held constant while the irradiating r.f.

field frequency of B_1 is swept. In a field sweep a controlled DC current passes through a set of sweep coils which increases or decreases the total magnetic field strength necessary to scan through the resonance whilst the r.f. field B_1 is kept constant.

If either the field B_o or the irradiating r.f. frequency (the source of B_1) is swept in a continuous fashion while the other is held constant there will be some point during the scan at which the field/frequency combination (B_o/B_1) is such that nuclear transition between the energy levels takes place. For example, if the field B_o is held constant, then at the precision frequency ν_o, the magnetisation M will be tipped from the z axis. The magnetisation M is the net magnetisation corresponding to the sum of all the individual nuclear magnetic moments. M_o is the equilibrium net magnetisation and $M = M_o$ only until r.f. excitation of the sample is initiated. A signal will be induced in the receiver coil which lies in the x, y plane, when M is tipped from the z axis.

The principal drawback to this technique is the time taken to obtain an individual spectrum. This may be in the order of 100-500 sec. Consequently, the total time necessary to obtain a spectrum requiring the computer controlled addition of several thousand scans would be very long.

1.10 Principles of Fourier Transform Nuclear Magnetic Resonance

An alternative method to irradiating at a single frequency is to irradiate all the frequencies simultaneously. This is done by use of an r.f. pulse. Pulse methods may be more easily understood if the co-ordinate axes of Figure 1.1 are replaced by a new set (x', y', and z') of axis. These new x'y' axes rotate about B_o

in the same direction as that in which the nuclear moments precess. The field B_0 lies along the z' axis in the rotating frame. If a second field B_1 is now applied perpendicular to this in the x' y' plane and is rotating at the precessional frequency, then the field B_1 will interact with Mo. In the rotating reference frame, the application of B_1 along the x direction causes M to precess about the x' axis. In a time tp (sec) the angle θ (rad) through which M precesses is given by:

$$\theta = \gamma B_1 \, tp \quad \text{rads} \qquad \ldots\ldots 1.31$$

This effect is shown in Figure 1.3.

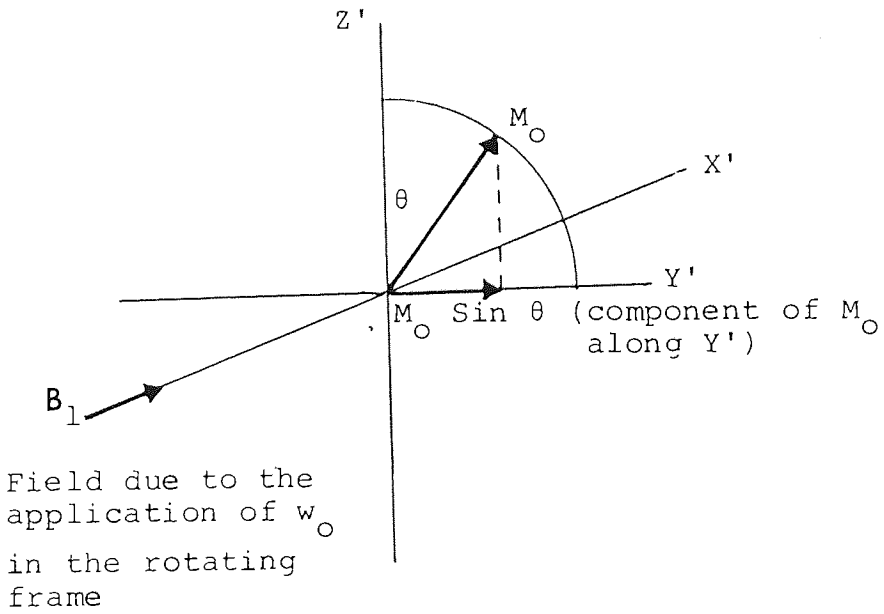

Figure 1.3: Application of an r.f. pulse with a frequency ω_0 for a time tp seconds on the magnetisation vector M_0.

The field B_1 arises from a pulse of r.f. radiation.

Equation 1.31 can be used to find the angle through which a pulse of a given duration (called the pulse width) will cause M to precess.

Following a pulse, the magnetisation M returns to its equilibrium value Mo by the T_1 relaxation process. As a result of being tipped by a pulse, the nuclear moments lie in such an orientation that a component of M is generated along the y' axis. Because the nuclei precess at slightly different frequencies (a consequence of field in homogeneity), the magnetisation vectors fan out in the x' y' plane (see Figure 1.4). This dephasing causes the signal to decay to zero in the x' y' plane and is called spin-spin or transverse relaxation. In addition, the nuclear moments lose energy to their surroundings (the lattice) and this results in the restoration of the z' components of magnetisation. This process is known as spin-latttice (or longitudinal) relaxation. A mathematical description on relaxation processes will be discussed in detail in Chapter Two.

If a 90° pulse is applied, the magnetisation will be tipped into the plane of the receiver coil and a signal corresponding to M_o would be obtained. The decay of this signal following the removal of the 90° pulse is determined by spin-spin relaxation. In a perfectly homogenous field, the signal arising from nuclei, with exactly the same Larmor frequencies would have a pure exponential decay called a Free Induction Decay (F.I.D).

For a system of several nuclei which differ in Larmor precession frequencies, interference effects can occur in the F.I.D. Such effects are superimposed on the exponential decay, as the magnetisation and the reference frequency comes in and out of phase. This complex F.I.D is measured as a function of time and contains all the frequency information of the spectrum. This may then be converted into the frequency domain by the mathematical process of Fourier transformation.

The normal sequence of events used in pulsed Fourier Transform NMR spectroscopy is that the sample is irradiated with a short (μs) pulse of r.f. radiation.

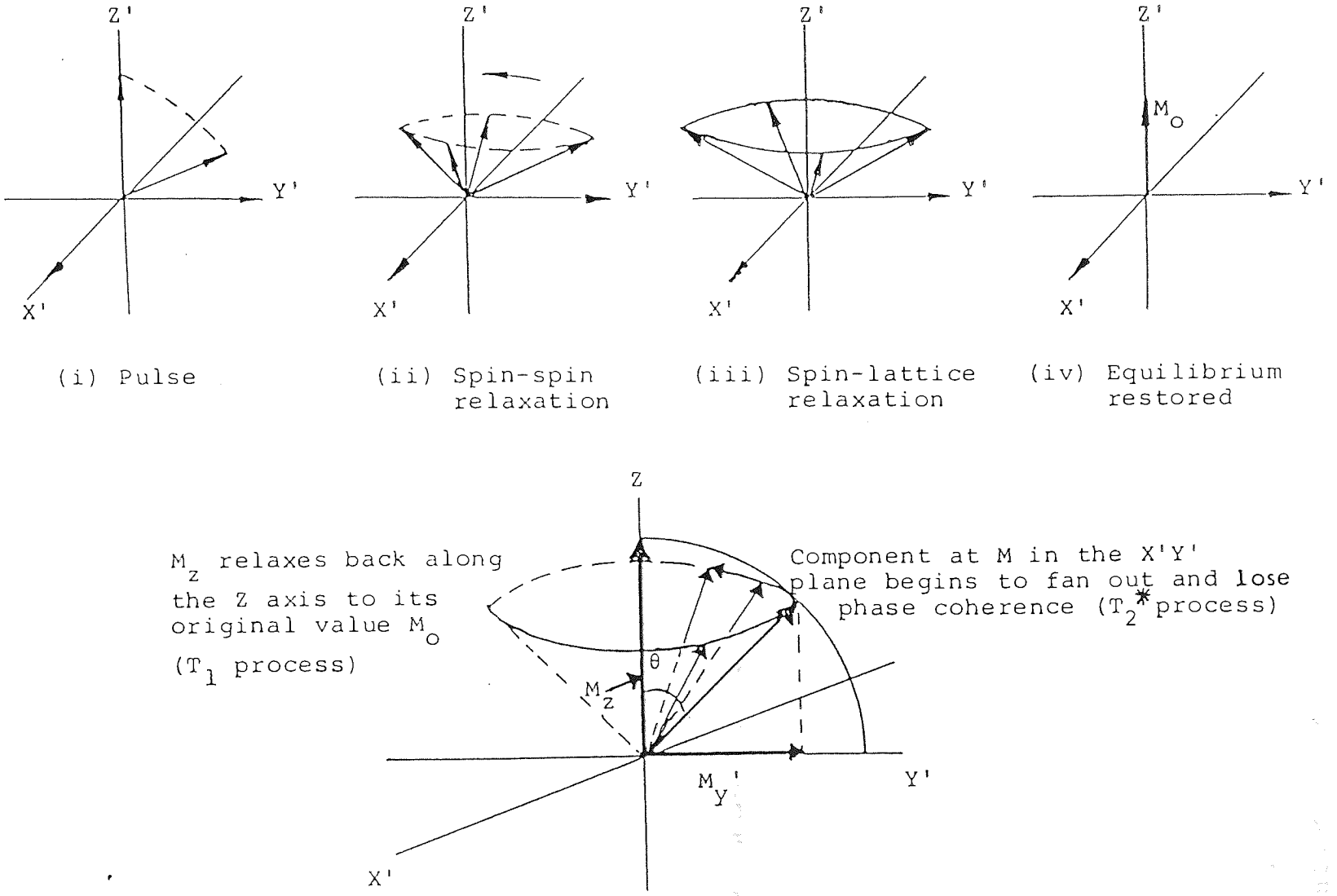

Figure 1.4 : Schematic representation of relaxation

Immediately following the pulse (in practice there is a micro-second delay called the recovery time, to prevent leakage of the pulse to the detector), the signal is detected through a receiver coil. The total time the receiver is operative in sampling the FID is called the acquisition time. The signal then passes through another detector which performs a subtraction process of a frequency less than the smallest frequency one expects to encounter. The object being to simplify the digitisation of the signal. For example, consider a proton spectrum recorded at 100 MHz. The various radiofrequency signals arising from the sample are all present in the region of 100 MHz, and caused to cover the chemical shift range present. For protons this would typically be 10 ppm or 1000 Hz, so the frequencies encountered may run from 100,000,000 Hz to 100, 001, 000 Hz. There is no objection in principle to attempt direct digitisation of the signals, however it is easier to note that it is only the chemical shift range of frequency that needs to be measured. Thus, subtraction of some reference frequency from the NMR signal, say 100 MHz, leaves the chemical shift range to be digitised.

The signal once again travels through a bandpass filter which has an electrical bandwidth limit. Consider a case where all the frequencies lie within the spectral range. Beyond this limit there exists the electrical noise which essentially is made up of an infinite range of frequency components (white noise). This causes a negating of signal sensitivity when time averaging the signal by way of fold back of the electrical noise within the spectral range. Thus, limiting the electrical bandwidth of the spectrometer can prevent this from happening. The electrical signal is then converted into a numerical form by a device known as the analogue-to-digital converter (ADC). The property of an ADC is that, presented with a voltage as its input, it outputs a binary number, representing the size of the voltage. This digitised signal then undergoes Fourier transformation to give a frequency domain signal which is stored in the computer. The spectrum is "outputted" on to a chart recorder to give a normal Lorentzian line shape.

Normally, several pulses are applied and the resulting F.I.D's stored in computer core. These are then averaged before Fourier transformation to give a better signal-to noise ratio than that obtained with one pulse. The principle behind this is that NMR signals occur in exactly the same place each time and therefore build up over a number of repetitions. The fate of the noise is slightly complicated. The noise does not "average out" as believed, but builds up more slowly than the signal. For over N repetitions of the experiment, during which the signal increases N times, the noise amplitude only increases by $\sqrt{N}$. Thus the signal-to-noise ratio improves by a factor of $\sqrt{N}$. Figure 1.5 represents a scheme for FT NMR.

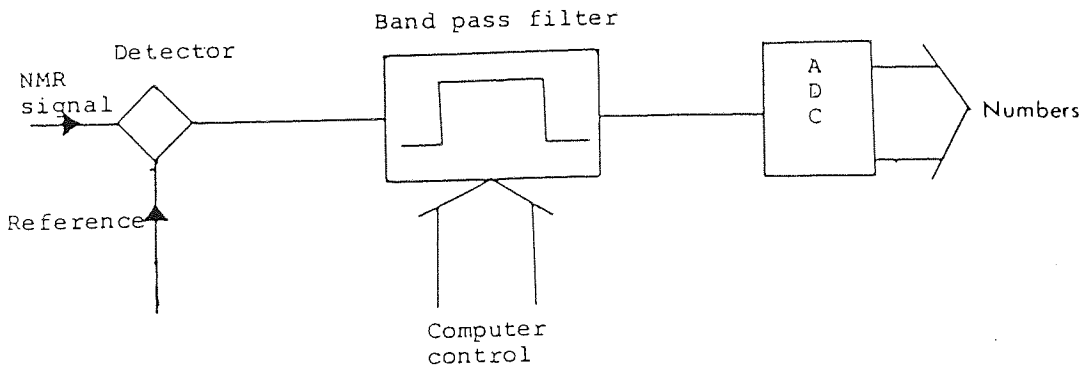

Figure 1.5: Schematic representation of FT NMR using a band pass filter and an ADC.

More detail on NMR instrumentation will be presented in a later chapter.

1.11 The Chemical Shift

The great utility of nuclear magnetic resonance spectroscopy arises from the fact that not every nucleus in a molecule resonates at identically the same frequency. This is due to the fact that the various nuclei in a molecule are surrounded by electrons, and exist in slightly different electronic environments from one another. The nuclei are shielded by the electrons which surround them. In a magnetic field, the circulating valence electrons of the nuclei generate counter magnetic fields which oppose the applied field. Thus, each nucleus in a molecule is shielded from an applied magnetic field to an extent that depends on the electron density that surrounds it. The greater the electron density around a nucleus, the greater is the applied field. The net field which the nucleus experiences is diminished by the counter field which shields it. A nucleus which experiences a lower applied magnetic field, will precess at a lower frequency. Each nucleus in a molecule will be in a slightly different chemical environment[12,13,14,15] and will, in consequence, have slightly different amounts of electron shielding which will result in a slightly different resonance frequency. These differences in resonance frequency are very small and until recently were difficult to measure at exact frequencies. Thus, a need for some reference arose. Tetramethylsilane is normally chosen as a reference for normal ^{1}H, ^{13}C and ^{29}Si spectrum. If nuclei in a molecule are in chemically identical environments, they often exhibit the same resonance frequency, and the nuclei are said to be magnetically equivalent. However, if the nuclei in the molecules are in a chemically identical environment but exhibit a different resonance frequency, then the nucli are said to be magnetically non-equivalent but chemically equivalent.

A mathematical interpretation of shielding can be written in the form of σ, the so called shielding or screening constant. If the applied field is B_o then the effective field experienced by a nucleus which has a shielding constant σ can be expressed as in equation (1.32).

$$B_{effective} = B_{applied}\ (1 - \sigma) \qquad \text{..... 1.32}$$

The positions of absorption with different resonant frequencies measured relative to the position of a reference can be expressed in the form of equation (1.33).

$$\delta = \sigma_{sample} - \sigma_{reference} \qquad \text{..... 1.33}$$

where δ is referred to as the chemical shift. More suitably the chemical shift can be expressed in the form of equation (1.33).

$$\delta = \frac{\nu_{sample} - \nu_{reference}}{\nu_{ref}} \times 10^6 \qquad \text{..... 1.34}$$

where the chemical shift δ is measured in numbers of parts per million.

CHAPTER TWO

RELAXATION PROCESSES IN NMR

NOMENCLATURE

S	Signal height
T_2^*	Effective spin-spin relaxation time
τ_c	Correlation time
$J(\omega)$	Spectral density
$K(\tau)$	Auto correlation function

2.0 RELAXATION PROCESSES IN NMR

This chapter continues the theme of nuclear magnetic resonance with a mathematical description of magnetisation, relaxation and the role of molecular motion and its implication to relaxation.

When a physical system is perturbed from its equilibrium condition and the perturbing influence removed, the system does not achieve equilibrium instantaneously but takes a finite time to readjust to the changed conditions. The effect of the perturbation can be seen by monitoring the system as it is allowed to return to equilibrium naturally.

In the case of NMR, for example, for nuclei with a spin one-half in a magnetic field B_o, the application of a r.f. field B_1 across the sample will at resonance, cause a change in the relative population of the two spin states α and β. These two spin states reach their original equilibrium via the two magnetic relaxation processes. Figure 2.1 depicts the two modes of relaxation of the spins after the application of a radio frequency field B_1.

2.1 Mathematical Description of Magnetisation and Relaxation

In 1946 Felix Bloch[16,17] gave a mathematical description of the magnetic properties of ensembles of nuclei in an external magnetic field. In order to derive the equations describing relaxation, it is convenient to discuss the behaviour of a macroscopic sample containing many identical molecules each with one magnetic nucleus. Thus, the total magnetic moment or magnetisation M of the sample is a sum of all the nuclear moments μ. This can be expressed as:

$$M = \sum_{j}^{i} \mu_{ij} \qquad \ldots\ldots 2.1$$

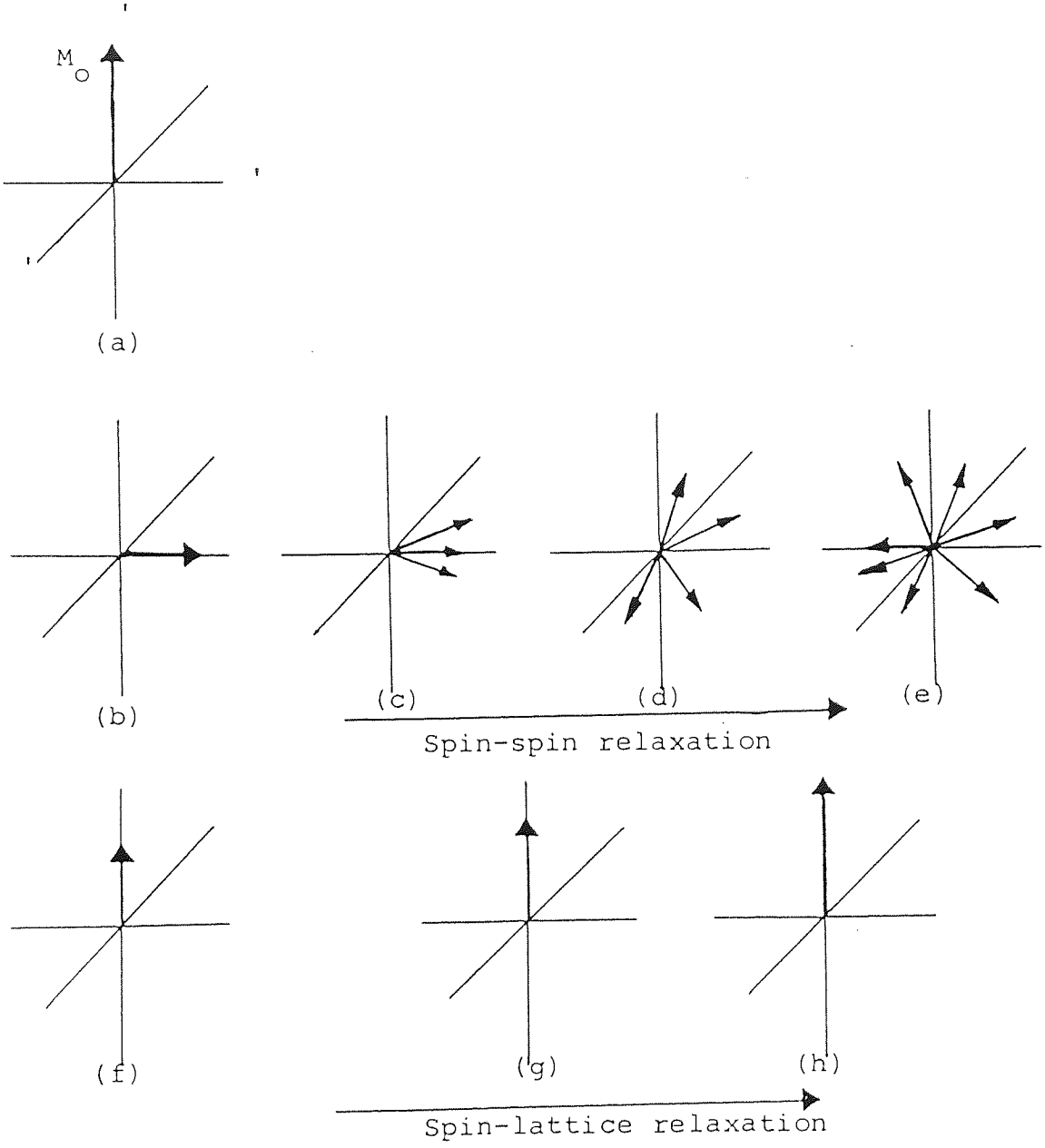

Figure 2.1: (a) The equilibrium magnetisation Mo.
(b) Transverse magnetisation produced in an NMR experiment.
(b-e) The loss of phase coherence of the transverse magnetisation (spin-spin relaxation).
(f-h) Re establishment of equilibrium magnetisation (spin-lattice relaxation)
Figure 2.1 is shown in a rotating frame of reference.

The summation $\Sigma\mu_{ij}$ represents the sum of all the nuclei nuclear magnetic moments from i to j.

If the magnetic moment of a nucleus is defined as:

$$\mu = \gamma \hbar I \qquad \text{..... 1.10}$$

then the summation $\sum_{j}^{i} \mu_{ij} = \gamma \hbar \sum_{j}^{i} I_{ij}$ 2.2

Where the summation $\sum_{j}^{i} I_{ij}$ now represents the sum of all nuclei with a nuclear spin quantum number I from i to j.

The magnetisation M can also be expressed in terms of the total spin angular momentum P. This is:

$$M = \gamma P \qquad \text{..... 2.3}$$

where $P = \hbar \sum_{j}^{i} I_{ij}$ and γ is the nuclear magnetogyric ratio.

As the sample is macroscopic, the effect of magnetic field B, can be predicted. The interaction of the magnetic field and the total magnetic moment gives a torque on the system changing the angular momentum P. The rate of change of the angular momentum can be expressed as:

$$\frac{dP}{dt} = \sum_{j}^{i} \mu_{ij} B \qquad \text{..... 2.4}$$

As P and M are related through equation 2.3 the rate of change of magnetisation can be expressed as:

$$\frac{dM}{dt} = \gamma \frac{dP}{dt} = \gamma \sum_j \mu_{ij} B = \gamma M B \qquad \text{..... 2.5}$$

Equation 2.5 relates the rate of change of magnetisation to the rate of change of the spin angular momentum. This is of the form that describes the motion of the magnetic moments μ as described in Chapter One. In the steady-state, due to the changing angular momentum, there is a precession of the nuclear spin system about the magnetic field direction with an angular velocity $\omega_o = -\gamma B_o$. This is known as Larmor precession and the corresponding frequency $\gamma B_o / 2\pi$ is the Larmor frequency.

Any system with a magnetic moment will show Larmor precession. The magnetic moment of the sample in nuclear resonance may, in addition, change by internal realignment of the individual nuclear spins. Indeed, when the sample is placed in a magnetic field B_o its moment changes from zero to an equilibrium magnetisation M_o.

The vector product of equation 2.5 may be resolved into its components using the unit vector i, j and k, thus:

$$M \times B = \begin{vmatrix} i & j & k \\ M_x & M_y & M_z \\ B_x & B_y & B_z \end{vmatrix}$$

$$= (M_y B_z - M_z B_y)i + (M_z B_x - M_x B_z)j + (M_x B_y - M_y B_x) k \qquad \text{..... 2.6}$$

The field B consists of the primary field B_o (along the z' axis) and the applied field B_1 which is at resonance with the nuclear precession and so is rotating in the xy plane with angular frequency ω. Thus the components of B are:

$$B_x = B_1 \cos \omega t \quad \text{..... 2.7}$$

$$B_y = -B_1 \sin \omega t \quad \text{..... 2.8}$$

$$B_z = B_o \quad \text{..... 2.9}$$

Thus, in the nuclear resonance experiment, there is a small oscillating magnetic field $2B_1 \cos \omega t$ in the x direction. This can be resolved into two components rotating in opposite directions with angular velocities $\pm\omega$. These may be considered independently, provided B_1 is small, and the effect on the nuclei of the component rotating in the opposite direction to the Larmor precession (the one with angular velocity $+ \omega$) can be neglected. The effective field induces a rotating magnetisation in the x, y plane which is monitored by the spectrometer. Thus, the field B acting on the sample is:

$$B = B_1 (i \cos \omega t - j \sin \omega t) + B_o k \quad \text{..... 2.10}$$

Substituting equations 2.7 to 2.9 into equation 2.6 gives:

$$\frac{dM_x}{dt} = \gamma (M_y B_o + M_z B_1 \sin \omega t) \quad \text{..... 2.11}$$

$$\frac{dM_y}{dt} = \gamma (M_z B_1 \cos \omega t - M_x B_o) \quad \text{..... 2.12}$$

$$\frac{dM_z}{dt} = -\gamma (M_x B_1 \sin \omega t + M_y B_1 \cos \omega t) \quad \text{..... 2.13}$$

The above equations of motion represent the motion of the magnetic moment of the sample which show Larmor precession. However, these equations fail to include the approach to thermal equilibrium. Bloch made the assumption that the z-component of the magnetisation M decays to its equilibrium magnetisation M_o exponentially. However, he allowed the components of M parallel and perpendicular to M_o to decay with different time constants T_1 and T_2 so that, with the z axis chosen along B_o

$$\frac{d(M_z)}{dt} = -(M_z - M_o)/T_1 \qquad \text{..... 2.14}$$

$$\frac{d(M_x)}{dt} = -M_x/T_2 \qquad \text{..... 2.15}$$

$$\frac{d(M_y)}{dt} = -M_y/T_2 \qquad \text{..... 2.16}$$

Thus, combining equations 2.11, 2.12 and 2.13 with equations 2.14, 2.15 and 2.16 respectively, results in:

$$\frac{dM_x}{dt} = \gamma\,(M_y B_o + M_z B_1 \sin \omega t) - \frac{M_x}{T_2} \qquad \text{..... 2.17}$$

$$\frac{dM_y}{dt} = \gamma\,(M_z B_1 \cos \omega t - M_x B_o) - \frac{M_y}{T_2} \qquad \text{..... 2.18}$$

$$\frac{dM_z}{dt} = -\gamma\,(M_x B_1 \sin\omega t + M_y B_1 \cos\omega t) - \frac{(M_z - M_o)}{T_1} \qquad \ldots\ldots 2.19$$

Equations 2.17, 2.18 and 2.19 take a simpler form if they are referred to a set of axis (x', y' and z') rotating with the applied field B_1, with an angular velocity $-\omega$ about the z axis. If the components of magnetisation in the plane perpendicular to B_o are designated u and v, then "u" is the component in the direction of B_1 along the x' axis and "v" is the component in the direction of B_1 along the y' axis. u and v are referred to as the in-phase and out-of-phase components of B_1, respectively. Thus:

$$\mu = M_x \cos\omega t - M_y \sin\omega t \qquad \ldots\ldots 2.20$$

$$v = M_x \sin\omega t + M_y \cos\omega t \qquad \ldots\ldots 2.21$$

The change in magnetisation M_y induces a signal in the receiver coils of the spectrometer. By using a phase-sensitive detector either u or v may be detected. The latter is normally used.

The rate of change of the in-phase component of magnetisation, u, can be expressed as:

$$\frac{du}{dt} = \frac{d}{dt}(M_x \cos\omega t) - \frac{d}{dt}(M_y \sin\omega t)$$

Differentiation of the above equation with appropriate mathematical manipulation reduces the above equation to:

$$\frac{du}{dt} = \gamma B_o v - \frac{u}{T_2}\omega v \qquad \ldots\ldots 2.22$$

If the Larmor angular velocity about B_o is denoted as

$$\omega_i = \gamma B_o$$

then substitution of the above equation into equation 2.2 gives

$$\frac{du}{dt} = (\omega_i - \omega)\, v - \frac{u}{T_2} \qquad \text{.....2 23}$$

Similarly the rate of change of magnetisation for the out-of-phase component, v, can be expresed as:

$$\frac{dv}{dt} = \frac{d}{dt}(M_x \sin \omega t) + \frac{d}{dt}(M_y \cos \omega t)$$

Following differentiation of the above equation and through appropriate substitution, the equation can be re-expressed as:

$$\frac{dv}{dt} = \gamma B_1 M_z - \gamma B_o u - \frac{1}{T_2} v + \omega u$$

On further substitution for $\omega_i = \gamma B_o$, the above expression further simplifies to:

$$\frac{dv}{dt} = \gamma B_1 M_z - \frac{v}{T_2} - u\,(\omega_i - \omega) \qquad \text{..... 2.24}$$

The rate of change of magnetisation M_z, from equation 2.19 can be expressed as:

$$\frac{dM_z}{dt} = -\gamma B_1 v - (M_z - M_o)/T_1 \qquad \text{... 2,25}$$

A visual picture of the transverse components of magnetisation vector with respect of fixed and rotating axis can be represented by Figure 2.2, when looking down the z axis.

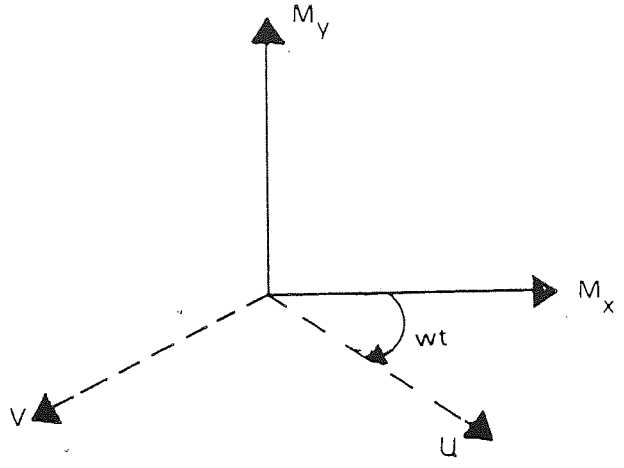

Figure 2.2: The transverse components of the magnetisation vector with respect of fixed and rotating axis (working down the z-axis)

2.2 Steady-State Experiments and Line Shapes

In normal steady state experiments, the spectrometer is tuned to observe the component of magnetisation 90° out of phase with the rotating field B_1, giving the absorption mode signal v. The in-phase component u which gives the dispersion mode signal, is occasionally observed; in high-resolution spectroscopy it provides a lock signal in order to maximise the field stability and also homogeniety. The values of u, v and M_z are given by solving the solutions of the Bloch equations in rotating axes (equations 2.23-2.25) with time derivatives equal to zero [10,17,18,19]. Thus:

$$M_z = \frac{M_o [1 + T_2^2 (\omega_i - \omega)^2]}{T_2^2 (\omega_i - \omega)^2 + 1 + T_1 T_2 \gamma^2 B_1^2} \quad \text{..... 2.26}$$

$$u = \frac{M_o \gamma B_1 T_2^2(\omega_i - \omega)}{T_2^2(\omega_i - \omega)^2 + 1 + T_1 T_2 \gamma^2 B_1^2} \quad \text{..... 2.27}$$

$$v = \frac{M_o \gamma B_1 T_2}{T_2^2 (\omega_i - \omega)^2 + 1 + T_1 T_2 \gamma^2 B_1^2} \quad \text{..... 2.28}$$

Similar expressions in frequency units may be obtained by replacing $\omega_i = 2\pi\nu_i$ and $\omega = 2\pi\nu$. Figure 2.3 shows the shape of the u and v signal predicted by the Bloch equation when $\gamma B_1 << (T_1 T_2)^{1/2}$. The v mode (absorption) signal has a Lorentzian line shape and the signal is at a maximum when ω_i=w and is proportional to $\gamma B_1 T_2$.

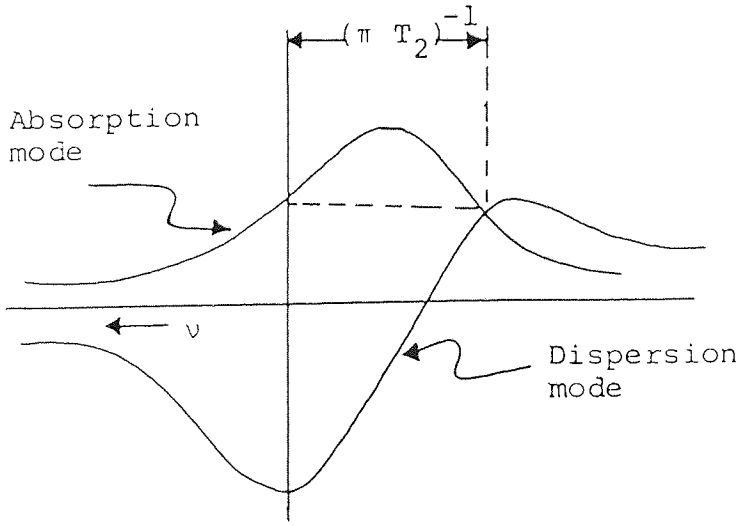

Figure 2.3 - Lorentzian absorption and dispersion lineshape

When $\gamma B_1 << (T_1 T_2)^{1/2}$, the population of the energy levels involved in the spin transitions do not depart appreciably from their values in the absence of B_1. Therefore $\Delta n \simeq \Delta n_o$, and the absorption mode signal is proportional to the line shape factor[10,20] which:

$$g(\nu) = \frac{2T_2}{1 + 4\pi^2 T_2^2 (\nu_i - \nu)^2} \qquad \ldots\ldots 2.29$$

This line shape factor depends on the probability, P, per unit time per transition of a spin being induced, such that, $P \propto \gamma^2 B_1^2 g(\nu)$. It also accounts for the fact that "spectral lines" are not infinitely sharp as there is some transition probability at frequencies differing slightly from exact resonance. The width of the absorption line at half-height and the peak-to trough separation of the dispersion line are both equal to $(\pi T_2)^{-1}$ in frequency units.

The absorption mode signal v is proportional to the power absorbed from the r.f. electromagnetic field. In fact it depends on B_1 and not on B_1^2 as may have been suggested by equation 2.28. This is because in a steady state NMR experiment the spin system can absorb energy from the radio frequency radiation at a rate, R, which depends on three other factors, these are:

(1) the probability, P, per unit time per transition of a spin being induced.

(2) the population difference between the spin-system.

(3) the energy change appropriate to the transition.

However, NMR spectrometers do not detect R directly, but rather the rate of induced magnetisation change in the direction of the receiver coil (d (My)/dt). This turns out

to be R/B_1 and so the observed signal height S is given by:

$$S \propto \gamma^4 B_o^2 N B_1 g(\nu)/T \qquad \text{..... 2.30}$$

where T in this case is temperature.

2.3 Factors Affecting Lineshapes

The lineshape predicted by the Bloch equation 2.29 is known as Lorentzian. This is the shape that would be observed in an ideal experiment if the relaxation of M_x and M_y were truly exponential with a single relaxation time T_2. In practice, the lines in NMR experiments are not often Lorentzian and may even be unsymmetrical. This is because "natural" line widths $(\pi T_2)^{-1}$ are so small that the observed widths are due to instrumental effects, such as the variation in B_o over the area of the sample. Thus, the lineshape in an indication of the field inhomogenity over the sample. This is sometimes known as inhomogeneity broadening. The effects of field inhomogeneity can be minimized by spinning a cylinderical sample about its long axis. If the magnetic field inhomogeneity is represented as $\gamma\delta B_o$ (expressed in Hertz) then T_2 can be replaced by an effective value known as T_2^*[20,21], where

$$\frac{1}{T_2^*} = \frac{1}{T_2} + \frac{1}{\gamma\delta B_o} \qquad \text{..... 2.31}$$

and the half-height linewidth is now given by:

$$\nu_{1/2} = \frac{1}{\pi T_2^*} \qquad \text{..... 2.32}$$

There are several other factors which effect the linewidth other than field inhomogeneity. These are:

(a) The effects of fluctuating fields, due to the magnetic moments of nuclei in other molecules as they excute thermal motion. This random fluctuating field may be resolved by Fourier analyses into oscillations at different frequencies and further subdivided into components perpendicular to B_o and those parallel to B_o. The components perpendicular to the static field which oscillate with the Larmor frequency induce transitions between the energy levels. This gives rise to a non-adiabatic (or non-secular) contribution to relaxation of both the longitudinal and transverse components of M. The linewidth (excluding the effect of inhomogeneity B_o) which is inversely proportional to T_2, is a measure of the uncertainty in the energies of the two states concerned. From the Heisenberg uncertainty principle the linewidth is inversely proportional to the lifetimes of these states. Thus, fluctuations which cause transitions between states result in both the changes of population associated with longitudinal relaxation (T_1) and an increase in linewidth associated with transverse relaxation (T_2). Both x and y components of the fluctuating field affect T_1 but M_y can only be affected by the x component of the non-secular contribution to the relaxation rate T_2^{-1}. However, there is a second contribution to T_2^{-1} arising from fluctuating fields in the z direction. This is the adiabatic (or secular) contribution and involves no energy exchange with the Lattice. It is related to variation in the total magnetic field in the z direction, and hence to linewidths. For a mobile liquid this contribution is usually equal to $1/2\, T_1^{-1}$ so that $T_1 = T_2$. The parameter T_2 itself has many sources of interaction but can be expressed as:

$$\frac{1}{T_2} = \frac{1}{T'_2} + \frac{1}{2T_1} \qquad \text{..... 2.33}$$

where T'_2 comes from energy fluctuations. Consequently, any mechanism affecting T_1 will effect $T_2$and of course $T_2 < T'_2$ and $T_2 < 2T_1$.

(b) The effects of nuclear magnetic dipoles. Any magnetic nucleus in a molecule supplies an instantaneous magnetic dipolar field, which is proportional to the magnetic moment of the nucleus. As the molecule tumbles in solution under the influence of thermal motion, this dipolar field fluctuates in magnitude and direction. This results in oscillating magnetic fields being produced with frequencies of oscillations which can and does interact with the applied r.f. magnetic field at the Larmor precession frequency. The effectiveness of the fluctuating dipolar fields in bringing about relaxation does not only depend on the Fourier components of motion at the Larmor frequency but also on the magnitude of the nuclear moments and the distance between the interacting nuclei. The static local magnetic field at a nucleus i due to another nucleus with a nuclear moment j can be expressed as:

$$B\ (\text{local}) = \pm \frac{\mu}{r^3_{ij}} (3 \cos^2 \theta_{ij} - 1) \qquad \text{..... 2.34}$$

In this expression, r_{ij} is the magnitude of a radial vector joining nuclei i and j, while θ_{ij} is the angle between this vector and the applied field B_o. Thus equation 2.34 modifies B_o:

$$B = B_o \pm \frac{\mu}{r^3_{ij}} (3 \cos^2 \theta_{ij} - 1) \qquad \text{..... 2.35}$$

When the molecules at which the magnetic nuclei reside are in motion, one must consider an average value of θ_{ij}. If the motion is random and rapid, $\cos^2 \theta_{ij}$ can be averaged over all space to an average value $\langle \cos^2 \theta_{ij} \rangle = 1/3$. Thus, using the value of $\langle \cos^2 \theta_{ij} \rangle = 1/3$ in equation 2.34 results in a zero local field being produced. Thus, there is no effect on the applied field B_o. However, in the case of viscous liquids or solids, $\langle \cos^2 \theta_{ij} \rangle \neq 1/3$ and this results in a finite value of the local field B_L. The effect of this gives rise to a line broadening[22,23,24].

(c) Relaxation by paramagnetic substances. Paramagnetic nuclei which have one or more unpaired electrons can contribute to relaxation of nuclei in two ways;

(i) dipolar relaxation by the electron magnetic moment.

(ii) transfer of unpaired electron density to the relaxing nucleus itself.

For example, the presence of molecular oxygen or other paramagnetic impurities, which produce strong local magnetic fields will reduce the spin-lattice relaxation time T_1. This results in a large broadening of the absorption line, and in some cases causes the actual NMR signals to remain undetected.

(d) Relaxation due to quadrupolar effects; Nuclei with spin $I >> 1/2$ will have an electric quadrupole moment. This occurs because the distribution of electric charge density inside the nucleus is assymmetrical (ellipsoidal) rather than spherical. In liquids molecular tumbling causes environmental fluctuating electric fields to interact with the quadrupole moment which induce transitions among the nuclear quadrupole energy levels. The resulting nuclear relaxation is observed in the NMR spectra just as though relaxation had occurred by a magnetic mechanism. For

reasons given in (a) this gives rise to line broadening.

2.4 Frequency Distribution of Molecular Motion

The frequencies of the motion of molecules in a liquid sample cover a wide range; at any given time some of the molecules are moving quite slowly while others are moving very rapidly. On average, in a non-viscous liquid, a molecule remains in one state of motion for about 10^{-12} sec. After this time it suffers a collision which changes its states of motion. If this molecule persists in some state of motion for a time of 10^{-12} sec, then its motion will have frequency components from 0-10^{12} Hz. This is analogous to the situation involving a pulsed oscillator in which a sine wave of frequency fc is turned on for a short time τsec. Thus, one does not only obtain a frequency component at the frequency fc, but also components over the range $(fc \pm \tau^{-1})H_z$. Thus, as the molecules move about in space they carry the nuclear spins with them and the motion of the nuclear magnetic moments generate fluctuating magnetic fields. These microscopic fluctuating fields if denoted by $\bar{b}$ behave in many respects like the B_1 field generated by an NMR transmitter.

Consider what the effect of these microscopic $\bar{b}$ fields are when they interact with the magnetisation M. In general one can express $\bar{b}$ as follows:

$$\bar{b} = ib_x + jb_y + kb_z \qquad \text{..... 2.36}$$

From equation 2.36, a static b_z field in laboratory frame is static in and rotating frame, but fields b_x and b_y which are static (i.e., not a function of time) in the laboratory frame rotates in the rotating frame. Thus, in order to perturb the magnetisation M from equilibrium it is necessary to exert a torque on it over a period of time. If both M and either b_x or b_y are fixed in the rotating frame one can thus

perturb M. If one assumes the magnetisation M has now been perturbed to a new position in which M now has components along x', y', and z' axis, then the torque acting on M can be expressed by the vector cross product of $\bar{b}$ and M. Thus, in the rotating frame:

$$(\bar{b} \times M)_{rot} = (ib_{x'} + jb_{y'} + kb_{z'}) \times (iM_{x'} + jM_{y'} + kM_{z'})$$

$$= i\,(b_{y'} M_{z'} - b_{z'} M_{y'}) + j\,(b_{z'} M_{x'} - b_{x'} M_{z'}) + k\,(b_{x'} M_{y'} - b_{y'} M_{x'}) \quad \ldots\ldots 2.37$$

All other possible terms are zero because of the relation for the unit vector product $i \times i = j \times j = k \times k = 0$. From equation (2.37) it can be seen that in the rotating frame, $b_{x'}$ fields provide relaxation mechanisms for $M_{y'}$ and $M_{z'}$. Similarly for $b_{y'}$ fields, one has relaxation mechanisms for $M_{x'}$ and $M_{z'}$. Fluctuations in $b_{z'}$, however interact effectively only with $M_{x'}$ and $M_{y'}$. Thus fluctuations in $b_{x'}$ and $b_{y'}$ are effective in both T_1 and T_2 relaxation processes and those of $b_{z'}$ effect T_2 relaxation processes. In summary;

$b_{x'}$ effects T_1, T_2 relaxation processes.

$b_{y'}$ effects T_1, T_2 relaxation processes.

$b_{z'}$ effects T_2 relaxation processes.

An alternative way of expressing the effects of microscopic $\bar{b}$ fields is: T_1 relaxation processes arise only from fluctuating magnetic fields with components in the x' and y' directions. Conversely T_2 processes arise from components in all three directions. In addition, a static component of $\bar{b}$ in the z' direction (rotating frame) is equivalent to a static components of $\bar{b}$ in the z direction (laboratory frame). Thus in the laboratory frame, T_2 processes are sensitive to zero frequency local magnetic fields. A static component of $\bar{b}$ in the x' and y' direction corresponds to a non static

component of $\bar{b}$ in the x or y direction. This means that high frequency processes can effect T_1, for example, $2\omega_o$[25,26].

In order to discuss the relaxation times T_1 and T_2 and how they are related to molecular motion in a more quantitative manner, it is necessary to introduce some new parameters. For molecules in some state of motion whether they are translating or rotating let τ_c be definition be the "average" time between molecular field fluctuations or the average time taken for a molecule to progress through one radian and its value represents the Fourier components of molecular motions. If τ_c is such that the Fourier components of these motions at the resonance frequency (ω_o) are large, then the relaxation times are expected to be most efficient; consequently the relaxation times will be a minimum. If, however, τ_c is too long or too short, then the Fourier components at ω_o would be smaller and the corresponding relaxation times T_1 and T_2 would be longer[26]. These deductions were made by Bloembergen[26] et al, whose results are shown in Figure 2.4 for a sample of glycerine with the dependence of $T_1(^1H)$ on the molecular correlation time τ_c at two different resonance frequencies is shown. Also shown is the effect of the molecular correlation time on T_2.

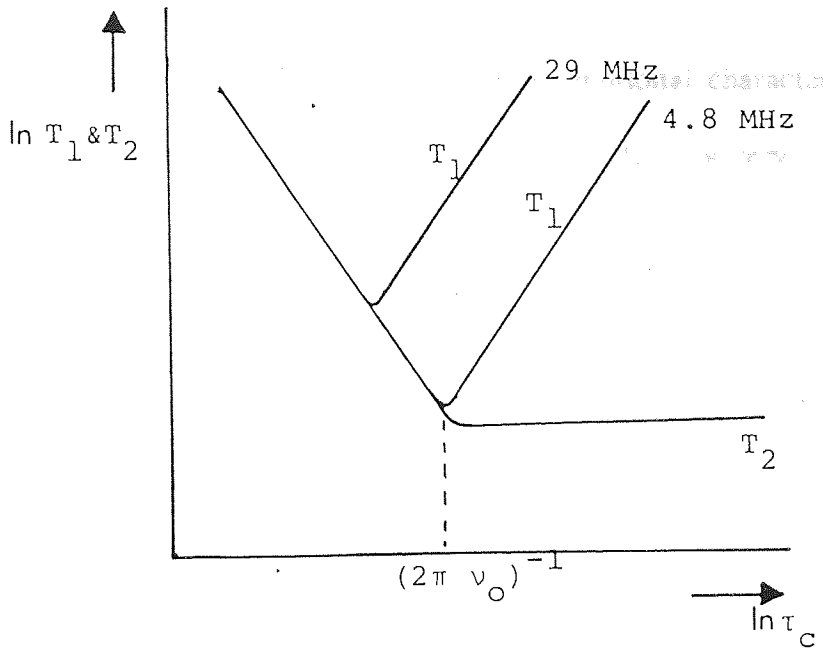

Figure 2.4 - A plot of T_1 and T_2 vs the correlation time τ_c

Referring to T_1 from Figure 2.4; in the high temperature region, to the left of the T_1 minima, T_1 is found to be frequency independent, and it decreases with decreasing temperature. This behaviour is typical of any molecule which is characterised by low τ_c values where $\omega_o\tau_c << 1$ as for small molecules in the liquid state. At both frequencies referred to, T_1 goes through a minimum and the value of T_1 at the minimum is proprotional to ω_o. This occurs whenever $\omega_o\tau_c \simeq 1$. In the low temperature region, to the right of the T_1 minimum, T_1 is frequency (ω_o) dependant and its values increase with decreasing temperature. This situation is found whenever $\omega_o\tau_c >> 1$.

When considering of molecular size and weight, small highly symmetric molecules often have short correlation times thus producing long T_1 values (ie. to the left of the minima). As the molecules increase in size they tumble less freely in solution leading to an increase in correlation time and a corresponding

decrease in T_1 (see Figure 2.4). In general, most motional characteristics of molecules may be represented by situations either to the left of, or very close to the T_1 minimum in Figure 2.4; this leads to a very useful general rule in these circumstances that T_1 values decrease with increasing molecular weight.

The functional form of T_2 dependent processes is much the same as that for T_1. However, since T_2 involves exchange of energy with nuclei rather than between the environment (lattice), the dependence on molecular motion is somewhat different from that of T_1. Processes giving rise to T_2 relaxation depend on high frequency (short τ_c) motion in the same way as T_1 processes. However, low frequency motion (such as chemical exchange) significantly shorten T_2. Hence, T_2 decreases monotonically with increasing τ_c and ultimately approaches a limiting value that is characteristic of a completely rigid solid lattice.

For a more quantitative analysis of T_1 and T_2 it is necessary to introduce two more parameters which are closely related to one another. These are, the correlation function k (τ), and its Fourier transform partner, the spectral density function J (ω). These two parameters are related by the expression:

$$J(\omega) = \int_{-\infty}^{\infty} K(\tau) \exp(i\,\omega\,\tau)\, d\tau \qquad \ldots\ldots 2.38$$

The spectral density function J (ω) as expressed by equation (2.38) provides a means of characterising the frequency distribution and the magnitude of the microscopic field b. The correlation function k (τ) (or sometimes called the

auto-correlation function) is related to a phase memory time or correlation time for the molecular motions. If k (τ) decays to zero in a short time, then the sample in question is characterised by a short correlation time τ_c; that is the molecular motions are very rapid.

If F (t) is a function which fluctuates randomly with molecular motion, that is, it describes the motion and the position of a rigid body and is a function of time, then the correlation function is defined as:

$$K(\tau) = < F(t)\, F^*(t+\tau) >_{AV} \quad \text{..... 2.39}$$

There <> represents the average over the ensemble of nuclei. The correlation function[20,27,28,29,30] can be represented by:

$$K(\tau) = K(o) \exp(-|\tau|/\tau_c) \quad \text{..... 2.40}$$

and the spectral density function is:

$$J(\omega) = < F(t)\, F^*(t) > 2\,\tau_c\,(1 + \omega^2\,\tau_c^2)^{-1} \quad \text{..... 2.41}$$

Figure 2.5 indicates how the information implicit in J(ω) varies with frequency.

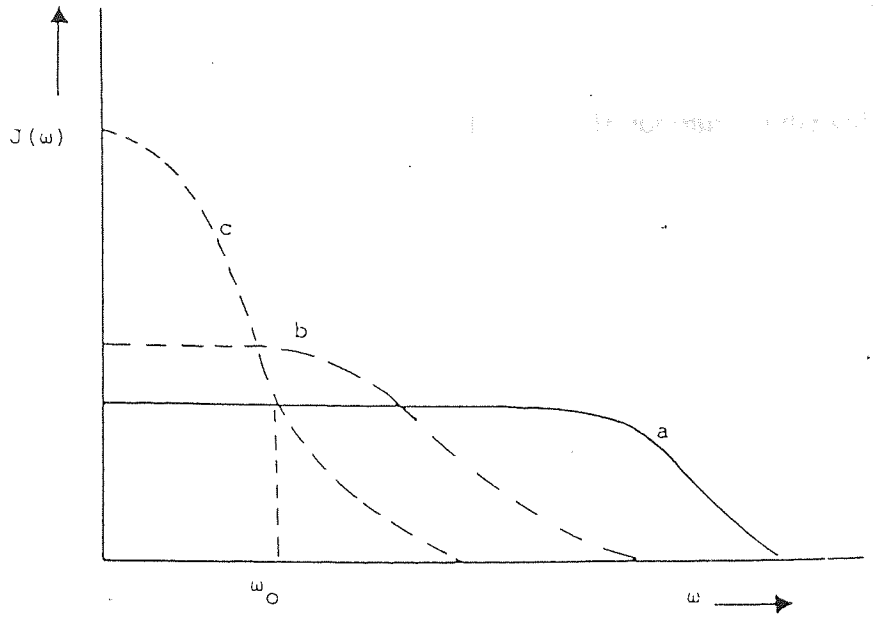

Figure 2.5: Plot of the spectral density function $J(\omega)$ vs the frequency ω case (a). For short correlation times $\omega_o \tau_c << 1$ case (b); and intermediate correlation times $(\omega.\tau_c \simeq 1)$; case (c) long correlation times $\omega.\tau_c >> 1$;

The area under the curves is constant and gives information on the amount of molecular energy available for molecular motion and changing τ_c changes only the way that the energy is distributed. If τ_c is short as in liquids (case a), the molecular motions are distributed over a very wide frequency range ($0 - \tau_c^{-1}$ Hz) and all the motional frequencies in this range have a small but equal probability of being found in any given molecule. If τ_c is long (case c), the very low motional frequencies have a very high probability of occurring, and all higher frequencies will be almost totally absent. In either case the Fourier components at the Larmor frequency will be small and T_1 will be long. In the intermediate region, (case b) where $\omega_o \tau_c \simeq 1$ the motional components at ω_o will be largest.

2.5 Spin-Lattice Interaction

The spin lattice relaxation time, T_1 depends not only on the value of the spectral density, $J(\omega)$ but also on the strength of the coupling between the spin system and the Lattice. A number of different physical interactions have been found to be important in coupling the nuclei to the lattice. These provide a link through which energy between these two systems can be exchanged. These interactions are:

(1) magnetic dipole-dipole interaction

(2) electrical quadrupole interaction

(3) chemical shift anisotropy

(4) scalar coupling interaction

(5) spin-rotation interaction

The above five processes will be discussed in the following chapters.

CHAPTER THREE

FACTORS AFFECTING SPIN-LATTICE RELAXATION TIMES AND THEIR REPRESENTATION BY VARIOUS MATHEMATICAL MODELS

NOMENCLATURE

W	Total spin transition probability
D	Diffusion coefficient
I	Moment of inertia
η	Viscosity
σ	Average distance between molecules
ρ	Density
μ	Reduced mass

3.0 Factors Influencing Spin-Lattice Relaxation Times

Spin-lattice relaxation times depends on a number of physical interactions which couple the nuclei to the lattice. This coupling provides a link through which energy between these two spin systems can be exchanged. The interactions mentioned briefly in Chapter Two are:

1 Magnetic dipole-dipole

2 Spin-rotation

3 Electric quadrupole

4 Chemical shift anisotropy

5 Scalar coupling

Nuclear magnetic dipole-dipole interactions are of principle interest here, for they are believed to play an important role in the acoustically induced changes that may be observed in spin-lattice relaxation times in the liquid phase. This chapter is devoted to the theory, experimental evidence for and models explaining these interactions. Chapter Four discusses the remaining four interactions.

3.1 Dipole-Dipole Relaxation

In general, any mechanism which gives rise to fluctuating magnetic fields at a nucleus is a possible relaxation mechanism. Simply, this can be expressed as:

$$T_1^{-1} = \sum_i R_i = E_c^2 f(\tau_c) \qquad \ldots\ldots 3.1$$

where E_c represents a specific constant for a particular dipolar relaxation interaction and τ_c is the correlation time.

At the molecular level, a given nucleus will be affected by the local dipolar field of its neighbours. Classically[8], the energy of interaction between two magnetic point dipoles μ_1 and μ_2 can be expressed in the form:

$$E = \frac{\vec{\mu}_1 \cdot \vec{\mu}_2}{r^3} - 3\,\frac{(\vec{\mu}_1 \cdot \vec{r})(\vec{\mu}_2 \cdot \vec{r})}{r^5} \qquad \text{..... 3.2}$$

where $\vec{r}$ is the radius vector between $\vec{\mu}_1$ and $\vec{\mu}_2$.

The appropriate quantum mechanical expression can be obtained by using $\mu = \gamma \hbar I$ and substituting into equation (3.2) to give:

$$H_{dd} = \gamma_1 \gamma_2 \hbar^2 \left[\frac{\hat{I}_1 \cdot \hat{I}_2}{r^3} - 3\,\frac{(\hat{I}_1 r) \cdot (\hat{I}_2 r)}{r^5} \right] \left[\frac{\mu_o}{4\pi} \right] \qquad \text{..... 3.3}$$

If I_1 and I_2 are treated as operators, then expanding the vector product from equation (3.3) and expressing the operators I_{1x} and I_{1y} in terms of raising and lowering operators I_1^+ and I_1^- respectively, and, transforming the cartesian co-ordinates to polar co-ordinates as shown in Figure 3.1, one obtains:

$$H_{dd} = \frac{\gamma_1 \gamma_2 \hbar^2 \mu_o}{r^3 4\pi} [A + B + C + D + E + F] \qquad \text{..... 3.4}$$

where

$$A = (1 - 3\cos^2\theta)\, I_{1z} I_{2z}$$

$$B = -1/4\,(1 - 3\cos^2\theta)\,[I_1^+ I_2^- + I_1^- I_2^+]$$

$$C = -3/2 \sin\theta \cos\theta\, e^{-i\emptyset}\,[I_{1z} I_2^+ + I_1^+ I_{2z}] \qquad \text{..... 3.5}$$

$$D = -3/2 \sin\theta \cos\theta\, e^{+i\emptyset}\,[I_{1z} I_2^- + I_1^- I_{2z}]$$

$$E = -3/4 \sin^2\theta\, e^{-2i\emptyset}\, I_1^+ I_2^+$$

$$F = -3/4 \sin^2\theta\, e^{+2i\emptyset}\, I_1^- I_2^-$$

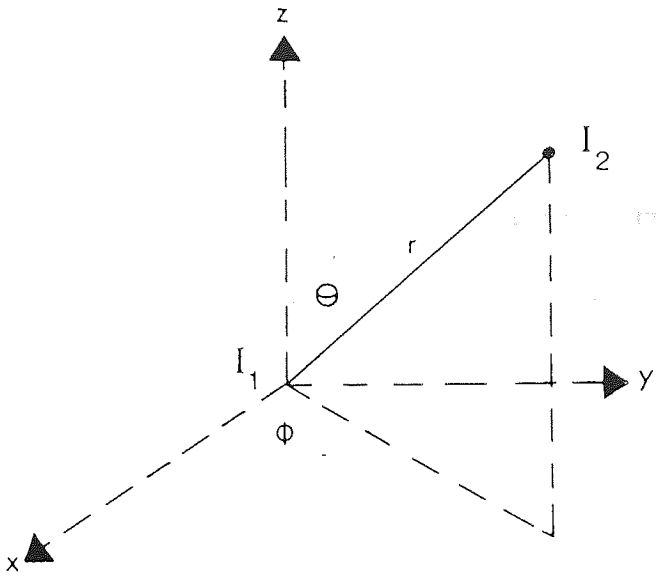

Figure 3.1: Definitions of geometry for dipole-dipole interaction of nuclei

The above formulations express the energy of magnetic interaction between one nucleus (specified here as nucleus 1) and a neighbouring magnetic moment (of which nucleus 2 is a typical example). The terms, A and B represent a flip of a pair of spins, C and D join states of energy which differ by $h\omega_0$ and represent a flip of one spin, and , E and F connect energy states that differ by $2h\omega_0$ and represents flip of both spins up or both spins down.

For each neighbour, the energy of interaction is found to involve three functions. These are, the distance r between the nucleus 1 and the neighbour 2, the angle θ between the direction axis of r and the magnetic field B_0, and the azimuth angle Ø, as measured from some fixed reference direction. The three functions are:

$$F_0 = (1 - 3\cos^2\theta)\, r^{-3}$$

$$F_1 = \sin\theta \cos\theta\, e^{-i\emptyset}.\, r^{-3} \qquad \ldots\ldots 3.6$$

$$F_2 = \sin^2 \theta \, e^{-2i\emptyset} \, . \, r^{-3}$$

where F_o is related to A and B, F_1 to C and D, and F_2 to E and F in the Hamiltonian H_{dd} of equation 3.5. In addition, F_o, F_1 and F_2 are related to transitions induced by spins. For example, the motion of the neighbour (say nucleus 2) at the resonance frequency ν_o produces at nucleus 1 an oscillating magnetic field of this frequency which is capable of inducing transitions. Furthermore, fluctuations of F_2 at frequency $2\nu_o$ can induce transitions; in the general case, when nucleus 1 and 2 are not identical, the frequency is not $2\nu_o$ but is equal to the sum of the precession frequencies of 1 and 2. Fluctuations of the remaining position functions F_o do not induce transitions.

By substituting equation (3.6) into equation (2.41) (Chapter 2) one obtains three spectral density functions J_o, J_1 and J_2, respectively, for all the neighbours. These spectral density functions are related to the transition probability of the spin system changing from a state α to a state ß by:

$$W_{\alpha\beta} = \frac{1}{\hbar^2} | < \alpha | H_{dd} | \beta > |^2 J (w_{\beta\alpha}) \qquad \ldots\ldots 3.7$$

The analysis of spin population (discussed in Chapter One), shows that the relaxation time T_1 is equal to twice the transition probability W. This is:

$$T_1^{-1} = 2W \qquad \ldots\ldots 3.8$$

W represents the total transition probability, which involves changes in energy $h\omega_o$

and $2h\omega_o$, as required by the parameters C and D and E and F respectively, in the dipolar Hamiltonian H_{dd}. Thus by using equation 3.7 and 3.8, for a nucleus with spin I = 1/2, the total transitional probability W, is found to be as expressed by equation 3.9:

$$W = 3/4\ \gamma^4 \hbar^2 I\ (I + 1)\ [(J_1\ (\nu_o) + 1/2\ J_2(2\ \nu_o)] \qquad \text{..... 3.9}$$

Thus, the relaxation time T_1, formulated from equations (3.8) and (3.9), can be expressed as:

$$T_1^{-1} = 3/2\ \gamma^4 \hbar^2\ I\ (I + 1)\ [J_1(\nu_o) + 1/2\ J_2\ (2\nu_o)] \qquad \text{..... 3.10}$$

This equation can also be written using the fact that J_1 and J_2 govern the intensity of the local field[24,26]. The result is:

$$T_1^{-1} = \gamma^2\ [b_x^2 + b_y^2]\ \frac{\tau_c}{1 + w_o\ \tau_c^2} \qquad \text{..... 3.11}$$

where b_x and b_y are the components of the local field in the rotating frame at the frequency $\omega_o = \gamma B_o$.

The effects of the fluctuating local fields on spin-lattice relaxation times have already been discussed in Chapter Two.

3.2 Intramolecular and Intermolecular Dipolar Contributions to Relaxation Proceses and their Representation by Mathematical Models

In general, for nuclei of spin one-half in liquids, spin-lattice relaxation times, T_1, are regarded to arise from dipolar-dipolar interactions. These interactions can be attributed to intra and inter molecular interactions.

The sum total of spin-lattice relaxation rates due to the above two interactions can be expressed as:

$$T_1^{-1} = T^{-1}_{1\ intra} + T^{-1}_{1\ inter} \qquad \ldots\ldots 3.12$$

where $T^{-1}_{1\ intra}$ and T^{-1}_{1inter} are the spin-lattice relaxation rates arising from the intra and intermolecular interactions, respectively.

In the case of intramolecular contributions, the molecule is considered approximately rigid, so the internuclear distance r is a constant and the "F" function from equations (3.6) and (3.7) has only to be averaged over orientations (θ, $\emptyset$).

Through the original calculations of spin-lattice relaxation rates for the intramolecular interactions, by Bloembergen et al[26] and later slightly corrected by Kubo and Tomita[31,32], the expression obtained for nuclei of non-identical spins can be written as:

$$T^{-1}_{1\ intra} = \frac{\hbar^2 \gamma_1^2 \gamma_2^2 \tau_c}{r^6} \qquad \ldots\ldots 3.13$$

where γ_1 and γ_2 represents the nuclear magnetogyric ratio for nucleus one and nucleus two, which have non-identical spins, τ_c represents an average rotational correlation time during local field fluctuations, and r is the distance between nucleus one and two.

For nuclei of similar spins Solomon obtained the expression which takes the form[33]:

$$T^{-1}_{1\ intra} = \frac{3}{2} \frac{\hbar^2 \gamma^4}{r^6} \tau_c \qquad \ldots\ldots 3.14$$

Solomon[33] gave a more complete derivation for non-identical nuclei.

In order to find the correlation time, τ_c, for the rotational motion of the molecule in a liquid, Bloembergen et al[26] extended the Stoke-Einstein-Debye theory[34,35,36] of dielectric dispersion. This is based on a model of a sphere turning in a viscous fluid and gives:

$$\tau_{(SED)} = \frac{4/3\ \pi\ a^3\ \eta}{kT} \qquad \ldots\ldots\ 3.15$$

where $\tau_{(SED)}$ is referred as the rotational correlation time obtained from the Stokes-Einstein-Debye model, η is the viscosity, and a is the radius of the sphere.

Intermolecular contributions to T_1 arising from the magnetic fields of nuclei in other molecules have also been related to the diffusion process. Bloembergen et al[26] applied their theory to water where there are two nuclei whose distances from the central molecule lie between r and r + dr. Using equation 3.14 for identical nuclei, and after averaging over all directions, τ_c is estimated as the time taken by a molecule to diffuse across a distance r. This is found to be $r^2/12D$, where D is the diffusion coefficient (noting that both molecules move). The total intermolecular contribution to T_1 is then obtained by multiplying by the number of nuclei per unit volume and also by 2 N (in water) and integrating over all the space outside a sphere of radius 2a, which corresponds to two spheres in contact. This gives:

$$T_1^{-1}\ \text{inter} = 2\,N \int_{2a}^{\infty} \frac{3}{2} \frac{\hbar^2 \gamma^4}{r^6}\ r^2/12D\ \times\ 4\,\pi\,r^2\,dr \qquad \ldots\ldots\ 3.16$$

$$= \frac{\pi\,N \hbar^2\,\gamma^4}{2Da}$$

The diffusion coefficient D has been related to the viscosity, by the Stokes-Einstein relation[35-38]:

$$D = kT/6\pi\eta a \qquad \text{..... 3.17}$$

Thus, combining equation 3.17 and 3.16 gives:

$$T^{-1}_{1\ inter} = \frac{3\pi^2\gamma^4\hbar^2}{KT}\eta N \qquad \text{..... 3.18}$$

Bloembergen[26] et al applied the above principles to water and calculated the spin-lattice relaxation times to be 5 seconds, which is thought to be in good agreement with the experimental value of $T_1 = 3.7 \pm 0.5$ seconds. The shorter experimental spin-lattice relaxation times was also attributed as possibly being under the influence of dissolved oxygen.

Intra and inter molecular dipolar contribution to T_1 have been studied by several other workers[39-50]. Discussed here, are the basic approaches for the intra and inter molecular dipolar contribution to T_1 that were extended for the Bloembergen et al theory by Gutowsky and Woessner [38,39]. They showed that the relaxation times for the ith nucleus could, in general, be expressed as:

$$T^{-1}_{1\ intra \equiv rot} = \hbar^2\gamma_i^2\left(3/2\,\gamma_i^2 \sum_{j}^{i} r_{ij}^{-6} + 4\,\gamma_f^2\,(I_f+1)\,I_f/3 \sum_{f}^{*}_{i} r_{if}^{-6}\right)\tau_{rot} \qquad \text{..... 3.19}$$

where the symbol f refers to non identical nuclei, the summation $\sum_{j}^{i}$ represents the sum over nuclei of the same species and Σ^* over all others. r_{ij} and r_{if} represents the mean distances for two nuclei in contract at the closest approach of nuclei in molecules of

similar and dissimilar spins, respectively.

The intramolecular dipolar contribution to the relaxation time T_1 is equivalent to saying that its contribution comes from the rotational motion of the molecules. For a spin 1/2, that is, $I_f = 1/2$, equation 3.19 can be expressed as:

$$T^{-1}{}_{1\ \text{intra} \equiv \text{rot}} = \hbar^2 \gamma_i^2 \left(3/2\ \gamma_i^2 \sum_{j}^{i} r_{ij}^{-6} + \gamma_f^2 \sum_{f}^{*} r_{if}^{-6}\right)\ \tau_{rot} \qquad \ldots\ldots\ 3.20$$

Similarly, the expression for the inter-molecular dipolar contribution to T_1 can be expressed in the form:

$$T_1^{-1}{}_{\text{inter = trans}} = \pi\hbar^2 \gamma_i^2\, N/a^2\ \left[6\ \gamma_i^2 \sum_{j}^{i} r_{ij}^{-1} + 16\ \gamma_f^2\ (I_f + 1)\ I_f/3\ \sum_{f}^{*} r_{if}^{-1}\right] \tau_{trans} \qquad \ldots\ldots\ 3.21$$

Thus, for nuclei of spin 1/2, one obtains the expression:

$$T^{-1}{}_{1\ \text{inter} \equiv \text{trans}} = 2\ \pi\hbar^2 \gamma_i^2\ \frac{N}{a^2}\ \left[3\ \gamma_i^2 \sum_{j}^{i} r_{ij}^{-1} + 2\ \gamma_f^2 \sum_{f}^{*} r_{if}^{-1}\right] \tau_{trans} \qquad \ldots\ldots\ 3.22$$

The translational correlation time can be expressed as

$$\tau_{trans} = a^2/12D \qquad \ldots\ldots\ 3.23$$

Using the equations expressing the rotational (τ_r) and translation (τ_t) correlation times (equations (3.15) and (3.17) and substituting them in equations (3.20) and (3.22) respectively, the following expressions for intra and inter molecular dipolar contribution to T_1 are obtained.

$$T^{-1}_{1\ intra} = \frac{2\pi\hbar\gamma_i^2\eta a^3}{3kT} \cdot \left[3\gamma_i^2 \sum_{j}^{i} r_{ij}^{-6} + 2\gamma_f^2 \sum_{f}^{*} r_{if}^{-6}\right] \quad .....3.24$$

$$T^{-1}_{1\ inter} = \frac{\pi^2\hbar^2\gamma_i^2\eta Na}{kT} \left[3\gamma_i^2 \sum_{j}^{i} r_{ij}^{-1} + 2\gamma_f^2 \sum_{f}^{*} r_{if}^{-1}\right] \quad ..... 3.25$$

Various models have been proposed for the correlation times, τ_c[51-60]. The rotational correlation times τ_r have been shown to be a factor of five or six times shorter than that predicted by the classical Stokes-Einstein-Debye's model (SED). In other words, the rate of rotation is faster than predicted, indicating that the frictional restraint must be lower than that represented by the Stokes coefficient. This discrepancy is attributed to the effective viscosity at the surface of a molecule which is not well represented by the bulk viscosity η. For example, Gierer and Wirtz[51] introduced the idea of a microviscosity factor as a dimensionless index that is applied to the viscosity in the SED model. The Gierer and Wirtz model is governed by the radii of the solute and solvent molecules. They introduced a microviscosity correction factor f whose ratio dependence is given by:

$$f = [6\, r_s/r + (1 + r_s/r)^{-3}]^{-1} \quad ..... 3.26$$

where r_s and r is the radius of the solute and solvent molecules. The rotational correlation times is now expressed as:

$$\tau_{GW} = f\,\frac{4\pi r^3\eta}{3kT} \quad ..... 3.27$$

The Gierer and Wirtz model has been extended for molecules which are non-spherical and are regarded as prolate (cigar shaped a=b<c) or oblate shapes (pancake shaped a<b=c) which takes into account of rotation off the symmetry axis[52-55]. For example, the Youngren and Acrivos model[55], for ellipsoidal molecules in which all the three axis have different lengths, the rotational correlation times τ_{YA} is expressed as:

$$\tau_{YA} = \frac{\lambda_i V_{ellipsoid} \eta}{6kT} \qquad \ldots\ldots 3.28$$

where λ_i is a function which depends on the solvent viscosity, angular velocity and the torque experienced by the rotating molecule in the "i" direction for rotation about the i axis. $V_{ellipsoid}$ is the volume of the ellipsoid in question. Several other workers[56-59] have demonstrated the superiority of this model over the SED model.

One model of particular interest is that presented by Hill[60]. She took a different approach towards the evaluation of the correlation time by following the model of a liquid corresponding to Andrade's[61] theory of viscosity which considers molecules of one layer vibrating and coming into contact with those of an adjacent layer. During this contact, the molecules will, in general, enter into a temporary union which is long enough for these molecules to acquire a common velocity of transition. However, owing to the fact that the period of vibration is longer than the period of temporary unity there is no possibility of association.

Hill's theory for the so-called "mutual viscosity" between the solute and solvent molecules predicts the dielectric relaxation times to be very similar to those experimentally observed. Referrring to the Debye's theory of dielectric dispersion in polar liquids for which the motion of the molecule is assumed to be

similar to that of a sphere of radius a imbedded in a viscous fluid, the dielectric correlation time, τ, was predicted to be:

$$\tau = \frac{4 \pi a^3 \eta}{kT} \qquad \text{..... 3.29}$$

(NB. Compare equation 3.15 and 3.29)

Hill[60] criticised the validity of using the viscosity, η, of the solvent as the only factor for calculating the dielectric correlation time. Instead, she proposed an alternative view through the use of a mutual viscosity between the solvent and the solute. The mutual viscosity, η_{AB}, for a binary mixture is deduced from the solution viscosity and is expressed in the form of:

$$\eta_m = (f_A^2 \eta_A \sigma_A/\sigma_M) + (f_B^2 \eta_B \sigma_B/\sigma_M) + (2 f_A f_B \eta_{AB} \sigma_{AB}/\sigma_M) \qquad \text{..... 3.30}$$

Here f_A and f_B are the mole fractions of A and B, respectively, σ_A and σ_B are the average distances between molecules in the liquids A and B, σ_{AB} is the average distance between A and B type molecules, and σ_M is the average distance between molecules in the mixture.

Using a model for the mutual viscosity, Hill deduced that the rotational correlation time for dielectric relaxation of molecules of type B in solution with molecules of type A is:

$$\tau_r = 1/2\, kT \; \{6 f_A \eta_{AB} \sigma_{AB} K_A^2 + 3 f_B (3 - \sqrt{2}) \eta_B \sigma_B K_B^2\} \qquad \text{..... 3.31}$$

where

$$K_A^2 = [(I_{AB} I_B)/(I_{AB} + I_B)] \; [(M_A + M_B)/(M_A M_B)] \qquad \text{..... 3.32}$$

and I_A and I_B are moments of inertia of A and B about their centre of mass, I_{AB} is the moment of inertia of A about the centre of B during collision, and K_B is the radius of gyration of a B type molecule.

The expression for the rotational correlation time, for dilute solutions is:

$$\tau_{rHill} = K_A^2 \sigma_{AB} \eta_{AB}/kT \qquad \text{..... 3.33}$$

where σ_{AB} and η_{AB} are obtained from equation (3.30), whilst σ_A and σ_B are calculated using equation (3.34)[62]. Equation (3.34) represents the empirical equation for calculating the volume occupied by a mole of substance using its mass and density. In addition, the average distance between molecules σ, can be calculated, if the molecule is assumed to be spherical.

$$V_A = N\sigma_A^3 = M_A/\rho_A \qquad \text{..... 3.34}$$

From equation (3.34), σ_A is the average distance between molecules A, M_A is the molar mass of molecule A, ρ_A is the density of molecule A, and N is Avagadro's number.

Similarly, the average distance between molecules in the mixture, σ_M, can be expressed as[63,64]:

$$(N_A + N_B)\,\sigma_M^3 = \left[\frac{M_A}{\rho_A} + \frac{M_B}{\rho_B}\right] \qquad \text{..... 3.35}$$

Substitution of equation (3.33) into equation (3.20) for nuclei of spin 1/2 gives:

$$T^{-1}_{1\ intra \equiv rot} = \hbar^2 \gamma_i^2 \left[3/2\ \gamma_i^2 \sum_j^i r_{ij}^{-6} + \gamma_f^2 \sum_f^* r_{if}^{-6}\right] K_A^2 \sigma_{AB} \eta_{AB}/kT \qquad \text{.....3.36}$$

Similarly, if one now looks at the intermolecular dipole-dipole contribution to T_1 through the Gutowsky and Woeossner equation [39] (equation 3.25), one can see that the translational correlation time (τ_{trans}) needs to be modified to obtain a better theoretical comparison with that observed. Hill[60] modified the Gutowsky and Woessner equation to account for the "mutual viscosity" and the average distance between molecules in a mixture.

The diffusion coefficient for an A molecule diffusing through a solution of A and B molecules is:

$$D = kT/6\,(\eta_{AB}\,\sigma_{AB}\,f_A + \eta_A\,\sigma_A\,f_A) \qquad \ldots\ldots 3.37$$

where f_A is the mole fraction of the A molecules in a solution of A and B molecules.

Using the expression for translational correlation time, equations (3.17) and (3.23), and substituting the "Hill's" diffusion co-efficient, equation (3.37), gives the expression:

$$\tau_{trans} = \frac{a^2\,(\eta_{AB}\,\sigma_{AB}\,f_A + \eta_A\,\sigma_A\,f_A)}{2kT} \qquad \ldots\ldots 3.38$$

Substitution of equation (3.38) into equation (3.22), one obtains the expression:

$$T^{-1}{}_{1\ inter \equiv trans} = \frac{\pi\hbar^2\,\gamma_i^2\,N}{kT}\,[3\,\gamma_i^2 \sum_j r_{ij}^{-1} + 2\,\gamma_f^2 \sum_f r_{if}^{-1}]\ x$$

$$(\eta_{AB}\,\sigma_{AB}\,f_B + \eta_A\,\sigma_A\,f_A) \qquad \ldots\ldots 3.39$$

Mitchell and Eisner[40,41] have calculated the correlation times of several molecules in carbon tetrachloride (CCl_4) and carbon disulphide (CS_2), using various different theories[65,66]. They found Hill's[60,62] theory to be the most suitable and in very good agreement to those obtained experimentally.

It is important to realize the significance of the diffusion constants as given by the Stokes-Einstein-Debye equation and the Hill's equation (equations 3.17 and 3.37 respectively), i.e.,

$$D = KT/6 \pi \eta a \quad \text{..... 3.17}$$

$$D = KT/6 (\eta_{AB} \sigma_{AB} f_A + \eta_A \sigma_A f_A) \quad \text{..... 3.37}$$

It can be seen from the two equations that the Hill's diffusion constant is dependant on the mole fraction of the solute and solvent. In addition, the diffusion constant values obtained[67] using the Hill's equation are about twice the values obtained using the Stokes-Einstein-Debye's equation. This may have a significant importance in the prediction and understanding of the acoustically induced changes observed in the spin-lattice relaxation times, T_1, in the liquid phase.

In the case of τ_{rot}, the expression for the rotational correlation time as expressed by Hill's equation is:

$$\tau_{rHILL} = K_A^2 \sigma_{AB} \eta_{AB}/KT \quad \text{..... 3.33}$$

where

$$K_A^2 = [(I_{AB} I_B)/(I_{AB} + I_B)] [(M_A + M_B)/(M_A M_B)] \quad \text{..... 3.32}$$

Comparison of equations (3.29), and the equation (3.33), suggests the rotational correlation time, τ_r, to be dependent on the moment of inertia, viscosity and the mass of the solute molecule. This again may have a significant importance in understanding of the acoustically induced changes observed in spin-lattice relaxation times, T_1, in liquid mixtures. However, it should be pointed out that the Hill's approach has limited success because of a residual error in the

prediction that τ_1 increases with the mass of the solute. In order to overcome this problem it may be suitable to use an average for τ_r in such a manner that a weighting of the mass distribution in the molecule is achieved. In addition, it may be possible to introduce some correction to account for electric forces which constrain the molecule to rotate about a certain axis. Making an assumption that intermolecular forces could influence anisotropic motion and that this is related to the molecular polarizability, the latter has been used to weigh the effective moment of inertia as expressed by equation 3.40.

$$I = \frac{1}{3\alpha} \Sigma I_i \alpha_i \qquad \text{..... 3.40}$$

This value of I was introduced in K^2_{AB} to get the effective correlation time. The influence of this type of correction is very small for benzene and cyclohexane. However, for chlorobenzene which has a dipole moment, it gives a correction of approximately 10%. Thus, it seems to indicate a real contribution to the description of molecular motion. The term K^2_{AB} was averaged with respect to the three moments of inertia, by using the expression:

$$K^2_{AB} = \frac{1}{3\mu} \sum_{i=1}^{3} \frac{I_{AB} I_{Bi}}{I_{AB}+I_{Bi}} \qquad \text{..... 3.41}$$

Comparison of this value with K^2_{AB}, gives a difference of less than 3%.

A critical review at Hill's theory on mutual viscosity can be summarised as follows:

(a) The theory accounts for the transfer of the solutes angular momentum to the intrinsic angular momentum of the surrounding solvent molecules. However, it fails to account for the transfer of angular momentum of the solute molecules to the flow angular momentum of

the surrounding fluid, and the associated long-range hydrodynamic effect.

(b) The theory is based on the Andrade's theory of viscosity[44] which is for molecules in a liquid vibrating at a high frequency ν, at some equilibrium position and varies slowly in time. In this case, the transfer of linear momentum arises from collisions between neighbouring molecules, which are momentarily closely associated so that no linear motions are possible. Hill extended Andrade's theory to include mixtures, and the effect of the transfer of angular momentum. The theories are derived for spherical molecules, and for rigid axially symmetric molecules. However, they would not be expected to work well for mixtures of molecules deviating from these type of structures. For example, flexible long-chain molecules.

(c) Further investigation is necessary for a more suitable model. A model which would account for the rotational molecular motion involving both microscopic (collisional) and collective (hydrodynamic) effects, in which the solutes linear and angular momentum are transferred to a layer of nearest solvent molecules by collision between the molecules.

In presenting the Gutowsky and Woessener equations and the Hills theory with all the discrepancies, the two theories give a firm foundation and a classical description on the factors which influence the intra and inter dipolar relaxation contribution to spin-lattice relaxation times T_1.

By performing experiments based on the idea that sound can effect the rotational and translational motion of molecules, one can already see the possible factors which may be influenced.

The absorption of sound in liquids arise due to the following

relaxation processes:

(a) translational

(b) rotational

(c) vibrational

(d) electronic

(e) structural

(f) conformational isomerism

(g) association equilibria

(h) chemical equilibria

(i) impurity effects

These factors which govern these relaxation mechanisms will be discussed in Chapter Five. It is then hoped, that the factors discussed in this chapter and Chapter Five can be combined, in a manner, which will lead to further information and understanding of the effects of sound and its influence on spin-lattice relaxation rates.

CHAPTER FOUR

OTHER RELAXATION PROCESSES

NOMENCLATURE

V	Electric Potential
x_α	Component of the radius vector from the centre of a nucleus
η	Asymmetry parameter
q	Field gradient
Q	Quadrupole moment
J	Scalar spin-spin coupling constant
$C_\perp$, $C_\parallel$	Diagonal components of the spin-rotation interaction tensor
τ_{SR}	Angular momentum correlation time
a_N	Hyperfine electron-nuclear spin coupling constant
τ_e	Correlation time experienced by nuclear spins due to the electron
τ_h	Exchange lifetime of the molecular complex between an ion and the molecule being relaxed
g	Electronic factor

4.0 Introduction

This chapter discusses and examines the importance of relaxation mechanisms which, in addition to the magnetic dipolar-dipolar relaxation mechanism already discussed, affect spin-lattice and spin-spin relaxation times. The relevant relaxation mechanisms are:

(i) Quadrupolar

(ii) Chemical shift anisotropy

(iii) Scalar

(iv) Spin-rotation

(v) Paramagnetic

These will be discussed briefly in this chapter.

4.1 Quadrupolar Relaxation

If a nucleus with a spin quantum number greater than one-half is considered, there is a relaxation process which occurs via the interaction with fluctuating electric fields as opposed to a magnetic field. Such a nucleus has an electric quadrupole moment in addition to a nuclear magnetic moment. This electric quadrupole moment arises from an asymmetry of the distribution in the electrical charge in the nucleus and does not depend on the net charge, unlike a spin one-half nucleus which possesses a spherical charge distribution. Quadrupolar nuclei do not have an electric dipolar moment, hence their energy is independent of orientation in a uniform electric field. However, in the presence of an electric field gradient, they precess about the net electric field, and in doing so provide a relaxation mechanism.

To develop a quantitative theory, one has to begin with a description of the classical charge density of a nucleus, ρ, and its interaction with a potential V due to external sources. The interaction energy E is represented as:

$$E = \int \rho(r)\, V(r)\, d\tau \qquad \ldots\ldots 4.1$$

Because the nuclear dimensions are much less than the average distance between the charges giving rise to V, the potential V(r) can be expanded in a Taylor's series about the mass centre of the nucleus. The expression can be written as:

$$V(r) = V_{(o)} + \sum_{\alpha} x_\alpha \left[\frac{\partial V}{\partial x_\alpha}\right]_{r=0} + \frac{1}{2} \sum x_\alpha x_\beta \left[\frac{\partial^2 V}{\partial x_\alpha x_\beta}\right]_{r=0} \quad \ldots\ldots 4.2$$

where x_α with $\alpha = 1,2,3$ stands for x, y and z respectively, and represents the components of the radius vector of the potential V in the three co-ordinate axis and has its origin at the centre of the nucleus. Defining

$$V_\alpha = \left[\frac{\partial V}{\partial x_\alpha}\right]_{r=0} \quad \ldots\ldots 4.3$$

and

$$V_{\alpha\beta} = \left[\frac{\partial^2 V}{\partial x_\alpha x_\beta}\right]_{r=0} \quad \ldots\ldots 4.4$$

where V_α and $V_{\alpha\beta}$ represents the electric field and the components of its gradient, respectively.

Combining equations (4.1), (4.2), (4.3) and (4.4) the interaction energy can be expressed as:

$$E = V(o) \int \rho \, d\tau + \Sigma_\alpha V_\alpha \int x_\alpha \rho \, d\tau + \frac{1}{2} \Sigma_{\alpha,\beta} V_{\alpha,\beta} \int x_\alpha x_\beta \, d\tau \quad \ldots\ldots 4.5$$

The first term gives the interaction of the nucleus taken as a point charge with the non-linear fields due to external sources; because it has no orientation dependence it has no effect on nuclear resonance. The second term involves the nuclear electric dipole moment. This term vanishes, since the centre of mass and centre of charge coincide. The third term involves the interaction of the so-called nuclear electric field at the nucleus and it possesses an orientation dependence. This third term is referred to as the electrical quadrupole. The next higher order term thought to be non-zero is the interaction involving the nuclear hexadecapole moment. The magnitude of these effects however, drops off rapidly as one proceeds to higher order so that the analysis here will be confined to a consideration of the quadrupole term.

Solving the third term in equation (4.5), the interaction energy between the nuclear quadrupole moments and the fluctuating electric field gradient can be represented as[68]:

$$E = \frac{1}{6} \Sigma_{\alpha,\beta} V_{\alpha,\beta} Q_{\alpha,\beta} \qquad \ldots\ldots 4.6$$

where $Q_{\alpha,\beta}$ is the nuclear electric quadrupole moment.

$$Q_{\alpha,\beta} = \int [3 x_\alpha x_\beta - \delta_{\alpha,\beta} r^2] \rho \, d\tau \qquad \ldots\ldots 4.7$$

where $x_\alpha x_\beta$ represents the co-ordinate of the nuclear electric quadrupole along the symmetry axis of the nucleus, $\delta_{\alpha,\beta} r^2$ represents the distance from the centre of the nucleus and ρ is the electric charge density.

An alternative way of expressing equation (4.1) is by using the Hamiltonian quadrupole operators. This is done using I_x, I_y and I_z as operators for the total angular momentum of the nucleus. Thus:

$$[I_x, 2.y_k] = iz_k, \text{ etc} \qquad \ldots\ldots 4.8$$

With the appropriate mathematical manipulation[68] equation (4.6), the effective quadrupole interaction expressed by the Hamiltonian can be represented as:

$$HQ = \frac{eQ}{4I\,(2I-1)}\,[V_{zz}\,(3I_z^2 - I^2) + (V_{xx} - V_{yy})\,(I_x^2 - I_y^2)] \qquad \ldots\ldots 4.9$$

From equation 4.9 two parameters V_{zz} and $V_{xx} - V_{yy}$ are redefined. This is done by defining two symbols, η and q, called the asymmetry parameter and the field gradient, respectively, by the equations:

$$eq = V_{zz} \qquad \ldots\ldots 4.10$$

and

$$\eta = \frac{V_{xx} - V_{yy}}{V_{zz}} \qquad \ldots\ldots 4.11$$

Abragam[28] considered the interaction between the nuclear quadrupole moment, and the local electric field gradient as:

$$HQ = I.Q\,(t)\,.\,I\,. \qquad \ldots\ldots 4.12$$

where Q(t) represents a certain tensor, with elements proportional to the quadrupole moments Q, and the field gradients V_{zz}, V_{yy}, V_{xx} etc. As the molecule reorients, components of the quadrupole coupling tensor becomes random functions of time and provides a relaxation mechanism for the quadrupolar nuclei. The quadrupolar contribution of this to spin-lattice relaxation time T_1 can be expressed as:

$$T_1^{-1} = \frac{3}{40}\left[\frac{2I+3}{I^2\,(2I-1)}\right]\left[1 + \frac{\eta^2}{3}\right]\left[\frac{e^2Qq}{\hbar}\right]^2 \tau_c \qquad \ldots\ldots 4.13$$

where the term (e^2Qq/h) is defined as the quadrupole coupling constant.

For nuclei with I > 1/2, the quadrupolar interaction is usually the dominant relaxation mechanism. However, this interaction may be weak if the molecule is symmetric as this would have no net electric field gradients[69,70].

Examples of the effectiveness of this relaxation mechanisms can be shown in typical examples of boron and nitrogen containing compounds. For ^{11}B in symmetric molecules, such as $^{11}BH_4^-$, where the quadrupolar coupling constant is zero, the relaxation time for the boride nucleus is 10 seconds, whereas in three co-ordinate Boron compounds, where the quadrupolar coupling constant is of the order of 3 MHz, the relaxation time are in the order of 10 msec. Similarly, in the highly symmetrical $^{14}NH_4^+$ ion, where the quadrupolar coupling constant is zero, the spin-lattice relaxation time, T_1, is of the order of 50 s with the relaxation being ^{14}N-H dipolar, whereas in acetronitrile, $CH_3C^{14}N$ it is 4 MHz with T_1 being 22 ms.

4.2 Chemical Shift Anisotropy

As previously discussed in Chapters One and Two, when an atom or a molecule is placed in a static magnetic field, the electrons produce a small auxiliary field. The direction and the magnitude of this field depends in a complex way on the electronic structure of the atom or molecule. The ability of the electrons to shield the nucleus depends in part on the direction of the magnetic field with respect to the electronic orbits. Thus, a nucleus experiences not the magnetic field, B_o, generated by the laboratory magnet, but rather a field, B_{loc}, which is expressed as:

$$B_{loc} = B_o - \sigma B_o = B_o (1 - \sigma) \qquad \ldots\ldots 4.14$$

where σ is called the shielding factor. This interaction can be represented by the

Hamiltonian, H_{cs}, as:

$$H_{cs} = -\gamma\hbar B.\sigma.I. \qquad \text{..... 4.15}$$

From equation 4.15, σ is referred to as the chemical shift tensor; thus, the magnitude of the shielding at a nucleus is dependent upon the orientation of the molecule in the magnetic field. In the liquid state, the rapid molecular motions of the molecules, averages the σ value[72] according to:

$$\sigma = \frac{1}{3}(\sigma_{xx} + \sigma_{yy} + \sigma_{zz}) \qquad \text{..... 4.16}$$

Although the nucleus on average sees an isotropic screening value represented by σ, on a shorter time scale, it sees fluctuations in the local magnetic field. Thus, if σ_{xx}, σ_{yy} and σ_{zz} are not equal, that is, if the chemical shift tensor is anisotropic, it produces a fluctuating magnetic field which can act as a relaxation mechanism.

McConnel and Holim[73] have shown that in liquids the relaxation rate can be expressed as:

$$T_1^{-1} = \frac{2}{15}\gamma^2 \beta_o^2 (\Delta\sigma)^2 \tau_c \qquad \text{..... 4.17}$$

From equation 4.17, $\Delta\sigma$ is equal to $(\sigma_{||} - \sigma_{\perp})$. $\sigma_{||}$ and $\sigma_{\perp}$ refers to the components of the shielding tensor parallel and perpendicular to the axis of symmetry in the molecule. In the case of the absence of axial symmetry the equation becomes more complicated[8]. The equation, in addition, shows that the relaxation

rate is dependent on the square of the field B_0. Thus this interaction is relatively unimportant at low fields but must be seriously considered at high fields such as those encountered in superconducting magnets. For protons, $\Delta\sigma = \sigma_{||} - \sigma_{\perp}$, is typically less than 10ppm for covalent hydrogens[74] and this relaxation mechanism is negligible for protons even when the high fields of superconducting magnets are used.

4.3 Scalar Relaxation

If a nucleus I is spin-spin coupled with a second nucleus S, it is possible for S to provide a fluctuating magnetic field and hence a relaxation mechanism at the first nucleus via scalar interactions involving the bonding electrons of the atom S. Since this mechanism relies on scalar spin coupling, it is called scalar relaxation. Fluctuations in the magnetic field can arise from two sources; firstly from any time dependence of the spin coupling constant that may occur, for example in systems undergoing chemical exchange, and secondly, from the time dependence of the excited state of spin S. To be efficient for spin-lattice relaxations, these fluctuations must be rapid (in the region of the Larmor frequency), and hence the mechanism is only efficient when exchange is fast or if the life time of the excited state of the nucleus S is short, such that, it has a broad line. In practice, this usually involves a quadrupolar nucleus.

The Hamiltonian interaction of the spin-spin coupling between the spin I and S, where I = 1/2 and S ≥ 1/2, can be expressed as:

$$H_S = \hbar\, I.A.S. \qquad \ldots\ldots 4.18$$

where $A = 2\pi J$ 4.19

and J is referred to as the scalar spin-spin coupling constant.

If one considers the relaxation of nucleus I, this can occur if the effective field, B_{loc}, fluctuates in time. This occurs when:

(i) A is time dependent, or

(ii) S is time dependent

Situation (i) is referred as scalar relaxation of the first kind. This arises, for example, in rapid chemical exchange systems, in which the rate of exchange is much greater than the rate of that induced coupling A (= $2\pi J$) and the spin-lattice relaxation times of both I and S. Thus, if the time the nuclei are uncoupled is short compared with the time they are coupled, then the muiltiplet structure disappears and only a single line is observed[75,76].

Situation (ii) is referred to as scalar relaxation of the second kind. This arises, for example, when a nuclei I is coupled to a quadrupolar nuclei S undergoing rapid relaxation. If the nucleus S, has a relaxation time, which is quite short compared with the relaxation time provided via the H_S interaction for nuclei I, that is T_{1S} (for nuclei S) is short compared with 1/A, then the local field produced at nuclei I is regarded to be fluctuating at a frequency comparable to the Larmor frequency of nuclei S. This will then induce relaxation of nuclei I.

In scalar relaxation of the first kind, the coupling A (= $2\pi J$) carries the time dependence, while for scalar relaxation of the second kind the time dependence originates with the coupled spin S. The formula for the relaxation time is the same in both cases and is given by[8]:

$$T_{1sc}^{-1} = \frac{2A^2}{3} S(S+1) \frac{\tau_{SC}}{1+(\omega_I-\omega_S)^2 \tau_{SC}} \qquad \ldots\ldots 4.20$$

where τ_{SC} is the correlation time for the nucleus S and ω_I and ω_S are the Larmor

frequencies of the two nuclei.

Scalar relaxation plays a significant role in the broadening of ^{1}H lines. For example, protons bound to a quadrupolar nucleus S, such as ^{14}N and ^{11}B, where the spin-spin relaxation times have similar values to the inverse of the spin coupling constants. However, such effects are not observed with nuclei such as chlorine and bromine because these nuclei have, as a rule, a much shorter relaxation time compared with the proton coupling constant, for scalar relaxation to be efficient. The contribution of the scalar relaxation mechanism can be recognised from a frequency dependence of T_1, that is when the coupling nuclei precesses with similar Larmor frequencies. For example a ^{13}C nuclei coupled to the quadrupolar ^{79}Br. As a consequence, ^{13}C nuclei bound to Br, relax relatively fast[77].

4.4 Spin-Rotation Relaxation

Relaxation can also arise from the local fields produced by spin-rotation interactions. A molecular system possessing angular velocity constitutes a rotating charge system and can thus give rise to a magnetic field at a resonant nucleus. Fluctuations in this field result from modulation of both the magnitude and direction of the angular momentum vector associated with the rotating molecule.

If one considers a particular electron and a given nucleus, then as the molecule rotates, the electron rotates about the nucleus at a radius, say R, then the rotational frequency ν_{rot} can be:

$$\nu_{rot} = \hbar J/2\pi I \qquad \text{..... 4.21}$$

where the molecule is in the Jth rotational state and I is the moment of inertia of the molecule. The current generated by the electron is then expressed as:

$$i = (e/c)\,\nu_{rot} \qquad \text{..... 4.22}$$

The magnetic moment associated with this circulating current is:

$$\mu_j = i\,(\pi R^2) = (eh/2\pi\, Mc)\, J \sim \mu_N J \qquad \text{..... 4.23}$$

where I is the moment of inertia, equal to MR^2; where M is the nuclear mass and $\mu_N$is the nuclear magneton.

The magnetic moment generated by the motion of the electron produces a local magnetic field at the resonant nucleus of the order of $\mu_N J/R^3$. For the hydrogen molecule the local field is about 35G, and for HCl the field at the hydrogen nucleus is about 10G[78]. Since this effect is proportional to the rotational velocity and inversely proportional to the moment of inertia of the molecule, one may anticipate, that, in general, the smaller the molecule the more important will be the spin-rotation interaction. Furthermore, symmetric molecules with little or no intermolecular interactions (such as hydrogen bonding) will be most affected since they will have greater angular velocities.

The Hamiltonian for this interaction, H_{SR}, is expressed as:

$$H_{SR} = \hbar\, I.\, C.\, J. \qquad \text{..... 4.24}$$

where I is the nuclear spin operator, J is the molecular rotation or the angular momentum operator, and C is the spin-rotation tensor.

Molecular collisions causes the molecule to experience changes in the direction (M diffusion) or in both the direction and the magnitude (J diffusion) in the angular momentum. This in turn causes fluctuations in the local field at the resonant nuclei in the molecule. For liquids undergoing isotropic molecular reorientation the spin-rotation contribution to T_1 is expressed as[72,79]:

$$T^{-1}_{1SR} = \frac{2}{3}\,\frac{IkT}{\hbar^2}\,(2\,C^2_{\perp} + C^2_{\parallel})\,\tau_{SR} \qquad \text{..... 4.25}$$

where I is the moment of inertia, $C_{\perp}$ and $C_{||}$ are the diagonal components of the spin-rotation interaction tensor C and τ_{SR} is the angular momentum correlation time. τ_{SR} is a measure of the time a molecule spends in any given angular momentum state. Thus, this is related to the time between collisions and clearly differs from the correlation time for molecular tumbling τ_c. For spherical molecules with diffusion-controlled proceses, Hubbard's equation[47] (4.26), applies:

$$\tau_c \tau_{SR} = I/6kT \qquad \ldots\ldots 4.26$$

In Chapter Three, various models were discussed which illustrated the rotational and translational correlation times to be proportional to the solution viscosity. Thus, comparing of equations (3.15) and (3.17) (from Chapter Three) with equation (4.26), it follows that τ_{SR} is inversely proportional to solution viscosity; as the solution temperature increases, τ_{SR} therefore also increases, unlike τ_c. From the equations, T_{1SR} is most efficient for small symmetrical molecules at high temperatures. At low temperatures, T_{1SR}^{-1} is inefficient and T_{1DD}^{-1} is efficient due to the slow molecular motion; as the temperature increases, T_{1DD}^{-1}, in general, decreases slowly due to the decrease in τ_c until T_{1SR}^{-1} becomes dominant and T_1 begins to decrease with temperature. If the relaxation mechanism were pure spin rotation T_1 would decrease linearly with temperature. Nuclei relaxed partially by spin rotation therefore shows a non-linear behaviour in T_1 as a function of

temperature.

4.5 Paramagnetic Relaxation

Paramagnetic atoms or molecules which contain one or more unpaired electrons can contribute to relaxation of nuclei in two ways. These are:

(i) dipolar relaxation by the electron's magnetic moment

(ii) transfer of unpaired electron density to the atom of the relaxing nucleus itself.

The electron has magnetic dipole and an unpaired electron will therefore generate a local magnetic field, which in general will have a non-zero average value. This local field is randomly modulated by molecular motion and consequently provide a relaxation mechanism. Because the electrons magnetic moment is very large, of the order of 10^3 times greater than the nuclear magnetic moment, the electron-nuclear dipolar relaxation is thus a much more efficient relaxation process than the nuclear-nuclear dipole relaxation.

The other important factor is the short electron spin relaxation time of the paramagnetic ion which causes the local field to fluctuate rapidly and induce fast transitions between the nuclear-spin states. Thermal motion will also modulate the anisotropic magnetic interaction in the usual way and contribute to the relaxation whether the observed nuclei are bound to the paramagnetic ions or to other nuclei in solution. Thus, if a nuclear spin in a solid or liquid were unable to move, the paramagnetic centres will produce little effect on the NMR spectrum; most of the nuclei being out of the sphere of influence of the unpaired electron. In practice, however, spin exchange and diffusion processes often allow all the nuclei in the material to have frequent encounters with the unpaired electron so that nearly all nuclei have similar relaxation behaviour. The observed relaxation is a weighted average over each of the different local nuclear environments.

If the ions' paramagnetism comes purely from spin angular momentum, its magnetic moment can be expressed as[81,24,72]:

$$\mu = \gamma_e \hbar [S (S + 1)]^{1/2} \quad \text{..... 4.27}$$

If there are other contributions, an effective magnetic moment μ_{eff} has to be used. In general, the spin-lattice and spin-spin relaxation rates are roughly proportional to μ^2_{eff} and to the concentration of paramagnetic species, N_s. In the narrowing limit, the two relaxation rates T_{1UE} and T_{2UE} due to the unpaired electron (UE), can be expressed as:

$$T_{1UE}^{-1} = (4S (S+1) \gamma_e^2 \gamma_I^2 / 3\hbar^2 r^6) \tau_c \quad \text{..... 4.28}$$

$$T_{2UE}^{-1} = T_{1UE}^{-1} + (S (S+1) a^2/\hbar^2) \tau_e \quad \text{..... 4.29}$$

In the second (scalar) term of this expression for spin-spin relaxation, a is the hyperfine electron-nuclear spin coupling constant. The correlation time, τ_e is related to the electron relaxation time and to the exchange life time τ_h of the molecular complex between the ion and the molecule being relaxed. This is expressed as:

$$\tau_e^{-1} = T_{2s}^{-1} + \tau_h^{-1} \quad \text{..... 4.30}$$

The effects of paramagnetic ions on nuclear relaxation has important application in chemistry and biology. For example, the "relaxation reagents" used in ^{13}C NMR provide an example of electron-nuclear relaxation. These reagents are usually transition metal complexes, the trisacetonylacetonate of chromium and iron (Fe^{3+}) being the most common, and their function is to dominate ^{13}C relaxation in the sample. In doing so they achieve two 'desirable' effects. Firstly, they shorten all T_1's, thus speeding up a pulsed experiment and secondly they eliminate the nOe.

This is especially useful in quantitative ^{13}C work and in studying ^{15}N where they can eliminate the negative nOe.

Interactions between the relaxation reagent and an organic molecule are far from clear. In some cases, a loose complex between the reagent and solute appears to form based on an interaction with any polar group. Under these conditions, the specific electron-nuclear relaxation rate depends on the inverse sixth power of the electron-nuclear distance[8,24,72].

An additional separate effect of paramagnetic species is in the use as shift reagents. Large chemical shifts are induced in metallo-organic compounds such as Lanthanides, where if the metal is paramagnetic, chemical shifts arise from either a contact interaction or pseudo contact interactions[8,20,24,29]. The former involves the transfer of some unpaired electron density from the metal to the ligand. The unpaired spin density can cause positive or negative chemical shifts depending on the electron distribution and electron spin correlation effects.

The pseudo contact interaction arises from the electron-magnetic dipolar fields experienced by a nucleus near a paramagnetic ion when the electron distribution is anisotropic. This anisotropy leads to anisotropic magnetic susceptibility, hence a nucleus experiences a shift.

It is important to distinguish between the requirements of a "shift reagent" and a "relaxation agent" although both are paramagnetic complexes. The shift reagent should be anisotropic and have a very fast electronic relaxation ($10^{-13}S$) in order to induce little line broadening. It must also complex, if only in a very loose way, with the solute. The relaxation reagent should be isotropic (hence producing no dipolar shift), relax more slowly ($10^{-6}s$) and not form any complex with the solute.

From discussions in this chapter and chapter three, various relaxation mechanisms and models have been invoked to explain the nature of spin-lattice and spin-spin relaxation times. It is envisaged that these two chapters and chapter five

can be combined, in a manner that, will lead to further information and understanding of the effects of sound in liquids and its influence on spin-lattice relaxation times.

CHAPTER FIVE

STRUCTURE OF LIQUIDS AND THE ABSORPTION OF SOUND IN LIQUIDS (I)

NOMENCLATURE

Z	Co-ordination number
P	Pressure
V	Volume
V_f	Free Volume
A_f	Free area
δ	Small increase in density
k_S	Adiabatic compressibility
P_A	Acoustic pressure
k_T	Isothermal compressibility
γ	Specific heat ratio
P_g	Probability of energy transfer during collisions in the gas phase
P_L	Probability of energy transfer during collision in the liquid phase
V_h	Volume of the hole
l_f	Mean free path in the liquid
V_c	Average velocity of molecules in the liquid phase
K_o	Compressibility of a liquid
τ_v	Structural or volume relaxation time
ΔF	Difference in free energy of two states
N_{AA}	Number of collisions between A molecules
P_{AA}	Probability of transfer of energy during collision of A-A molecules

τ_{AA}	Vibrational relaxation time for A-type molecules surrounded by A type molecules
$\ddot{\theta}$	Angular acceleration
$\dot{\theta}$	Angular velocity
$\ddot{X}$	Linear acceleration
$\dot{X}$	Linear velocity

5.0 Introduction

The basis on which this research was initiated and performed rested entirely on the hypothesis that sound (or to be more precise ultrasound) can be used to perturb natural molecular motion in the liquid phase. The effects of the perturbation could then be observed through their influence on NMR relaxation times. The emphasis in this chapter is directed towards examining and understanding the effects of ultrasonic waves and, the information that may be obtained relating to the structure of matter and molecular processes.

In order to understand the effects of ultrasound in liquids, one must first understand the properties of liquids. Thus, the first part of this chapter addresses questions such as: How does one define a liquid? Does it have a finite structure? Can it be approximated to the behaviour of an ideal gas or to a solid structure? How does it behave under the influence of volume, pressure and temperature variations?

In Chapter Three various mathematical models were presented to give an account of the factors affecting spin-lattice relaxation times. These models led to expressions for translational and rotational diffusion of molecules in liquids. In addition, expressions involving the effects of size and shapes of molecules on diffusion and the so-called "mutual viscosity" of solution were discussed.

Discussions on translational and rotational diffusion of molecules in liquids will not be presented again. However, diffusional parameters that may be affected via the effects of ultrasound absorption will be discussed.

In the second part of this chapter are discussed the absorption and dispersion of ultrasound in liquids in terms of the physical mechanisms, relevant equations and its frequency dependance. Mathematical models to account for sound absorption and molecular motion will also be presented.

In the following chapter (Six), three other areas of relevance will be discussed. These are: acoustic nuclear magnetic resonance (ANMR), with reference

to acoustic nuclear magnetic resonance in liquids, the effects of ultrasound absorption in liquids and its possible influence on NMR relaxation times, and finally acoustic cavitation in liquids with reference to sonochemical reactions.

This chapter presents some of the highlights of physical acoustics without deep analysis in places. It is, however, hoped that sufficient understanding is obtained to enable the initial hypothesis to be given some credibility. For readers who wish to acquire a deeper insight of the analytical derivation of ultrasound absorption in liquids they should consult Matheson[80], Stumpf[81], Kinsler and Frey[82], Bayer and Letcher[83], Lindsay[84], Hertzfeld and Litovitz[85], Morse and Ingard[86], Stephens and Bate[87], Mason[88] and Kruus[89].

5.1 Properties of Liquids and Their Structure

There are essentially three distinct phases of matter: solids, liquids and gases. By making a comparison of these three different phases it is hoped that a very good approximation to the properties of liquids will evolve.

5.2 The Solid State

There are three main types of solids: crystalline, glasses and polymers and these are formed under the influence of ionic, covalent and van der Waals forces.

The main feature of a solid is in its long-range order. It has an ordered repeating lattice structure with only occasional empty lattice sites, due to misplaced molecules and other breaks in the regularity. Further more, a typical molecule will spend a comparatively long time oscillating about the same equilibrium position in the lattice, migrating to another lattice site only occasionally. In this highly ordered solid, the translational kinetic energies of the molecules are negligible and the molecules vibrate about equilibrium positions under the influence of strong intermolecular forces.

If one chooses any internal molecule as a reference for any other molecule, however far removed, it will bear some definite spatial relationship to the initial reference molecule. A molecule will also have a certain number, Z, of nearest neighbouring molecules on adjacent sites. Z is known as the co-ordination number of the lattice. The Z nearest neighbours of a given molecule will lie on a sphere of larger radius than the subject molecule.

Consider what happens as the temperature of a solid is raised. The result is as that the temperature is raised more and more, the molecules begin to vibrate increasingly. However, these vibration still occur in a well defined system of lattice sites and so long-range order is still preserved. If now the temperature of the solid is raised further, a conflict arises between the ordering influence of the intermolecular forces and the disordering influence of the increasing thermal motion of the molecules. When the solid melts into a liquid, the original long-range order is destroyed, but a great deal of local or short-range order remains.

At the melting point there is usually a volume increase of 5-15%[90] indicating that the molecules in a liquid possess more "elbow room" than those in the solid. There is also evidence that a volume increase on melting is related not so much to an increase in distance between neighbouring molecules, but to a general decrease in the co-ordination number Z. For example, if Z were twelve in the solid state, then it might on average be reduced to nine in the liquid state; in other words, each molecule in a liquid can be regarded as being surrounded by nine nearest neighbours and three empty sites or "holes".

In the liquid state the value of Z is related to its value in the solid state. It has been shown, in general, that the values in the liquid state Z_L, and in the solid state, Z_S, can be expressed as [91,92]:

$$Z_L \simeq Z_S - 1 \qquad \ldots\ldots 5.1$$

5.3 The Gaseous State

Molecular motion in a gas is completely chaotic, in striking contrast to molecular motion in solids where molecules vibrate in an orderly fashion on a set of permanent sites. Gas molecules move around in their enclosure and it is often assumed that any intermolecular forces existing between the molecules is negligibly small. The only interaction between molecules envisaged are those occurring when two molecules collide but these are comparatively rare if the density is low and where the molecules are far apart for most of the time thus rendering the effect of intermolecular forces negligible. If the density of the gas increases, the molecules will be closer together. The question is: how does this effect the intermolecular forces between the molecules and what can be said about such forces. The fact that there are cohesive forces present, which hold the molecules together in liquids and solids, suggests that the net forces between the molecules are attractive. However, if one tries to compress an ordinary liquid or solid, this would present certain difficulties, suggesting that the forces between two molecules becomes strongly repulsive below a certain molecular separation. To deal with this situation the molecules must be regarded not as mass points but rather as nearly "rigid spheres" of diameters σ. σ represents the minimum possible distance between the centres of two molecules. The idea of replacing "point molecules" by rigid spheres of finite diameter σ, is a convenient way of saying that when the distance r between two molecules decreases to about σ, a very strong or infinite repulsion between them occurs. When r is greater than this, the force is of attraction, which decreases as r increases. However, if r becomes fairly large, say of the order of five molecular diameters as in a gas of low density, this attraction is virtually zero.

One of the outstanding discoveries in the field of gaseous theories was due to van der Waals. He showed there is an approximate balance between the

effects of the short-range repulsive forces and the long-range but weaker attractive forces. He represented the repulsion simply by replacing the "point" molecules of a perfect gas by rigid sphere of a finite diameter σ. The kinetic theory of gases leads to the equation of state for one mole of gas in the form:

$$PV = RT \qquad \text{..... 5.2}$$

where V is the volume of an enclosure occupied by a gas. van der Waals proposed the total available volume at any instant is not V as for point molecules but less because of the finite volume of the molecules. V is replaced by (V-b) where b turns out to be approximately four times the volume of a molecule in the enclosure. Thus;

$$b = \frac{2}{3} N \pi \sigma^3 \qquad \text{..... 5.3}$$

The attraction is dealt with by assuming that attraction between the molecules is equivalent to some internal pressure P' causing the molecules to crowd closer together. Thus, the pressure P' must be added to the applied pressure P.

van der Waals further suggested that P' is proportional to the square of density of the gas which means that P' is inversely proportional to the square of the volume, for a constant mass of gas. Thus equation 5.3 is modified to[90,93] to equation 5.4.

$$\left(P + \frac{a}{V^2}\right)(V - b) = RT \qquad \text{..... 5.4}$$

If a liquid is now regarded as a highly compressed gas, then in some critical region the density of gas can be increased continuously from a low value appropriate to a gas to a high value approaching that of a liquid.

5.4 Liquid State

In summary, the main characteristics of a gaseous state are its random motional molecular behaviour, the translational motion of the molecules is great and there is relatively little molecular interaction. In a solid state the main characteristics are fixed sites for the individual atoms or molecules and very little translational movement.

By contrast in a liquid state, there is a great deal of translational motion of the molecule but the cohesive intermolecular forces are strong enough to form a condensed state. Thus, given a quantity of liquid, like a solid and unlike a gas it occupies a definite volume. On the other hand, the molecules have so much freedom that a liquid unlike a solid flows very readily and easily takes up the shape of the vessel it occupies.

It has long been realised that a liquid is unable to resist shearing stress permanently because of its disordered structure. It would be expected that a solid with nearly perfect lattice structure would resist shear. This is because such a configuration is likely to be one in which the potential energy of a typical molecule is nearly a minimum value. In other words, work is required to displace it from its lattice site. If one has a periodic lattice structure with only occasional imperfections, neighbouring rows of molecules can change their relative positions by a shear and this movement can be shown to require a small amount of energy than that in a solid with a nearly perfect lattice structure. If as in a liquid there is no lattice structure, then a great many molecular locational configurations with very nearly the same potential energy exist which can be occupied in turn. Thus, a shear deformation which does not alter the density or the mean distance between the molecules can take place relatively easily.

So far no mention has been made about the structure of liquid without referring either to a solid or gas like structure. In the subsequent sections, theories which describe the structure of liquids by considering their own characteristics and

properties will be discussed. These theories are: the "Cell theory", which uses a similar model to that for a regular lattice structure with all lattice sites occupied, the "Hole theory", which uses a similar model to the cell theory but with some of the lattice sites unoccupied, the "Tunnel theory" based on a partially disordered lattice structure; and the "Monte Carlo" and "Molecular Dynamic" models in which the available volume is divided into large cells containing many molecules and an averaging is performed by direct numerical methods.

For the readers who wish to know more on the subject of liquids and their properties, they should consult Kruus[89], Temperley and Trevena[90], Barker[94], Barker and Henderson[95], Hirschfelder[96], Murrell and Boucher[97], and Marcus[98].

5.5 The Cell Model

The cell model for a liquid was first introduced by Lennard-Jones and Devonshire[99,100]. This model considers a dense assemble of N molecules occupying a volume V at temperature T in which each molecule is constrained by its neighbours to occupy a limited region in space - a "cell". The simplest cell model makes the following assumption:

(i) The total volume may be subdivided into cells.

(ii) The centres of the cells form a regular lattice, (however, the order is only local and not long range.

(iii) The cells are all identical but may be distinguished by their position in the lattice (the molecules are indistinguishable).

(iv) Each cell contains one molecule, hence, there are N cells and the volume per cell equals the volume per molecule, V/N.

(v) Each molecule moves independently in its cell.

(vi) The effect of the molecules in the cells neighbouring a given cell

which contains a molecule in question is such that, the cell is "smeared out" uniformly over a sphere of radius a.

The physical picture behind this is that the free volume is defined as the volume available in a cell for the centre of a molecule to move as shown in Figure 5.1.

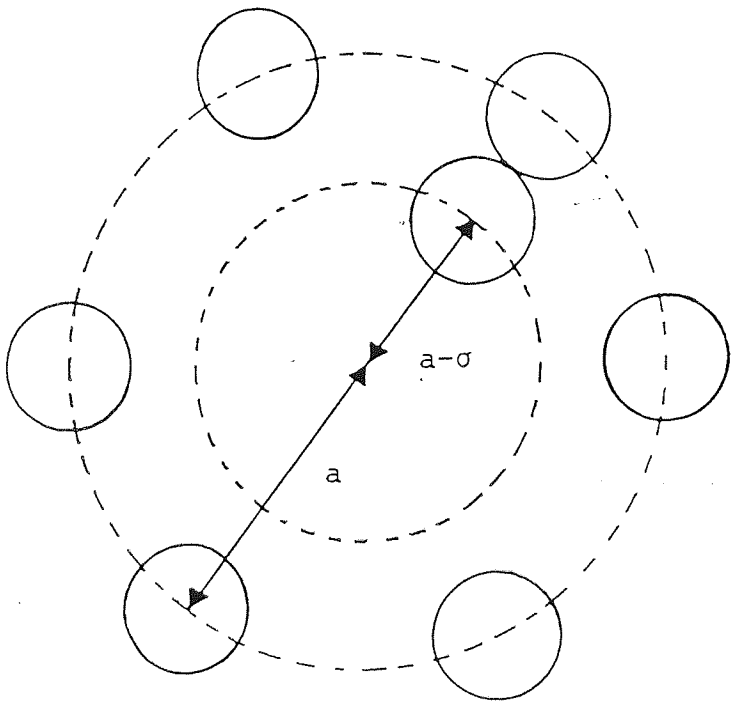

Figure 5.1: Central plane section of a typical cell

For an assembly of hard spheres of diameter σ, the minimum distance the central molecule can move from the cell centre to collide with a neighbour is (a - σ). Thus the maximum value of the free volume per molecule, V_f, is:

$$V_f = \frac{4\pi}{3} (a - \sigma)^3 \qquad \text{..... 5.5}$$

A more general equation is written in the form:

$$V_f = \frac{4\pi\gamma^1}{3N} (V^{1/3} - V_o^{1/3})^3 \qquad \text{..... 5.6}$$

where V represents the volume of liquid occupied by N molecules in a regular closed packed lattice, V_o represents the minimum volume of liquid when the nearest neighbours throughout the liquid are in contact (ie. $a=\sigma$), γ^1 represents a constant for a particular cell lattice type. For example, $\gamma^1 = \sqrt{2}$ for cubic closed packed and a hexagonal closed packed lattice and $\gamma^1 = 3\sqrt{3}/4$ for a body centered cubic lattice.

Lennard-Jones and Devonshire also considered a more sophisticated cell model by assuming inverse 12-6 power distance interactions[101,102] between the molecules. To obtain V_f in this case, they introduced the idea of "smearing". For a close-packed lattice, there are twelve nearest neighbours and each cell is a dodecahedron formed by the planes which perpendicularly bisect the lines joining adjacent cell centres. In the smearing approximation this dodecahedron is replaced by a sphere, ie. the twelve neighbouring molecules could be "smeared" with uniform probability distribution over the surface of this sphere.

The assumption in LJD theory is that each molecule is surrounded by twelve nearest neighbours. If the liquid expands the density decreases, and it is more likely that the average number of nearest neighbours Z will be less than twelve. Another method of achieving the same result is to suppose that some "holes", or empty cells, exist in the liquid; that is equivalent in saying that Z is reduced. Such a "hole" model will be discussed in the following section.

5.6 The Hole or Free Volume Theory

If the temperature of a liquid is raised both density and the apparent number of nearest neighbours, Z, decrease still further. These facts suggest that one

ought to allow for the presence of vacant lattice sites or holes. The presence of holes and their more or less random distribution in the lattice would explain at least part of the disorder in liquids which gives rise to the entropy increase on melting. Furthermore, the presence of holes would give a basis for understanding the relative ease of diffusion and flow in liquids in terms of a "vacancy diffusion" mechanism. It was this latter consideration which originally led Eyring[103,104,105,106] to postulate the presence of holes in liquids.

Consider a fixed lattice of cells, each cell having a volume V_{cell}. Let there be N_o cells which are empty and randomly distributed in addition to the N singly occupied cells. The volume per cell is now:

$$V_{cell} = V/(N + N_o) \qquad \ldots\ldots 5.7$$

where V is the total volume.

This is related to the free volume V_f, from equation 5.7:

$$V_f = (Z/Z_o)\, V_f^o + (1 - Z/Z_o)\, V_{cell} \qquad \ldots\ldots 5.8$$

where Z_o, is the lattice co-ordination number which does not vary with density or temperature and $Z = (1/2)\, Z_o\, N^2/(N + N_o)$. This is the average co-ordination number. Several other authors[107,108,109] have made modifications to the above theory.

As discussed earlier, on melting a solid, a volume increase of approximately 5-15% is observed. This has two effects: first, it increases the volume simply by increasing the number of sites at the same time keeping the intermolecular distance constant, and second, when two or more molecules share a vacancy, the lattice structure is destroyed, so that it no longer has long range order. Long range order is also blurred by a distribution of hole volumes around the vacancy as a mean.

Dynamic vacancies of molecular size are likely to occur also since they leave all but nearest neighbours of the vacancy relatively undisturbed. In order to take possession of a vacancy, a nearest neighbour must have sufficient kinetic energy to push back the other neighbours competing for the vacancy. This means it must have enough excess kinetic energy to equal or exceed the mean kinetic energy which the competing neighbours can put in the vacancy, since kinetic energy density is proportional to the pressure. The molecules that have been pushed back by the energized nearest neighbour to become part of the hard volume of the liquid.

5.7 The Tunnel Theory

This model was devised by Barker[94,110] and conceives molecules as moving in straight tunnels whose walls are formed by neighbouring lines of molecules. Figure 5.1 can also represent a view down along a tunnel axis and the inner area can then represent a "free area", A_f, analogous to the free volume of the cell model. A_f is the area available to the centre of each molecule perpendicular to the tunnel axis.

The theory was then developed by considering two approximations for A_f. The first of these is a "smearing approximation" which gives:

$$A_f = \pi (r - \sigma)^2 \qquad \ldots\ldots 5.9$$

where r is the distance between the axis of neighbouring tunnels.

A second and better approximation is to write:

$$A_f = \pi (r - \sigma')^2 \qquad \ldots\ldots 5.10$$

where σ' is the average closest distance of approach of the central molecule of diameter σ to the line of centres of similar molecules that are equally spaced.

5.8 The Monte Carlo and Molecular Dynamic Computer Simulations of a Liquid

In a Monte Carlo (MC) method[90,93,94,95,98], a particle is given a random displacement and the potential energy for the new configuration is calculated. Repetition of this procedure generates a chain of configurations. The overall average of a property then converges to the cononical ensemble average as the chain increases in length. In this chain, a configuration is counted again if the subsequent move is rejected.

A typical MC calculation involves the generation of hundreds of thousands of configuration for a model of hundreds of particles.

In a molecular dynamic[90,93,94,95,98] (MD) method, it describes essentially a microcononical essemble. Here both the velocity and the position of each particle is initially specified. The motion of the particles are then followed by numerically solving the classical equation of motion, assuming a given interparticle potential energy.

5.9 The Compressibility of Liquids

As this chapter is concerned with the effects of sound pressure, it is important to consider the effects of pressure on liquids in terms of compressibility.

Liquids, as a class, are more compressible than solids and much less compressible than gases. The compressibility of all liquids decrease with increase of pressure: at first rapidly and then more slowly as the pressure becomes higher. The initial high value of the compressibility occurs because of a decrease in the intermolecular spacing. The smaller values at the higher pressure are thought to be due to a decrease in volume of the actual molecules themselves once they are nearly in contact with their neighbours.

The compressibility of most liquids increases as the temperature rises. This is due to the fact that, as the temperature rises, collision between molecules

become more vigorous and because the molecules are not completely rigid, their effective volume will decrease.

5.10 Liquid Viscosity

The viscosity of a liquid is a measure of the forces that work against movement or flow when a shearing stress is applied. In molecular terms, the molecules in a liquid are held together much more strongly than in a gas. In liquids, viscosity may be thought of as a measure of the forces needed to overcome the mutual attraction of the molecules so that they can be displaced relative to each other. The more strongly the molecules are held together, the smaller the flow for a given shearing stress.

The effects of temperature are such that, as the temperature is raised, the frequency with which the molecules move or vibrate increases. This results in altering the average intermolecular separation a. Thus, with increasing temperature, the random kinetic energy of the molecule helps to overcome the intermolecular forces and reduces the viscosity. One may say that in a liquid the molecules are so close together, that considerable energy must be expended in dragging one molecular layer over its neighbours.

The viscosity of a liquid can be expressed as[111,112]:

$$\eta = \frac{h N_A}{V_m} \exp\left(\frac{E}{RT}\right) \qquad \text{..... 5.11}$$

where h is the Planck's constant, N_A is the Avagadvo's number, V_m is the volume per mole of the liquid and E is the molar activation energy for surmounting the energy barrier.

The energy barrier E can be regarded as the energy needed to create a hole in the liquid big enough to receive a molecule. This is found to be of the order of 0.4 times the latent heat of vaporisation L_v. The numerical value, 0.4, arises from the fact that there is already some free volume in the liquid for a molecule to move. Consequently, the viscosity can be reexpressed as[93,111,112]:

$$\eta = \frac{h N_A}{V_m} \exp\left(\frac{0.4\, L_v}{RT}\right) \qquad \ldots\ldots 5.12$$

To discuss the effects of pressure on liquid viscosity, it is easier to regard the energy barrier E as the energy required to open up a hole for the transposed molecules. Equation 5.11 can be written in the form:

$$\eta = A \exp\left(\frac{E}{RT}\right) \qquad \ldots\ldots 5.13$$

If an external pressure, P, is applied, the energy expended to form a hole is increased by PV_h, where V_h is the volume of the hole. The thermal energy for activated flow is then increased from E to $E + PV_h$. The viscosity then becomes,

$$\eta = A \exp\left(\frac{E + PV_h}{RT}\right) \qquad \ldots\ldots 5.14$$

which can also be expressed as:

$$\eta = \eta_o \left(\frac{PV_h}{RT}\right) \qquad \ldots\ldots 5.15$$

A plot of ln η plot against P gives a straight line of slope V_h/RT for which V_h turn out to be approximately 15% of the volume per mole of the liquid (V_m).

In molecular terms, the molecules are pushed closer together, or in terms of the alternative way of describing the molecular jumps, more work must be done to open up a vacant site.

Table 5.1 summarises the basic differences between the mechanism responsible for viscosity in gases and liquid.

Fluid		Effect of temperature (T)	Effect of pressure (P)
Gases	momentum transfer	η increases as $T^{1/2}$	None
Liquids	Intermolecular forces	η decreases as $\ln \eta = A + \frac{B}{T}$ (A & B are constants)	η increases as $\ln \eta = A + KP$ A is a constant K is the bulk modulus.

Table 5.1: Shows basic differences between the mechanism responsible for viscosity in gas and in liquids

5.11 Molecular Acoustics

Molecular acoustics is the study of molecules and their interaction with elastic sound waves. When an elastic wave passes through a medium in which there exists an equilibrium, the effect on the equilibrium depends on the frequency of the wave. If the period of the elastic wave is much longer than the time constant (or relaxation time) for the alteration of the position of equilibrium, the latter is disturbed by the wave. If on the other hand the period of the wave is much shorter than the

relaxation time, the wave will not "see" the equilibrium which consequently remains undisturbed. When the period is comparable to the relaxation time changes in the velocity of propagation and absorption coefficient of the elastic wave will occur. From measurement of these changes the relaxation time and rate constants of the equilibrium may be determined. Since the period of an elastic wave can range from $1\text{-}10^{-15}$ sec a wide range of equilibria can be studied.

Experimentally it is possible to produce waves with frequencies as low as few Hertz or as high as approximately 10^{10} Hertz. The acoustic spectrum may be divided roughly into four regions; Infrasonic (10^{-2}-10 Hz), audible (10 Hz-14 KHz), ultrasonic (14 KHz-10^{9} Hz) and hypersonic (> 10^{9} Hz). Information on molecular processes will in general be obtained from studies of the ultrasonic and hypersonic regions.

There are two types of elastic waves: longitudinal and transverse waves. These two types of elastic waves are also alternatively referred to as compressional and shear waves respectively. Sometimes the term "ultrasonic" is used to describe both types of wave motion although it should strictly be confined to longitudinal waves. In a shear or transverse wave the displacement of the particles of the medium is at right angles to the direction of propagation of the wave. However in a longitudinal wave the particles move in the direction of wave propagation.

When a medium experiences a small shear strain there is no volume and temperature change. Hence a shear wave propagating in a medium does not induce a temperature variation in phase with the displacement of the medium, and any equilibria which are present are not disturbed. The medium may respond to the shear wave by viscous flow (as in a liquid), or by elastic deformation (as in a solid). The change from viscous to elastic behaviour (viscoelastic relaxation)[80,113,114] occurs when the period of the shear wave becomes comparable to the time for an elementary diffusive motion of the molecules of the medium.

An ultrasonic longitudinal wave contains both shear and a pure compressional component. If the period of the alternating compression wave is short, a longitudinal wave will propagate adiabatically and the local temperature of the medium (not the same as the bulk of the medium) will alter in phase with its changing volume. Hence, any equilibrium which is sensitive to temperature or pressure will be disturbed by the passage of a longitudinal wave. In liquids this includes chemical equilibria, molecular energy transfer between the translational, vibrational and rotational degrees of freedom, rotational isomerisation and the flow of liquid molecules between packing of high and low density[80,114-120].

5.12 Sound Absorption in Liquids

When studying molecular dynamics and mechanisms the first question which one may ask is: why does a liquid absorb sound energy? From an energy stand point a liquid may be represented as a system of boxes each containing energy of a certain type as shown in Figure 5.2 which are now all coupled to another in some manner. By this is meant that energy can be transferred from one box to another. For example, if one raises the temperature of any one box, energy will flow from this box to the others until equilibrium is reached. The time it takes for equilibrium to be achieved depends on the details of the coupling process. In liquids, the important means of coupling is relaxational. In this type of coupling, if one raises the energy of one box above equilibrium, then this energy will decrease exponentially with a time constant, called the relaxation time to the equilibrium value. This differs from the resonance case where the energy would oscillate back and forth. That is to say, an overshoot in energy transfer occurs in the resonance process.

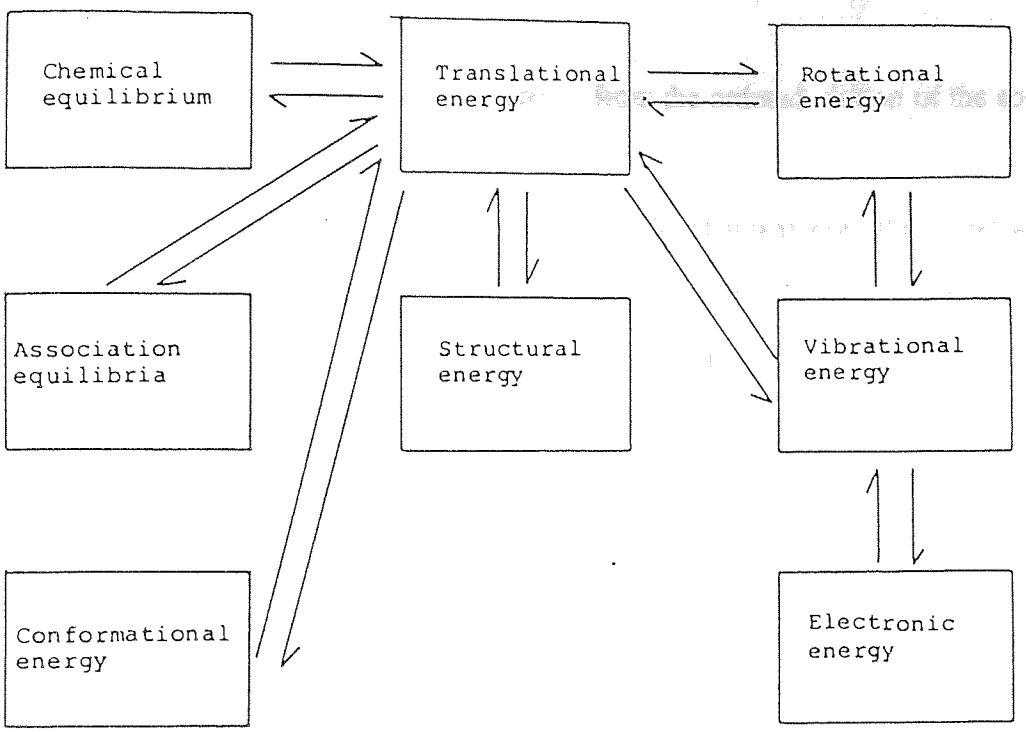

Figure 5.2: Schematic representation of possible energy states in a fluid

A sound wave in passing through this liquid, increases the energy in one or more of these boxes almost instantaneously. For example, the compression accompanying the wave can cause a temperature rise in the translational energy of the molecules in the liquid. If now, no energy leaks to the other boxes, then, when decompression occurs, the increased translational energy is returned to the ordered elastic energy of the wave. The temperature is then restored to its initial value prior to the compression cycle. However, because of relaxation coupling, some of the translational energy is coupled to other boxes (or forms of energy) during the compression half cycle. Owing to the time lags in the energy transfer, this energy does not get back into the translational box until the sound wave is in its decompression cycle. Hence, this energy returns out of phase. The effect of this out-of-phase energy is to decrease the height of the peaks and the depth of troughs of the sonic wave. The result is sound absorption. Absorption[114,116,117] occurs when energy flows from the peak to the trough of a sound wave, because the

net effect of this process is to remove energy from the ordered motion of the sound wave.

The next question one may ask is: "In what way does the sound wave interact with a liquid?" In attempting to answer this question, one should think of the effects of compressing a gas, since sound is a pressure wave. Imagine a volume element of gas to be compressed quickly as it is done by a sound wave. The translation motion of the molecule will adjust nearly instantaneously, and since the pressure that adjusts the gas is determined solely by this translation motion, the pressure adjusts immediately to the volume changes. After the compression is completed, some of the translational energy of the molecule goes more slowly into the rotational and vibrational energy, and the pressure decreases accordingly. If the gas is allowed to expand to its initial volume, the work delivered by the gas during the expansion is less than that absorbed during the compression. Therefore, during each cycle, there will be a net energy transfer to the internal degrees of freedom of the molecules, which will heat the gas and attenuate the sound.

The magnitude of this energy loss will depend on the ratio between the length of the cycle and the "relaxation time" of the transfer from translational to internal energy of the molecule. In the extreme case, when the gas is expanded immediately after compression, before such transfer can take place, the gas will behave as a monoatomic gas, and only viscosity and heat conduction will cause attenuation. On the other hand, if both compression and expansion take place very slowly, so that thermal equilibrium between all internal modes of motion is continuously established, relaxation attenuation will be important in some intermediate range of frequencies.

In order to understand the effects of sound waves in fluids, it may be easier to relate the effects of acoustic pressure in the gas phase and then build up a model of what may be happening in the liquid phase.

If one assumes that gas compression is adiabatic (the entropy content of the gas remains nearly constant during compression), then the pressure changes caused by sound (also referred to as acoustic pressure) if represented as P_A on the equilibrium pressure P, can be interpreted in terms of changes in the density ρ of a fluid. This has been shown to be:[82,86,89,120-122]

$$\rho + \delta = \rho + \left(\frac{\delta \rho}{\delta P}\right)_S P_A = \rho + \rho k_S P_A \qquad \text{..... 5.16}$$

where δ represents a small increase in density and k_S in the adiabatic compressibility.

Similarly, changes in the equilibrium temperature T, due to the acoustic pressure can be expressed as:

$$T + T_A = T + \left(\frac{\delta T}{\delta P}\right)_S = (\gamma - 1)\frac{k_S}{\beta} \qquad \text{..... 5.17}$$

where T_A is a small increase in temperature, γ is the ratio of specific heats and ß is the fractional change in volume (or density) with temperature at constant pressure. (called the co-efficient of thermal expansion)

Using the equation of state for perfect gas, $MP = RT\rho$ for which $k_S = 1/\gamma P$, the changes in density and temperature from equations (5.16) and (5.17), respectively, can be expressed as:

$$\delta = \rho k_S P_A = \frac{M}{\gamma RT} P_A \qquad \text{..... 5.18}$$

$$T_A = \frac{(\gamma-1)}{\gamma R \rho} P_A \qquad \text{..... 5.19}$$

From equation (5.18) one can see that the ratio between the changes in density, δ, and the acoustic pressure, P_A, is independent of the equilibrium pressure but is inversely proportional to the equilibrium temperature of the gas. In addition, the ratio between the changes in temperature, T_A, and the sound pressure, P_A, is independent of temperature but is inversely proportional to the equilibrium density ρ.

In fluids with very large thermal conductivity, the temperature of the fluid is practically unchanged by the passage of a sound wave. In this case the isothermal compressibility, k_T, is directly applicable and the change in density of the fluid is expressed as:[80,82,86,89,96]

$$\rho + \delta = \rho + \left(\frac{\partial \rho}{\partial P}\right)_T P_A = \rho + \rho k_T P_A \qquad \text{..... 5.20}$$

$$\text{Thus, } \delta = \rho k_T P_A \qquad \text{..... 5.21}$$

Having illustrated that sound wave perturbs matter either directly by a change in pressure or due to a temperature rise accompanying a change in volume in the gas phase, it may be wise to ask whether, pressure or temperature changes or both play a role in the energy loss in a given liquid.

Sound velocity measurements[80,111,113,116,121,123] in liquids reveal a great deal of information relating to the absorption of sound. The sound velocity C in a liquid can be obtained by the following expression;

$$C = \left[\frac{1}{\rho k_S}\right]^{1/2} = \left[\frac{\gamma}{\rho k_T}\right]^{1/2} \qquad \text{..... 5.22}$$

where k_S, k_T and γ have the usual meanings.

If, for some reason, the volume change is out of phase with the pressure then sound absorption occurs. In an adiabatic compression, this out of phase relation can be accounted for, by assuming that k_S is complex. If $k_S = k_T/\gamma$, either a complex γ or k_T can cause k_S to be complex.

If one assumes that a box has two energy states as shown in Figure 5.3, differing by a Gibbs' free energy, ΔF, and separated by an energy barrier of height ΔF, the relative population of molecules in the two states is given by:

$$K_{eq} = \frac{n_2}{n_1} = \exp\frac{-\Delta F}{RT} = \exp -\frac{\Delta E + P\Delta V - T\Delta S}{RT} \qquad \text{..... 5.23}$$

where K_{eq} is an equilibrium constant, ΔE is the difference in energy between the two states, ΔV the difference in volume, ΔS the difference in entropy, and n_2/n_1 is the number of molecules in state 2 divided by the number in state 1.

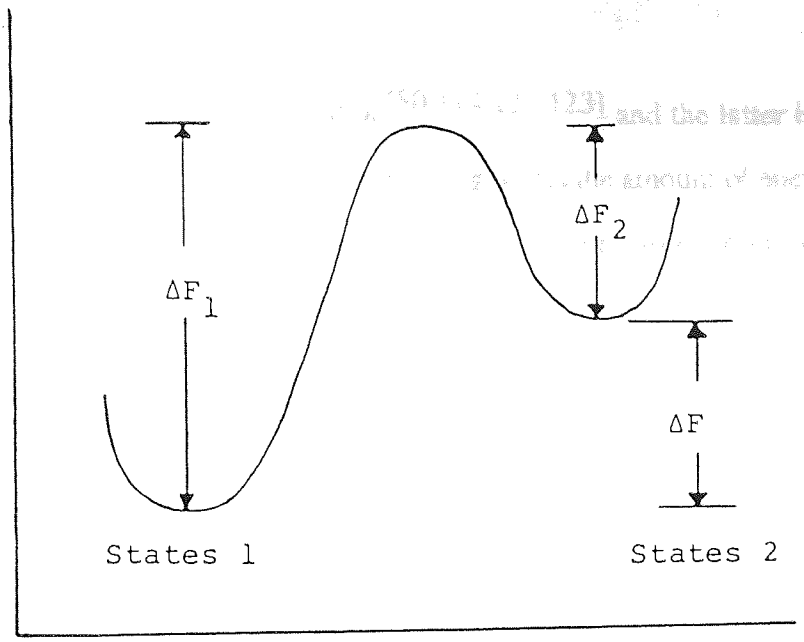

Figure 5.3: The difference in two energy states

For one energy state box to exchange energy with another, the ratio n_2/n_1, (K_{eq}), must be changed (the number in the excited state must increase or decrease). This can be done by changing the temperature in which case the governing equation determining the amount of shared energy is:

$$\frac{\partial \ln K_{eq}}{\partial T} = \frac{\Delta H}{RT^2} \qquad \ldots\ldots 5.24$$

where ΔH is the difference in enthalpy between the two states. It can also be done by the change in pressure (causing ΔF to change) in which case the governing equation is:

$$\frac{\partial \ln K_{eq}}{\partial P} = -\frac{\Delta V}{RT} \qquad \ldots\ldots 5.25$$

Equation (5.24) leads to a complex or relaxing specific heat and a complex γ. Equation (5.25) leads to a complex or relaxing isothermal compressibility. The

former case is called thermal relaxation[80,114,121,123] and the latter isothermal volume relaxation. Equation (5.24) and (5.25) governs the amount of energy which a given energy box will accept, when there is a change in pressure or temperature.

The height of the energy barrier between the two states determines the rate at which this two-state system can except energy and thus determines the relaxation time for the process. Thus, if the ultrasonic frequency region in which a maximum energy change occurs is related to ΔF_1 and ΔF_2, then the relaxation time can be expressed in the form:

$$\tau = \frac{h}{kT} \frac{e^{\Delta F_2/RT}}{1 + e^{-\Delta F/RT}} \qquad \ldots\ldots 5.26$$

where h is Planck's constant and k is Boltzmann's constant. When the value of ΔF is small compared to ΔF_2, the expression reduces to:

$$\tau \simeq \tau_o \exp(\Delta F_2/RT) \qquad \ldots\ldots 5.27$$

The factor exp $(\Delta F_2/RT)$ expresses the probability that a molecule will have sufficient energy to overcome the barrier ΔF_2. It can be seen that the bigger the barrier height, the longer the relaxation time.

It should be emphasised that sound absorption in a liquid ultimately results in all the energy of the wave being converted into heat by the non-ideal nature of the liquid. The three main causes of sound absorption are viscosity, thermal conduction and relaxation effects. Sound absorption can also be treated as being due to a time lag between the pressure variations in a sound wave and the associated density variations.

In the following sections, the phenomena of relaxation and the various relaxation processes that exist in liquid, sound absorption losses due to viscosity and heat conduction will be discussed.

5.13 Thermal Relaxation

Every polyatomic molecule possesses a number of degrees of freedom; these are of two kinds: external and internal. The external degrees of freedom (also possessed by a monatomic species) are three in number, corresponding to the three translational velocity components of the molecule. Translational energy obtained directly from the acoustic wave, is passed on from molecule to molecule by collisions with virtually no time-delay. The internal degrees of freedom correspond to the vibrational and rotational motion of the molecules. For one of these internal modes to be excited it is necessary for energy to be transferred from one of the external degrees of freedom. Such a transfer of energy from an external to an internal degree of freedom requires a certain finite relaxation time in which the internal modes lag slightly behind the external modes. This is called thermal relaxation and it involves a consideration of the transition from a translational energy state to an excited internal state.

Consider the thermal mechanism of sound absorption. The effect is due to a rise in temperature accompanying an adiabatic compression and the fact there is a time lag for transfer of energy from external to internal degrees of freedom. It has been shown[81,86,88,89,115,124] that the absorption coefficient per wavelength, $\alpha\lambda$, can be expressed as:

$$\alpha\lambda = \frac{k_T (\gamma - 1)}{\pi\rho} \left[\frac{C_i}{C_p}\right] \frac{\omega\tau}{1 + \omega^2 \tau^2} \qquad \ldots\ldots 5.28$$

where C_i is the internal relaxing specific heat contribution and τ is the relaxation time for coupling translational energy into the internal degree of freedom involved. One can better understand the factors that determine the energy changes due to thermal relaxation by considering equations (5.28) and (5.19). From thermodynamics, a change in temperature for a given volume change is proportional to k_T. Thus for a given amplitude of a sonic wave, the rise in temperature is proportional to $k_T (\gamma - 1)$. The ratio C_i/C_p is simply the fraction of the total energy shared by the internal degrees of freedom. The quantity $\omega\tau/(1 + \omega^2 \tau^2)$ expresses mathematically the relaxational absorption, which is, the energy that is stored internally in a small volume during a compression. However, due to time lags, this energy is restored to the external degrees of freedom at a time when the decompression half-cycle is present in the volume under consideration. Thus, energy from the peak has appeared in the trough not by moving through space under the action of a temperature gradient but because of time lags in transfer of energy between internal and external degrees of freedom. If one now considers the effects in terms of ultrasonic frequencies, then, at low frequencies the compression and decompression occurs very slowly. This suggests it has time to come back in phase, hence the absorption is low. This absorption per wavelength, $\alpha\lambda$, increases with frequency because as the period of the sonic wave gets shorter, the shared energy becomes more out of phase and thus causes a greater loss. However, as the frequency increases there is less time for energy to transfer into other degrees of freedom. Therefore, a smaller fraction of the energy gets shared and this tends to decrease the loss from the sonic wave. At very high frequencies, almost no energy is shared and the loss drops towards zero. Thus, equation 5.28 reexpressed such that frequency

dependance is now given by the expression:

$$\alpha\lambda = \omega\,\tau/(1 + \omega^2\,\tau^2) \qquad \text{..... 5.29}$$

As mentioned earlier, C_i/C_p is simply the fraction of the total energy shared by the internal degrees of freedom. If one considers the internal degrees of freedom as having only two states, then C_i can be expressed by the following equation:

$$C_i = \left[\frac{(\Delta H)^2}{RT^2}\right]\left[\frac{e^{-\Delta F/RT}}{(1+e^{-\Delta F/RT})^2}\right] \qquad \text{..... 5.30}$$

If equation (5.30) is plotted as a function of temperature, as shown in Figure 5.4a, it can be seen that C_i exhibits a maximum. For the two-state system, C_i, goes to zero at low temperature because so few molecules can get sufficient free energy to get into the excited state following a small increase in the temperature. At very high temperatures, almost 50% of the molecules are in the upper state and a further increase in temperature causes little change in the relative population of the two states. Thus, the degree of freedom can accept little energy.

If there are many states present, as in the case with the harmonic oscillator with frequency ν, the specific heat is given by Planck-Einstein equation;

$$C_i = R\left[\frac{h\nu}{kT}\right]^2\left[\frac{e^{h\nu/kT}}{(e^{h\nu/kT}-1)^2}\right] \qquad \text{..... 5.31}$$

where h is Planck's constant, and k is Boltzmann's constant.

Using equation (5.31) and plotting a graph of internal specific heat versus temperature for many states, one obtains a graph as shown in Figure 5.4b ,where the system exhibits no peak in C_i as a function of temperature.

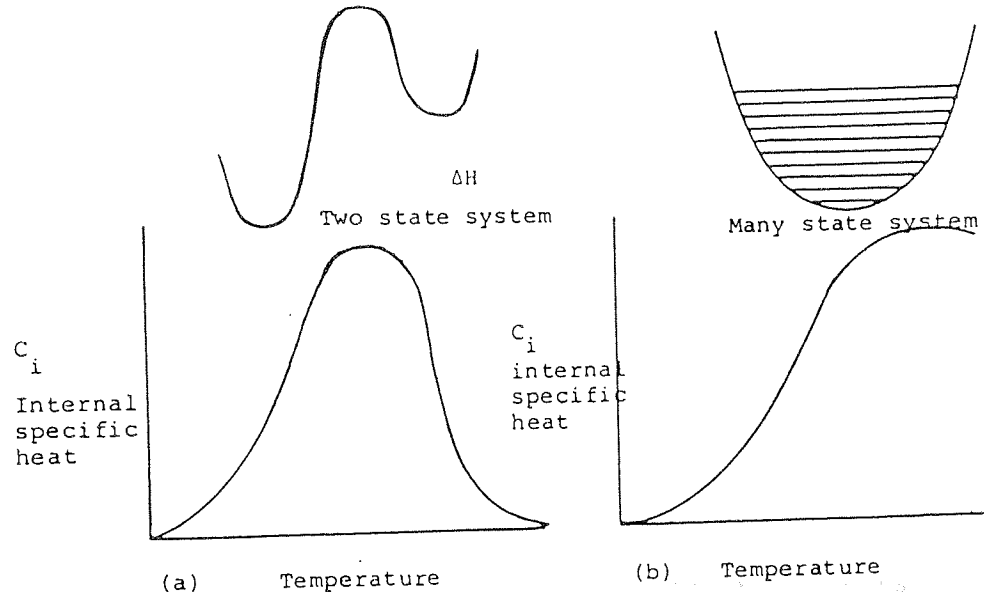

Figure 5.4: a and b showing specific heat vs temperature for a two-state and for many-state system respectively.

5.14 Vibrational Relaxation

In this case, the energy of the translational (external) degrees of freedom is transferred to the vibrational (internal) modes[80,90,125,126] and the corresponding relaxation times are of the order of 10^{-10}S or less. If one assumes that the mechanism of energy transfer in the liquid phase is the same as that in the gas phase, this would mean that energy transfer would be due to collisions with exceptionally high energy and that co-operative actions of molecules or cluster is insignificant. In this type of collisions the molecule in question comes particularly close to and interacts with another single molecule exclusively and not with the cell wall, or with a group of molecules in a complex. The relaxation time involved in this binary collision process can be represented as:

$$\tau = [\tilde{N}\,\tilde{P}]^{-1} \qquad \ldots\ldots 5.31$$

where N is the number of collisions per second and P is the probability that during collision, energy transfer takes place. This involves a change in the energy state. If the process in gas and liquid state is the same then:

$$\tilde{P}_g = \tilde{P}_l \qquad \ldots\ldots 5.32$$

where $\tilde{P}_g$ and $\tilde{P}_l$ represents the probability of energy transfer taking place in the gas and liquid phase, respectively.

As τ is the quantity which is directly obtainable from ultrasonic experiments, one must evaluate $\tilde{N}$ in order to determine $\tilde{P}_l$ so that the gas and liquid values can be compared. The problem that arises in attempting to evaluate $\tilde{N}$ is whether it is wise to apply gas theories to liquids. However, one has got to persue a theory in order to obtain approximations to the experimental results.

$\tilde{N}$ can be obtained from the following expression:

$$\tilde{N} = V_c/l_f \qquad \ldots\ldots 5.33$$

where V_c is average velocity of the molecules in the liquid phase and l_f is the mean free path in the liquid.

The evaluation of l_f is not simple because in liquids the volume of the molecules itself is an appreciable part of the volume which the liquid occupies. Thus in order to calculate mean free paths one must calculate a value for the "free volume".

The concept of free volume which is the volume available in a cell for the centre of a molecule to move about, has already been discussed in Sections 5.1-5.10. In addition to the three models, (cell, hole and tunnel), Eyring and Hirschfelder[127] proposed a cell model for dense gases and liquids. They

considered the molecules as rigid spheres of diameter σ, and that all the molecules are fixed but one, which is allowed to move freely, the "wanderer", around in the cell made up of six nearest neighbours. If molecules occupy the lattice points of a cubic lattice, the distance between the centres of the molecules would be given as;

$$R = (V/N)^{1/3} \qquad \ldots\ldots 5.34$$

where V is the volume the liquid occupies, N is the number of molecules in that volume and R is the distance between the centres of the molecules. It can be seen that from the centre of the "wanderer" molecule it is free to move a distance:

$$l_f = 2R - 2\sigma = 2\,(V/N)^{1/3} - 2\sigma \qquad \ldots\ldots 5.35$$

l_f is the mean free path of the molecule as given by the cell model. Several other methods[128-133] are now available for the estimation of the mean free paths.

The pressure dependance of the relaxation time τ, allows a test of equation (5.35). Combining equations (5.31) and (5.35), one obtains the following expression for the pressure dependance of τ:

$$\tau_p/\tau_o = \frac{l_{fp}}{l_{fo}} = \frac{(V_p/N)^{1/3} - 2\sigma}{(V_o/N)^{1/3} - 2\sigma} \qquad \ldots\ldots 5.36$$

where τ_p and τ_o, l_{fp} and l_{fo}, V_p and V_o are the values of the pressures at pressure P and atmospheric pressure, P_o, respectively. The only problem remaining before comparing this expression with experiment is to know σ, the effective diameter of the molecule.

Litovitz[134] performed experiments on CS_2 at various pressures and obtained values of τ_p/τ_o. The results were then correlated using Eyring and Hirschfelder's model. He used σ, the effective distance of CS_2 as 4.32Å, in comparison to Eyring and Hirschfelder's theoretical value of 4.44Å. The results, as presented in Table 5.2, give good agreement between the experimental and theoretical values of τ_p/τ_o at various pressures. In addition, the probability $\tilde{P}$ evaluated from the experimental values of τ in the gas and liquid state by using equations (5.31) and (5.32) for CS_2 at 298°K are found to be 1.49×10^{-4} and 1.03×10^{-4}, respectively. This unusual agreement suggests that a change in state has very little effect on the fundamental mechanisms of the energy transfer processes.

In conclusion, it appears that the theory for binary collisional processes[80,88] as a mechanism, for thermal relaxation phenomena, appears to be a good one. However, a more refined value of the finite size of the molecule would give even a better account of thermal vibration relaxation process, on the basis of collisional processes in dilute gases, dense gases and in liquids.

P Kg/cm^2	τ_p/τ_o (theoretical) $\sigma = 4.32$	τ_p/τ_o observed
1	1.0	1.0
500	0.83	0.87
1000	0.67	0.65

Table 5.2: Pressure dependance of vibrational relaxation time of carbon disulphide

5.15 Isomeric Relaxation

Molecules of certain chemical compounds can exist in two different geometrical forms possessing different energies. The two forms are known as isomers and both arise from a rotation of groups about the vallence bonds.

When an acoustic wave is propagated the accompanying pressure and temperature changes perturbs the equilibrium in a manner which causes a change in the relative amounts of isomers. This is as a consequence of absorption of acoustic energy which causes a relaxation from one isomeric form to the other. The relaxation times involved here are much longer than those in vibrational relaxation and are of the order of 10^{-6} seconds.

Karpovich and Lamb[88,135] showed the existence of isomeric relaxation. An example of this type of loss is found in esters such as methyl acetate and ethyl acetate as shown in Figure 5.5. The absorption here, is thought to be due to a perturbation of the relative concentrations of molecules in the two planar configurations;

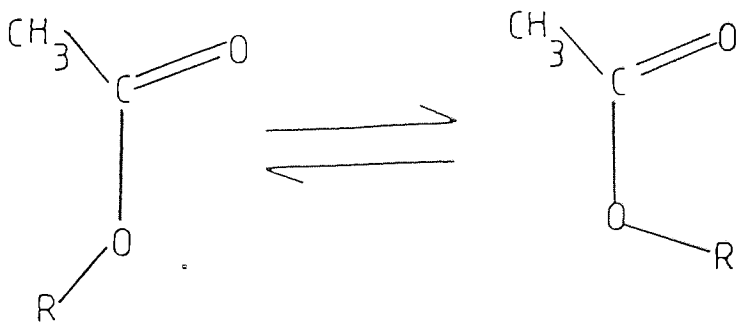

where R is either a CH_3 or C_2H_5 group.

Figure 5.5: The two different states of methyl and ethyl acetate

If one reflects on the process by which relaxation takes place one must think of the possible routes for the transfer of energy. For this one may visualize the following two possible routes:

(1) The energy can be transferred directly from the translational energy of the system by a collisional process. In this case the relaxation time would be sensitive to the type and number of collisions. For example, raising the pressure and squeezing molecules closer together, thereby reducing the effective free volume, as discussed in Section 5.12, should shorten the relaxation time as in CS_2.

(2) A second possible source of energy is through coupling with other internal degrees of freedom of the molecule, such as vibrational modes. Collisions that excite the vibrational modes (although the relaxation times are usually quite short compared to the rotational isomeric times) can transfer its energy to the isomeric forms, thereby perturbing the equilibrium between the two states.

The second mechanism of energy transfer should be independent of the number of collisions per second and of the pressure.

A mathematical expression for the relation between the relaxation frequency, and the relative population of the two states, can be expressed as follows: consider a two state equilibrium as described by equation 5.37:

$$A \underset{k_{21}}{\overset{k_{12}}{\rightleftharpoons}} B \qquad \text{..... 5.37}$$

For a two state reaction of the type necessary for acoustic relaxation, the above equilibrium can be expressed as:

$$\frac{dn_2}{dt} = k_{12}\, n_1 - k_{21}\, n_2 \qquad \text{.....5.38}$$

where n_1 and n_2 are the fraction of molecules (expressed in gram molecular weight) in state one and two respectively, k_{12} and k_{21} are the rate constants for the translations 1 to 2 and 2 to 1 respectively and t is the time.

At equilibrium the relative population in the two states is given by:

$$n_2/n_1 = k_{12}/k_{21} = \frac{\exp(-\Delta E_1/RT)}{\exp(-\Delta E_2/RT)} = \exp(-\Delta E/RT) \quad \ldots\ldots 5.39$$

where ΔE is the difference in activation energy between the two states, R is the gas constant and T is the absolute temperature.

The relaxation frequency may be expressed[80,135,136] in terms of reaction rate and energy parameters as;

$$f_c = \frac{(k_{12} + k_{21})}{2\pi} \quad \ldots\ldots 5.40$$

For most practical cases, $k_{21} >> k_{12}$, so expression 5.40 becomes:

$$f_c = \frac{k_{21}}{2\pi} \quad \ldots\ldots 5.41$$

5.16 Structural Relaxation

Sound absorption in some liquids,where relatively large intermolecular forces exists, results in relaxation due to volume changes and not a temperature change. To visualise this more clearly consider a sound wave with an alternating compression of low frequency. In this case the volume fluctuations are able to remain in phase with the applied pressure variations by the flow of liquid molecules between positions of high and low density. As the compressional frequency increases, the liquid structure is not able to adjust itself to the pressure variations sufficiently quickly. Thus this results in structural relaxations.

If structual relaxation is as a direct result of volume changes, then some concept of structure, or at least a degree of order, must be visualized. This order could be similar to the solid phase of a substance, but over a very short range. Furthermore, if this short range order is incomplete and many neighbours are missing, that is to say there are "holes" present in the liquid lattice, as described in the hole theory (see Section 5.6), the liquid can naively be thought of as small crystalline groups continuously breaking and forming.

The variations in temperature and pressure accompanying a sound wave, will cause changes in the degree of order present in a liquid. The concept here is that the molecules of the liquids under the influence of acoustic pressure wave will "flow" into lattice positions so as to increase packing by occupying the holes or vacancies in the liquid. The "flow" or structural rearrangement process takes a finite time and thus the volume changes in the liquid are out of phase with the pressure.

If one considers the compressibility K_o of a liquid, one finds that it is roughly composed of two parts:

$$K_o = K_{relax} + K_\infty \qquad \ldots\ldots 5.42$$

The first term, K_{relax}, involves the flow of molecules from one lattice site to another (ie. changes in lattice structure) and this takes a finite time. The second term, K_∞, involves simply a decrease in the liquid lattice spacings and is for most purposes instantaneous.

If one compresses a liquid in times which are short, compared with the times necessary for structural changes or rearrangements, one can measure the compressibility, K_∞, at high frequencies. Conversely at low frequencies, where the structural changes are able to remain in phase with the pressure variations, as at low frequencies, the compressibility K_o, can be obtained. In this manner, one can

investigate certain properties of the liquid, which are due only to the existence of its lattice. These are termed as the solid-like properties of a liquid.

The frequency dependence of the compressibility of a liquid[80,137,138] can be expressed in the form of equation 5.43, if a single relaxation time is present.

$$K = K_{\infty} + \frac{K_{relax}}{1 + \omega^2 \tau_v^2} \qquad \ldots\ldots 5.43$$

In the above equation, τ_v represents structural or volume relaxation time.

A development of structural relaxation in terms of molecular quantities has been accomplished by Hall[137]. He showed that ultrasonic energy changes, due to the structural relaxation process (which is a non-thermal process), could be expressed in terms of the absorption per wavelength ($\alpha\lambda$). This is expressed as:

$$\alpha\lambda = \frac{\pi K_{relax}}{K_o} \frac{\omega\tau_v}{1 + \omega^2 \tau_v^2} \qquad \ldots\ldots 5.44$$

where τ_v, is the structural relaxation time. At low frequencies ($\omega \tau_v << 1$), the above equation 5.44 reduces to equation 5.45.

$$\alpha\lambda = \frac{\pi K_{relax} \tau_v}{K_o} \qquad \ldots\ldots 5.45$$

To calculate K_{relax} and τ_v, Hall suggests that there are two types of packings in which the molecules can exist. One, state one is characterized by a smaller volume and a lower free energy, and the other state by an open packing with a larger volume and higher free energy. If one now considers water as a system, then the first state involves a closed packing system with twelve nearest neighbours, and the second state has four nearest neighbours tetrahedrally arranged about the central water molecule.

Using this two state theory, he showed that:

$$K_{relax} = \frac{V}{RT}\left[\frac{\Delta V}{V}\right]^2\left[\frac{e^{-\Delta F/RT}}{(1+e^{-\Delta F/RT})^2}\right] \qquad \text{..... 5.46}$$

and that

$$\tau_v = \frac{kT}{h}\exp\left(\frac{-\Delta F^*}{RT}\right)\left[1+\exp\left(\frac{-\Delta F}{RT}\right)\right] \qquad \text{..... 5.47}$$

where ΔV is the difference in volume between state one and state two only, ΔF^* is the activation free energy for this process and is assumed to be the same as for shear viscosity, ΔF is the difference in free energy of the two states and is chosen by fitting the data at zero degrees centrigrade. This theory has been tested by measuring the sound absorption as a function of pressure[139]. From thermodynamics, one finds that the pressure part of ΔF, is simply $P\Delta V$. Thus knowing or assuming the value of ΔF at atmospheric pressure one can predict ΔF at any other pressure (eg. $\Delta F_p = \Delta F_{atmos} + P\Delta V$). Knowing this, values for sound absorption can be calculated as a function of pressure.

5.17 Impurity Effects

In this section, the effects of the presence of impurity molecules on the environment in a pure liquid will be discussed.

Consider two separate liquids composed of molecules A and B respectively. From equation 5.31, the relaxation time for a pure liquid can be expressed as:

$$[\tau_{pure}]^{-1} = \tilde{N}_{AA}\tilde{P}_{AA} \qquad \text{..... 5.48}$$

where $\tilde{N}_{AA}$ represents the number of collisions between A molecules, $\tilde{P}_{AA}$ is the probability of transfer of energy during collision of A-A molecules

If liquid B is now mixed with liquid A, the relaxation time for the "impure" liquids can be expressed as:

$$[\tau_{impure}]^{-1} = \tilde{N}_{AA}\tilde{P}_{AA} + \tilde{N}_{AB}\tilde{P}_{AB} \qquad \text{..... 5.49}$$

or alternatively:

$$[\tau_{impure}]^{-1} = (1 - x)\frac{1}{\tau_{AA}} + x\frac{1}{\tau_{AB}} \qquad \text{..... 5.50}$$

where $\tilde{N}_{AB}$ is the number of collision per sec of unlike molecules (AB), P_{AB} is the probability of energy transfer during a collision of A molecule and the impurity molecule B, x is the mole fraction of impurity B molecules, and τ_{AB}, is the vibrational relaxation time for A-type molecules surrounded by B type molecules.

If a collision between AB molecules is much more effective than between AA molecules, then the presence of a few impurity molecules (in this case, B represents the impurity molecules) can significantly affect the relaxation frequency.

Another way of interpreting the above theory, is to consider the effects of impurities in terms of energy losses. When two liquids are mixed, each of which separately exhibit a thermal loss due to vibrational relaxation, then in the mixture, the presence of unlike molecules can cause the relaxation time to be less than in the pure liquids. This would be so if the collisions of unlike molecules were more effective than those of like molecules in producing energy transfer. In this case, each species acts as an impurity for the other. Because of this, a minimum will be observed in the relaxation time at some intermediate concentration of the mixture. Since the absorption is proportional to the effective relaxation time in the mixture, the absorption coefficient will exhibit a minimum at this concentration. Figure 5.6 shows the effect for a solution of benzene in carbontetrachloride[140]. In this case the main cause of absorption is vibrational relaxation.

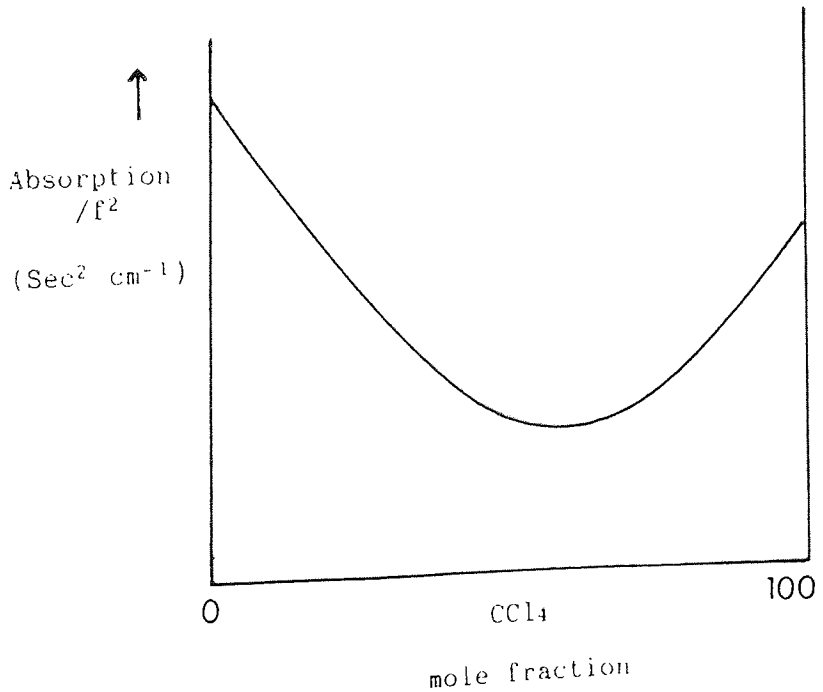

Figure 5.6: Ultrasonic absorption in mixtures of benzene and carbontetrachloride

In some mixtures a maximum is observed for absorption as a function of concentration. This is due to a structural relaxation effect involving unlike molecules. For example, if liquids A and B each are composed of molecules which tend to associate, then, upon mixing there will be a tendency to form some structural aggregate composed of A and B molecules. The presence of the sonic wave perturbs this AB structure in much the same way as it perturbs the AA or BB structure in the pure liquid. An example of this is ethanol/water mixture. Figure 5.7 shows sound absorption in ethanol/water system with increasing alcohol concentration[141].

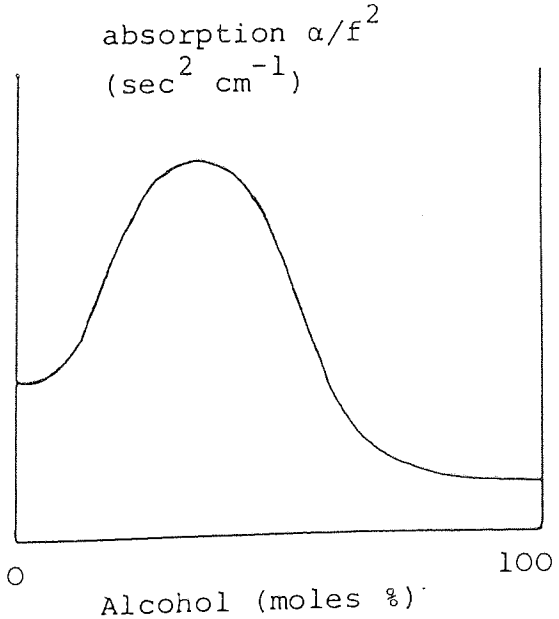

Figure 5.7: Sound absorption in ethanol/water mixture

Liquid mixtures which exhibit relaxation times which are independent of environment (eg. rotational isomeric relaxation), show that the value of absorption decreases without exhibiting a minimum or maximum. This is due to dilution of the number of absorbers (ie. molecules per cubic centimeter exhibiting rotational isomersion). An example of this is crotonaldehyde mixed with n-Hexane[142] as shown in Figure 5.8.

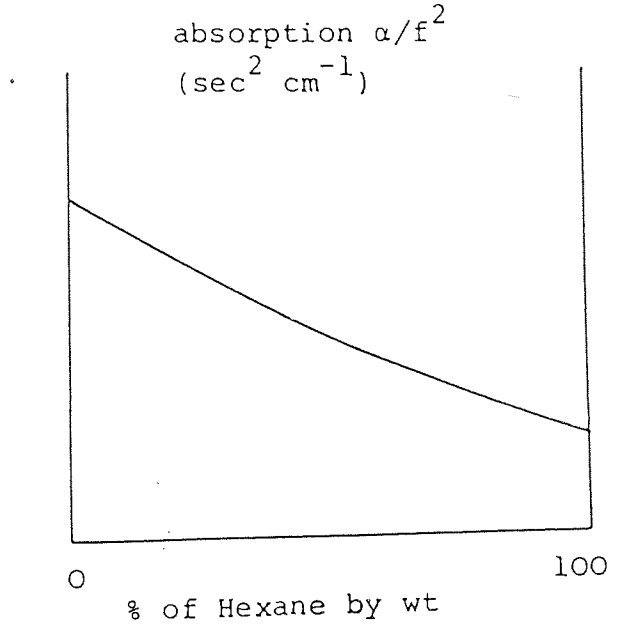

Figure 5.8: Sound absorption in crotonaldehyde n-Hexane

5.18 Crude Mathematical Model for the Effect of Ultrasound on Molecular Rotation

In this section, a crude approximation of the amount of ultrasonic energy required to rotate a molecule is presented. The model does in no way take account of factors such as intermolecular forces which holds the molecules together to form a liquid, the degrees of freedom a molecule would possess in terms of translational and vibrational motions, effects of viscosity, size, shape and symmetry of molecules, and the energy lost during molecular collisions. Although it is implicitly recognised that the total ultrasonic energy delivered into a liquid sample does not go directly into giving molecules energy for rotation the following derivation does, however, provide an approximation for the amount of power required to cause the molecules to rotate.

Consider a loaded stick model for ultrasonic molecular rotation, as shown in Figure 5.9 in which m represents the mass of a molecule of length, x, and M represents the mass of an added heavy atom at one end, such that M is a integral of the m.

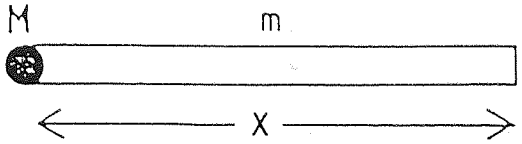

Figure 5.9(a): A loaded stick model

An example of this is 4-bromo-azobenzene, as shown in Figure 5.10 where the bromine atom acts as a mass of the added heavy atom at one end.

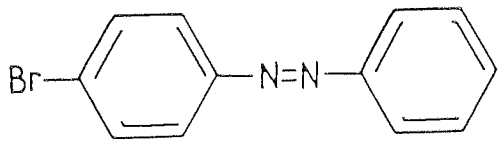

Figure 5.10: Structure of 4-bromo-azobenzene

In order to relate the rotational motion of a molecule to the amount of ultrasonic energy necessary for this type of motion, an expression relating the moment of inertia, I, to its angular acceleration, $\ddot{\theta}$, must first be obtained. This can then be related to the power delivered by the ultrasound. Consider the model as shown in Figure 5.9(b) as a basis for calculating the required relationship.

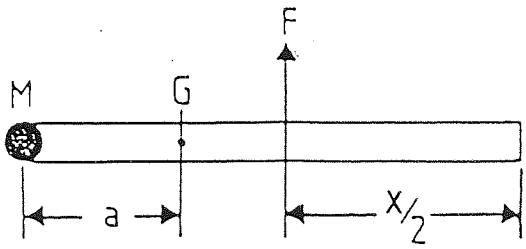

Figure 5.9(b): Showing loaded stick model with its centre of gravity G and a force F

In order to get rotation, the molecule will have to rotate about its centre of gravity. If F is the force which acts at right angles to the molecular axis, and at the centre of the molecule, (not the centre of gravity), then taking moments about G:

$$Ma = m\left(\frac{x}{2} - a\right) \qquad \text{..... 5.51}$$

Through mathematical manipulation, the equation reduces

$$Ma + \frac{ma^2}{2x} = \frac{m}{2x}(x - a)^2 \qquad \text{..... 5.52}$$

$$\text{if } nm = M \qquad \text{..... 5.53}$$

then equation 5.53 becomes;

$$nma + \frac{ma^2}{2x} = \frac{m}{2x}(x - a)^2 \qquad \text{..... 5.54}$$

which reduces to:

$$a = \frac{x}{2(n + 1)} \qquad \text{..... 5.55}$$

Equation 5.55 gives a relationship between a, x and n, a factor of mass of molecule.

Squaring equation (5.55) gives:

$$a^2 = \frac{x^2}{4(n+1)^2} = a^2(n+1) = \frac{x^2}{4(n+1)} \qquad \text{..... 5.56}$$

Multiplying (5.55) with x, gives:

$$ax = \frac{x^2}{2(n+1)} \qquad \text{.....5.57}$$

Taking moments of inertia I about G gives:

$$I = \int_0^a \rho x^2 dx + \int_0^{x-a} \rho x^2 dx + Ma^2 \qquad \text{..... 5.58}$$

Integrating the above equation and assuming that the density ρ of the stick is equal to m/x and not m/x^3, that is, the stick has no thickness, and also substituting for $M=nm$ gives:

$$I = m\left(\frac{x^2}{3} + a^2 - ax + na^2\right) \qquad \text{..... 5.59}$$

Substituting equation 5.56 and 5.57 into equation (5.59) gives;

$$I = m\left(\frac{x^2}{3} + \frac{x^2}{4(n+1)} - \frac{x^2}{2(n+1)} + \frac{nx^2}{4(n+1)^2}\right) \qquad \text{..... 5.60}$$

$$= mx^2\left(1/3 - 1/4(n+1)\right)$$

The equation of rotational motion is given as $I\theta$, and this can be equated as:

$$I\ddot{\theta} = F\left(\frac{x}{2} - a\right) = F\,\frac{x}{2}\left(\frac{n}{n+1}\right) \text{ (by substituting 5.55).} \qquad \ldots\ldots 5.61$$

Substituting equation 5.60 into 5.61 gives:

$$\ddot{\theta} = \frac{F}{mx^2} \; \frac{\frac{x}{2}\left(\frac{n}{n+1}\right)}{\left(\frac{1}{3} - \frac{1}{4(n+1)}\right)}$$

$$= \frac{F}{2mx} \; \frac{3n}{(n + 1/4)} \qquad \ldots\ldots 5.62$$

For a reasonable effect n should be about 1/4. Thus by assuming various values of n,

the factor $\dfrac{n}{(n + 1/4)}$ would give;

n	$\dfrac{n}{n + 1/4}$
0.1	0.286
0.2	0.444
0.25	0.5
0.3	0.545
0.4	0.615
0.5	0.666

Thus if n = 1/4 (ie. 1/4 of the mass of the molecule) then

$$\ddot{\theta} = 3/4\left(\frac{F}{mx}\right) \qquad \ldots\ldots 5.63$$

The force exerted on a molecule of a similar size to the stick model can be obtained substituting mx for the force F, where m is the mass of the molecule and x is the linear acceleration, equation (5.63) can be expressed as:

$$\ddot{\theta} = \left(\frac{3}{4x}\right) \ddot{x} \qquad \text{..... 5.64}$$

and angular velocity θ is related linear velocity x as:

$$\therefore \dot{\theta} = \frac{3}{4l} \dot{x} \qquad \text{..... 5.65}$$

For an acoustic wave of intensity w (watts m^{-2}), this is related to the density, ρ, of the medium under investigation, the acoustic velocity, c, and the linear velocity, q, with which the particle is moving in the form[81,82]:

$$\rho c q^2 = w \qquad \text{..... 5.66}$$

In this case $q = \dot{x}$. Thus combining equation 5.65 and 5.66, a relation between the angular velocity and acoustic power is obtained. This can be expressed as:

$$\dot{\theta} = \frac{3}{4} \frac{1}{x} \left[\left(\frac{w}{\rho c}\right)\right]^{1/2} \qquad \text{..... 5.67}$$

In order to approximate w, a value of ρc for water (1.5×10^6 kg m^2 s^{-1}) is used, and a bond length of 0.2nm from which x is approximated as 1nm. Thus:

$$\dot{\theta} = \frac{3}{4} 10^9 \left(\frac{1}{1.5 \times 10^6}\right)^{1/2} w^{1/2} \qquad \text{..... 5.68}$$

To express the angular velocity θ, in terms of the angle movement (in radians)

$$\text{If } \theta = \frac{1}{j\omega}\dot{\theta} \qquad \text{..... 5.69}$$

Thus at 1MHz $\omega = 2\pi \times 10^6$ radians^{-1}, θ is:

$$\theta = \frac{3}{4}\,\frac{10^9}{2\pi \times 10^6}\,\frac{1}{1.22 \times 10^3}\sqrt{w} \qquad \text{..... 5.70}$$

For $\theta = 1$ radian

$\sqrt{w} = 10.22$
$w = 104.46$ watts

Thus, the amount of power delivered per unit area can be expressed as 104.46 w m^{-2} (0.01 w cm^{-2}). This result suggests that sound waves with an acoustic power of approximately and as low as 0.01 w cm^{-2} is sufficient to rotate a molecule through one radium.

Throughout this chapter various theories and models have been presented to account for and understand the absorption of sound inliquids. With this understanding, the following Chapter Six discusses its implication and the effects it would have an NMR spin-lattice and spin-spin relaxation times for systems which are subject to ultrasound and at the same time investigated by NMR.

CHAPTER SIX

SOUND ABSORPTION IN LIQUIDS (II)

NOMENCLATURE

η	Ratio of the acoustic transition probability in the liquid state to the acoustic transition probability in the solid state.
α_n	Absorption coefficient. It is the ratio of power per unit volume absorbed from the ultrasonic wave by the nuclear spin system to the acoustic power per unit area introduced into the sample.
ε	Relative deformation (strain) of the liquid produced by sound waves
$g(\omega)$	Form factor. It provides information related to the probability of transition of a nuclear spin and the absorption of energy under the influence of a periodic interaction induced by sound waves passing through the medium.
P_o	Hydrostatic pressure
P_A	Maximum amplitude of acoustic pressure
P_K	Blake threshold
σ	Surface tension of the liquid

6.0 Introduction

This chapter is divided into two parts. The first half discusses and examines two important and entirely separate techniques using sound waves. These two techniques are known as acoustic nuclear magnetic resonance (ANMR) and acoustic cavitation. The aim, through these discussions is to provide several interesting concepts and ideas. For example, it will lead further into the theoretical treatment of the effects of sound in liquids, afford information on types of instruments necessary to perform the experiments proposed, induce ideas and aid the design of the types of experiments and experimental procedures, and more importantly to elucidate areas where caution is necessary when interpreting the results obtained.

In the second half, the aim is to combine the first five chapters including the first part of this chapter and discuss the original hypothesis on which this research is based, which is, can sound be used to purturb natural molecular motion in the liquid phase and detect such effects via changes in NMR relaxation times.

6.1 Nuclear Acoustic Resonance

This section discusses the use of sound waves (also referred as acoustic waves) to excite nuclear spins. The technique is known as acoustic nuclear magnetic resonance (ANMR). The technique has similar principles implicit in a conventional NMR experiment but instead of using a radio-frequency (rf) field, sound (in the Megahertz region) is used to exicte nuclear spins. The theory and experimental evidence for ANMR will be presented with particular attention being paid to acoustic quadrupolar resonance and acoustic nuclear magnetic resonance in liquids.

In ANMR, the energy exchange or the internal interaction capable of coupling energy between the acoustic wave and the nuclear spin system takes place

through the periodic modulation of the following;

(i) Magnetic dipole-dipole interaction between neighbouring spins.

(ii) Dynamic electric quadrupole interactions. The nuclear electric quadrupole moment of a nuclear spin system is effected by changes in the electric field gradient.

(iii) Hyperfine interaction between electron and nuclear spins in paramagnetics arising from covalent mixtures.

(iv) Hyperfine interactions between electron and nuclear spins in ferromagnetic fields at the nucleus arising from indirect d-d orbital coupling through s-d orbital exchange polarisation.

(v) Interaction of nuclear magnetic moment with the small radiofrequency magnetic field associated with a transverse acoustic wave propagating in a metal

If the periodic modulation frequency of these interactions (which is at the same frequency as that of the acoustic wave) coincides with the Larmor precessional frequencies of the spins, then a strong resonant absorption can occur. For a detailed treatment of these interactions as well as the treatment of ANMR, the reader is referred to several books and reviews[8,83,88,143-148].

In order for interaction between nuclear spins and the acoustic wave to occur, several other general conditions must be satisfied of which the most prominent are:

(i) Conservation of energy; the frequency ν, of the wave must satisfy $E = h\nu$, where E is the energy difference of the levels between which the transitions are considered, so that ν must be a resonant frequency.

(ii) Selection rules; the matrix element corresponding to the transition must be different from zero. This requirement restricts ultrasonically

induced transitions to change $\Delta m = \pm 1$ and $\Delta m \pm 2$.

(iii) There must be a sufficient net number of spins in the lower energy state in order to have a reasonable probability that some of these spins will make transitions to a higher energy state under the influence of the ultrasonic wave.

The mechanism that permits fulfillment of the third condition is of particular interest because it is directly related to the mechanisms considered in ultrasonic absorption. Indeed, the foremost process by which a sufficient supply of spins in the lower energy state is assured consists of the interaction of the spins with thermal energy. This interaction tends to restore thermal equilibrium that is disturbed by the transition of spins from lower to higher energy states.

In the case of an acoustic wave, fluctuations in the magnitude of internal interactions due to acoustic energy, provides a relaxation mechanism by means of which the exicted spins give up their energy to the surrounding lattice. For any one of these internal interactions, two forms of coupling energy between the spin system and acoustic energy have been found to be important[149,150]. The first form consists of direct spin transitions, accompanied by the absorption (or emission) of acoustic energy having a resonant frequency. The second form consists of an indirect or Raman-type process. This involves two acoustic energies having frequencies ν_{L1} and ν_{L2} well in excess of the resonant frequency ν_o. One half of the acoustic energy is absorbed by the spin system and another frequency modified by ν_o, is emitted. Conservation of energy then requires, $\nu_{L1} - \nu_{L2} = \pm 2$ ν_o. If a net de-excitation of nuclear spins, leading towards thermal equilibrium can be produced by thermal acoustic energy then the inverse process of a net absorption of energy by a nuclear spin system from an ultrasonic wave, should also be possible. This general reasoning led Kastler[151] and Altshulter[152,153] to

propose that ultrasonic attenuation due to interactions of the acoustic waves with nuclear spins should be observable.

Figure 6.1 shows a comparison of conventional NMR and acoustic excitation of nuclear spins.

From an experimental point of view, two approaches to making measurements have been followed. The first approach consists of attempting to measure directly the attenuation of an ultrasonic beam at a given frequency as a function of a static magnetic field strength (applied externally). When the magnetic field reaches a magnitude such that the splitting of the nuclear spin energy levels corresponds to the ultrasonic frequency an increase in the attentuation occurs. This experimental approach is analogous to the conventional NMR, the ultrasonic wave having replaced the alternating magnetic field of the same frequency. The major experimental difficulty of this method comes from the smallness of the absorption. The amplitude absorption coefficient is approximately 10^{-6} or less and the ultrasonic methods commonly used are not suitable for measuring such coefficients less than about 10^{-3}. Consequently, very elaborate methods need to be used for measurements of such attenuation[154]. The second method consists of measuring the effect of an ultrasonic wave indirectly. This involves measuring the saturation effects. When an alternating r.f. magnetic field of an appropriate frequency is applied to the sample under investigation in the presence of a static magnetic field, the resulting normal NMR resonance signal is observed before saturation is reached. Subsequently, an ultrasonic wave of the same frequency is also introduced and causes additional upward spin transitions to occur, thus leading to a decrease of the spin population in the lower level. The alternating r.f. magnetic field then "sees" a smaller population from which transitions can take place. If the amplitude of the ultrasonic wave is high enough, it will effectively produce saturation. The power absorbed by the nuclei will decrease, and the resonant NMR signal initially observed in the absence of the ultrasonic wave will also decrease. One thus observes the

(1) Nuclear magnetic resonance.

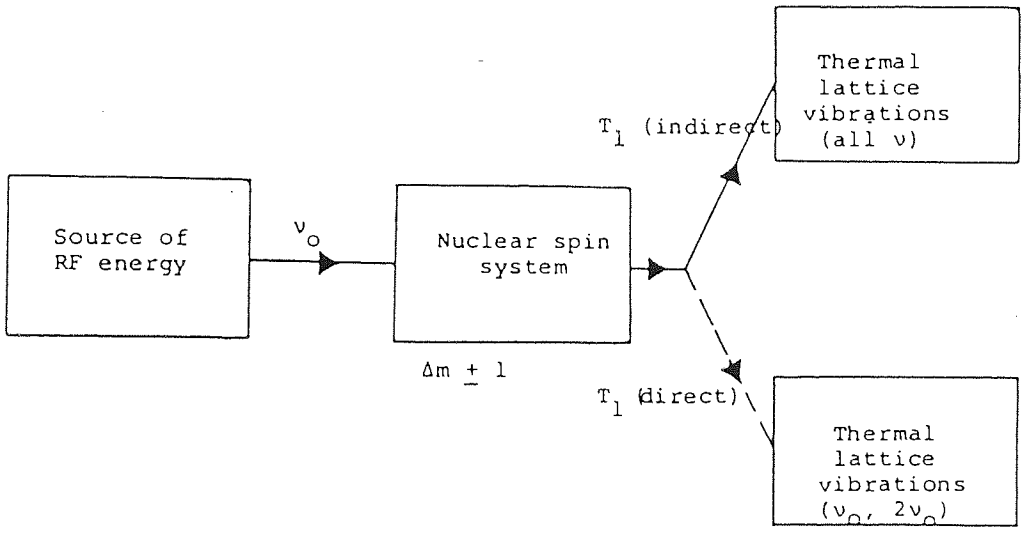

(2) Acoustic Nuclear spin-sound (phonon) absorption.

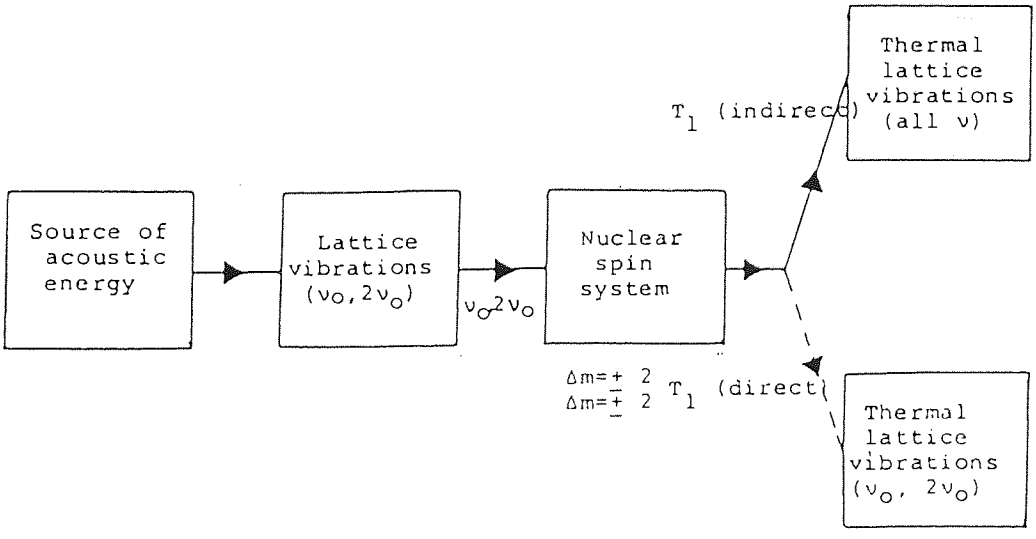

Figure 6.1: A comparison of conventional NMR and acoustic excitation of nuclear spins. The mechanism of excitation differ markedly; the relaxation processes, however are the same.

effect of the ultrasonic wave by measuring the intensity of the NMR signal as a function of the ultrasonic amplitude[154,155].

6.2 Coupling through Electric Quadrupole Moment

Among the interactions whose modulation by acoustic waves causes transitions between nuclear spin levels, is one involving the nuclear electric quadrupole moments, and the electric field gradients produced by the acoustic wave.

The nuclear electric quadrupole interaction can be expressed as:

$$H = Q:\nabla E \qquad \text{..... 6.1}$$

where Q, is the nuclear electric quadrupole moment and ∇E, is the electric field gradient.

The coupling of acoustic energy to the nuclear spin system is accomplished by the time-varying field gradients resulting from the action of an externally induced acoustic wave so that the effect of the acoustic wave is to create a time-varying strain in the locality of the nucleus. If the field gradient is now expanded to second order three terms relating to the strain produced are obtained. These are, a constant term which represent a static field gradient in the absence of strain, a linear term in the strain component which represents a direct spin-acoustic energy coupling and a quadratic term in the strain components which represents the indirect or Raman type interactions[83,88,144,156]. Thus,

$$q = q_o + q_1 \varepsilon + \frac{1}{2} q_2 \varepsilon^2 \qquad \text{..... 6.2}$$

where ε, represents the peak strain caused by the longitudinal acoustic wave.

The above three terms have been explained in terms of their effects on spin-transitions.

Indeed, the great bulk of work that is reported in the literature on ANMR is in materials with quadrupolar nuclei[83,88,157-162]. The reason for this lies in

the ratio of the electric quadrupole energy to the magnetic dipole interaction energy which is of the order e^2Q/μ^2, where e, is the charge on the electron and μ is the nuclear dipole moment. This ratio is generally between 10 and 10^3 in magnitude and so the effect of the quadrupole interaction will always be greater than that of the magnetic dipole-dipole interaction. Resonant transitions via dynamic electric quadrupole coupling can occur at both the Larmor frequency (called $\Delta m = \pm 1$ transitions) and twice the Larmor frequency ($\Delta m = \pm 2$).

6.3 ANMR in Liquids

A considerable controversy remains in the literature on whether it is possible to carry out ANMR in liquids[147,152,167-174]. Kessel[147,163] discusses the possibility of ANMR in inviscid liquids. The arguments presented are that both quadrupolar and dipolar interactions depend on a random vector that has zero mean and is characterised by a correlation time, τ. By straight forward reasoning the acoustic transition probability for a given substance in the liquid state, denoted by P_l is related to the acoustic transition probability for the same substance in the solid state, P_s by:

$$\eta = \frac{P_l}{P_s} = \frac{\tau}{T_2} \qquad \ldots\ldots 6.3$$

Thus, if $\tau = 10^{-11} - 10^{-12}$ seconds, and η is very small, then ANMR is not observable.

Iolin[166-168] suggested two mechanisms which would lead to the observation of narrow ANMR lines in liquids when they have a low and finite viscosity. The first, is a reorientation of the axis of an anisotropic molecule under the influence of the sound wave, and the second, is a modulation of the scaler

spin-spin interaction between nuclei in the same molecule. In both cases, the effect of the sound wave is proportional to the high-frequency shear modulus of the material. For aqueous solutions the high-frequency shear modulus parameter is taken to refer to the solute molecules rather than to the solvent. Iolin estimated that these effects should lead to an ANMR absorption coefficient α_n of the order of 10^{-4} cm^{-1} for longitudinal waves. The absorption coefficient, α_n, represents the ratio of power per unit volume absorbed from the ultrasonic wave by the nuclear spin system to the acoustic power per unit area introduced into the sample.

Alekseev and Kopvillem[169] showed that an acoustic wave could modulate the amplitude of spin-echoes even if the sound frequency was not at resonance with the Larmor precession frequency. Their argument is as follows; in the presence of sound, the state of the liquid is altered as the molecules perform, in addition to the Brownian motion, motion induced by the variation in sound pressure. The details of motions are irrelevant to the spins but the power spectrum density of the motion at resonant frequency J (ω) is crucial for ANMR excitation. Thus, ANMR may be distinguished from the Brownian excitation if $J(\omega)_{Br} < J(\omega)_{ANMR}$. In the simplest case this is:

$$\varepsilon^2 g(\omega) > 2\tau_c/(1 + \omega^2 \tau_c^2) \qquad \ldots\ldots 6.4$$

where τ_c, is the correlation time, ε is the relative strain of the sound wave and $g(\omega)$ is the form factor of the ANMR line. The form factor $g(\omega)$ comprises information related to the probability of transition of a nuclear spin and the absorption of energy, both under the influence of a pure periodic interaction induced by sound waves

passing through the medium[147]. If τ_c and $g(\omega)$ are approximately 10^{-12}s and 10^{-4}s respectively, then a strain of approximately 10^{-4} is required in order to observe ANMR.

An ANMR experiment was performed on H_2O: $CuSO_4$. $5H_2O$ for protons in water at 16 MHz, with a sound frequency 2.1 MHz and at power level of $72W/cm^2$. A 7% sound amplitude modulation effect was observed through which they concluded that it was possible to carry out ANMR at a lower sound frequency than the Larmor resonant frequency.

Finally, if the liquid has a finite conductivity, the sound wave will induce time-varying currents which in turn produce time-varying magnetic fields and cause nuclear transitions. The effect is called the dynamic Alpher-Rubin effect[170] and has been shown to reduce spin-lattice relaxation times liquid gallium.

Further experimental evidence to confirm that ANMR exists in liquids was presented by Bowen[164,165] and Antokol'sikii et al[171]. Bowen found acoustic saturation of the NMR line, at resonant frequency in an aqueous colloidal solution of As_2S_3 with a reduction in T_1 from 1.8 seconds to 1.3 seconds, whereas in aqueous solution of NaCl and $CuSO_4$, and various other organic liquids no effect was observed. Antokol'skii et al observed strong acoustic paramagnetic resonance from Fermy's salt in aqueous solution.

6.4 Acoustic Cavitation: Introduction

Cavitation is defined as the formation of one or more pockets of gas or "cavities" in a liquid. The word "formation" refers to both the creation of a new cavity or the expansion of a pre-existing one to a size where macroscopic effects can

be observed. The cavity's gas content refers to the liquid's vapour, some other gas, or combination thereof. Sometimes these cavities are referred to as "bubbles" or "voids" depending on the relative amount and type of gas.

Cavity formation in response to an alternating pressure field (i.e., an acoustic field) is called acoustic cavitation. It also refers to bubbles being stimulated into motion by an acoustic field.

During the negative part of the acoustic cycle, when the local pressure falls below the ambient pressure, a preexisting bubble may begin to grow. When the acoustic pressure turns positive the bubble growth slows and is finally reversed. The degree of growth and collapse during a given acoustic cycle and the life time of the bubbles in the acoustic field depends on the acoustic pressure amplitude, the ambient pressure, the acoustic frequency and the characteristics of the liquid and dissolved gases. Several authors have characterised theoretically the phenomenon of cavitation from the treatment of bubble dynamics[175-196]. A brief mathematical treatment is given below.

6.5 Mathematical Treatment of Acoustic Cavitation

When an acoustic wave propagates through a liquid, the local pressure varies with time and space. If a bubble due to air or vapour pressure of liquid is present in the liquid, its radius will expand and contract in response to these pressure changes. For low amplitude pressure excursions, these bubble motions are periodic and may last for many acoustic cycles. This phenomenon is called stable cavitation. Under certain conditions, however, these bubble motions become irregular and lead to a rapid collapse of a bubble during a single acoustic half-cycle. This phenomenon is called transient cavitation.

Cavitation has been classified into two types: the stable and transient. Stable cavities are bubbles that oscillates radially about some equilibrium size and often persist for many acoustic cycles. Transient acoustic cavities, on the other

hand, exist for only one or two acoustic cycles and will expand to at least two or three times their original size during the negative acoustic pressure half-cycles before violently collapsing during a single compression half-cycle. During the final stage of collapse, the velocity of the liquid/gas interface approaches the speed of sound in the liquid and the temperature and pressure within the cavity will become enormous ($> 300^{o}$ and 10,000 bar, where 1 bar = 10^{5}P ~ 1 atm)[180-182]. Stable cavitation bubbles may sometimes grow by a process called rectified diffusion[175,176,179] and become transformed into transient bubbles. During the compressional phase of the acoustic cycle, the bubble will shrink causing gas to diffuse out of the bubble. During the rarefaction phase of the cycle, on the other hand, the bubble expands causing gas to diffuse into the bubble. Since the surface area is larger when the bubble expands, a net increase of gas in the bubble occurs. This process competes with the natural tendency for the bubble to shrink. For certain critical conditions which depends on bubble size, the intensity of ultrasound and the concentration of dissolved gas in the liquid, bubbles below the resonance size will grow to become transient bubbles. For example, the threshold intensity for bubble growth in water at 1 MHz is found to be about 6 mW/cm^{2} within a period of 10 msec[187]. Thus, transient caviation can therefore be regarded as a complex process that can be conveniently divided into three stages: nucleation, growth and collapse.

When an acoustic wave propagates through a liquid, the total external pressure P_t experienced by a microscopic volume element is composed of two parts, a hydrostatic part and a time varying part. Thus P_t may be expressed as:[178,180]

$$P_t = P_o + P_A \sin (2 \pi f t) \quad \ldots. 6.5$$

where P_o is the hydrostatic pressure (usually the atmospheric pressure), P_A is the maximum amplitude of the acoustic pressure and f is the frequency of the wave transmitted into the fluid.

P_A is related to the intensity I of ultrasound transmitted into the fluid

(defined as the energy transmitted per second per cm^{-2} of fluid). This can be expressed as:

$$I = P_A^2 (2\rho c)^{-1} \qquad \text{..... 6.6}$$

where ρ and c are the density and velocity of the fluid, respectively.

Noltingk and Neppiras[178] have shown that in order to produce a bubble of radius R, a critical pressure, P_k, referred to as the Blake threshold, must exceed the acoustic pressure, P_a ($P_a = P_A \sin(2\pi ft)$).

$$P_k = P_o + \frac{2}{3\sqrt{3}} \left[\frac{(2\sigma/R)^3}{P_o + 2\sigma/R} \right]^{1/2} \qquad \text{..... 6.7}$$

where σ is the surface tension of the fluid and R is the radius of the bubble.

For small bubbles to be produced, $2\sigma/R >> P_o$ and equation 6.7 can be expressed in the form:

$$P_k = P_o + 0.77 (\sigma/R) \qquad \text{..... 6.8}$$

These bubbles by the process of rectified diffusion are transformed into transient bubbles where they expand to a radius of at least twice their initial size before collapsing violently.

Noltingkand Neppiras[178], and Flynn[175,190] showed for an adiabatic collapse of the bubbles, the maximum pressure, P_{max}, and temperature, T_{max}, within a bubble at the moment of collapse can be expressed as:

$$P_{max} = P \left[\frac{P_t (\gamma-1)}{P} \right]^{\gamma/(\gamma-1)} \qquad \text{..... 6.9}$$

and

$$T_{max} = T_o \left[\frac{P_t (\gamma-1)}{P} \right] \qquad \text{..... 6.10}$$

where P is the pressure in the bubble at its maximum size, T_o is the ambient temperature of the liquid. They also showed that the maximum bubble radius, R_{max}, at the time of collapse can be related to the maximum temperature, T_{max}. This can be expressed as:

$$T_{max} = T_o (\gamma - 1) \left[\frac{R_{max}}{R_o} \right]^3 \qquad \text{..... 6.11}$$

where R_o is the minimum bubble size.

Results of calculations made by Flynn[178,190] predict that transient cavitation at 1MHz with a pressure amplitude of 6 bar, and at an average intensity of 24 W/cm^2, for a bubble filled with argon gas with an initial radius of 1μm will expand to a maximum radius of 7.4μm and then will collapse giving rise to a peak pressure of 28,000 bar and a maximum temperature of 10,000°K. Several authors[191,194] have reported similarly large pressure and temperatures to exist at low frequencies[191,194].

Bubble size depends mostly on the frequency of sound transmitted into the fluid. As the frequency is increased[184,195,196] the production of cavitation in liquids decreases. One explanation given for this is that, when the compression and rarefaction cycles are short, the finite time required for the rarefaction cycle is too small to permit a bubble to grow to a size sufficient to cause disruption of the liquid. Alternatively, if a bubble was produced during rarefaction, the time required to collapse that bubble may be longer than that available in the compression half-cycle.

6.6 Sonochemical Reactions

In studies of the chemical effects of ultrasound, one has to look primarily for the answer to the question, "Why do any chemical reactions occur when a system is irradiated with high intensity ultrasound?"

It has been established that the presence of gas or vapour bubbles in liquids that are subjected to ultrasound at sufficiently high sound intensity, will cause the bubbles to cavitate. The liquid serves as an efficient medium for carrying energy of high intensity sound wave from the source to the interfaces between the small bubbles and the liquid. In the adiabatic compression of a sound wave, the production of a high temperature is dependant upon the existence of a large difference between the adiabatic and isothermal compressibility. For sound waves of intensities between 5-10 W/cm^{-2} travelling through a liquid the temperature difference due to the adiabatic compression is of the order of a few degrees in the liquid. At these intensities, a small bubble of gas may reduce its volume appreciably or even collapse producing heat which raises the temperature to several hundred degrees. Moreover, if the bubbles resonate in the sound field, the amplitude of vibration and the temperature reached inside them are increased considerably. A temperature gradient in the gas bubble is then set up, and this produces periodic temperature variations in the liquid adjoining the gas bubble. These combined effects of temperature are sufficiently high to explain the chemical effects observed.

If one assumes this model, there are two possibilities for thermal effects. The chemical reactions could be gas-phase thermal reactions taking place in the gas bubble, or they might take place at the liquid-gas interface but still be due to the high gas temperature in the bubbles. These same thermal processes are responsible for the absorption of energy from the sound waves.

Doulah[197] proposed an alternative to the above theory which in essence requires that the collapsing bubbles in a cavitating ultrasonic field convert acoustic energy into hydrodynamic energy due to release of elastic waves and these

in turn disintegrate into small water eddies. In a cavitation field, the molecules will thus undergo a dynamic force due to the eddies. When this force exceeds the bond strength in the molecule, the molecule degrades into small stable fragments. Fragments which are unstable recombine until a stable molecule is formed.

Several investigators[198-207] have shown the importance of using sound waves at various frequencies and intensities either to initiate or promote chemical reactions. The energy for the reactions, obviously, comes via the large temperature and pressure changes during the violent collapse of bubbles. Examples of reactions induced by sound waves are discussed below.

(a) Radical Generation

Generation of OH and H radicals by sonolysis of water[180,208,209] have been shown to exist via the use of spin-trap agents and electron-spin resonance spectroscopy (ESR). The purpose of spin-trap agents[210,211] is to convert short-lived radicals into relatively longer-lived radicals which can then be observed using ESR:5,5-dimethylpyroline-N-oxide (DMPO) was used during the experiments performed in the course of this research. The structure (DMPO) is shown in Figure 6.2.

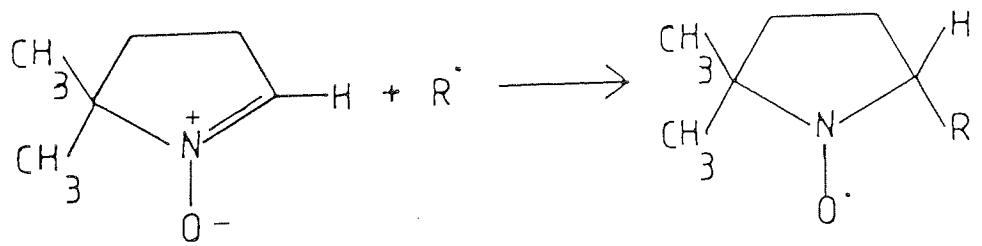

where R = $\dot{O}H$ or $\dot{H}$

Figure 6.2: Use of 5,5-dimethyl pyrroline-N-oxide (DMPO) as a spin-trap agent

Other spin-trap agents such as α-4-pyridyl-1-oxide-N-tert-butyl nitrone and pentamethylnitrosobenzene have been used to show the presence of $\dot{O}H$ and $\dot{H}$ radicals[211].

(b) Polymerisation reactions

Polymerisation studies using ultrasound have been performed either with solutions of monomers or polymers. The scission of monomers or polymer bonds due to ultrasound (depolymerisation) supplies new chain carriers for polymerisation.

Kruus et al [202-204] studied bromobenzene (a), isoprene (2-methyl 1,3-butadine) (b), methylmethacrylate (2-methyl-propenoic acid, methyl ester) (c) and styrene (ethenylbenzene or vinylbenzene) (d). He suggested that the polymerisation of these molecules was via a radical process.

Figure 6.3 shows the possible mode of bond scission and the molecular fragmented ions, that lead to polymerisation.

(a)

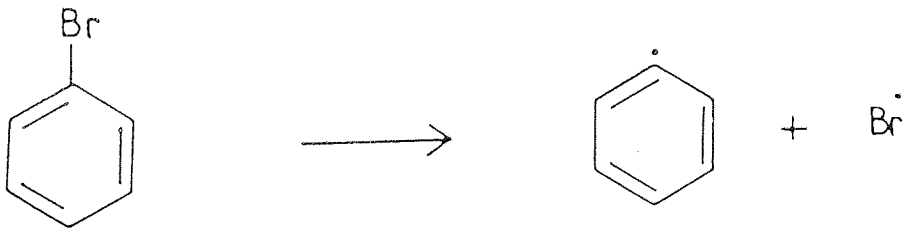

(b) $CH_2 = \underset{\displaystyle CH_3}{\overset{|}{C}} - CH = CH_2 \longrightarrow \begin{cases} \dot{C}H_3 + CH_2 = \dot{C} - CH = CH_2 \\ CH_2 = \dot{C} - CH_3 + \dot{C}H = CH_2 \end{cases}$

(c) $CH_2 = \underset{\displaystyle CH_3}{\overset{|}{C}} - \underset{\displaystyle O}{\overset{\|}{C}} - O - CH_3 \longrightarrow \begin{cases} \dot{C}H_3 + CH_2 = \dot{C} - CO - O - CH_3 \\ CH_2 = \dot{C} - CH_3 + .\dot{C}O - O - CH_3 \\ \dot{O} = CH_3 + CH_2 = C(CH_3) - C\dot{O} \\ \dot{C}H_3 + CH_2 = C(CH_3) - CO - \dot{O} \end{cases}$

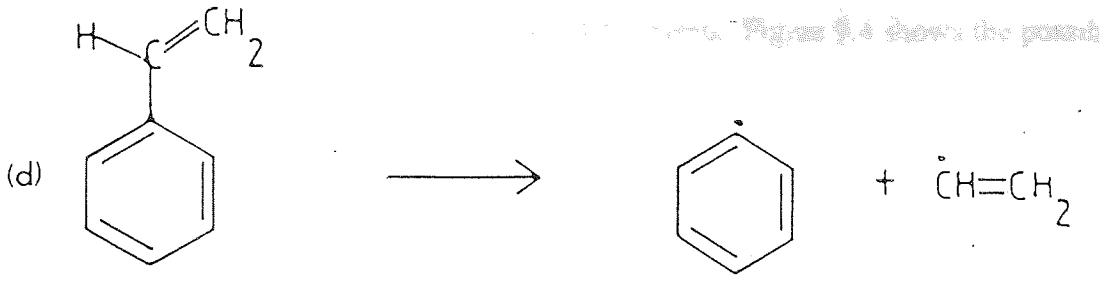

Figure 6.3: Compounds used to study polymerisation via a radical process

Using methylmethacrylate as an example, Dupont et al[203] gave the reaction mechanism for the polymerisation outlined below;

(a) Bond breaking due to cavitation

$M \longrightarrow P_i + P_j$; Rate α cavitation rate (M effectively constant)

(b) Initiation of polymerisation

$P_i + M \longrightarrow P_{i+1}$; Rate α P_i (M effectively constant)

(c) Propagation

$P_{i+1} + M \longrightarrow P$; Rate α P_{i+1} (M effectively constant)

(d) Termination

$Pa' + P_b \longrightarrow P_{a+b}$ or $P_a + P_b$; Rate α $(P)^2$

Kruus,[202] like many other authors, found difficulty in detecting the radicals or the polymerized product owing to the short life-time of the radicals and the low concentration of the polymerised product. Tabata et al,[212] and various other authors[213-216], overcame this by using spin-trapping agents. Tabata[212] using pentamethyl nitrosobenzene (PMNB) as a spin-trapping agent in the ultrasonic degradation of polymethamethacrylate not only showed the possible radical products that are produced in the degradation of polymethylemethacrylate but also

proved which of the radicals is generally produced. Figure 9.4 shows the possible radical products.

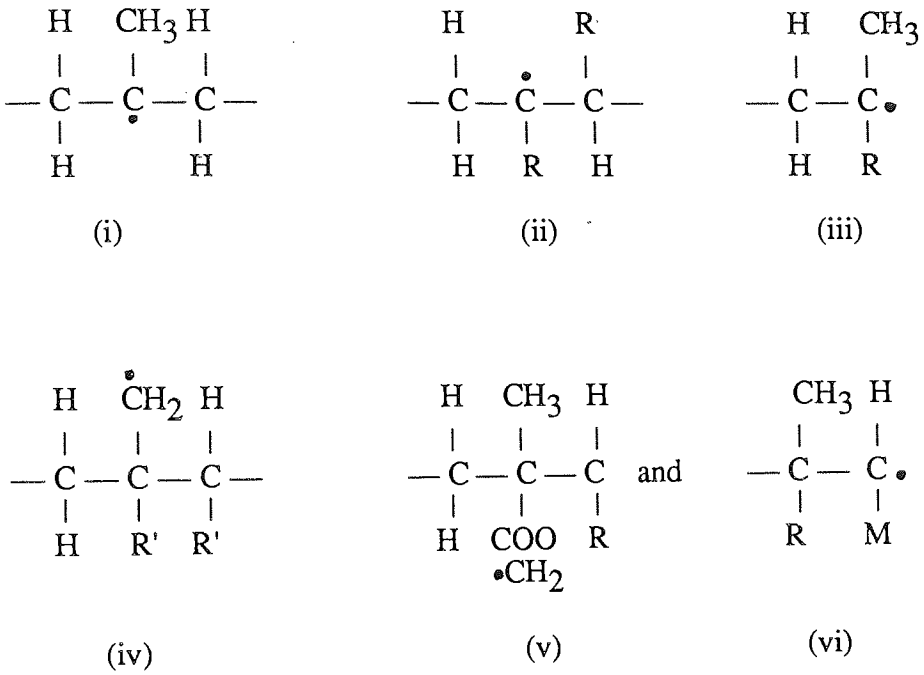

Figure 6.4: Possible radical products that could be trapped using PMNB

Using ESR and computer simulation Tabata revealed that radical (vi) was produced.

If ultrasonic degradation proceeds via scission of bonds within molecules, then degradation should depend on the strength of bonds that sustain the stress. Encinia et al[219] using polyvinyl pyrolidine showed that the rate of degradation is much faster when a few (C-C) bonds are replaced by much weaker (O-O) bonds. They performed their experiments by incorporating peroxide linkages in poly (vinyl pyrolidine). The results revealed that, PVP containing oxygen degrades more readily, the limiting intrinsic viscosity was considerably smaller and the rate was ten times that of untreated PVP of a similar molecular weight. From this it was deduced that O-O bonds were ruptured at a rate 5000 times greater than the C-C bonds.

(c) Rates and Product of Chemical Reactions

It has been shown by several authors[201,207] that ultrasonic irradiation can substantially improve and change the rates of reaction and product yields of a

wide range of reactions. The results of experiments performed suggest that increases in reaction rates are due to the high temperatures reached within the cavitation bubbles and also due to an increase in the frequency of collisions between ions generated by the cavitation pressure gradient and temperature rise[220,221,222].

Examples shown in Figure 6.5 refer to phase-transfer catalysis[207,223] and one in which the reaction pathway is switched[224].

(i) For N-alkylation:

$$R_2N + KOH \rightleftharpoons R_2 N^- K^+ H_2O$$

$$R_2 N^- K^+ + R' Hal \longrightarrow R_2 NR' + KHal$$

For N-methyl indole synthesis

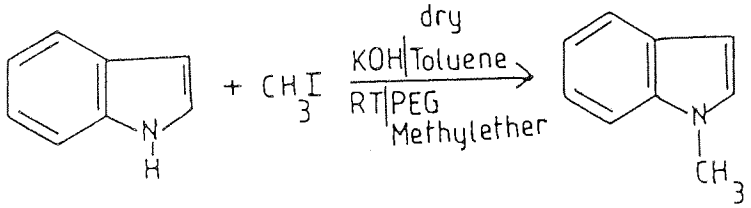

Reaction time	Yield %
5 hrs (with no ultrasound)	60
0.5 hrs (with ultrasound)	65

(ii) Ether synthesis

$$RO^- M^+ + R' Hal \longrightarrow R OR' + M^+ Hal$$

$$EtBr + PhOH \xrightarrow[RT \mid PEG\ methylether]{KOH \mid dry\ toluene} Et—O—Ph$$

2 hrs (with no ultrasound)	44%
2hrs (with ultrasound)	80%

(iii) Changes in reaction pathways

Reaction between 4-methylbenzyl bromide and toluene in the presence of potassium cyanide and alumina, under normal conditions, yield the

Friedel-Craft adduct (a) (75%) after 24 hours, whereas under sonication the major product is benzyl cyanide (b), (77%).

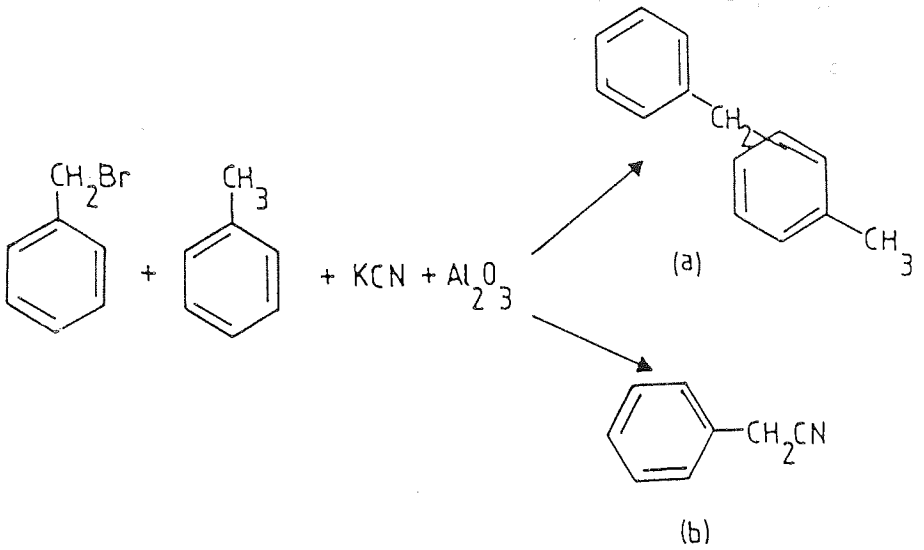

Figure 6.5: Effects of ultrasound on reaction rates and products

6.7 Observation of the Effects of Sound Absorption in Liquids using NMR (Theory)

The aim of this section is to correlate the principles discussed to this point and discuss the original hypothesis on which this research is based.

The first question must really be "Why is there such an interest in NMR relaxation times?"

From a chemists point of view, there are two reasons why one is interested in relaxation times. The first is that relaxation parameters are related to the structural features of molecules and also their motion. Unfortunately these relationships are not understood in such detail as are those involving chemical shifts and coupling constants. In fact, although relaxation measurements are sometimes used to a good effect in structure elucidation, it still seems to be difficult to lay down rigorous guidelines for their application.

The second aspect is that, consideration of relaxation processes is critical to the design of NMR experiments simply because one needs some idea of relaxation times to achieve optimum sensitivity in any experiment.

The intention from the original hypothesis is to develop a technique that could significantly reduce the relaxation times for nuclei with naturally long relaxation times and hence reduce the overall time for the acquisition of NMR spectra.

The next obvious question is "Why are relaxation times, namely spin-lattice relaxation times, T_1, often long?"

The first point to note is that, there should be absolutely no problem in principle with dissiapating the tiny energies of NMR spins into the general thermal energy of the sample because they are negligible compared to the thermal energy of the sample.Therefore, it is not a lack of somewhere to send the energy but a lack of means to move it there that slows down the relaxation. It is already known that for closely spaced energy levels, the probability of spontaneous emission is extremely low ($\simeq 10^{-25}$ per second) and can be neglected. Thus, relaxation must occur via stimulated emission and the observation that T_1 tend to be rather long implies that there do not happen to be suitable stimuli available. In other words, the nuclear energy levels are not connected very well with the surrounding environment

In developing theories for relaxation, one tries to think of sources for suitable fields to stimulate the spins transitions. Chapters Two, Three and Four refer to several sources which could stimulate spin transitions and thereby contribute to spin-lattice relaxation times. These are dipole-dipole interactions (DD), quadrupole (Q), chemical shift anisotropy (CSA), spin-rotation interactions (SR), scalar interaction (SC) and interactions arising with unpaired electrons (UE). The overall spin lattice relaxation rate can then be expressed as the sum of all the individual relaxation rates arising from these interactions, that is equation 4.0.

$$T_1^{-1} = T_{IDD}^{-1} + T_{1Q}^{-1} + T_{1CSA}^{-1} + T_{1SR}^{-1} + T_{1SC}^{-1} + T_{1UE}^{-1} \quad \text{..... 4.0}$$

Considering the simplest case, that is, for a nuclei of spin-half in solution. The dominant source of stimulation for the spin transitions are the dipolar-dipolar

interactions between nuclei. Equation 4.0 can now be approximated to:

$$T_1^{-1} = T_{1DD}^{-1} \qquad \text{..... 6.12}$$

Spin-lattice relaxation times may be subdivided into intra and intermolecular contributions. These results from the rotational and translational motions of molecules, so that, T_1 may be written in the form of equation 6.13

$$T_{1DD}^{-1} = T_{1(rot)}^{-1} + T_{1(trans)}^{-1} \qquad \text{..... 6.13}$$

Equation 6.13 takes the same form as equation 3.12 .

The contribution arising from rotational motion of nuclei to $T_{1(rot)}$ has fully been expressed as[38,39]:

$$T_{1(rot)}^{-1} = \hbar^2 \gamma_i^2 \left(3/2\, \gamma_i^2 \sum_{j}^{i} r_{ij}^{-6} + \gamma_f^2 \sum_{f}^{*} r_{if}^{-6}\right) \tau_{rot} \qquad \text{..... 3.20}$$

Similarly, the contribution arising from the translation motion of nuclei to $T_{1(trans)}$ has been expressed as[38]:

$$T_{1trans}^{-1} = 2\pi\hbar^2 \gamma_i^2 \frac{N}{a^2} \left[3\gamma_i^2 \sum_{j}^{i} r_{ij}^{-1} + 2\gamma_f^2 \sum_{f}^{*} r_{lf}^{-6}\right] \tau_{trans} \qquad \text{..... 3.22}$$

Equation 3.20 and 3.22 can be simplified as as follows;

For rotational motion:

$$T_{1(rot)}^{-1} = A\,\tau_{rot} \qquad \text{..... 6.14}$$

where $A = \hbar^2 \gamma_i^2 \left[3/2\, \gamma_i^2 \sum_{j}^{i} r_{ij}^{-6} + 2\gamma_f^2 \sum_{f}^{*} r_{lf}^{-6}\right]$

and τ_{rot} is the rotational correlation time.

For translational motion:

$$T^{-1}{}_{1(trans)} = B\tau_{trans} \qquad \text{..... 6.15}$$

$$\text{where } B = 2\pi\hbar^2\gamma_i^2 \frac{N}{a^2}\left[3\gamma_i^2 \sum_j^i r_{ij}^{-1} + 2\gamma_f^2 \sum_f^i r_{if}^{-6}\right]$$

and τ_{trans} is the translational correlation time.

Expressing equation (6.13) in terms of equations (6.14) and (6.15) gives:

$$T^{-1}_{1DD} = A\tau_{rot} + B\tau_{trans} \qquad \text{..... 6.16}$$

Equation 6.16 has two implications. The first is that the energy of interaction between nuclei is time dependent. By causing the spins to move more randomly with respect to each other, the interaction energy will be distributed in frequency and time.

The second is that the spin-lattice relaxation rate could be altered by a change in either or both the translation and rotational motions of the molecules. This could easily be achieved by changing the temperature of the system.

The frequency dependence of the interaction energy which gives information on the amount of molecular energy available for molecular motion is called the spectral density $J(\omega)$. This information is related to the intensities and probabilities of molecular motion at the Larmor resonance frequency ω_o.

Calculation of the exact spectral density for any real molecular motion has never been solved. The difficulty is that the molecular motion (or atomic motions) are extremely complicated. In Chapter Two, the spectral density was expressed as:

$$J(\omega) = \frac{\tau_c}{1 + \omega^2\tau_c^2} \qquad \text{..... 2.41}$$

where τ_c is the correlation time and is a measure of the time between the field fluctuations.

Examination of the second implication that the spin-lattice relaxation rate could be altered by a change in temperature, reveals that this is possible via a change in the correlation time τ_c. In effect τ_c represents an average of the translational and rotational correlation times.

The effect of temperature on spectral density and spin-lattice relaxation rates can be explained in the following manner. At low temperatures molecules have long correlation times, one therefore expects that the spectral density will be bunched at low frequencies. As the temperature is raised, the spectral density will become spread out over a larger and larger frequency region. If one now samples this spectral density at a specific frequency, as relaxation processes do, a smaller, then a larger and finally a smaller value of $J(\omega)$ is obtained, as the temperature is raised from very low to a very high temperature.

To illustrate numerically the effects of temperature on spectral density, $J(\omega)$ as a function of the correlation time, τ_c, consider the following: From equation 2.41, let τ_c have three different values of 10^{-10}s, 10^{-6}s and 10^{-2} seconds, corresponding to fast, intermediate andslow molecular motions, respectively. If ω is the resonant Larmor frequency (ω_o) at 10^{-6}Hz, then the numerical values of spectral density, $J(\omega)$, are 10^{-10}S, 0.5×10^{-6}S and 10^{-10}S, for fast, intermediate and slow molecular motions, respectively. These results illustrate that the greatest contribution to the spectral density, $J(\omega)$ comes from intermediate molecular motions. In other words, the greatest contribution from molecular motion is achieved when molecules have large components of molecular motions at the Larmor

resonant frequency, ω_o. Chapter Two, Figure 2.5, illustrates the behaviour of spectral density for three types of motions discussed.

Changes in spectral density results in changes in spin-lattice relaxation times. A graphical representation (Figure 2.4) and explanation of such behaviour has been described in Chapter Two.

From Figure 2.4, Chapter Two, it can be seen that spin-lattice relaxation times are at a minimum when the spectral density contribution is at the resonant frequency and is at a maximum.

If sound is expected to perturb natural molecular motion, the first question regardless of which of the parameters it may effect is, "Can the effects of sound be treated as another mechanism by which the spin-lattice relaxation rate is altered?" If the answer to this is "yes", then the next question would be "Are the effects of sound, if expressed in terms of its relaxation rate as T^{-1}_{ULT}, additive to the existing contributions embraced by an overall spin lattice relaxation rate, T^{-1}?" If the answer to this is "yes", so that, that it can be expressed as an additive term, then for nuclei of spin-half in solution, the effect of sound can be expressed similar to equation (6.12).

$$T^{-1}_1 = T^{-1}_{1DD} + T^{-1}_{1ULT} \qquad \text{..... 6.17}$$

Re-expressing equation 6.17 by using equation 6.16, gives:

$$T_1^{-1} = A\tau_{tot} + B\tau_{trans} + C\tau_{ULT} \qquad \text{..... 6.18}$$

where A, B, τ_{rot} and τ_{trans} have the usual definitions. C represents some constant and τ_{ULT}, represents a correlation time in which sound is used to force a modulation on the natural molecular motion of the molecules.

If sound is introduced in the megahertz frequency range, it will then

attempt to modulate the molecular motion in this frequency region. The rotational and translational correlation times for natural molecular motion are in the order of 10^{-12} seconds and 10^{-10} seconds, respectively, in mobile liquids. Thus, substituting these numerical values for the correlation times with τ_{ULT} as 10^{-6} seconds (a megahertz frequency modulation) into equation (6.18), gives equation 6.19:

$$T_1^{-1} = A\ 10^{-12} + B\ 10^{-10} + C\ 10^{-6} \qquad \ldots\ldots\ 6.19$$

It can be seen from equation 6.19 that a modulation in the megahertz frequency range has a greater effect on the spin-lattice relaxation rate than either or both the rotational and translation motion of the molecules. This implies that sound, or to be more precise, ultrasound, could be used to reduce spin-lattice relaxation times by increasing the spectral density at the resonant frequency.

The basis of the above hypothesis, rests entirely on the assumption that, the spin-lattice relaxation rate as affected by ultrasonic modulation of the magnetic dipolar-dipolar interactions are additive effects.

If one now introduces the discussion on ultrasound absorption in liquids from Chapter Five, with figure 5.2 in mind, the effects, for example, of a compressional wave will be to cause a change in the translational, rotational and vibrational energies of molecules. Therefore, during a compression cycle, the molecules attain an excess of energy from the perturbation caused by the sound pressure. This increased energy of molecules is returned to the ordered elastic energy of the wave during the decompression cycle. However, because of relaxational coupling some of this energy is transferred to other boxes of energy during the compression cycle. Due to time lags in energy transfer from one box to another, energy initially absorbed from the compression cycle does not get back until the decompression cycle starts, therefore the energy is out of phase and this results

in sound absorption. In molecular terms, the translational energy is the one which is directly accessible to the ultrasonic wave. Its energy is then passed on from molecule to molecule by collisions. The internal degrees of freedom corresponds to the vibrational and rotational motion of the molecules. One of these internal modes can be excited, if the necessary energy can be transferred from the translation energy. Such a transfer of energy from an external to an internal degree of freedom requires a certain finite relaxation time, so that the internal modes lag slightly behind the external modes. In the case of energy transfer between translational and rotational modes, translational and vibrational modes, and vibrational and rotational modes, the corresponding relaxation times are of the order of 10^{-12} - 10^{-14}S, 10^{-12} - 10^{-10}S, and 10^{-9} - 10^{-6}S respectively.

If one separates the various motions executed by the molecules and considers the period of that motion, they can be represented as in Table 6.1.

Motion	Electronic	Vibrational	Rotational	Translational	Nuclear precession
Periods	~ 10^{-16}	~ 10^{-14}	~ 10^{-12}	~ 10^{-10}	10^{-6}

Table 6.1: Various molecular motions and the period of that motion as encountered by molecules.

Any energy that is absorbed by the molecule from the acoustic wave will be as a result of energy exchange between other degrees of motion. This energy exchange occurs only during a collision, and for this to be effective the duration of collision must be comparable to the period of the motion in which the energy is stored. For example, taking the case where there is an energy exchange between the translation and vibration modes. For a molecular collision to be effective in changing the vibrational energy of the molecule, the duration of collision should be comparable to the period of the vibration. A typical molecular relative translational velocity at room temperature is $5 \times 10^{2}ms^{-1}$. However, the distance over which intermolecular forces are effective during a collision is of the order of 10^{-10}m.

Hence the time which two molecules spend closer than 10^{-10}m, which is, the duration of the collision, will be about 4×10^{-13} seconds. A typical molecular vibration frequency of 3×10^{13}Hz has a period of about 3×10^{-14} seconds. Thus, only those molecular collisions in which the relative translational velocity is much higher than average will lead to vibrational-translational energy transfer. For further discussion see Chapter Five on thermal and vibrational relaxation.

For an effective coupling between translational, rotational and vibrational modes, the frequency at which the motion must be driven by sound must be of the order of 10^{10} Hz - 10^{14} Hz. This is far above the frequency range that was initially proposed in terms of the liner additivity rule of the relaxation rate as expressed in equation 6.17.

The discussion on acoustic cavitation in the first half of this chapter suggests that transfer of energy from external degrees of freedom to internal degrees of freedom could take place via the formation of stable cavitation. Once the gas or vapour bubble is nucleated, its periodic oscillation can cause a maximum transfer of energy to the external degrees of freedom at the gas to liquid interface. Because there is a time lag in energy returning back from the internal modes to the external mode, the effect becomes more pronounced as time goes on owing to the fact that there is a superimposition of energies each time. The implication of this discussion is that, as there is a superimposition of energies, the molecules will have more and more energy to translate, rotate and vibrate, and therefore one does not need really have to work at very large frequencies. The only flaw in this discussion however concerns the efficiency of the coupling of energies between the internal modes and external mode, and between the external mode and periodic oscillations of the bubble. If the coupling of energies between the external mode (translation motion) and the periodic oscillation is poor, a null effect on the translational motion will be observed. In addition, as a result of this, a null effect will be observed on the coupling of energies between translational and the rotational and vibrational energies

of the molecules. Conversely, if the coupling is very efficient, a large effect on the translational motion will be observed and as a result a large increase in energy of the rotational and vibrational modes of the molecules will result.

In terms of spin-lattice relaxation rates, an efficient coupling between the sound wave (or more precisely the acoustic energy) and the external and internal modes of freedom of molecules will either lead to an increase or decrease in the correlation time τ_c, depending on which part of the curve in Figure 2.4 the molecules are at initially. For molecules which lie to the far left of the T_1 minimum, (that is for molecules which are moving very quickly and have short correlation times τ_c), a gradual increase in the correlation time decreases the spin-lattice relaxation times, up to a point where $\tau_c^2\,\omega^2 \sim 1$; a further increase in the correlation time now causes the relaxation times T_1 to increase. Similarly, for molecules which lie to the far right of the T_1 minima, (that is for molecules which are moving relatively slowly) a decrease in the correlation time τ_c, that reflects faster translational or rotational motions, will cause a decrease in the relaxation times, T_1, up to a point where $\tau_c^2\,\omega^2 \sim 1$ further decrease in correlation times will now increase the relaxation times. In terms of spectral density, in the fast exchange limit, the component at the Larmor frequency is small, but increases as the molecular reorientation rate is slowed down. Most small organic molecules in non-viscous solvents are in this category. This means that any factor which slows the molecular motion shortens the spin-lattice relaxation times. A minimum is reached near the conditions for intermediate molecular tumbling rates and any further slowing of the motion reduces the component at the Larmor frequency and therefore increases the

relaxation times.

Bowen[164,165] showed by acoustic saturation of the NMR line at the resonant frequency for protons (18 MHz) in an aqueous colloidal solution of As_2S_3, a reduction of spin-lattice relaxation time of about 27%.

In another NMR experiment by Alekseev and Kopvillem[169] on an aqueous solution of $H_2O.CuSO_4.5H_2O$ the protons in water at 16 MHz, when subject to sound at a frequency of 2.1 MHz showed a 7% decrease in sound amplitude modulation effect. They concluded that it was possible to carry out ANMR at a lower sound frequency than the Larmor resonant frequency.

In the following section are discussed the effects on NMR relaxation times in terms of the effects of structural relaxation, impurities, liquid viscosity, changes in compressibility of liquids that are effected by sound absorption in liquid.

Chapter Five discusses in depth the structure, properties and sound absorption in liquids. Concepts such as cell, hole, tunnel, compressibility of liquids, and other theories describe the behaviour and properties of liquid. The theories suggests that molecules in a liquid have more space to move around, compared to that in a solid and less to that in gases. The volume increase in going from a solid phase to a liquid phase is in the order of about 10-15%. Structural relaxation, which results in volume changes of a liquid, due to sound absorption in liquids suggest that a reduction in volume occurs by causing the molecules to move closer to one another. By forcing molecules closer to one another would increase the efficiency and the probability of the number of collisions owing to the fact that each molecule now has a smaller volume in which to move freely. Impurity effects as discussed already, suggest that the presence of unlike molecules may produce a better molecular arrangement and therefore a greater probability of energy transfer during collisions than those of like molecules. Conversely, if the molecular arrangement is poor (in terms of packing), then the probability of energy transfer during collision will also be poor.

Results obtained from studies of structural relaxation, impurity effects and compressibilities reveal a great deal of information about the properties of liquids. If one now performs experiments using sound waves in a liquid and at the same time performs an NMR experiment to measure its spin-lattice relaxation rate, one may either observe a distinct change or a null effect on the relaxation rate. If a null effect is observed, several conclusions could be drawn from this failure. These being, an inefficient coupling of energy between the sound wave and the external mode of freedom, a poor transfer of energy from external mode to the internal degrees of freedom and a poor molecular packing which gives a larger free volume for the molecule to move around before colliding with another molecule.

Chapter Three discusses and demonstrates the dependence of spin-lattice relaxation rates on viscosity. It discusses the effects of liquid mixtures which gives rise to the so-called "mutual viscosity". In Chapter Five the effects of temperature and pressure on viscosity were discussed. In this section the effects of viscosity on spin-lattice relaxation rates is discussed through the changes brought around by temperature and pressure.

The effects on viscosity of increasing temperature will be to reduce it . This is due to the fact that molecules are moving and vibrating faster as the temperature is raised. In terms of the spectral density, $J(\omega)$, this will be spread over a larger frequency region with a larger number of molecules having frequency components at the resonant Larmor frequency than before. As a result an increase in spin-lattice relaxation rate is observed. As the temperature continues to rise, the viscosity continues to decrease, owing to the fact that molecules now have even more energy to move or vibrate. The spectral density will now have an even larger frequency spread than before. However, the frequency components at the resonant frequency will be less and as a result will decrease in spin-lattice relaxation rates. The effects of temperature on relaxation rates have already been discussed earlier in this section.

If sound is treated as a continuous and alternating pressure wave, then perhaps the effects observed at various pressures on a liquid could be extrapolated to explain the effects of sound in a liquid.

The effects of pressure on a liquid are several fold. It induces changes in volume, density and viscosity. The pressure applied to a liquid reduces its volume and as a result its density increases. In molecular terms, by increasing pressure the molecular reorientation becomes increasingly more hindered and anisotropic in nature due to the closer proximity of the neighbouring molecules. This also results in enhancing the rotational and translational coupling.

If the viscosity of a liquid is a measure of the forces that work against movement or flow then as a result of hindered motion, the viscosity will increase. Equations (3.36) and (3.39) in Chapter Three describes the effects of viscosity on spin-lattice relaxation rates. The equations re-expressed below shows the effects of viscosity on the intra and inter molecular dipole-dipole contribution to spin-lattice relaxation rates for liquids with nuclei having spin one-half (I = 1/2).

$$T_1^{-1}{}_{intra} = \hbar^2 \gamma_i^2 \left[3/2\, \gamma_i^2 \sum_{i \neq j} r_{ij}^{-6} + \gamma_f^2 \sum_{f}^{*} r_{if}^{-6}\right] K_A^2\, \sigma_{AB}\, \eta_{AB}/KT \qquad \ldots\ldots\ 3.36$$

$$T_1^{-1}{}_{inter} \frac{\pi \hbar^2 \gamma_i^2 N}{KT} \left[3\, \gamma_i^2 \sum_{i \neq j} r_{ij}^{-1} + 2\, \gamma_{if}^2 \sum_{f}^{*} r_{if}^{-1}\right] x \left[\eta_{AB}\, \sigma_{AB}\, f_{AB} + \eta_A\, \sigma_A\, f_A\right] \qquad \ldots\ldots\ 3.39$$

where η_{AB} is the mutual viscosity of a binary liquid containing solution A and B,

and η_A is the viscosity of pure liquid A.

From the equations it can be seen that the spin-lattice relaxation rates increase with increasing viscosity. These results are supported by Artaki and Jonas[225] who showed the pressure effects on the coupling between rotational and translational motions of viscous fluids. Table 6.2[225] shows the effects of pressure on spin-lattice relaxation times, T_1, viscosity, η ,and volume V, at various temperatures. The conclusions made from their observations were that, by increasing the pressure, it reduces the available volume of liquid necessary for molecular motion, and, as a consequence, its density and viscosity increases. For molecules which are highly anisotropic, the presence of neighbouring molecules changes the anisotropic character of the reorientational motions, causing the rotational-translation coupling parameters to increase. In contrast, molecules which are highly symmetric, the coupling parameters for translational and rotational motion decrease with increasing density.

For a given constant molar volume available for molecular motion, reducing the kinetic energy of molecules may reduce the frequency of reorientation. However, the actual nature of the reorientations which couple to the translational motions remains uneffected. Therefore, volume rather than kinetic energy plays the decisive role in determining the degree of coupling.

In supporting the hypothesis, that sound could be used to perturb natural molecular motions in the liquid phase, and that these effects could be observed through their influence on NMR relaxation times, various ideas, theories, models, and other related experimental observations have been presented. The following chapter discusses the instrumentation, experimental methods and conditions which were developed to facilitate and test the above hypothesis.

Table 6.2: Shows the effects of pressure on spin lattice relaxation time T_1, viscosity η, and volume V, in liquids (results obtained from reference 225)

Compound	Pressure (bars)	T_1 (ms)	η (cP)	V (cm^3/mole)	T_1 (ms)	η (cP)	V (cm^3/mole)	T_1 (ms)	η (cP)	V (cm^3/m
		Temp - 20°C			Temp - 45°C			Temp - 70°C		
Isopropyl benzene d_5	1	222	1.58	134.0	106.5	3.06	130.9	37.4	7.98	128.1
	1000	108	3.76	127.7	43.7	7.14	125.6	8.79	31.6	123.7
	2000	53.7	8.98	123.8	16.0	19.9	122.0	1.53	117.0	120.2
	3000	24.8	18.5	121.0	4.62	5.41	119.7			
	4000	10.8	37.4	118.9	1.25	133.7				
		Temp - 43°C			Temp - 21°C			Temp - 5°C		
Cis decalin d_{10}	1	494	2.17	157.8	348	3.36	154.0	257	4.97	151.9
	500	349	3.62	152.4	232	5.61	149.5	170	9.79	148.0
	1000	241	5.70	149.0	150	9.3	146.5	107	18.2	145.1
	1500	178	9.3	146.3	104	16.5	144.0	70	35.4	143.2
	2000	130	14.7	144.0	69	28.3	142.4	46	71.3	141.6
	2500	92	24.6	142.3	46	51.6	141.2			
	3500	67	65.8	140.2						
		Temp - 10°C			Temp - 20°C			Temp - 40°C		
Sec-Butyl cyclohexane d_5	1	205								
	1000	85.9	2.39		158	3.02		90.8	5.6	
	2000	34.5	4.31		63.9	11.5		30.2	25.4	
	3000	13.3	28.9		23.3	39.3				
	4000	5.3	103		8.8	148		8.41	122	
	5000	2.2	1306		3.3	615		2.55	594	
		Temp - 0°C			Temp - 35°C			Temp - 55°C		
Toluene d_8	1	860	0.81	104	410	1.42	100.3	253	2.55	98.3
	1000	555	1.49	98.4	240	3.16	95.9	120	5.84	94.1
	2000	350	2.77	94.9	131	6.38	92.9	60.0	13.2	91.0
	3000	217	4.98	92.4	70	13.3		29.9	31.2	

CHAPTER SEVEN

INSTRUMENTATION AND EXPERIMENTAL METHODS

NOMENCLATURE

A_t	Acquisition time
t_p	Length of pulse
HSP	Homospoil pulse
DESPOT	Driven Equilibrium-Single Pulse Observation of T_1
PZT	Piezoelectric ceramics made of lead titanate zirconate
Q	Mechanical Q of transducers ($Q = \frac{fo}{\Delta f}$)
k_p	Planar electromechanical coupling
f_n, f_m	Frequencies of maximum and minimum impedance
us ≡ μs	Microsecond
m ≡ M	Magnetisation

7.0 Introduction

This chapter discusses the instruments, experimental methods and conditions which were developed to facilitate and test the hypothesis on which this thesis rests.

The chapter is divided into three sections. The first section continues the discussion from Chapter One on the principles of Fourier transform (FT) NMR spectroscopy and describes various methods for measuring NMR relaxation times.

The second section discusses instruments, experimental methods and conditions which were developed to generate and transmit sound into a liquid sample while at the same time performing NMR T_1 measurement, within a FT NMR spectrometer. It also discusses the performance and reliability of the individual instruments that were designed and built.

The third section discusses instruments, experimental methods and conditions which were developed to perform sonochemical reactions via the effects of acoustic cavitation.

7.1 Principles of FT NMR (II)

Continuing the discussion from Chapter One (Section 1.10), on the principles of FT NMR, it can be said that most FT NMR techniques use a method that simultaneously excites all the resonances of a given type of nucleus. The signal induced in the receiver coil is a complex waveform that is a superposition of the resonances of all the nuclei resonating within the frequency range of the exciting device. The complex waveform is sampled as a function of time and is referred to as the time-domain spectrum. This process can be repeated a given number of times with each response being coherently added and stored in a digital computer. After the desired enhancement in the signal to noise ratio has been achieved, the frequency spectrum (called the frequency-domain spectrum) can be obtained by Fourier transformation of the time-averaged time-domain spectrum.

The frequency-domain, f (ν), and the time domain, f (t), are related by the mathematical procedure of Fourier transformation as follows:

$$f(\nu) = \int_{-\infty}^{\infty} f(t)\, e^{-i\omega t}\, dt \qquad \ldots\ldots 7.1$$

$$f(t) = 1/2\pi \int_{-\infty}^{\infty} f(\nu)\, e^{i\omega t}\, d\omega \qquad \ldots\ldots 7.2$$

Since the time-domain spectrum is a complex waveform representing the response of all nuclei of a particular type in the sample, Fourier transformation of the time-domain spectrum separates the complex waveform into various frequency and intensity components.

The mathematical process of Fourier transformation is facilitated by the use of a computer. Consequently prior to transformation the FID is converted from the analogue signal into the digital form before it is added to the memory. This is achieved by means of an analogue-digital converter (ADC). In practice, in order to determine a spectrum covering a range of frequencies, ΔHz, according to the sampling theory, each incoming signal must be sampled at least twice within a single period of the incoming signal. As a consequence of the sampling theory, the acquisition of a frequency spectrum ΔHz in width, requires a minimum sampling rate of 2Δ points per second. If the selected computer memory size is N, the FID has to be acquired in a time A_t which fulfills the condition

$$2\Delta \,.\, A_t = N \qquad \ldots\ldots 7.3$$

The longer the acquisition time the better defined the spectrum and higher the resolution, which is defined by

$$R\,(Hz) = \frac{1}{A_t} \qquad \ldots\ldots 7.4$$

An increase in computer size, N or a decrease in the frequency range, ΔHz, enhances the digital resolution.

7.2(a) Basic Components of FT NMR Spectrometers

As discussed earlier, FT NMR spectrometers acquire spectral information in a very short time. In order to do this the FT spectrometer transmitter must generate higher powers, capable of producing B_1 in the range of 10-400 Gauss at the sample and stimulate the whole resonance spectrum and nutate the corresponding magnetization before any transverse decay occurs. The pulsed NMR receiver must consequently be able to handle large voltages and recover very quickly to detect the nuclear signal without interferences. Thus, the transmitter and the receiver circuits are suitably designed for pulse operations. Furthermore, several supplementary units such as a programmer and a system for acquiring and processing the data are provided. Figure 7.1 shows the basic scheme of an FT NMR spectrometer.

7.2(b) The r.f. Gate Unit and the Pulse Programmer

In order to produce pulse sequences, the transmitter is equipped with a gate which can be switched "on" or "off" by means of a pulse generator. The output of the r.f. transmitter which contains a very stable quartz crystal oscillator is gated to produce pulses which are fed through amplifiers to attain the desired power level. When and for how long in any channel the r.f. gate will be opened is controlled by the pulse programmer. Usually the r.f. switch is "on" in the presence of a dc pulse signal from the pulse programmer and otherwise in the "off" position.

7.2(c) The r.f. Power Amplifier

The value of the r.f. magnetic field B_1 used in FT NMR spectrometers has to be high in order to ensure a sufficiently uniform distribution of r.f. power across the spectrum. Typically the required r.f. power for pulse spectroscopy is about 100 Watts, and following a pulse, less than 10^{-9} of the output power is radiated, so that the interferogram obtained by the receiver is without interference.

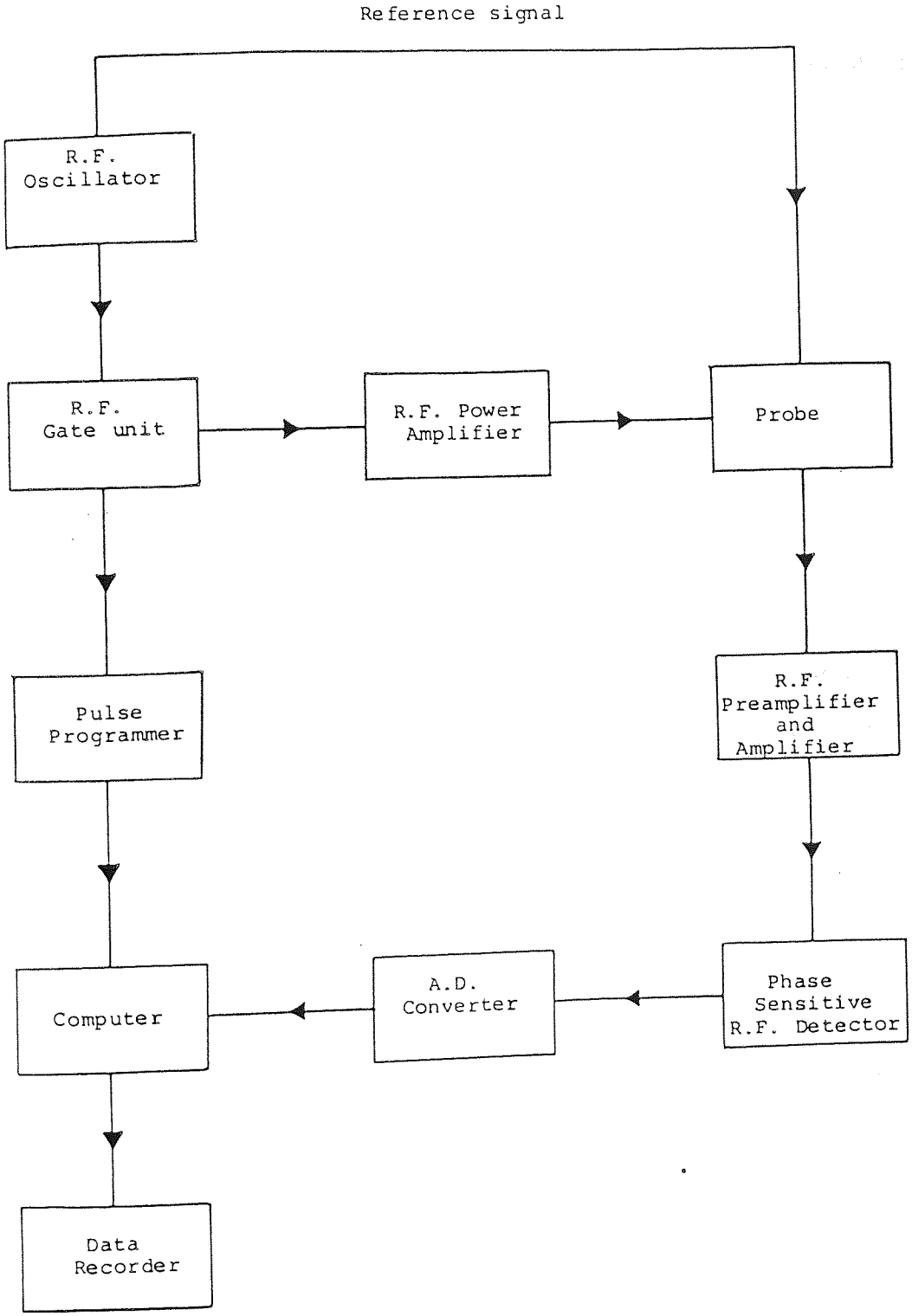

Figure 7.1: Basic Diagram of a F.T. NMR Spectrometer

B_1 is chosen to be large enough for the condition

$$\gamma B_1 >> 2\pi\Delta \qquad \text{..... 7.5}$$

to hold where Δ (in Hertz) is the entire range of chemical shift measured. If for a 90° pulse equation 1.30 is expressed as:

$$\gamma B_1 t_p = \pi/2 \qquad \text{..... 1.30}$$

then, from equation 7.5 the value of t_p is

$$t_p << \frac{1}{4\Delta} \qquad \text{..... 7.6}$$

Equation 7.6 suggests a need for short intense pulse for FT NMR.

7.2(d) The Probe

The FT NMR probe must be able to handle the large voltage present while the pulse is on, and to recover rapidly from the powerful pulse. In addition, in some cases, it must continuously deliver noise modulated or coherent decoupling power to the sample at a second r.f. frequency without interfering with the processing of the FID signal.

The probe must have facilities for essentially locking the magnetic field strength to the pulsed NMR frequency. This is usually achieved using a separate C.W. r.f. signal that enables locking to a heteronucleus.

Moreover, the probe should have spinning facilities and a temperature detector necessary for conducting variable temperature studies.

7.2(e) The Receiver

The essential features of the receiver are that it should recover very quickly from any overloads generated by the absorption of the r.f. pulse. In addition, the receiver and transmitter should be well isolated from one another to

achieve minimum overload condition and the required fast recovery time.

During the free precession period after the pulse, the nuclear signal enters the receiver (r.f. detector) as a band of radiofrequencies near the basic transmitter frequency. Passage through a phase sensitive detector results in a series of audio frequencies which are filtered by being fed through a low pass filter having a band width usually just equal to the chosen spectral width. Because single phase detection is not able to distinguish between positive and negative frequencies, the r.f. carrier has to be positioned so that all the audio frequencies have the same sign. If the r.f. carrier is placed at the end of the spectrum and the set spectral width is bigger than the chemical shift range Δ, the frequencies can be digitized unambiguously. However, if the spectral width is set to a value smaller than Δ, some of the frequencies corresponding to lines at the other end of the spectrum can be folded. It is, therefore, necessary to set the spectral width larger than the chemical shift range to avoid folding the spectrum. The discrimination between +ve and -ve frequency can be performed by using an experimental technique called quadrature detection[228]. This employs two phase sensitive detectors to distinguish between high and low frequencies; for this the r.f. carrier frequency should be placed in the middle of the spectrum.

7.2(f) The Analogue-to-Digital Converter (ADC)

In order for the signal to be stored and processed by the spectrometer computer, it is necessary to digitize the signal. A device known as the Analogue-to-Digital computer (ADC) does exactly this; it samples the free induction decay signal, which is an analogue signal at selected time intervals and converts each voltage measured to a binary number that can be stored in the corresponding memory location of the computer. The rate with which the spectrum of width Δ(Hz) must be collected by the ADC is twice the spectral width 2Δ. Ideally, the FID should be sampled until its amplitude has fallen off to zero to avoid line shape distortions. If a signal is sampled over a period of time known as the acquisition

time, t_{ac}, this defines a total of $2\Delta \cdot t_{ac}$ sampling points. Since each point is stored, a memory of N words is needed (ie. $N = 2\Delta \cdot t_{ac}$). This is related to the digital resolution of the instrument (via equations 7.3 and 7.4) and not the actual resolution due to the magnet homogeneity.

7.2(g) The Computer

A computer basically consists of input and output units, storage and arithmatic units. To use it, a program is read into the storage unit. It controls the transmitter and receiver functions, stores and processes the FID and transfers the results to display units like the oscilloscope or a chart recorder. In addition the computer is also used to carry out mathematical manipulations of data acquisition and coherent addition of repeated signals to improve the signal-to-noise ratio. Furthermore, FT data processing can be carried out during the whole process between the above mentioned steps or after them.

Memory locations are counted in multiples of K which stands for 2^{10} = 1024. The word length determines the amount of data or their magnitude that can be stored in each memory location. In general computers with a memory of 12K can be regarded as the minimum requirement for a FT spectrometer.

In order to achieve a reasonable signal-to-noise ratio, many pulses have to be applied sequentially. This means that each "scan" have the same characteristics. If, for example, there is a change in field homogeneity, this will cause the observed peak shapes to change on different passes, and as a result the final spectrum will be damaged. This problem can be overcome by the computer. In one approach, the height of an absorption peak of a reference compound (lock signal) is monitored. With field homogeneity optimized, the peaks show a maximum height. Any change from the optimal conditions is detected. The error signal is then used to control the shim current and return the field to the optimum value.

7.2(h) The JEOL FX 90Q FT NMR Spectrometer

The JEOL FX 90Q FT NMR spectrometer was the instrument used for carrying out the work reported in this thesis. Whilst it has a proton resonance frequency of 89.56 MHz, the instrument can be used to detect all NMR active nuclei in five different ranges of frequencies[229]. The instrument uses tunable 10mm and also 5mm probes. It has a range of facilities which permit digital quadrature detection (DQD), light pen control and autostacking of spectral data. The basic units of the spectrometer are present in the block diagram shown in Figure 7.2.

7.2 (i) The Magnet System

The instrument is provided with an electromagnet, fed by a voltage and current regulated power supply system, that produces a magnetic field of 2.11 tesla. The magnet is mounted in a compact thermostatted console to help maintain its stability. Several controls are provided to improve the magnetic field homogeneity. These adjust the current in the shim coils placed on the probe assembly between the pole-faces.

7.2(j) Transmitter, Receiver and Data Systems

The transmitter system has three channels: observation, irradiation and lock oscillator units. The lock oscillators units have a reference frequency of 44 MHz provided by a master clock unit. The OBS OSC unit has a 4 phase generator which is used to generate the OFFSET components of the OBS r.f. output. The gate of the oscillator is operated by the PG 20 pulse programmer, generating the desired r.f. pulse sequence. Two IF reference signals at 0° and 90° out of phase are taken to the OBSIF amplifier unit in the DQD system. The frequency of the reference signal is then adjusted for the selected nucleus at the wide band local oscillator unit. The next stage is amplification of the r.f. frequency output which is done in the r.f. power amplifier unit. When the r.f. signal reaches the probe, the sample absorbs

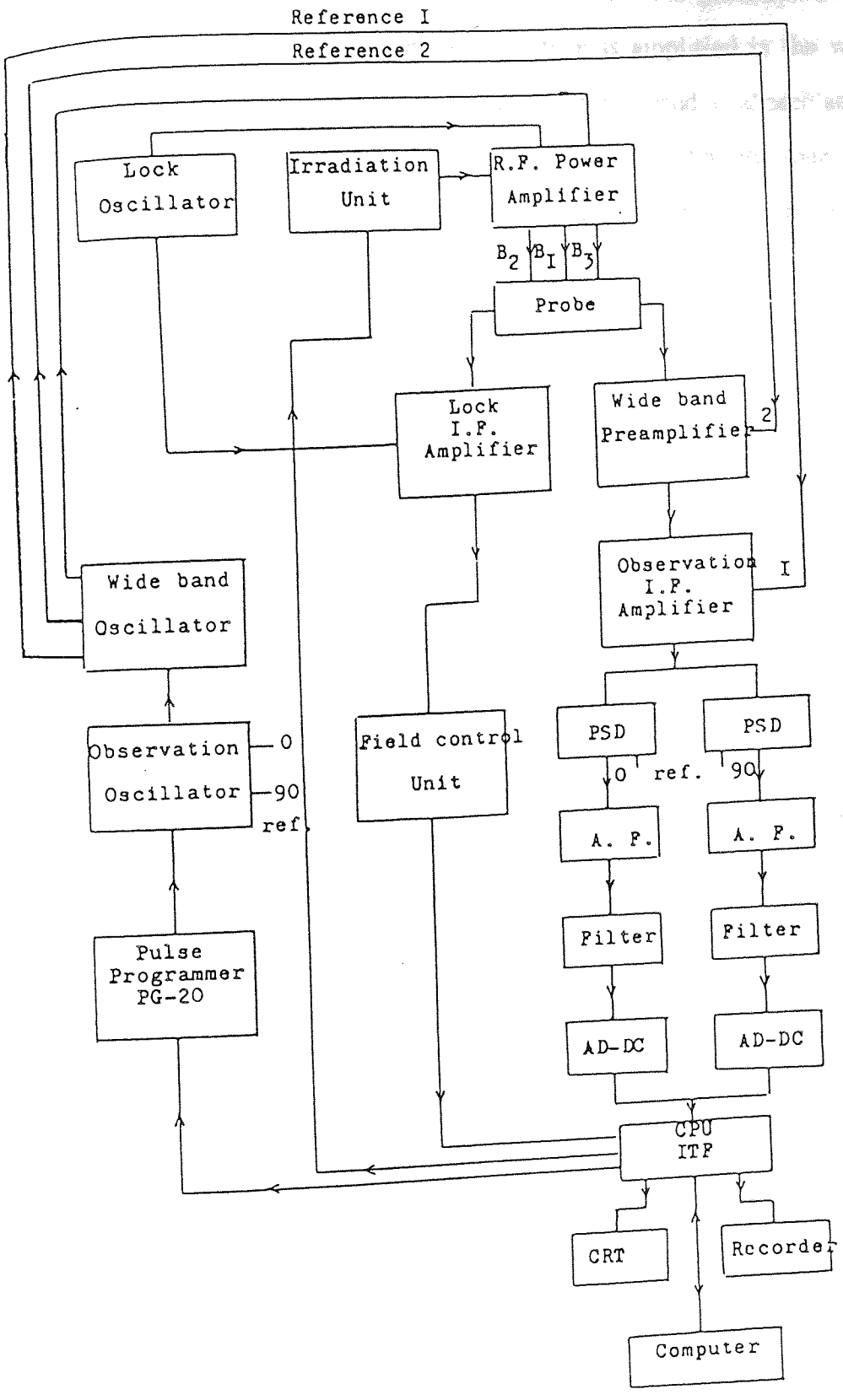

Figure 7.2: Schematic representation of the basic units in the JEOL FX 90Q NMR spectrometer.

most of the energy generated at the transmitter coil. The FID generated after the r.f. pulse, is detected by the receiver coil and then is amplified in the wideband preamplifier unit where a reference signal from the wideband local oscillator unit is used to reduce the signal levels when they are mixed. An additional stage of amplification and frequency reduction, is achieved in the OBS IF amplifier where a further 0° and 90° reference signals from the OBS OSC unit are used to get the audio frequencies that are at 0° and 90° out of phase. At this stage, it can be seen that the detection system has two phase sensitive detectors (PSD) instead of the usual one in the digital quadrature detection (DQD) technique. The advantage of DQD system is that FT NMR can be carried out with the excitation pulse placed in the centre of the observation range. This allows the observation band width to be reduced to only half that required for single pulse detection (SPD), resulting in a $\sqrt{2}$-fold improvement of the signal-to-noise ratio. Since the r.f. is delivered at the centre of the spectrum, the efficiency of the r.f. power is enhanced 4 times when compared with SPD.

The AD-DA unit receives filtered signals which are converted to digital form. Then they are transferred via the CPU (controller) to the computer where the information is stored. When it is required, the FID is transformed to get the spectrum signal to digital form. The DA unit changes the information to analogue signals which can be recorded or displayed on the oscilloscope screen.

On the FX 90Q spectrometer, the conversation between the operator and the computer is facilitated by using a light pen unit. After pointing to a particular function or command on the screen this order is transferred to the CPU unit which establishes a link between the computer and the spectrometer units controlling its operations. In this way, the pulse mode, irradiation mode, frequencies etc can be selected.

The lock signal is obtained as in any continuous wave spectrometer. The Lock OSC unit produces an r.f. signal at the appropriate resonance frequency and this is amplified in the r.f. power amplifier. The field control unit produces a

sawtooth signal which modulates the magnetic field, and allows the observation at the lock resonance signal which is phase sensitive detected at the LOCK IF amplifier unit; this receives a reference signal from the LOCK OSC unit. In addition to being used for lock, the signal can also be used for rapid monitoring of the adjustments to the resolution of the magnet. The r.f. oscillator for the lock signal can be used with two nuclei namely $^{2}D/^{7}Li$. The ^{2}D nuclei for internal lock and the ^{7}Li nuclei as an external lock in a separate probe.

The r.f. irradiation oscillator units used for double resonance studies can be selected according to the experiments that involve either noise irradiation or selective r.f. output. In both cases the irradiation power has to be amplified, but at different levels that are controlled by the irradiation selector unit which is linked to the r.f. power amplifier. The noise irradiation modulation width can be selected to be 0.5, 1, 2.5 and 5 KHz. Normally 1 KHz is used to irradiate protons when detecting ^{13}C. In the case when selective r.f. power is used for double irradiation, the r.f. power can be manually adjusted to the required level, and the OFFSET of the r.f. irradiation field can be similarly adjusted in a continuous fine range covering $\pm$ 5 Hz.

7.2(k) The Probe

The probe is placed between the poles of the magnet and has several modules. These are:

(1) The permabody; this is the fixed main part of the probe on which the sample insert is mounted. Within it, irradiation and detection coils and a thermocouple are mounted. The spinner has a device for detecting the sample spinning rate. This is achieved by a photosensor placed on the top of the permabody. Air is used to spin the sample tube, and water is used to keep the temperature of the permabody constant.

(2) The radiofrequency tunable module, this has five ranges of frequencies with five independent impedance matching channels and the fine tuning which maintains optimum sensitivity over the range of frequencies needed for observing the various nuclear resonances.

(3) The irradiation module; this enables the tuning of the irradiation circuit so that most of the energy is used in the irradiation coil to produce a maximum field. This is indicated by a minimum in the standing wave ratio meter deflection (SWR).

(4) The sample insert; this is exchangeable for different sample tube sizes and holds the sample coil that is wound around the glass tube. At the bottom of the insert there is a plug that permits electrical connections of the coils to the spectrometer.

(5) NMR Lock; this serves to maintain a fixed relation between the magnetic field and frequency of the NMR instrument and so enhance system stability. There are two methods of NMR lock, namely, the internal lock which refers to that method whereby the lock sample (deuterium solvent) is mixed with the sample to be measured, and the external lock (^{7}Li) which uses a lock sample that is kept separate from the sample to be measured.

7.2(l) Autostacking Program

The different operations that can be carried out by the computer are contained in the autostacking program which consists of the:

(1) normal program

(2) stacking program

(3) analysis program

The work carried out in the present thesis used only the normal program which is always used for routine measurements. The basic operations require the setting of pulse width, pulse mode, pulse repetition, frequency range, observation frequency, irradiation mode, irradiation frequency and the OBSET

which has to be placed in the middle of the spectrum. The number of scans is selected according to the nuclei and sample concentration. When the accumulation ends the FID is adjusted with mathematical parameters which modify the final spectra in terms of S/N resolution, line shape etc. In addition, several other measurements can be made on the screen via the light pen of line width, chemical shift intensity etc. Finally the data can be printed on a alpha numeric printer or recorded on a conventional chart.

The computer JEC-980B has a memory of 24K words. The progam is stored in the initial 8K words memory; the remaining memory 16K words are used as the entire spectral data memory.

7.3 Relaxation Time Measurements

There are several pulse techniques to determine spin-lattice relaxationtimes, T_1.[29,72,230-246] The most common techniques being the inversion recovery (IR), saturation recovery (SR) and the progression saturation (PS). However, the work reported in this thesis uses a newly revised pulse technique, referred to as the Driven Equilibrium Single Pulse Observation of T_1(DESPOT), instead of the three mentioned techniques mentioned above. Each technique has its advantages and disadvantages[227,235]. One feature that has to be considered when selecting the method most suitable to a particular problem is the implicit time scale of each method. This assumes considerable importance for nuclei of low natural abundance, and low sensitivity, particularly when studied at low concentration. The SR, PS and DESPOT are faster and more convenient than the inversion recovery. However, the pulsing requirements in the PS methods are more rigorous. The effect on determined T_1's of misset pulse lengths and variable offset were studied by Levy and Peat[227]. They showed that the PS method gives 5-10% more systematic errors than IR and SR in the determination of spin-lattice relaxation times. In the case of DESPOT it has features similar to those of the PS method, in

that it involves driven-equilibrium experiments, but depends on a systematic variation of the pulse angle θ, and does not involve the use of variable delay times. DESPOT has also been shown[247,248] to be over 100 times more rapid to use than the IR method, under similar conditions.

7.3(a) Driven equilibrium single pulse observation of T_1 (DESPOT)

The Driven Equilibrium Single Pulse Observation of T_1 is (DESPOT)[247-248], a method for measuring spin-lattice relaxation times T_1 that is one of the most versatile techniques in terms of the ease of instrumentation and also in terms of the time saved in obtaining T_1 values. This technique is likely to succeed and supersede techniques like the inversion recovery(236), saturation recovery(243-244), the progressive saturation methods(245-246) and other modified techniques(230,232,234).

The procedure for DESPOT involves a repeatedly applied pulse θ at a fixed interval of time until an equilibrium cycle is obtained. A field spoiling z gradient pulse (FS) is applied after acquisition, which destroys phase coherence of nuclear vectors in the x-y plane, so removing M_x and M_y vectors. The remaining magnetisation vector M_z increases slightly between field spoiling and the next nutation pulse and in the steady state, the increase is exactly matched by the decrease caused by (θ - fS) resulting in an equilibrium cycle independent of t_i but dependent on T_1. The cyclic process is outlined in Figure 7.3. Figure 7.3(a) depicts the approach to equilibrium and Figure 7.3(b) shows the equilibrium cycle.

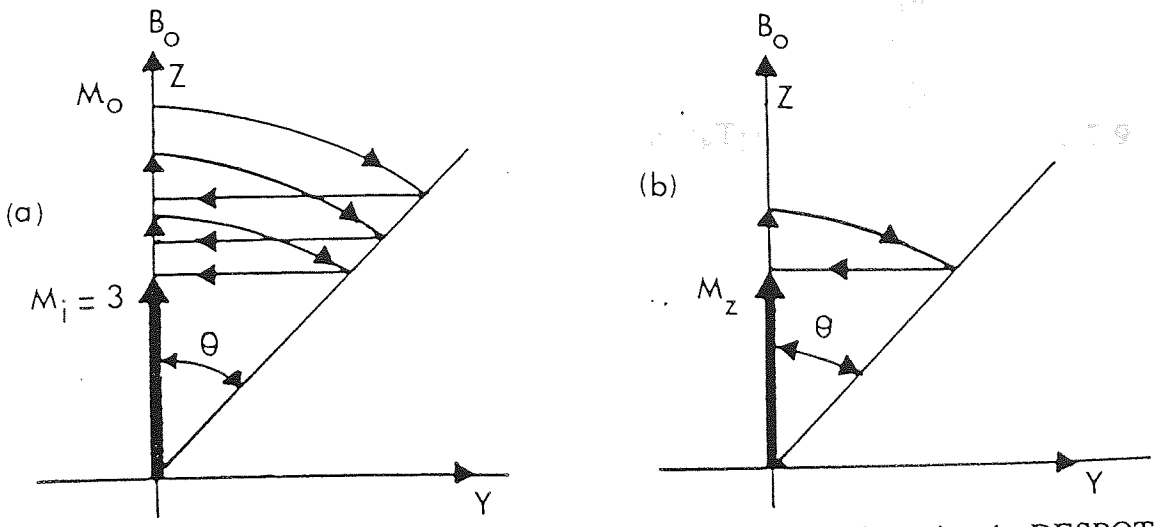

Figure 7.3(a) and (b): The approach to equilibrium magnetization using the DESPOT pulse sequence

Prior to attainment of this cycle, non-acquisition dummy pulses are employed and acquisition (A) of data is allowed only after sufficient dummies for attainment of the steady state have been applied. The number of dummy pulses varies with the nutation angle θ (proportional to pulse width). The minimum number of dummy pulses required has been assessed by experiment and computer simulations. The relevant DESPOT pulse train may be represented as:

$$(\theta - FS - t)_n - (\theta - (A) - FS - t^*)_m \qquad \ldots\ldots 7.7$$

The sequence $(\theta - FS - t)_n$ represents the system being subjected to rapid multipulsing at an angle θ, requiring n non-sampling or dummy pulses, in order to attain a steady state. Following the attainment of a steady state, the equilibrium magnetisation, M_{zeq}, is acquired (A) by m acquisition pulses in a sequence of the form $(\theta - A - FS - t^*)_m$. The times t and t* ensure that the dummy and the acquisition sequences have a constant total pulse repetition time t_i, such that $t_i = FS + t$ and $t_i = FS + A + t^*$ in the respective cases. 7.8

The DESPOT equilibrium magnetisation is given by:

$$M_{zeq} = M_o (1 - \exp(-t_i/T_1) / (1 - \cos\theta \exp(-t_i/T_1) \quad \ldots\ldots 7.9$$

which upon rearrangement gives;

$$M_{zeq} = M_{zeq} \cos\theta \exp(-t_i/T_1) + M_o(1 - \exp(-t_i/T_1) \quad \ldots\ldots 7.10$$

From the equation, a plot of $M_{zeq} \cos\theta$ obtained at different values of θ gives a straight line with a gradient of $\exp(-t_i/T_1)$ and an intercept of $M_o (1 - \exp(-t_i/T_1))$. From the gradient of the regression T_1 values can be obtained.

The geometrical configurations of the detector coils in the NMR instruments, provides signal intensities, I, that derive from the magnetisation normal to the direction of B_o and it is necessary to appreciate that for the magentisation, M, at some angle, θ, to the direction of B_o, the following equation holds;

$$I = KM \sin\theta \quad \ldots\ldots 7.11$$

where K is a spectrometer constant.

For a steady state, the equilibrium magnetisation intensity I_{eq} can be expressed as:

$$I_{eq} = KM_{eq} \sin\theta \quad \ldots\ldots 7.12$$

from which $I_{eq}/K\sin\theta$ can be substituted for Mz_{eq} in equation 7.10 for practical use.

An alternative method of determining T_1s, stems from differentiating equation 7.9 with respect to the nutation angle θ. This predicts that a plot of signal intensity, I, versus pulse widths, t_p, for various nutation angles, will show a peak maximum when

$$\cos\theta = \exp(-t_i/T_1) \quad \ldots\ldots 7.13$$

so that T_1 can readily be estimated from this condition.

Figure 7.3(c) illustrates for plots of signal intensity, I, versus pulse width, t_p (μs) for various pulse angles in the range $\theta = 0^o$ to $\theta \sim 90^o$, for ^{13}C nuclei in ethylbenzene.

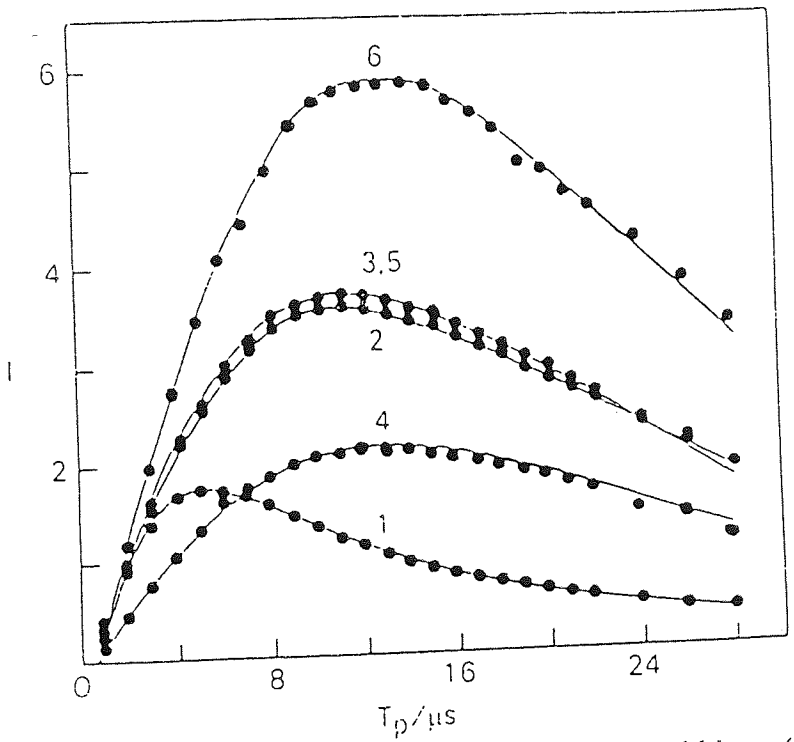

Figure 7.3(c): Plots of signal intensities, I, against pulse width, t_p (μs) for pulse angles in the range of θ=0 to θ=90°, for the ^{13}C NMR resonances of ethylbenzene

There exists a further possibility for deducing T_1 that involves measurement of intensities at two pulse angles only if signal intensities I_1 and I_2 are measured for two pulse angles θ_1 and θ_2 it is possible to deduce T_1 from equation 7.14:

$$\ln \frac{(I_1 \sin\theta_2) - I_2 \sin\theta_1)}{(I_1 \sin\theta_2 \cos\theta_1 - I_2 \sin\theta_1 \cos\theta_2)} = \frac{-t_i}{T_1} \qquad \ldots\ldots 7.14$$

The choice of effective pulse, flip (nutation) angles, using two pulse angles for the measurement of T_1, should be such that a good signal to noise ratio as well as a significant difference in signal intensities between the two pulse angles is observed.

Table 7.1 illustrates the number of non-sampling or dummy pulses suitable for the measurement of spin-lattice relaxation time, T_1 for carbons. Here a value of T_1 is first assumed, and with the value of a pulse repetition time, t_i, that is going to be used, gives the ratio of t_i/T_1, from which the required number of non-sampling, or dummy pulses at various angles (or pulse widths) are obtained. The table also shows a comparison of the magnetisation, M_z, achieved after the required number of dummy pulses with the true magnetisation, M_{zeq}, observed experimentally, for a particular nutation angle θ.

The DESPOT method requires the use of a homospoil pulse applied on the z axis. This sudden change in homogeneity can interupt the lock signal and cause the loss of homogeneity[250,254]. As a result, errors in relaxation times will be observed.

7.3(b) Determination of the 90° pulse width using DESPOT

The DESPOT technique implicitly requires an accurate knowledge of the pulse width, t_p, corresponding to the nutation angles θ, that are required for the experiment. This is usually done by determining t_p for $\theta=90^o$. The 90 degree pulse width is determined by taking a suitable sample which enables intensity variations with increasing pulse widths to be measured. Conventionally 5 T_1's are allowed between pulses to determine the maximum signal intensity, (90^o) or the null (180^o).

dummy analysis

ti/T1 ratio= 0.02

angle (deg)	pw us	dummies req'd	mz	mequ
0	0	1	999.99	999.99
3	0.8	123	941.05	936.46
6	1.5	157	790.57	786.67
9	2.3	149	624.36	621.33
12	3	128	482.74	480.36
15	3.8	107	374	372.19
18	4.5	89	293.53	292.15
21	5.3	74	234.29	233.21
24	6	62	190.26	189.4
27	6.7	52	157.1	156.36
30	7.5	44	131.67	131.02
33	8.3	38	111.8	111.28
36	9	33	96.08	95.65
39	9.8	29	83.45	83.11
42	10.5	25	73.25	72.91
45	11.3	22	64.81	64.52
48	12	20	57.74	57.54
51	12.7	17	51.93	51.68
54	13.5	16	46.85	46.71
57	14.2	14	42.62	42.47
60	15	12	39.01	38.83
63	15.8	11	35.8	35.67
66	16.5	10	33.02	32.92
69	17.3	9	30.6	30.52
72	18	8	28.47	28.4
75	18.8	7	26.59	26.53
78	19.5	6	24.93	24.86
81	20.3	5	23.47	23.38
84	21	4	22.16	22.06
87	21.8	4	20.87	20.87
90	22.5	1	19.8	19.8

*-No of dummies required exceeds 550
Mz value after 550 dummies

Table 7.1: The number of non-sampling, or dummy pulses required for measurement of spin-lattice relaxation times T_1, for carbon-13 nuclei.

A more rapid alternative is to use DESPOT itself. Usually an excess of 100 dummy pulses are used for any given pulse width prior to measurement of the signal intensity, as this would certainly ensure that magnetisation, M, has been driven to equilibrium. The null condition for a DESPOT nutation angle of 360^{o} is then sought.

By increasing the pulse width around the expected 360^{o} position until the lineshape splits into two equal intensities, one of +ve intensity and one of -ve intensity, this gives the value of the pulse width corresponding to the nutation angle of 360 degrees.

Figure 7.4a shows a DESPOT 360 degree pulse determination for a ^{13}C nucleus.

DESPOT 360 degree pulse determination

data fitted to cubic equation

$$y(int.) = a*x^3 + b*x^2 + c*x + d$$

where:-
a= -0.32411858 b= 108.23732
c= -11706.995 d= 408244.09

Data Table

pulse width microsecs	Expt. int	Calc. int.
90	-4926	-4945.6071
95	-4996	-4969.7858
100	-4245	-4200.7863
105	-2693.5	-2881.6984
110	-1559.75	-1255.6158
115	600	434.37732
120	2065	1945.1967
125	2865	3033.7435
130	3507	3456.931

pulse width(y=0)= 113.7±.1us
int.= 2.3963623 at 113.7 us

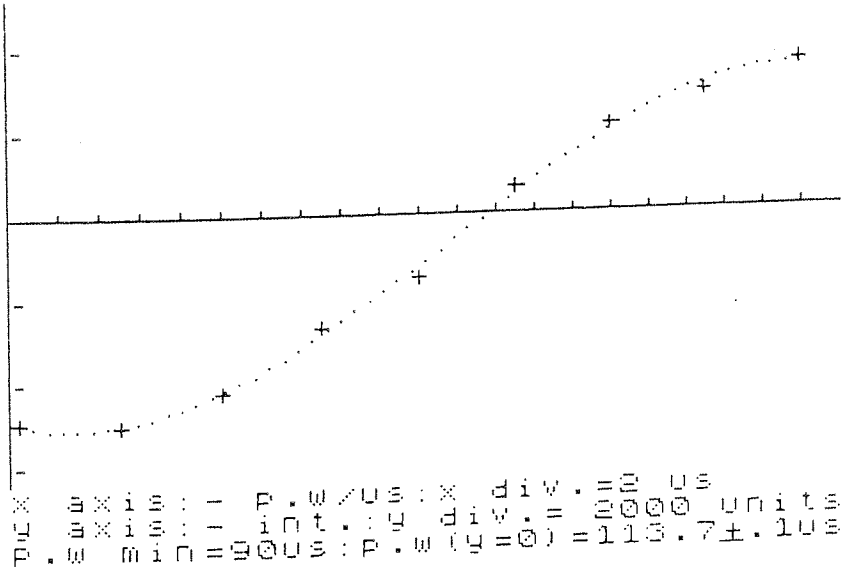

Figure 7.4 (a): A DESPOT 360° degree pulse determination of ^{13}C nucleus.

7.3(c) Selection of optimum parameters for T_1 measurements

Once a pulse sequence has been selected for measurement of relaxation times, a number of practical problems remain to be solved regardless of the nature of the sequence. These problems can arise from the following factors[227]:

(a) quantity of sample

(b) sample state (solvent, paramagnetic impurities etc)

(c) temperature control problems

(d) instrument resolution and sensitivity stability

(e) effective nutation angles

(f) computer limitation

(g) data processing

(h) non-exponential relaxation behaviour

The size of the sample can effect the value of T_1[29,249,250] because the B_1 field is not entirely homogeneous inside the transmitter coil over the entire sample length. If the sample occupies a larger volume than the area influenced by B_1, then the value of B_1 at a point away from the centre of the coil can be very different from that at the centre. This means that physically remote nuclei which are away from the large influence of B_1 affect the value of the true relaxation times when they diffuse into the central region of the coil. Furthermore, if a system is saturated to a low B_1 regions and appear to relax more quickly. It has been established, usually, that(227) for ^{13}C T_1's $\leq$ 50 seconds and for samples $\leq$ 30mm in length, the effect of diffusion is negligible. Moreover, sample tube diameter can also affect the amount of diffusion a system undergoes during measurement of T_1 experiments.

The values of spin-lattice relaxation times, T_1, are very dependent on sample purity. It is important, therefore, to use uncontaminated compounds and to prepare solution in clean containers.

The presence of dissolved oxygen or other paramagnetic impurities in the sample can significantly affect the value of relaxation times. This is particularly true for protons which are located at the periphery of the molecules, and experience dipolar-dipolar interactions with the paramagnetic sources so that the latter provide become the most important relaxation mechanism. For example, the relaxation time, T_1, for pure benzene is approximately 4.8 seconds in normal air saturated samples, but after degassing by chemical processes[251] it is found to be 24.8 sec at 309° Kelvin.

Good temperature control is very important to the accurate measurement of T_1. The identification of temperature problems is relatively easy because the observed T_1 either increase or decrease (see Chapter 2) according to the change in temperature and the type of relaxation mechanism of the nuclei under study. It is also known(252,253) that there are samples (especially ionic solvent) that when they are irradiated (eg. ^{13}C decoupling experiments) become hotter because of dissipation of the decoupling signal power.

The handling of acquired data is an important factor in determining the accuracy of measured T_1's. If for example the spectral resolution changes slightly during the course of an experiment, the analysis of T_1 using peak heights alone is dubious. Therefore, only signal areas should be used. However, it is possible to impose a small exponential weighting factor on the FID which broadens the signals and masks resolution instabilities so that heights can be used to represent M_z with some confidence.

For further discussion on optimizing parameters for T_1 measurements see Brevard and Granger[234], and Shaw[72].

7.3(h) Spin-lattice relaxation time measurement using DESPOT

Three different computer analysis programmes requiring experimental data obtained from the DESPOT pulse sequence were used to obtain numerical values of the relaxation times. These programmes are: the curve fit, the linear fit and the two point curve fit.

The curve fit programmes fits intensity/pulse width pairs initially to a cubic equation. This fit is then used to determine the nutation angle, θ, corresponding to the peak maximum. At this point, the condition $\cos\theta = \exp(-ti/T_1)$ is fulfilled, permitting calculation of the spin-lattice relaxation time T_1.

The linear fit programme permits the analysis of the experimental data which is manipulated to fit a linear DESPOT equation. This programme gives a value for the relaxation times from the gradient and a value for the equilibrium magnetisation (M_o) from the intercept of the linear regression.

The two point curve fit analysis programme is based on equation 7.14. This involves measurement of intensities at two pulse angles which are then used to calculate the relaxation times and also simulate a graphical plot of signal intensities at various pulse widths.

Figures 7.4(b), (c) and (d) shows experimental numerical data for signal intensities/pulse width pairs, and graphical plots used to calculate spin-lattice relaxation time for the para carbon-13 nuclei in ethylbenzene using the three methods. The results appear to show similar values within acceptable experimental errors.

despot-t1 from peak max.

Ethyl Benzene
S. Patel
15/1/86
para carbon

fitted cubic curve

$$ax^3 + bx^2 + cx + d$$

a= 0.461 b= -35.663

c= 804.857 d= -850.681

90 deg pulse= 27 us
delay time= 4 s
pulse offset = 0.6 us

pulse width us	expt. int	calc int
3	1268	1137.8923
7	3157	3048.3103
11	4325	4257.2641
15	4785	4753.861
19	4694	4731.7473
23	4426	4397.7914

spin lattice relaxation time = 7.233 seconds
equilibrium magnetization(m0)= 9233.0527

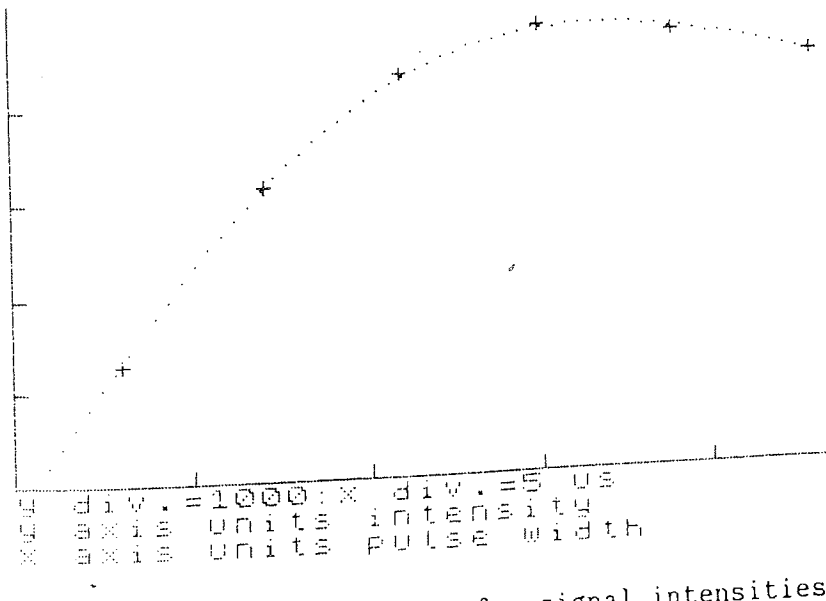

Figure 7.4 (b): Experimental data for signal intensities/ pulse width pairs, and graphical plots used to calculate spin-lattice relaxation time for the para carbon-13 nuclei in ethylbenzene. The results are obtained using a curve fit programme.

DESPOT-T1 from Mz vs Mzcos θ

Ethyl Benzene
S. Patel
15/1/86
para carbon

fitted line
ax + b = y(int.)

a= 0.571 b= 3940.137
correlation coeff.= 0.9996

90 deg pulse= 27 us
delay time= 4 s
pulse offset= 0.599 us

pulse width/us	intensity
3	1268
7	3157
11	4325
15	4785
19	4694
23	4426

data table

x	y	y calc'd
8819.1337	8909.8229	8980.9107
7885.8048	8494.2666	8447.4457
6073.6127	7456.1649	7411.6468
4146.2261	6331.4624	6310.006
2419.9252	5281.0675	5323.3002
1073.736	4554.3809	4553.8557

spin lattice relaxation time= 7.151 seconds
equilibrium magnetization(M0)= 9196.74

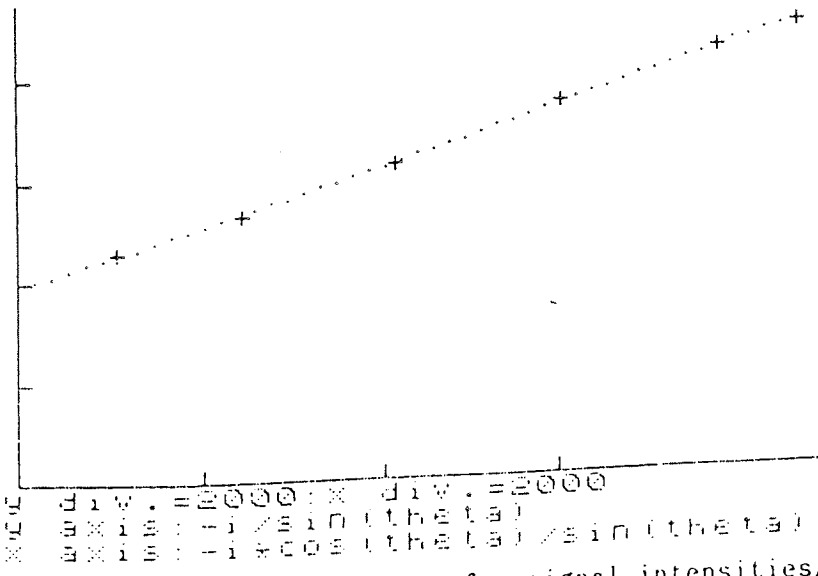

Figure 7.4 (c): Experimental data for signal intensities/ pulse width pairs, and graphical plots used to calculate spin-lattice relaxation time for the para carbon-13 nuclei in ethylbenzene. The results are obtained using a linear fit programme.

2-point curve fit analysis programme

```
pulse width 1= 7 us
pulse width 2= 19 us
pulse offset= 0.6 us
90 deg pulse= 27 us
intensity 1/1= 3157
intensity 1/2= 4694
intensity 2/1= 3157
intensity 2/2= 4694
pulse repetition 4 secs
T11= 7.529 secs
T12= 7.529 secs
M01= 9362.17
M02= 9362.17
int max 1 at 15.838 usecs
int max 2 at 15.838 usecs
```

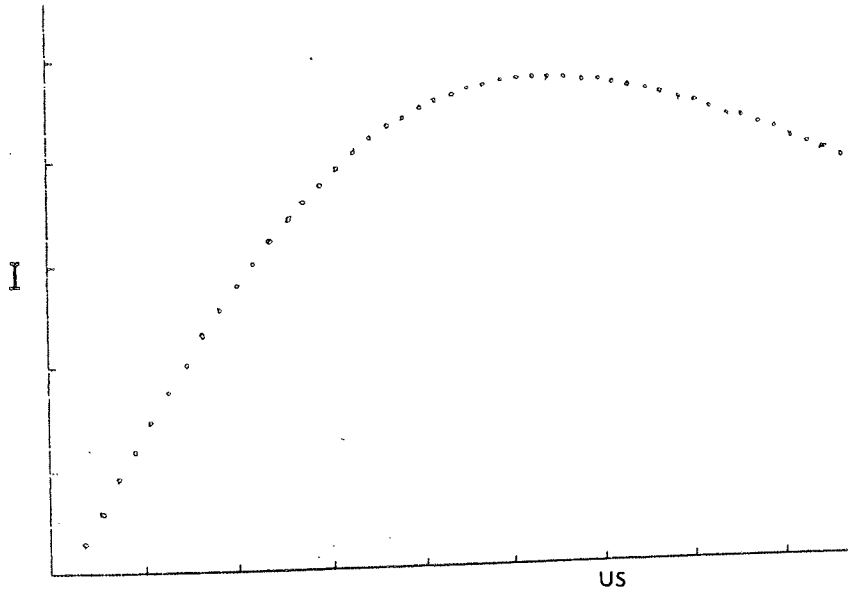

Figure 7.4 (d): Experimental data for signal intensities/ pulse width pairs, and graphical plots used to calculate spin-lattice relaxation time for the para carbon-13 nuclei in ethylbenzene. The results are obtained using a 2pt curve fit programme.

7.4(a) Introduction: Instrumentation and Experimental Methods using Sound

Two different types of instruments were necessary for investigating the two areas of research described in this thesis.

To investigate the effects of molecular perturbations by sound in the liquid phase and to observe these effects through their influence on NMR relaxation times required the use of instruments which could generate ultrasound frequencies in the mega-Hertz region and power levels ranging from as low as 0.1 watt cm^{-2} to as high as 30 watts cm^{-2} in addition to an NMR instrument.

To investigate the effects of acoustic cavitation on chemical reactions required the use of instruments which could generate sound frequencies in the KHz region and power levels ranging from as low as 5 watts cm^{-2} to as high as 150 watts cm^{-2}.

The two areas of research will now be discussed in terms of instrumentation and experimental methods.

7.4(b) Generation and Transmission of Sound

In order to facilitate the presently described studies, various instruments had to be designed, constructed and adapted. This was due to the fact that no such instruments were commercially available. This in fact was one of the greatest problems in the research. Even to the present time, this equipment is being designed and redesigned in order to make it more adaptable and easier to use. The following ideas were put forward before the design and construction of the type of instruments and equipment required to undertake such a study had begun;

(a) An ultrasonic instrument which could generate frequencies from 1 Mega-hertz and above, and with an adjustable output power ranging from as low as 0.5 watts cm^{-2} to as high as 50 watts cm^{-2}.

(b) A unit or a component which could convert this high frequency low power electrical energy into acoustic (sound) energy.

(c) A means by which the acoustic energy could be delivered into a liquid sample contained within a NMR tube that is spinning between the magnetic poles of the NMR instrument. The NMR tube is to be filled with a liquid sample to a depth of 35mm in length, in a total NMR tube length of 130mm and an inside diameter of 9mm.

(d) In delivering the acoustic energy into a liquid sample, it has to be ensured that the NMR instrument resolution, the electronics and the electromagnet are not effected. Thus any equipment that has to be designed has got to be non-magnetic or at least far away as possible for it not to have any influence upon the magnetic fields of the NMR instrument.

(e) Any acoustic components or units which are inserted directly into the liquid sample, must not contaminate the liquid in any manner that would effect the NMR relaxation times.

Having laid a foundation for designing, constructing and adapting an ultrasonic instrument which could transmit acoustic energy into a liquid sample, within an NMR tube, the basic requirements for this may be summarised as follows:

(a) A ultrasonic frequency generator which can generate frequencies from 1 mega-hertz and above.

(b) A power amplifier, with an adjustable output power ranging from as low as 0 watts to high as 50 watts cm^{-2}.

(c) Transducers, which will convert electrical energy to acoustic energy.

(d) A probe, which is long and of a maximum outside diameter of 5mm which will either act as a medium through the sound energy will be transmitted, or have a transducer mounted on it, which can be lowered into the liquid sample held with the NMR tube.

If a 5mm diameter probe is to be inserted into a 9mm diameter NMR tube, which is spinning there is only a 2mm free annular space between the probe and the inside wall of the NMR tube. This suggests that great precision is necessary

for inserting the probe vertically into the NMR tube. Hence one needs to build equipment which would have three degrees of movement, in the x, y and z direction, and also have tilting mechanisms. The following sections deal with specification on each of the instruments designed, constructed and adapted in order to perform the experiments.

7.4(c) The Frequency Generator

During the course of this research two types of commercial frequency generator were used. In the initial stages, the first type of frequency generator used (Farnell instrument No LFM3) produced a selected frequency from 10 Hz to 10 MHz of either a continuous wave form or a square wave form, with an adjustable output power ranging from 1mV to 20V. The only drawback with this instrument was in the accuracy of selecting and tuning to a precise frequency. Thus, resonating a transducer at a particular frequency proved difficult.

The second type of instrument used (Yaesu FT57GX/FP757 HD PSV) was in effect a digital r.f. transceiver. The instrument consisted of a power supply, a frequency generator which operates with an accuracy of ±0.1Hz in the frequency range from 1 MHz to 30 MHz an adjustable output power from 1W to 100W and a watt meter (Yaesu VSWR) which measures both the forward and reflected power levels of up to 500W.

7.4(d) The Power Amplifier

In view of the lack of availability of suitable commercial equipment it was decided to test the working hypothesis of this thesis using single apparatus designed and constructed in house.

The first type of frequency generator used required building a power amplifier of the type broad-band. This was necessary so that the output power could be increased to a suitable higher value.

The first power amplifier built was of the "push-pull" type (Figure 7.5), which when connected to a power amplifying stage (Figure 7.6) would operate in a frequency range from 200 KHz to 10 MHz, with adjustable output power ranging from 1V to 80V (80 W). However, after having built and tested the amplifier it proved to work for a very small frequency range and with a very large power attenuation with increasing frequency.

The second amplifier built (Figure 7.7) was of a simpler construction using a copper coil wound on a ferrite rod. This proved to work much better with greater stability.

7.4(e) The Tuner

A tuner was designed and built, which maximized the forward power delivered to the transducer (Figure 7.8). This was necessary in order to match the impedence of the power supply, frequency generator and the power amplifier to that of the transducers. However, the frequency bandwidth in which the tuner could operate well was found to be narrow.

A second commercially purchased tuner proved to be more suitable (Figure 7.9) (type ATU SPC-300). This has a frequency coverage ranging from 500 KHz to 29.9 MHz, an input and an output impedance ranging from 50-750 hms, and 2 ohms to 2.5K ohms, respectively, and a power capability of 400 Watts. Figure 7.10 shows three ways of connecting a tuner (A.T.U.) to a transreceiver.

7.4(f) Transducers

(i) Generation of Ultrasonic Waves

Ultrasonic waves are derived from mechanical vibrations generated in a substance by causing it to vibrate at some point at the required frequency. There are numerous ways of generating these vibrations and can be classified as being piezoelectric, magnetostrictive or mechanical[82,113,255-260] in origin. Only the piezoelectric effect will be discussed here.

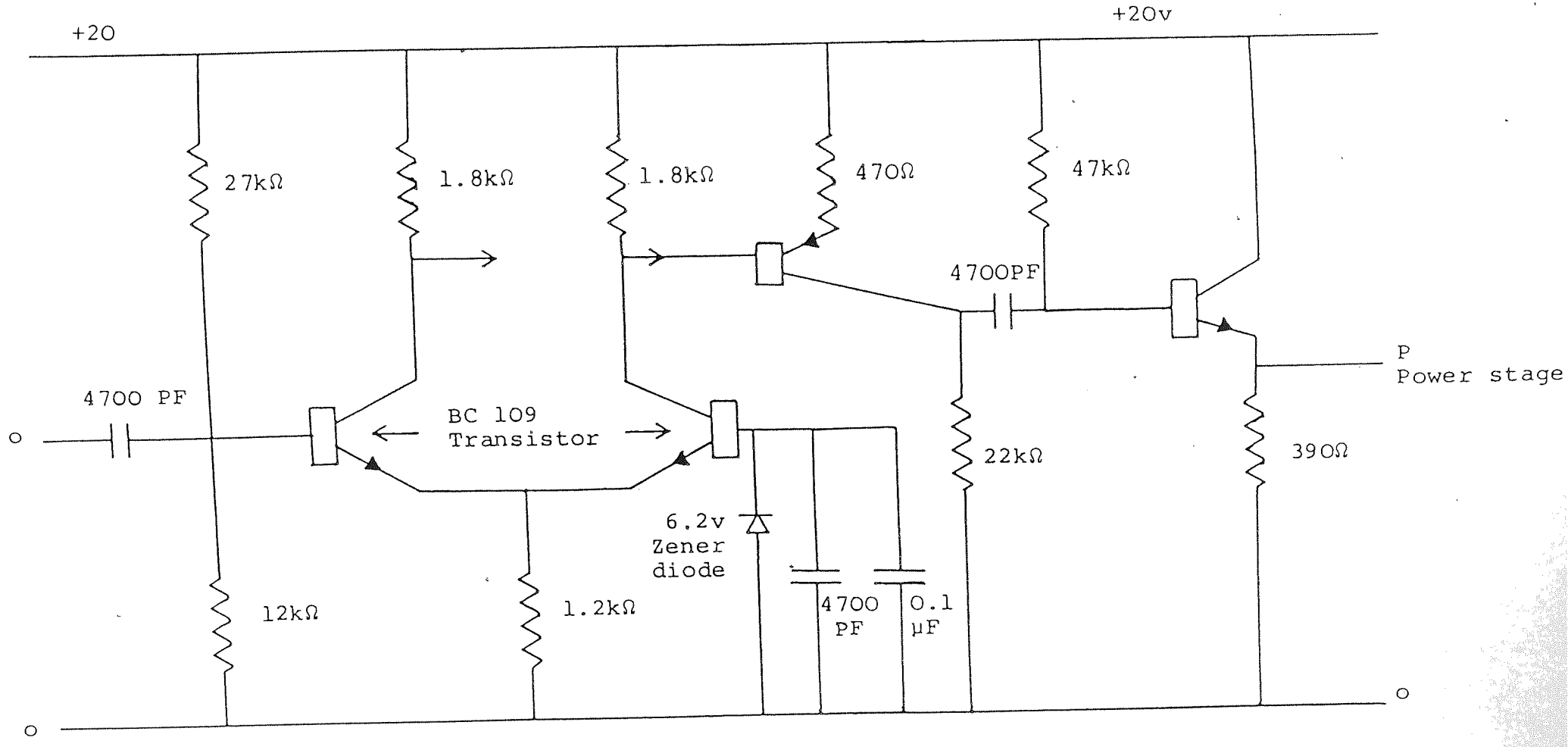

Figure 7.5: Push-pull amplifier (A)

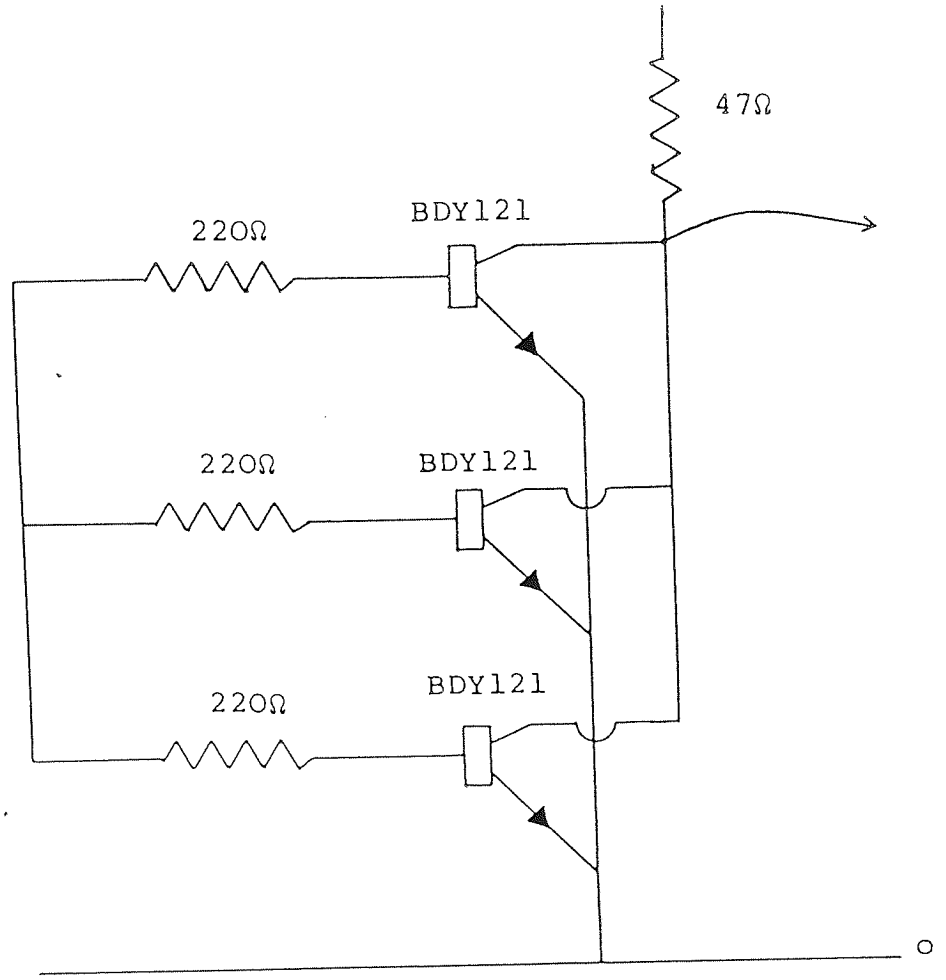

Figure 7.6: Power amplifying stage

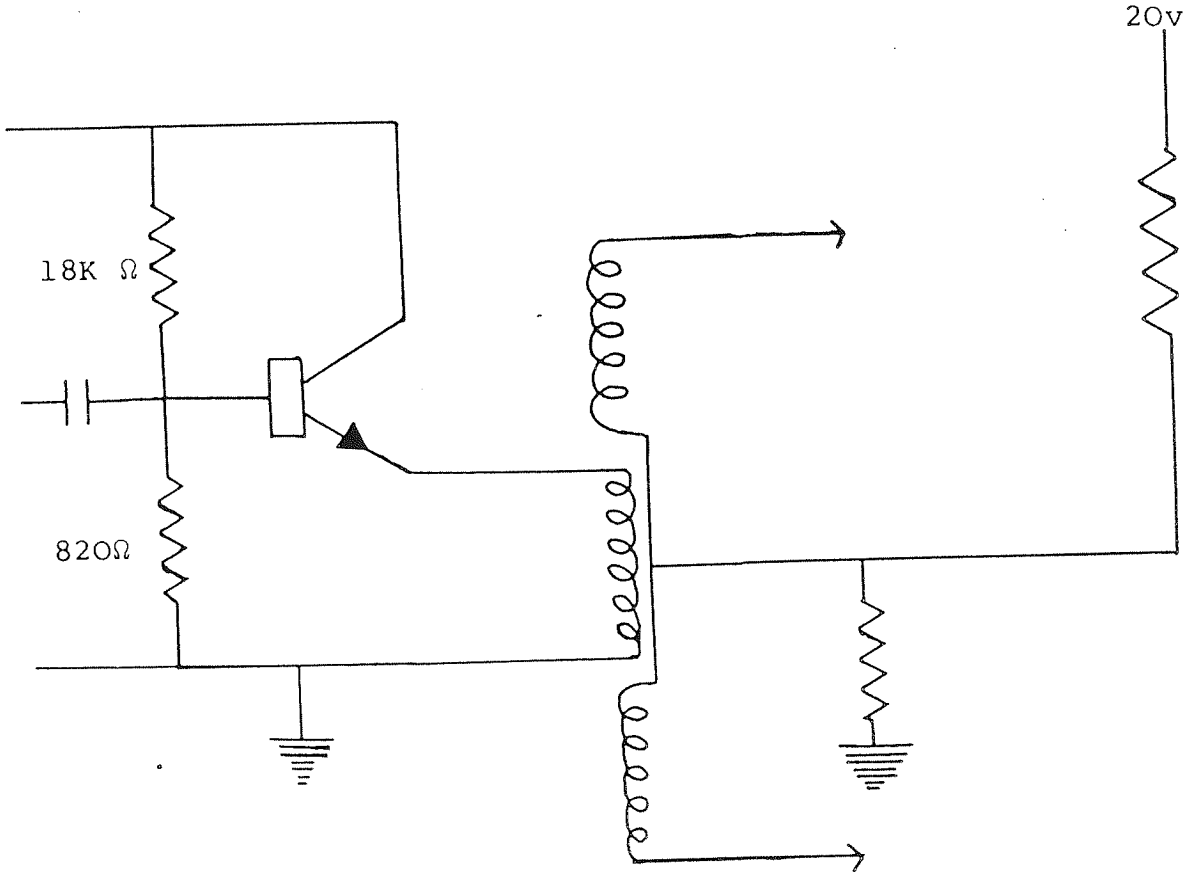

Figure 7.7 : Transformer type amplifier (B)

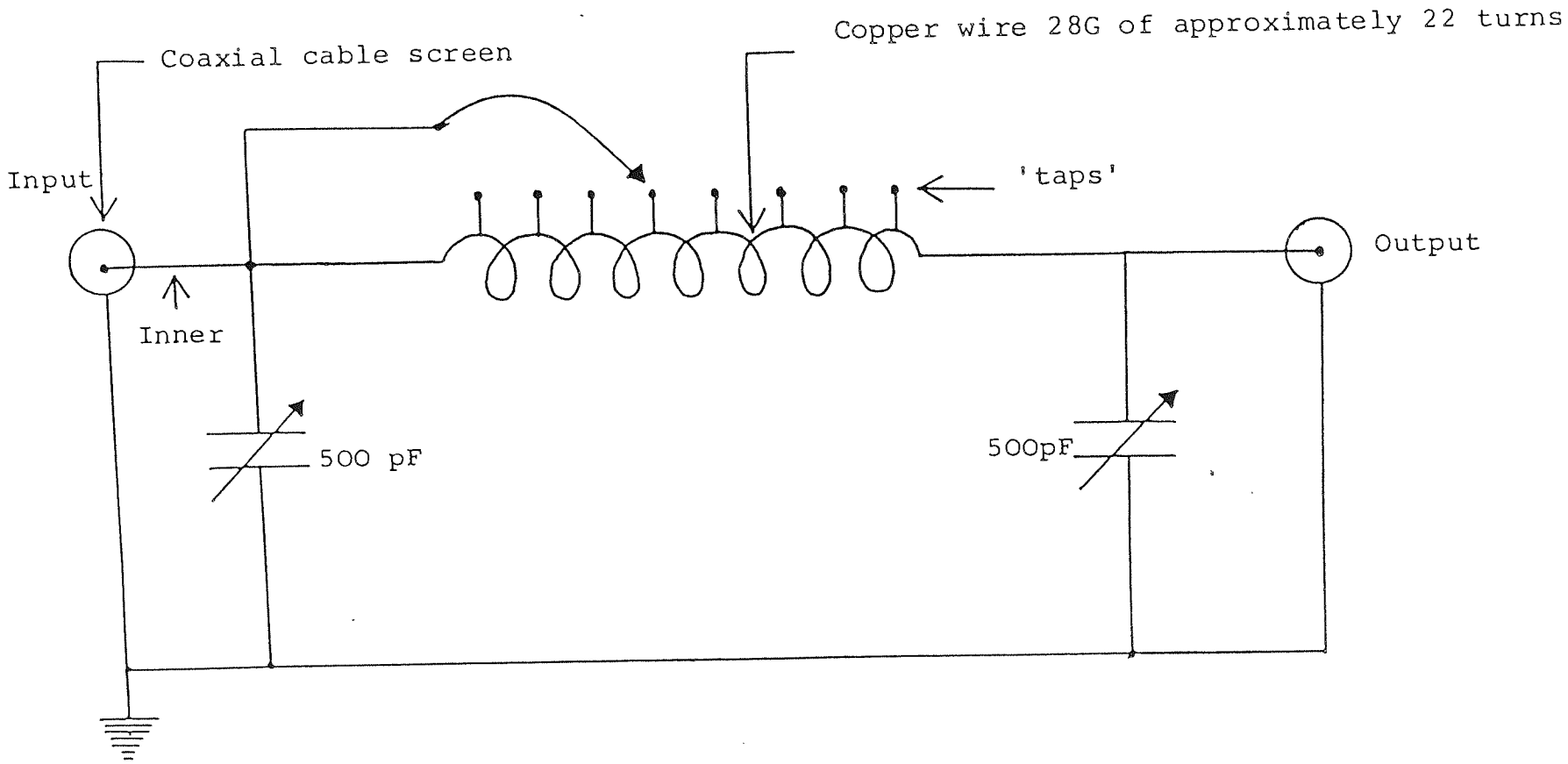

Figure 7.8 : Tuning circuit for transreceiver (home made tuner)

A.T.U. CIRCUIT DIAGRAM. (S.P.C. 300/3000)

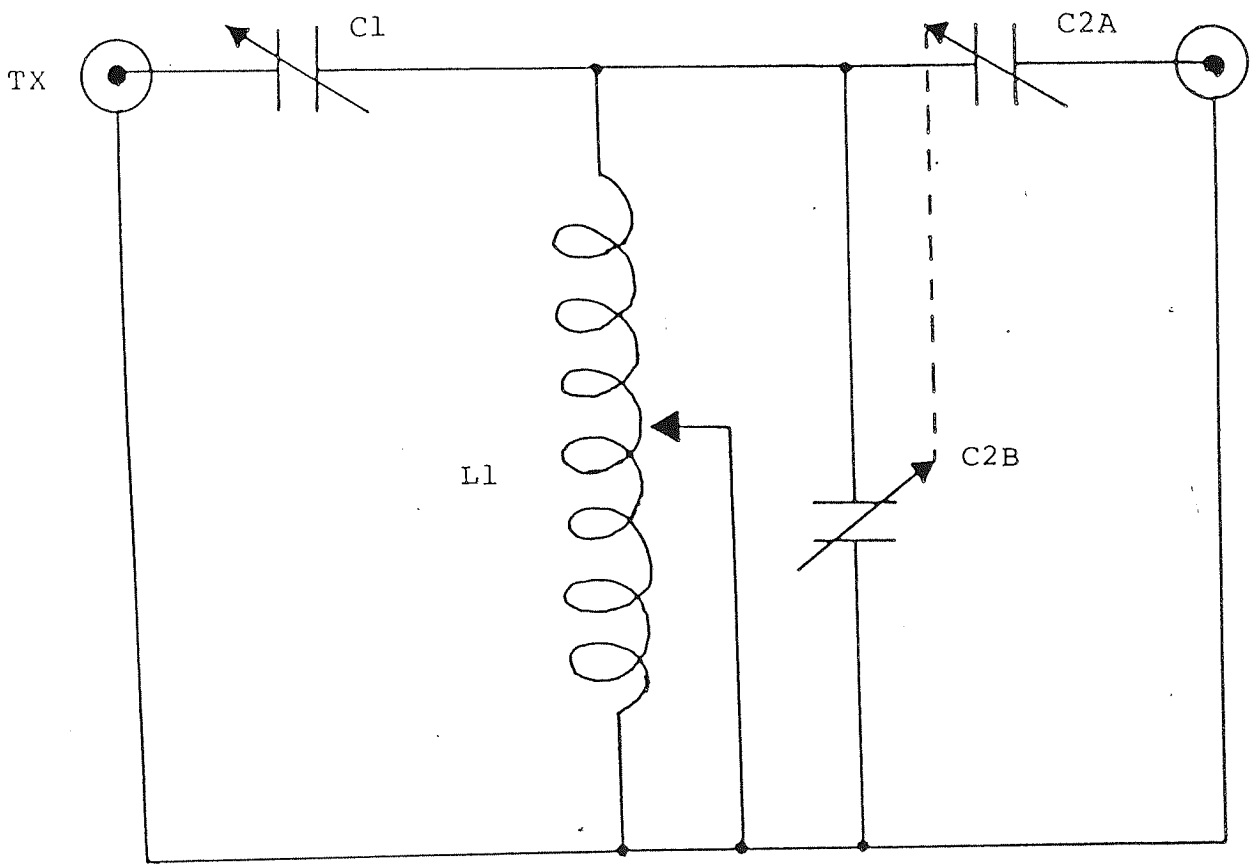

C1 - 200 PFD

C2 A&B - 200 & 200 PFD

L1 - Roller coaster

- 28 micro henries

Figure 7.9 : Circuit diagram for a commercially purchased tuner

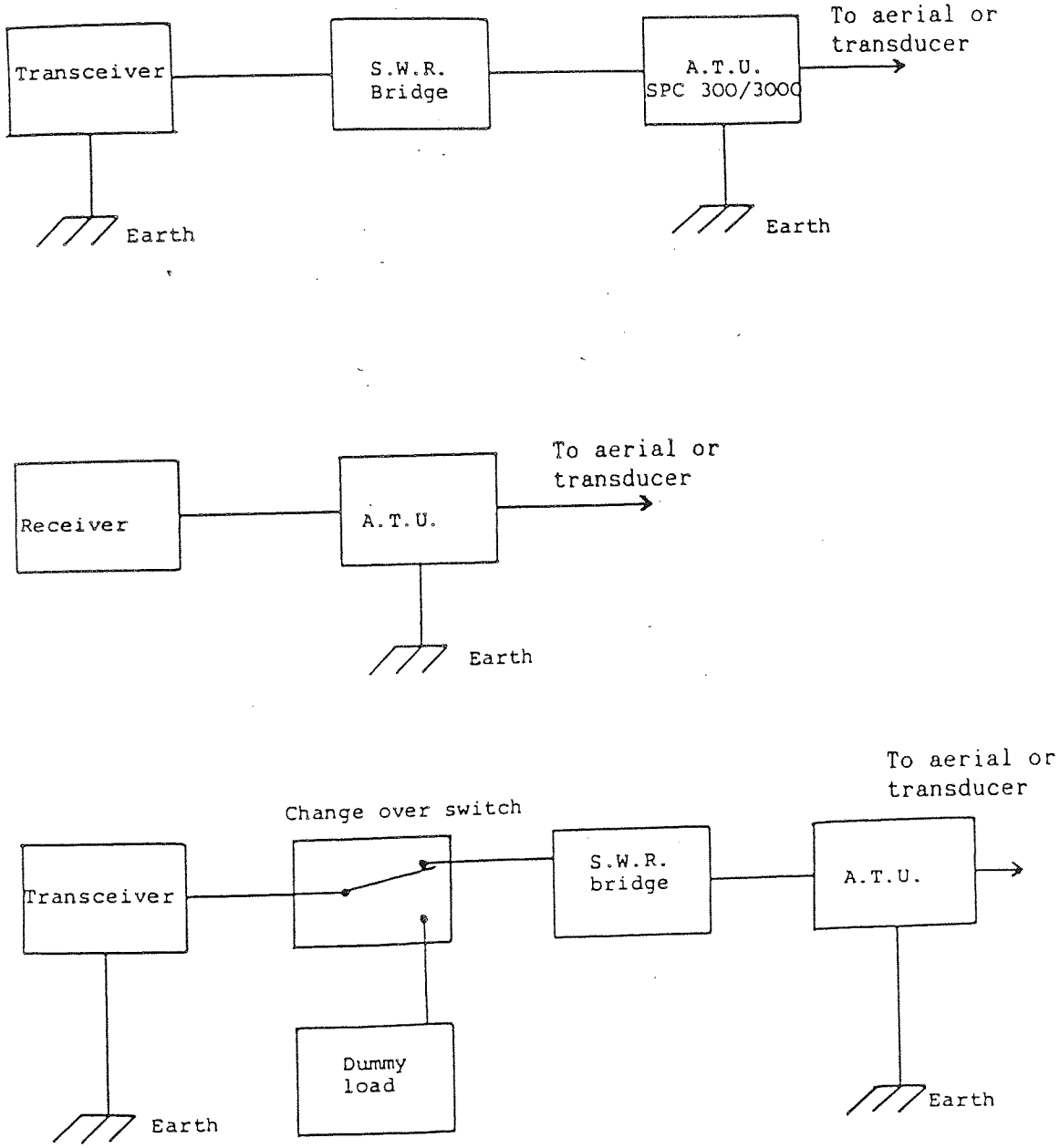

Figure 7.10: Three ways of connecting a tuner (A.T.U.) to a transceiver.

Some crystalline substances change their shape slightly when a voltage is applied across two opposite ends of a crystallographic axis (a straight line through the centre of the crystal). Examples of such materials having this property include quartz, barium titanate, lead titanate zirconate, lead strontium titanate zirconate and copolymers of vinylidene fluoride and trifluoroethylene[261-266]. When a high frequency alternating voltage is applied across a piezoelectric material, the shape of the material will alternate in harmony with the applied voltage, thus sending out mechanical waves at that frequency, into any substance with which it is in contact.

Materials which have the property to resonate as a result of applying alternating voltages and current are called transducers. By definition, a transducer is "a device that is actuated by power from one system to supply power to a second system", that is, a transducer is a device which converts energy from one form to another (in this case from a r.f. signal to sound of the same frequency).

(ii) Transducers Used

The types of transducers used in this work are of a modified PZT Lead zirconate titanate ceramic. This type of ceramic was chosen for several reasons[255,259,267-280] viz: PZT element, when compared with other ceramics, enables its volume to be substantially reduced for the same power input, or to have an increased power handling capacity for the same volume change. It has a high electromechanical coupling factor, a low dielectric loss (meaning that heating is kept to a low value), a high curie point which permits it to operate at high temperatures and also allows soft soldering without being depolarized (or loose its piezoelectric properties) and has a high dielectric constant which minimises cable loading effects on its performances. Table 7.2 lists some of these properties for the two types of transducers used during the course of this research[281].

Ceramic properties	Ceramic type: PZT 4A	Ceramic type: PZT 5A
Mechanical Q 0° psi	> 500	75
1000 psi	> 400	25 approx
2000 psi	> 200	25 approx
density ρ	7.5	7.75
Thermal conductivity W/m°C	2.1	1.5
Heat capacity J/Kg °C	420	420
Curie point °C	328	365
Tmax (max operating temp	200	250
k_p (planar electromechanical coupling, radial mode)	-.58	-.60
V_3^D (velocity of a compressional wave parallel to polar axis)	4600	4350
Transducer tollerance	± 7 - 10%	± 7 - 10%

Table 7.2: Some of the characteristic properties the ceramic transducers PZT 4A and PZT 5A(281).

The necessity for the PZT transducers to operate at large powers, have a high mechanical Q, and to be able to sustain large temperatures were very important from the point of view of the following experimental considerations.

(a) The maximum size of the probe was 5mm in diameter. This suggested that a transducer (PZT ceramic) had to be of the same order in size if it was to be mounted either at the top or bottom of the probe.

(b) If there were large electrical and acoustic impedance mismatches between the various generator components and the transducer, and between the transducer and the probe this would result in a great deal of power being reflected back into the transducer. This will result in causing the transducer getting hot. This in turn would result in changes of the overall performance of the transducer. For example, Figure 7.11(a) illustrates the changes in the mechanical Q versus temperature for

transducers of the type PZT 4A, 5A, 8 and 5H. As can be seen from the graph the PZT-4A transducer is more stable compared to the PZT-5A transducer in the temperature range of 0° to 150°C. Figure 7.11(b) illustrates the changes in the planar coupling factor, k_p, versus temperature for the various types of transducers. From the graph the planar coupling constant varies with increasing temperature for both PZT 4A and 5A transducers.

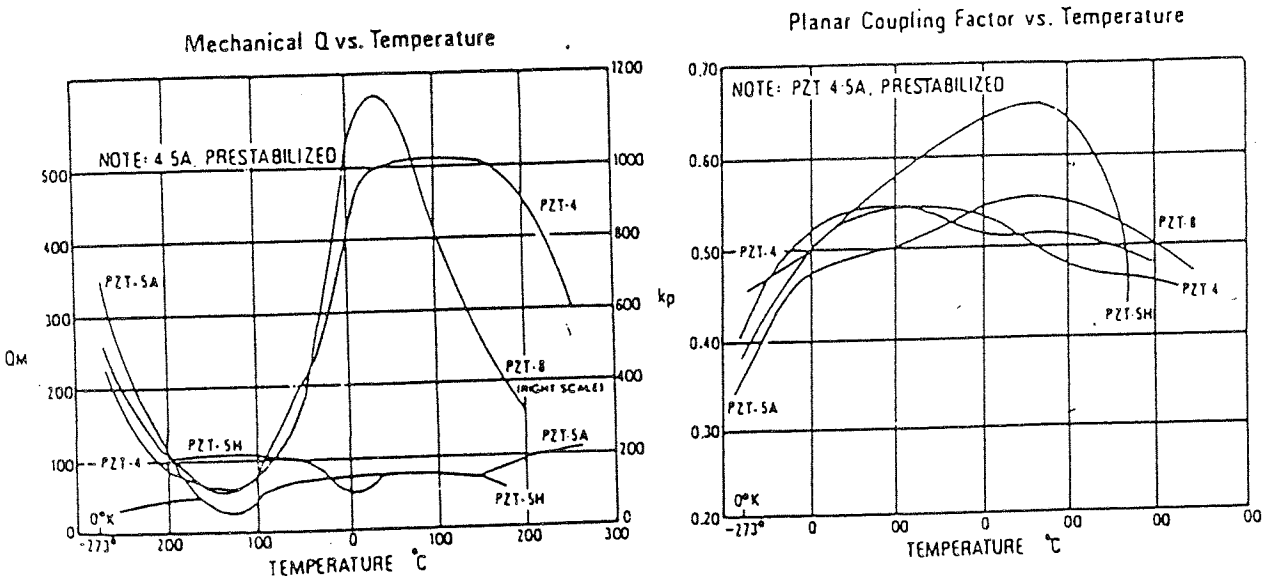

Figure 7.11(a) Illustrates changes in mechanical Q versus temperture for transducers of the type PZT 4A, 5A, 8 and 5H.

Figure 7.11(b) Illustrates changes in the planar coupling factor, k_p, versus temperature for transducers of the type PZT 4A, 5A, 8 and 5H.

(iii) Measurement of Resonance Frequency of Transducers

Due to a 10% tollerance in the natural frequency of the transducers, the exact resonance frequency had to be determined. Two approaches were followed:

(1) Use can be made of two transducers that operate at the same natural frequency. Figure 7.12 shows a circuit diagram for measuring the resonance frequency of the transducers. By slowly adjusting the frequency of the oscillator, the first transducer oscillated. This in turn induces oscillations in the second transducer, which in turn induced a voltage. This induced voltage was also observed using the oscilloscope.

By measuring the difference in power (through a difference in voltage) using the oscilloscope, between the first and second transducer, it was possible to determine the natural frequency of the first transducer. When the amount of power delivered through the first transducer at a specific frequency was almost equal to the power received through the second transducer, the first transducer was considered to dissapate all its acoustic energy by resonating at its natural frequency. It should be pointed out that a tuner should not be used for balancing the impedance as this would change the natural resonance frequency.

The method described above, was not particularly suitable as it relied on the second transducer to have the same characteristics to that of the transducer.

(2) This involves using a single transducer and a thin copper wire (coil) wound in the shape of a cylinder. The transducer was connected to a frequency oscillator and a double beam oscilloscope and the copper coil connected directly to the same oscilloscope with a resistor in series. The transducer was then lowered directly into the centre of the copper coil, and the total coil system placed in a suitable inert solvent like cyclohexane. Figure 7.13 illustrates the experimental set up.

By slowly adjusting the frequency of the oscillator the signal strength of the radio-frequency pick-up varied. The signal strength corresponded to the amount of power transmitted by the transducer into cyclohexane. When the transducer resonated at its natural frequency, the signal strength was found to be a maximum.

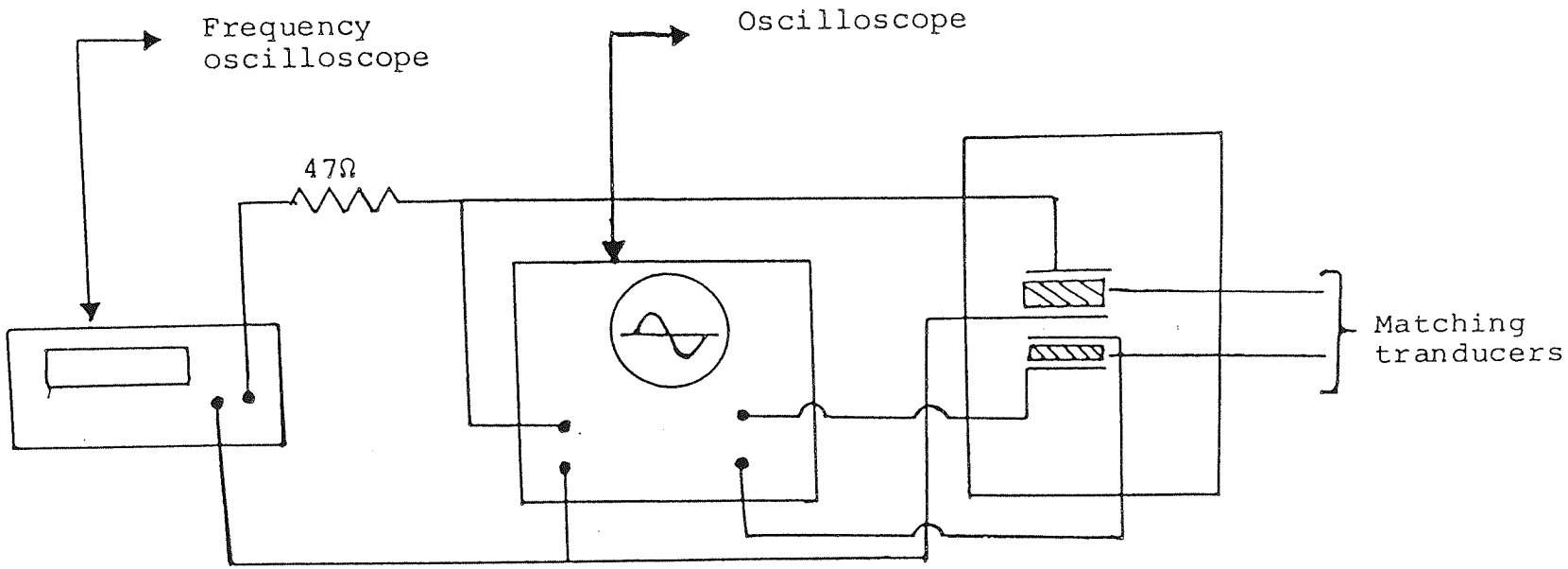

Figure 7.12: A circuit diagram for measuring the exact resonance frequency of a transducer using two transducers

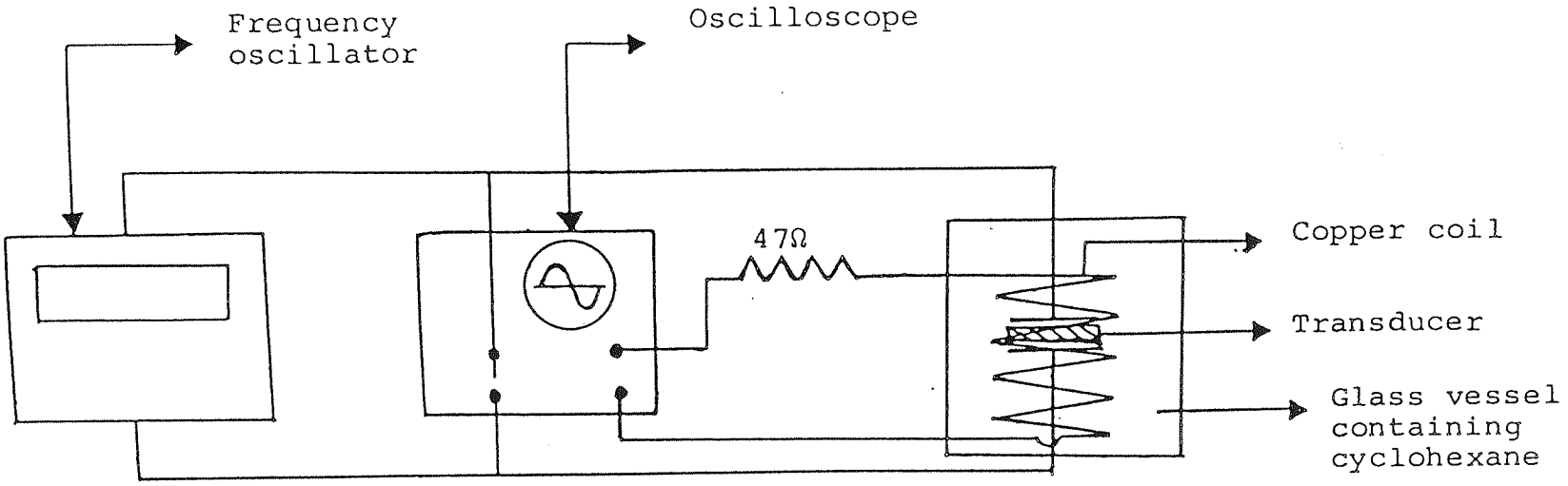

Figure 7.13 : A circuit diagram for measuring the resonance frequency of a transducer using a copper coil.

(iv) Measurement of Transducer and Frequencies of Maximum and Minimum Impedance

The frequency of minimum and maximum impedance was determined using the electrical circuit shown in Figure 7.14. This uses a frequency oscillator, a 1Ω, resistor a 100Ω, a variable resistor, an oscilloscope and a PZT ceramic. Using constant power and varying the frequency of the oscillator, a meter deflection peaked sharply at the frequency of minimum impedance, and a sharp null indicated the frequency of maximum impedance. The magnitude of minimum and maximum impedance differed so greatly that it was necessary to change the value of resistance R for the two measurements.

The magnitude of the minimum impedance was determined by adjusting the oscillator to the frequency of minimum impedance as shown in Figure 7.14(a). By substituting a calibrated variable resistor (such as a decade resistor) as shown in Figure 7.14(b), the value of minimum impedence was obtained by carefully adjusting the variable resistor until it had a similar reading to that obtained with the ceramic.

(v) Handling and Soldering to Ceramic Materials

Although PZT ceramics are robust materials and will withstand high stresses, they should be handled as glass, in order to avoid chipping and cracking.

Soldering to ceramic surfaces was one of the most common causes of thermal shock. If the user required to solder electrodes, or wires, special advice and instruction should be followed. These are that when soldering electrodes on to ceramic surfaces:

(1) The soldering iron should never come in contact with the ceramic body (use minimum of 15W minimum).

(2) The contact eletrode should be tinned with solder leaving a tiny blob of solder on the end, just sufficient to make the solder joint.

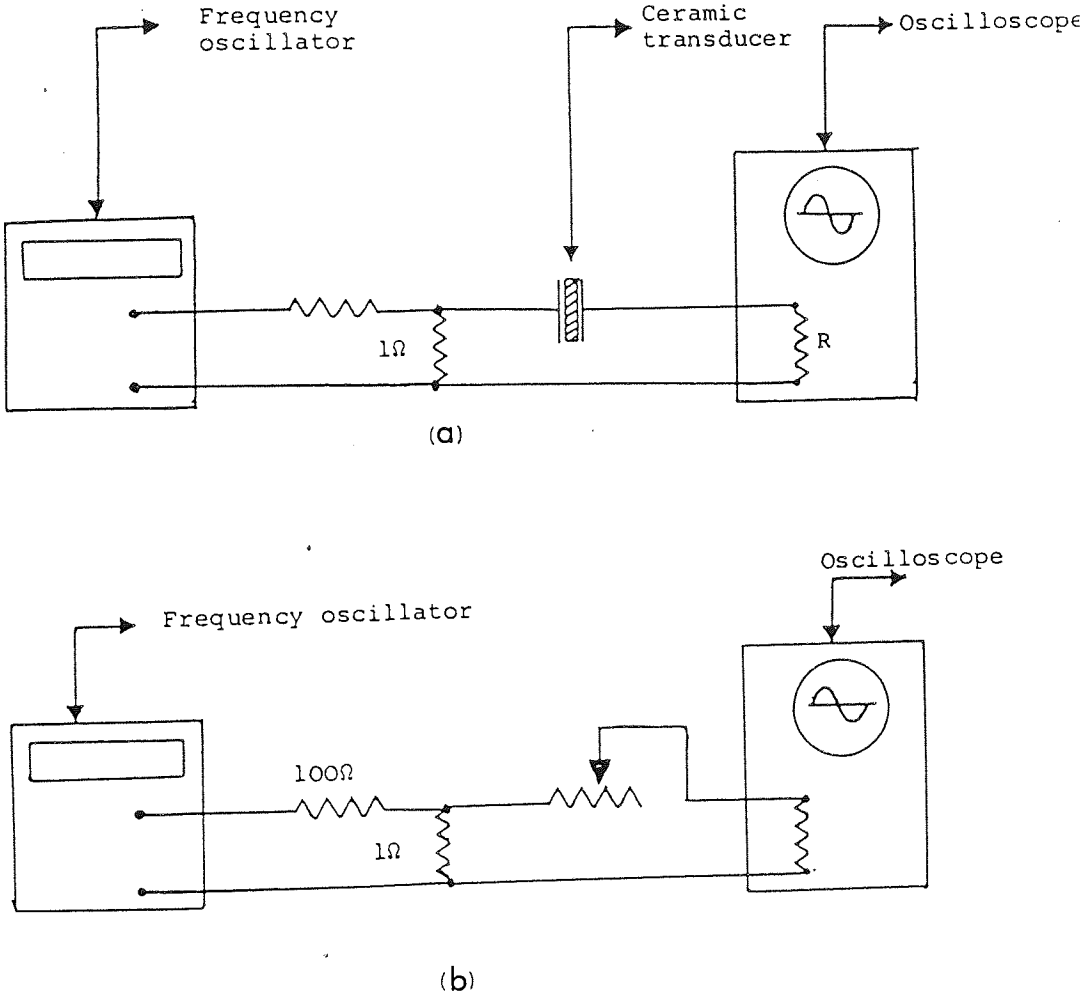

Figure 7.14 (a) & (b): Circuits for determining transducer frequencies of minimum and maximum impedance.

(3) Place the ceramic on a copper block and then place the electrode in the electrode in the required position. The copper block acts as a heat sink.

(4) Commence heating the electrode about 10mm above the ceramic, slowly lowering the iron down the electrode. Heat will conduct along the electrode at the same time warming the required area of ceramic. As soon as the solder has melted remove the iron and allow the joint to cool naturally. Such a joint will stand a very high strength test (~ 35 x 10^6 Nm^{-2}) when properly prepared. Burnishing the area to be soldered helps to increase the mechanical strength of the bond. This is done by rubbing the surface gently with the rounded end of a small steel rod.

Two methods were used to solder the electrodes onto the ceramics:

(1) Using copper foil of thickness 0.0254 mm. The foil was tinned and cut in the shape as shown in Figure 7.15(a). Following the above instructions the tinned copper foil was soldered to the ceramics.

(2) Using a single strand of copper wire stripped from an electrical cable. The wire was twisted to form a circle of an approximate dianeter of 4mm, and then tinned. The circle end of wire was then placed onto the ceramic and then point soldered, following the above instructions.

Figure 7.15(b) shows the electrodes connected to the ceramic. The electrodes have their leads (tails) facing 180° opposite each other.

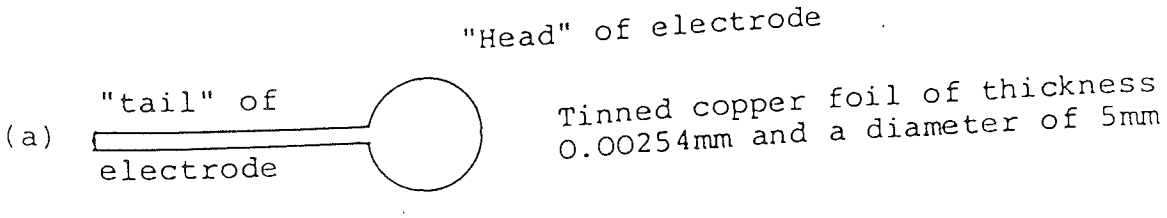

Figure 7.15(a): A tinned copper foil used for soldering onto a ceramic

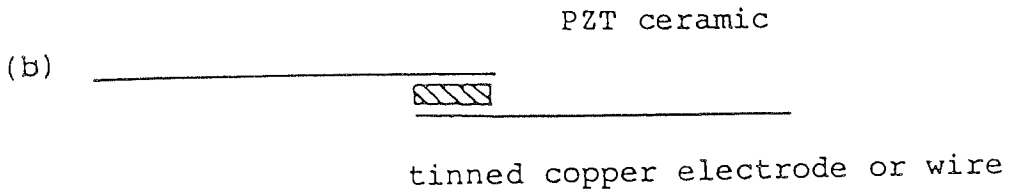

Figure 7.15(b): A tinned copper electrode or wire soldered onto a ceramic with its leads placed 180° opposite to each other.

(vi) Use of adhesives for coupling electrodes to PZT ceramics

When PZT ceramics need to be bonded to metals, plastics, or other ceramic materials, the use of epoxy resins and cyanoacrylates, such as "Araldite" range is recommended.

The use of adhesives such as super glue and silver loaded epoxy resins were experimented with in order to form electrical connections between the electrode and the ceramic. The electrical connections were made under pressure leaving a very thin sandwich layer of adhesive between the electrodes and the ceramic.

The electrical connections made in the ways described proved to be successful but only to some limited extent. This is because using these adhesives, other problems arose which led to changes in the acoustic properties of the ceramics being changed. These changes occurred in the natural resonance frequency at which the ceramic vibrates, the acoustic and electrical impedances, which in turn resulted in heat being generated across the ceramic, a greater amount of power being reflected back into the ceramic and whenever the joined ceramic/electrode system came in contact with organic solvents, the adhesive began to dissolve thus losing its electrical connections.

Another material used as a non-bonded electrical conducting electrode under pressure was aluminium foil. In this case the surface of the aluminium foil was prepared using fine grade emery paper to remove the oxide layer and then wiped clean. The reason for choosing aluminium electrodes as opposed to copper electrodes was because it has a similar acoustic impedance to that of the PZT ceramic and of the fused silica rod. The fused silica rod in this case was used as a probe through which sound was transmitted into a liquid sample contained in a NMR tube.

7.5(a) Transmission of Sound into Liquid Sample

The discussion so far, has been directed towards the generation of ultrasound using frequency oscillators, power amplifiers, tuners and type PZT ceramics transducers. The following sections deal with various methods adopted to transmit sound into a liquid sample contained in a NMR tube and is at the same time spinning between the poles of an NMR electromagnet.

7.5(b) The Scaffolding Rig

Owing to the size of the NMR tube (130mm in length and 9mm inside diameter) and the large magnetic fields produced by the electromagnet, it was decided that a probe of approximately 1 metre in length and about 5mm in diameter had to be used. The transducers were then mounted either on the top or bottom of the probe and then lowered into a liquid sample contained in a NMR tube.

A scaffolding rig was constructed which has three Cartezian degrees of motion, with a tilting mechanism incorporated which could be used to lower an ultrasonic probe into a NMR tube with great precision. Figure 7.16(a) illustrates (not to scale) the total construction of the ultrasonic probe mountings. The probe is held vertically in a scaffolding rig above an NMR tube and the electromagnet. Figures 7.16(b) and (c) show various components constructed to hold the silica rod rigidly at the centre and prevent it from wobbling.

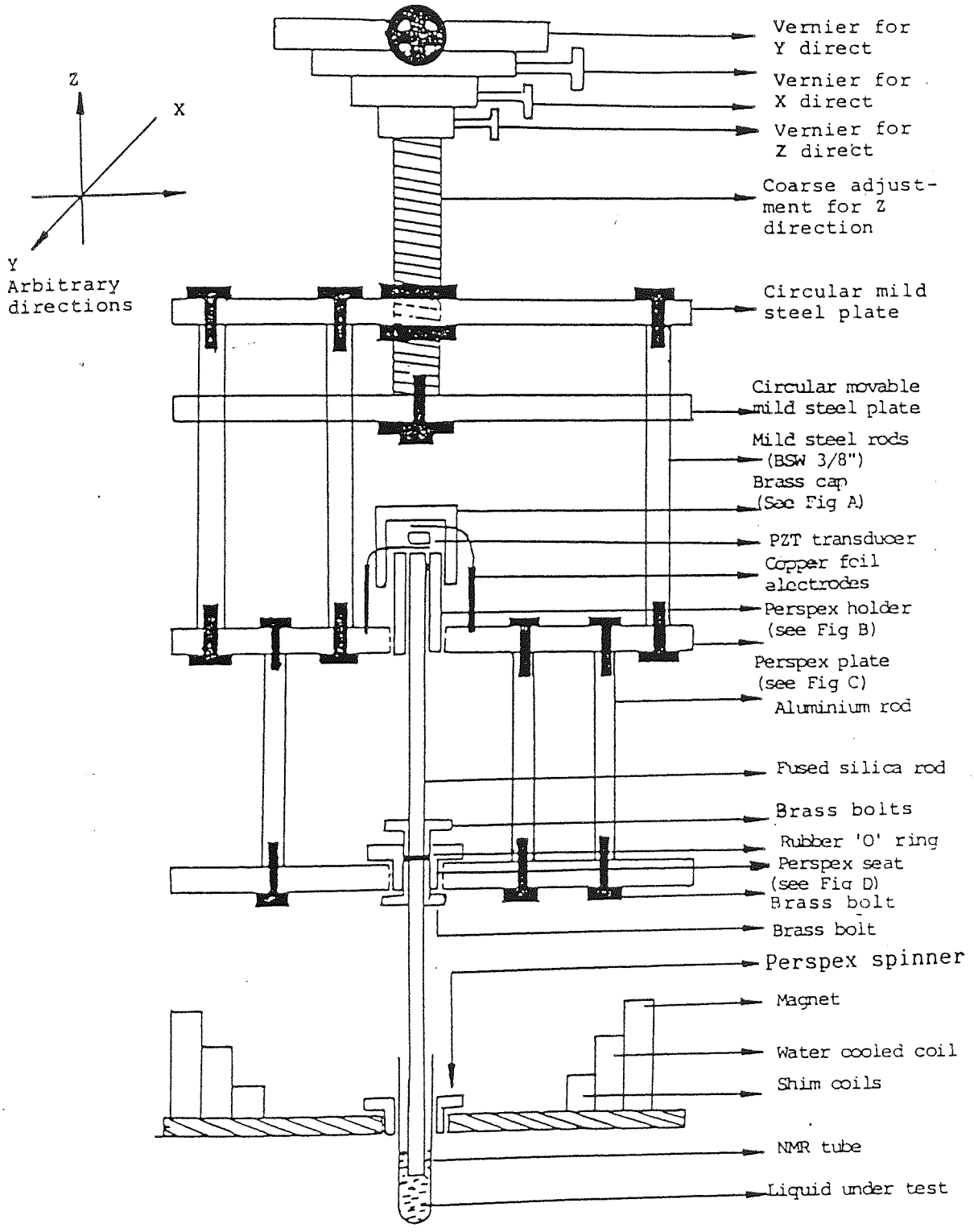

Figure 7.16(a): Total ultrasonic mounting for NMR instrument

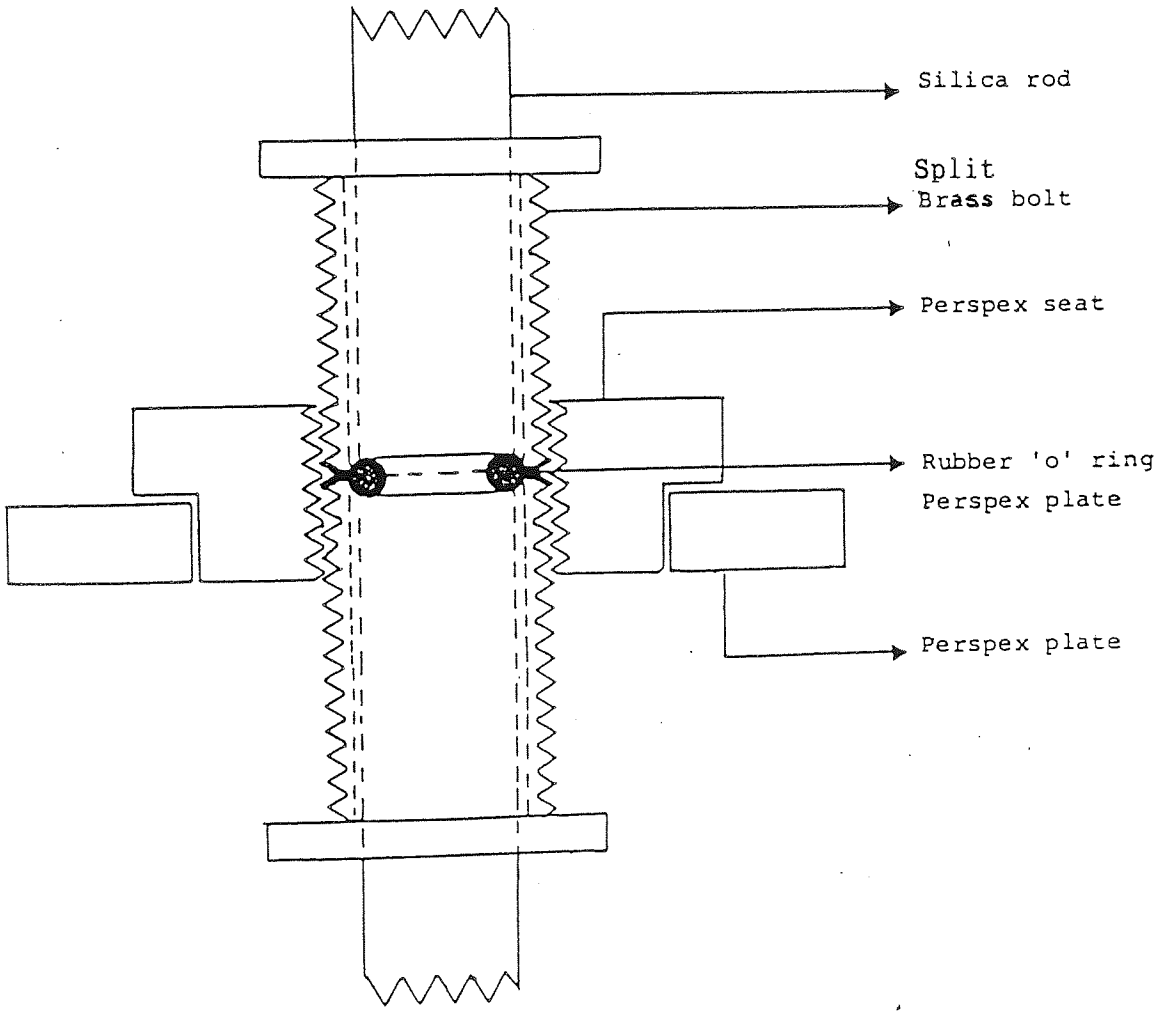

Figure 7.16(b): Silica rod held rigidly at the centre of the plate by brass bolts/rubber 'o' rings/ perspex seat

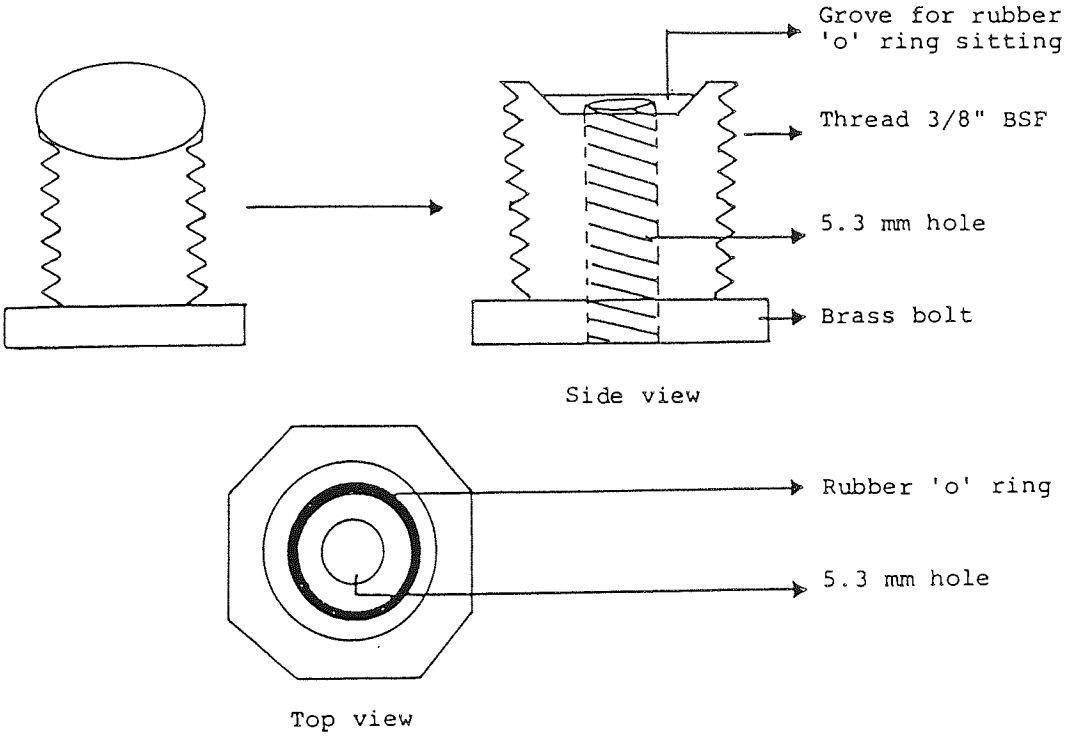

Perspex seating design

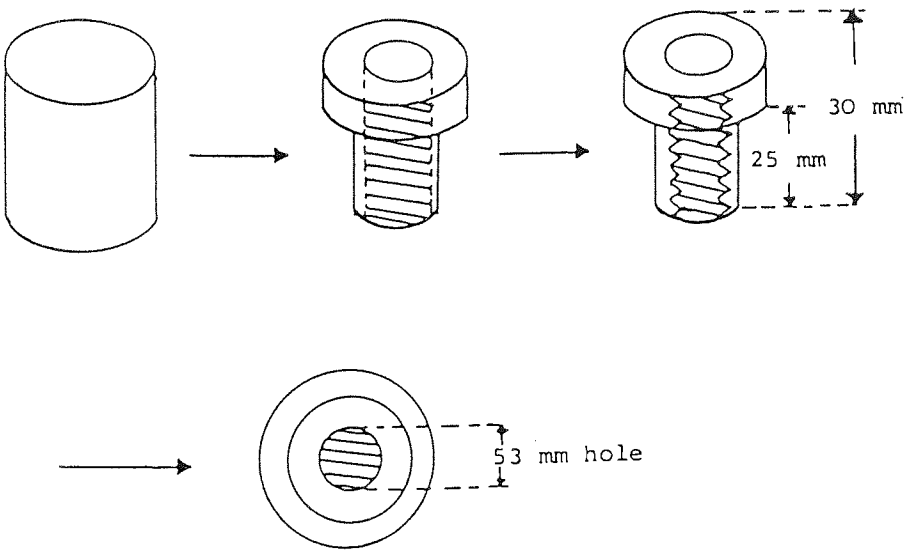

Figure 7.16(c): Some of the components constructed to hold the silica rod

7.5(c) The Probe

Principally there were three different types of probe designs with each having several different modifications. These were:

(i) a fused silica rod which had transducers mounted on the top end of the rod. The two ends of the rod were polished flat so that a fine contact was achieved between the electrode of the transducer and the top surface of the rod, and to minimize the scattering of sound emission at the bottom end of the rod. The silica rod was the medium through which the sound travelled. The transducers were kept on the top of the silica rod with various compressional fittings.

Fused silica was chosen as a probe because it has several similar characteristics to those of a PZT transducer and the other materials used in conjunction. These characteristics being, similar acoustic impedance and velocity of sound through it. Table 7.3 illustrates some of the physical properties of a PZT ceramics and of the various materials used. More importantly was viewed that a silica rod would not act as a radio-frequency receiver, picking up spurious radio frequencies from the environment which would effect the NMR instrument.

(ii) Fibre reinforced tufnol tubes. This type of design had transducers mounted with compressional fittings. In this case it was the transducer mounting assembly that is lowered into the liquid sample contained in the NMR tube.

(iii) Glass tubes sealed flat at one end. This design enabled two long tinned wires to be used as electrodes that ran parallel and on opposite sides of glass tube walls, with the transducers connected at the lower end. The transducers were either just floating in air (not in contact with a backing material) or joined by adhesives to the sealed end of the glass tube. Again it was the transducer mounting assembly that was lowered into the liquid sample.

Material	Density kg m^{-3} x 10^3	Speed ms^{-1} Bar x10^3	Bulk x10^3	Characteristic impedances g cm^{-2} s^{-1} Bar x10^6	Bulk
(PZT) Lead zirconate titnate	7.50		4.60		3.30
Aluminium	2.71	5.10	6.30	1.39	1.70
Brass	8.50	3.40	4.37	2.98	4.00
Copper	8.90	3.70	5.00	3.30	4.40
Steel	7.70	5.05	6.10	3.90	4.70
Quartz	2.65	5.45	5.75	1.45	1.53
Titanium	4.5	5.08	6.10		2.77
Teflon	2.2		1.35		0.30
Water	9.98		1.48		0.148
Benzene	8.79	1.326			0.117
Bromoform	28.9		0.928		0.268
Chloroform	14.98		1.005		0.151
Cyclohexane	7.79	1.284			0.100
Air	12.10		3.43		$41.5x10^{-6}$

Table 7.3: Physical properties of various materials[90] used.

7.5(d) Transducer Mountings

With reference to each of the three types of probes, various transducer mountings were constructed to facilitate the transmission of sound into a liquid sample. The construction of these mountings will now be discussed.

(i) Transducer mountings using a silica rod as a probe. Various types of transducer mountings were designed and constructed in which the transducer was sandwiched between the electrodes and held firmly in contact with the top surface of the fused silica rod as the transducer oscillated. However, the transducer/electrode assembly and the silica rod could not be held too rigidly as this would have

dampened the oscillatory motion of the transducer.

The transducer mountings described above were of the "hat" type designs. In these designs, the transducer, the electrodes and silica rod are held together by one of the following types of fittings:

(i) push-fit

(ii) screw-on

(iii) compressional

(iv) tensional

Figures 7.17-7.21 illustrate the five different prototypes of "hat" designs constructed.

Figure 7.17 illustrates prototype 1. This consisted of a brass cap which simply push fits onto a perspex holder containing the transducer, electrodes and the silica rod assembly. This design had a great deal of damping on the oscillatory motion of the transducer which resulted in large heating effects being produced which further led to changes in the characteristic properties of the transducer.

Figure 7.18 illustrates prototype 2. This had a screw-on type fitting. It consisted of aluminium nut with threads for screwing onto a fibre-reinforced tufnol. In addition it also had a aluminium 'T' piece which sat between the nut and the tufnol which maintained the transducer, the electrodes and the silica rod in contact. This type of design also had large heat losses being produced at the transducer. This was as a result of the transducer being heavily damped.

Figures 7.19, 20 and 21 illustrate three prototypes with compressional and tensional fittings. Prototype 3 consisted of a brass 'T' piece held under a brass strip which in turn was held under compression by a spring. The brass strip maintained the transducer, electrodes and silica rod all in contact. In addition the brass strip prevented the transducer being thrown off the silica rod thus forcing a continuous contact between them as the transducer oscillated. This prototype construction had similar heating losses to that of prototype 2. Prototype 4

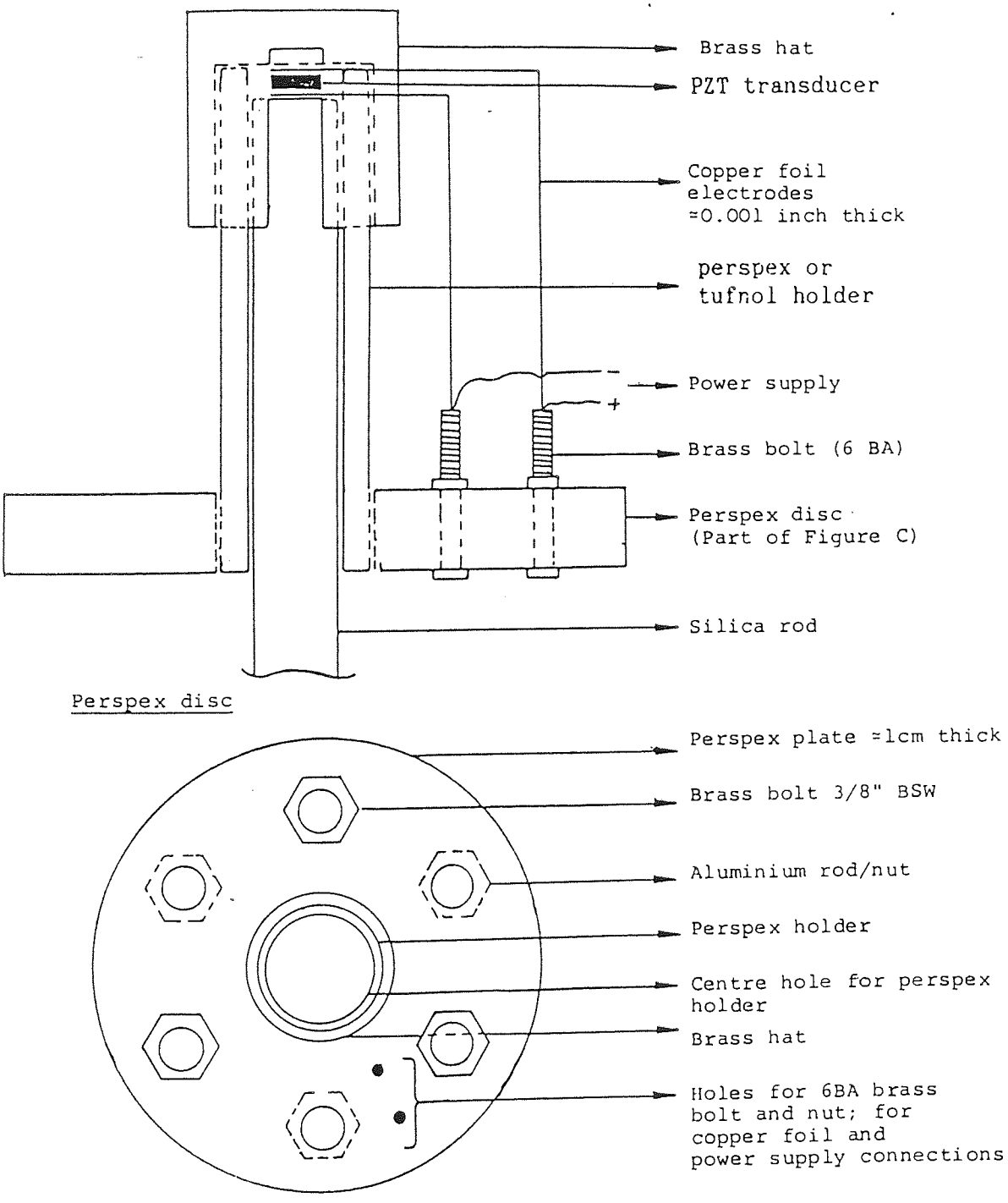

Figure 7.17: Prototype 1; using a brass hat and perspex holder construction of a "push-fit" fitting.

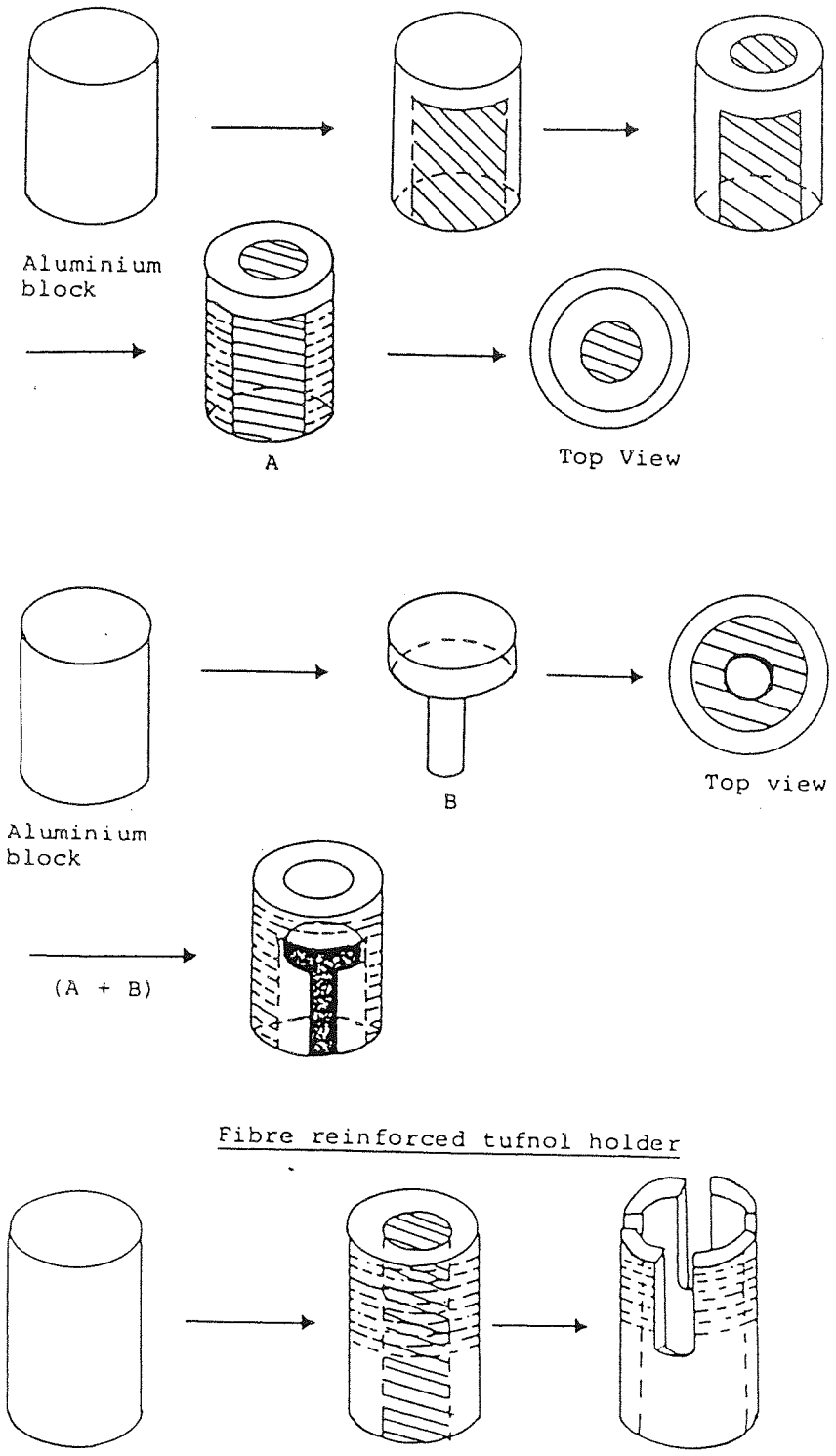

Figure 7.18 (a): Prototype 2; Construction of aluminium "T" piece and hat for a "screw" type fittings.

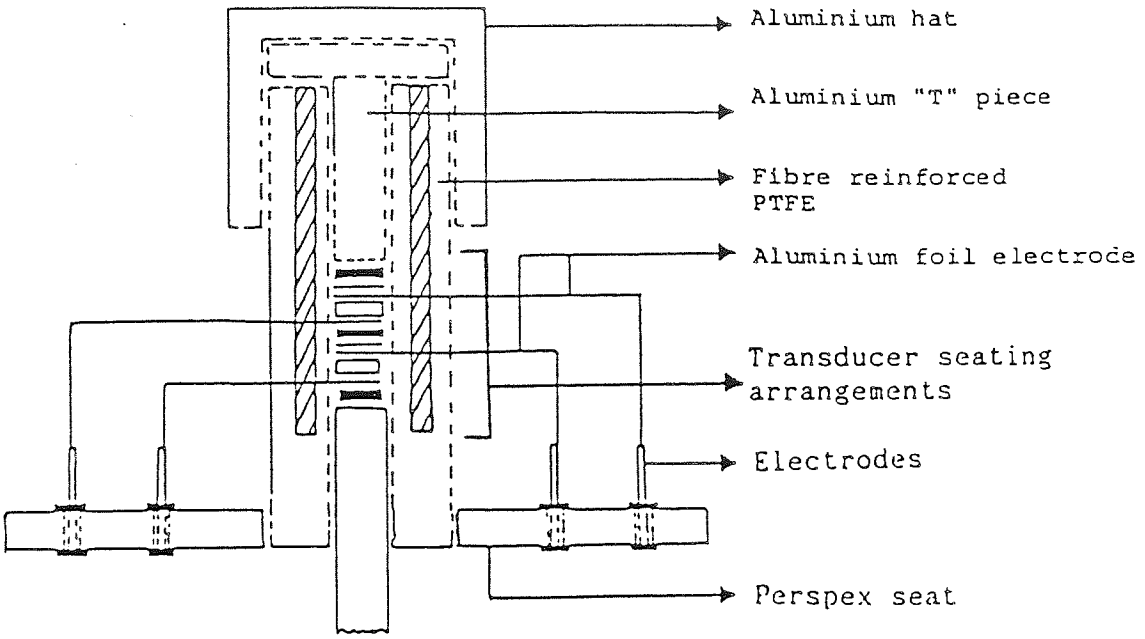

Enlarged view of transducer seating arrangements

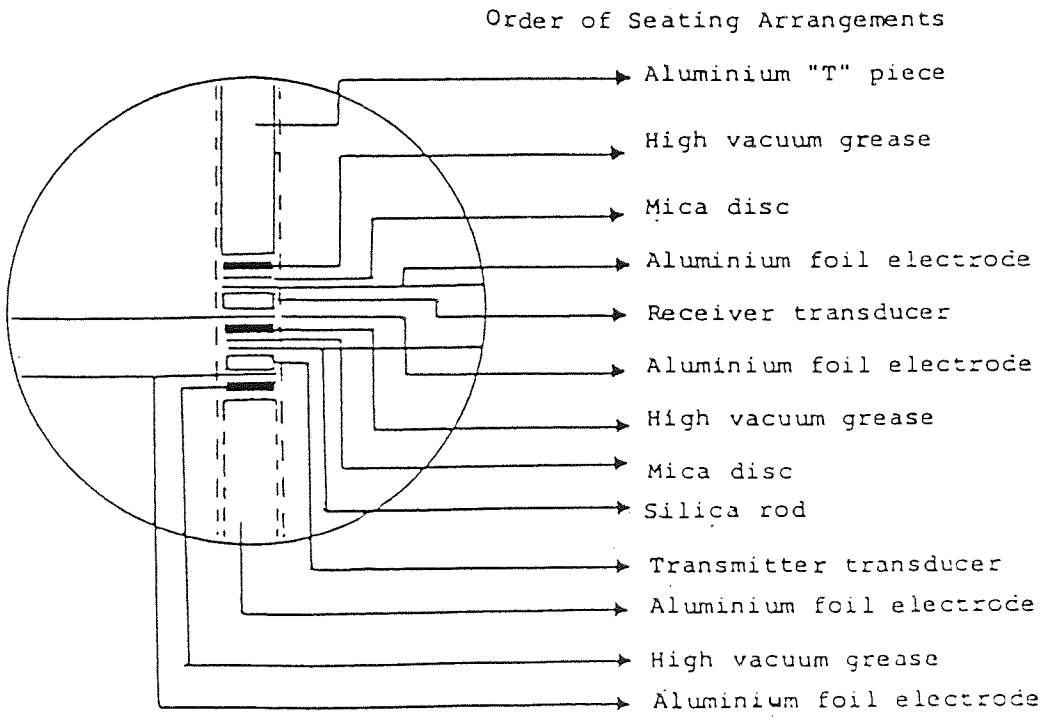

Figure 7.18 (b): Total assembley of aluminium nut and "T" piece with a fibre reinforced tufnol holder.

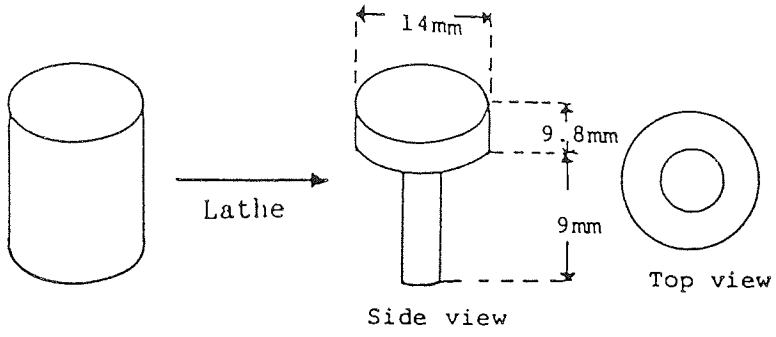

Perspex/PTFE holder: Prototype 2

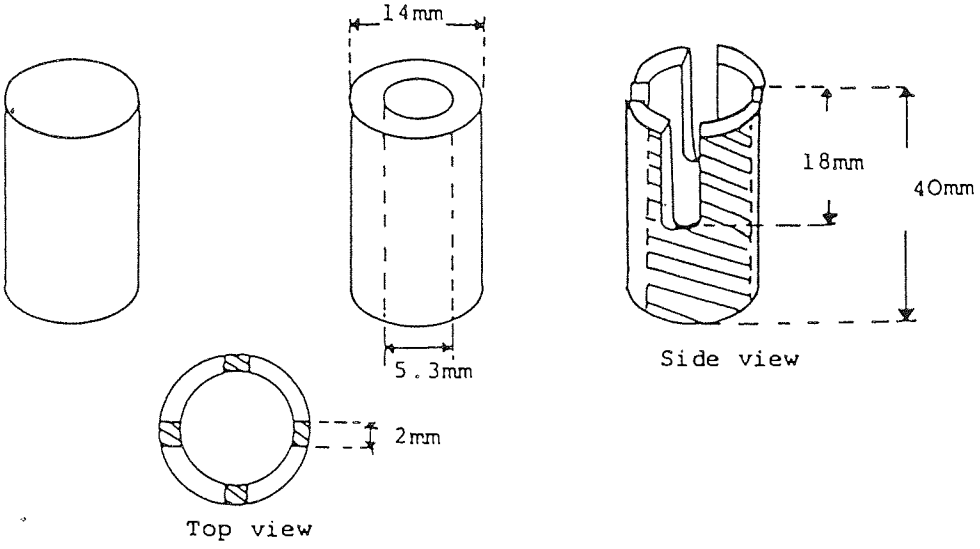

Brass strip

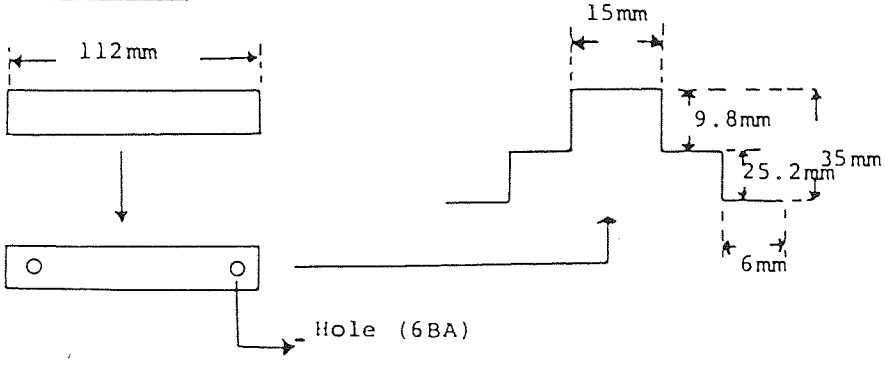

Figure 7.19 (a): Prototype 3; Construction of brass "T" piece for compressional fittings.

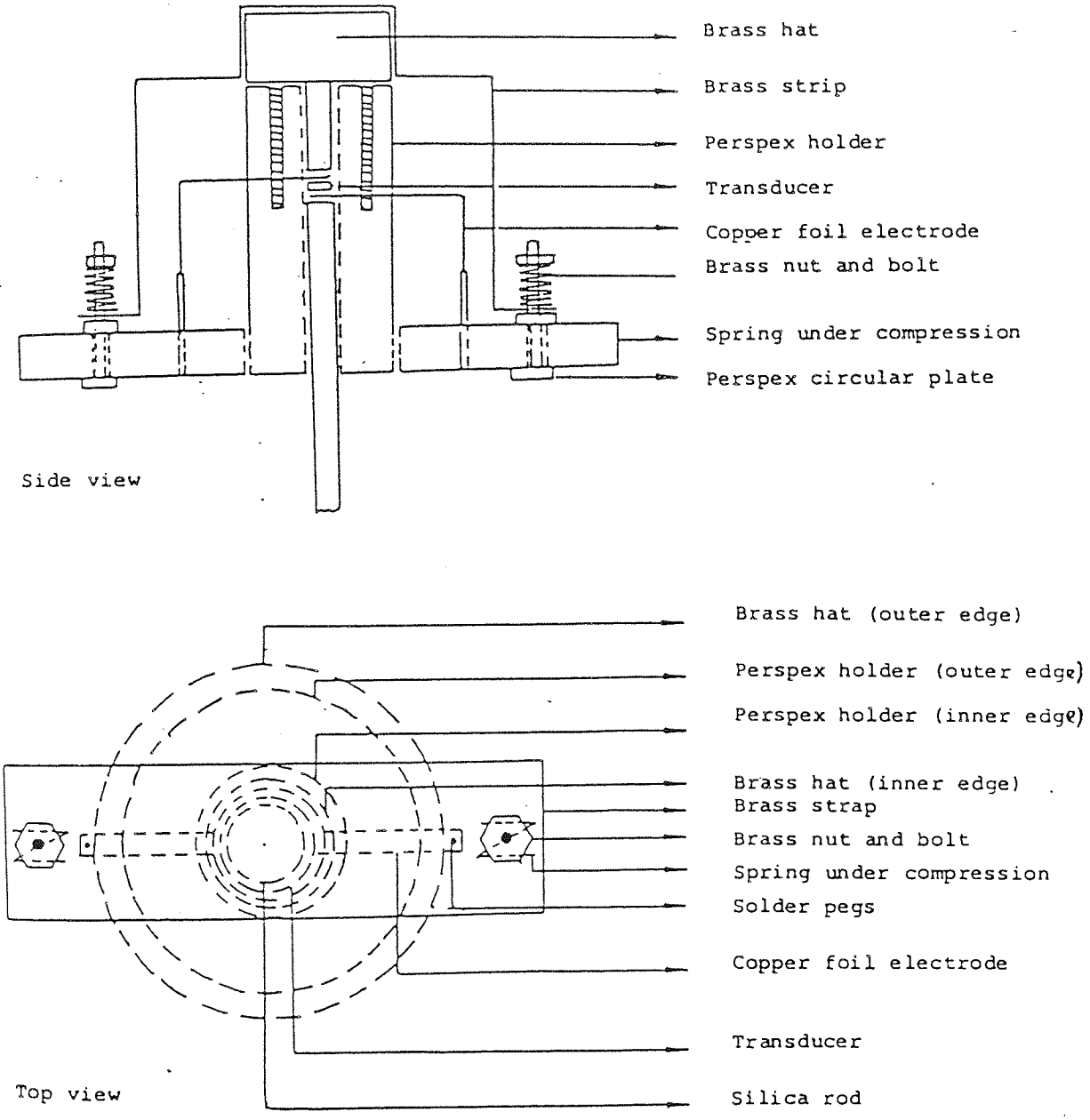

Figure 7.19 (b): Prototype 3; Total assembly of a brass "T" piece with a brass strip and a perspex holder.

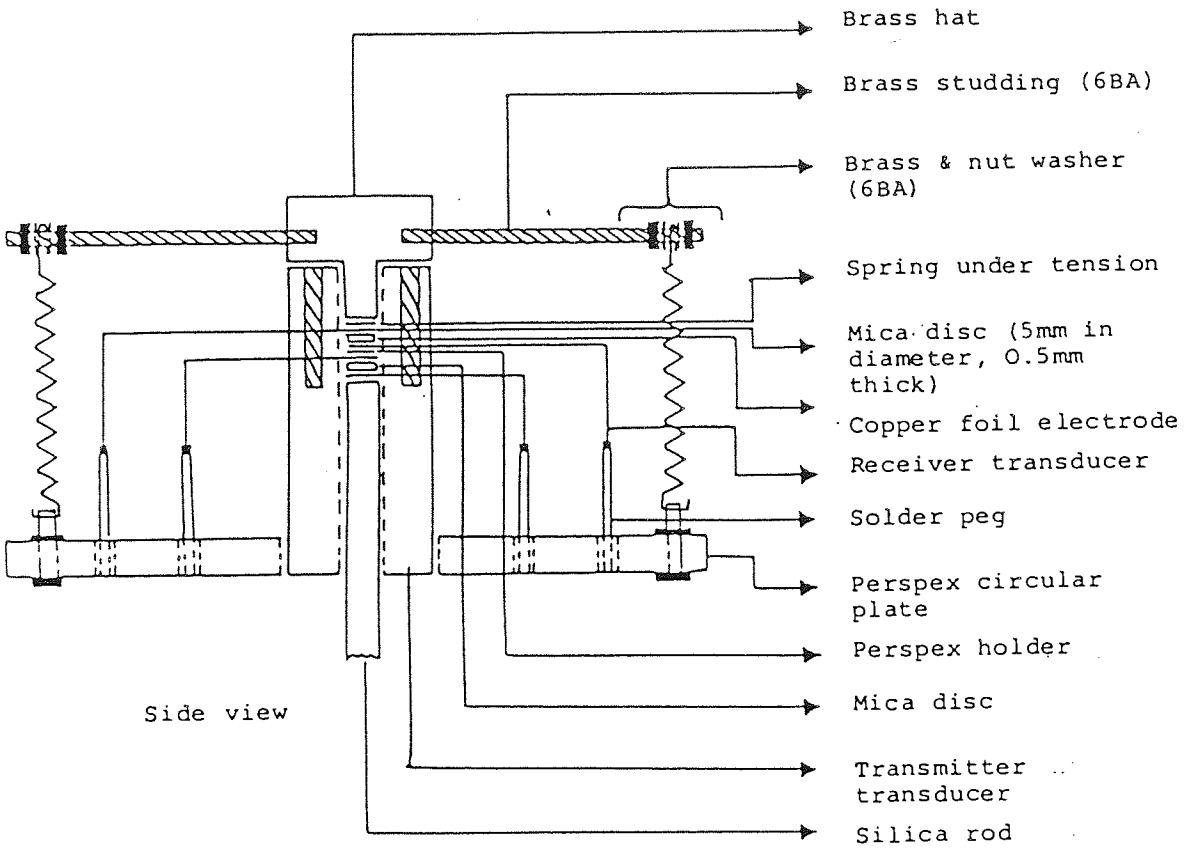

Enlarged view of transducer seating arrangements

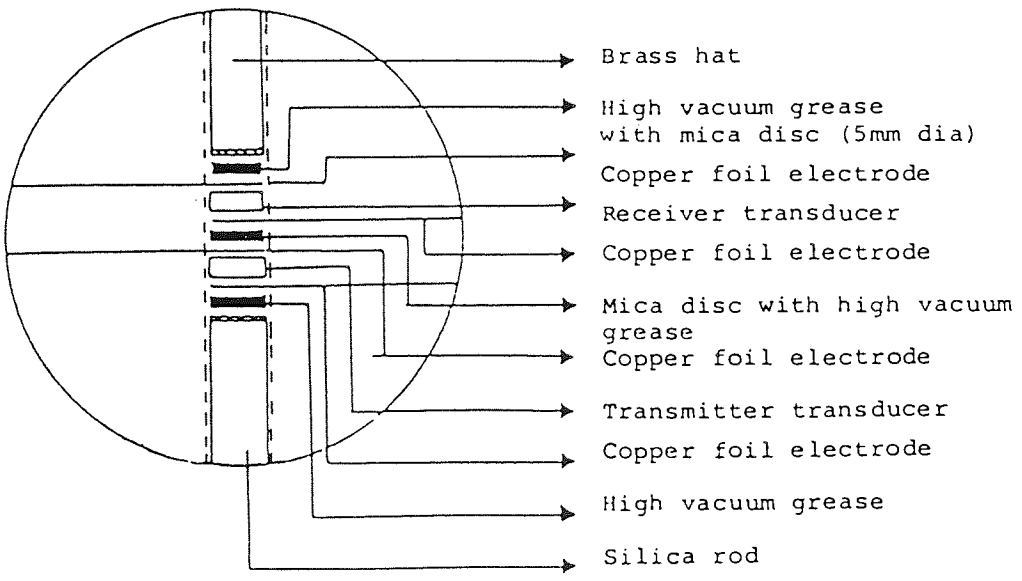

Figure 7.20: Prototype 4; Total assembly of brass "T"piece, brass studding and a perspex holder with a tensional spring type fitting.

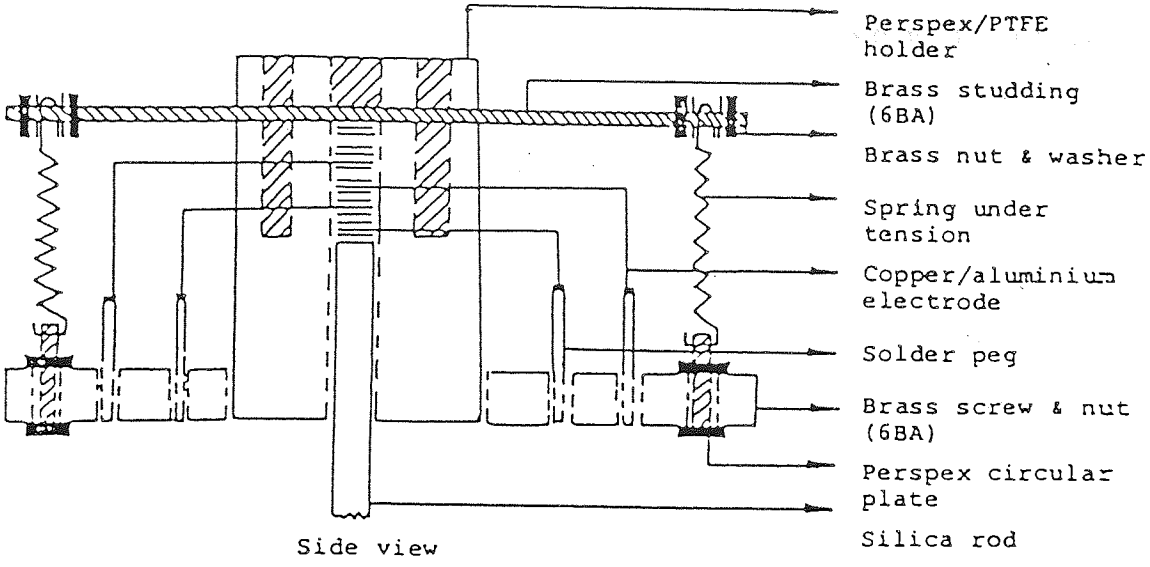

Side view

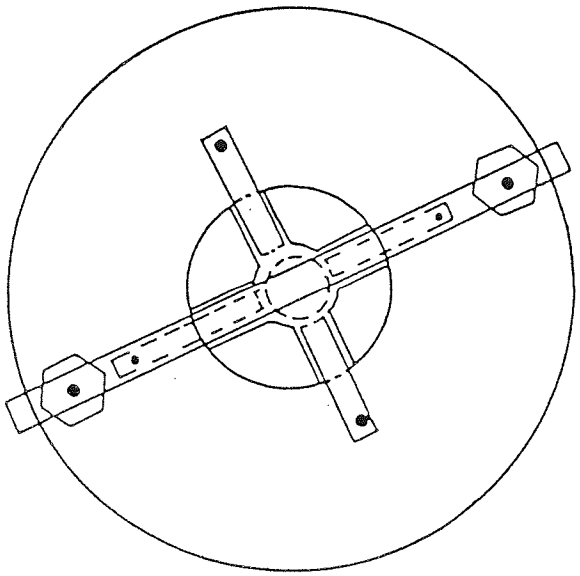

Top view

Enlarged view of transducer seating arrangements

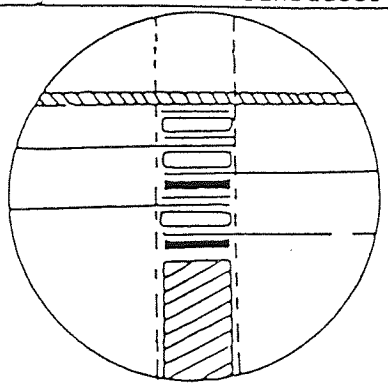

Order of seating arrangements

Brass studding (6BA)
Mica disc (5mm)
Brass disc
Mica disc
Copper foil electrode
Receiver transducer
Copper foil electrode
High vacuum grease
Mica disc
Copper foil electrode
Transmitter transducer
Copper foil electrode
High vacuum grease
Silica rod

Figure 7.21: Prototype 5; Total assembley of brass studdings and a perspex/PTFE/tufnol holder(s) with a tensional spring type fitting.

replaced the brass strip with a brass studings which is screwed into the brass "T" piece which was then held under tension by small springs. This type of construction did neither improve the transmission of sound through the silica rod nor did it minimize the heat losses across the transducer. Prototype 5 used a brass studding across the sandwiched transducer instead of the brass 'T' piece. Due to point contacts, the heat generated across the transducer was minimised as well as decreases the damping in the oscillatory motion of the transducer being decreased.

Several different types of materials were used as holders in which the transducer, the electrodes and the silica rod were housed. The variations in the materials used arose from an attempt to overcome the large heating effects which led to the materials being deformed. The materials were perspex, teflon fibre reinforced tufnols. Fibre reinforced tufnols proved to be the most suitable material, withstanding temperatures up to 300°C. Four slits were made at right angles to one another on these holders in order for the electrodes to be inserted through them. From the prototypes constructed, it was also possible to use more than one transducer. The use of a second transducer was merely for detection purposes, thus allowing observation of the first transducer being oscillated.

High vacuum grease and micra discs were also used between the silica rod and the electrode, and between two electrodes having opposite voltages, respectively. It was viewed that both these materials would increase contact between the various materials and also prevent electrical short circuiting, thus increasing the efficiency with which the transducer oscillated and transmitted the sound waves through the silica rod. This type of design had a good degree of success, however, both materials caused large damping in the oscillatory motion of the transducers.

Although all these prototypes worked with a good degree of success, several problems remained the effects of which were difficult to minimize any further. These were:

(i) For electrodes bonded to the transducer by adhesives, the inclusion of a bonding layer through which the acoustic waves had to pass, caused an attenuation

of the sound as a result of an acoustic impedance mismatch.

(ii) Using a long length of silica rod in order to keep the scaffolding rig as far away as possible from the electromagnet resulted in the number of multiple reflections of sound waves within the silica rod being large. This led to the total acoustic energy dissapated at the other end of the silica rod being reduced, this is as a result of a combination of constructive and destructive interference of waves.

(iii) A difference in acoustic impedance between the transducer, and the electrodes, silica rod and any other materials, used led to large damping effects in the oscillatory motion of the transducer. This resulted in heat being generated across the transducer. As a direct consequence of heat generation, it further caused changes in the physical properties of the transducer. These changes further resulted in a poor performance in the transduction of electrical energy to acoustic energy.

It was concluded that using a transducer mounted on the top of the silica rod resulted in some unavoidable problems. In order to minimize these problems it was decided that the transducers should be mounted at the bottom end of a rod or a tube such that it would either still allow the use of a shorter-length of silica rod as the ultrasonic probe or allow the transducer mounting assembly to be lowered into the liquid sample contained in the NMR tube.

Four different types of transducer mountings were designed and constructed. The first two types of transducer mountings were those constructed using fibre reinforced tufnol tubes, and the remaining two types were using glass tubes sealed at one end. These will now be discussed.

(ii) Transducer mountings constructed with fibre reinforced tubes. These mountings had a compressional type fitting. Figures 7.22 and 7.23 illustrate the two main types of transducer mountings. Figure 7.22 illustrates the use of either a paper reinforced tufnol tube or a phenolic based resin tube which has a hollow perforated asbestos reinforced tufnol sleeving screwed underneath. The transducer was maintained under compression by a spring which was held between a high quality

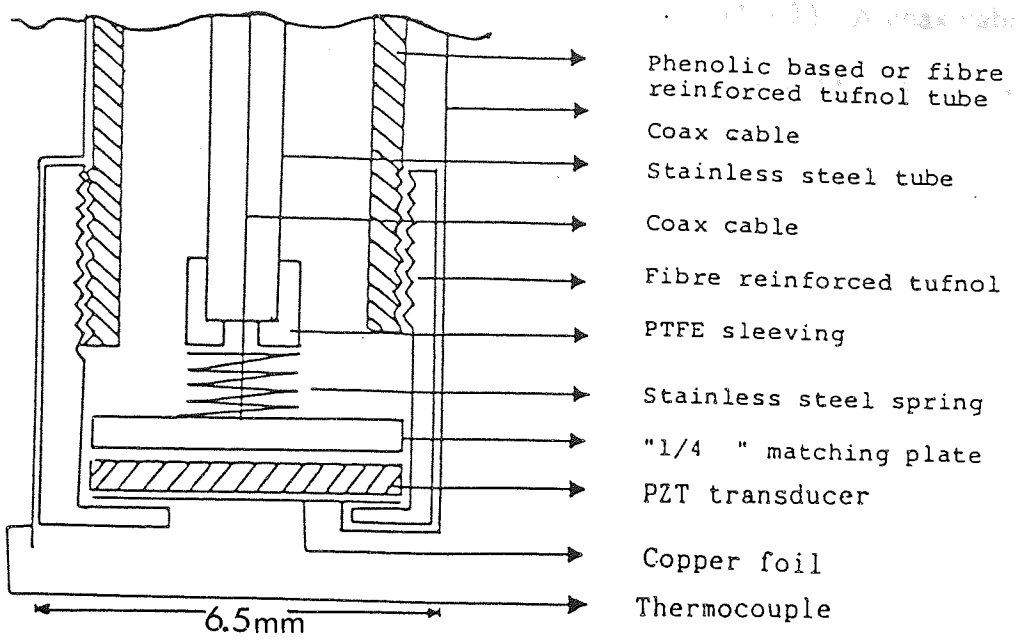

Figure 7.22: Transducer mountings constructed with fibre-reinforced tube. This has a compressional type fitting.

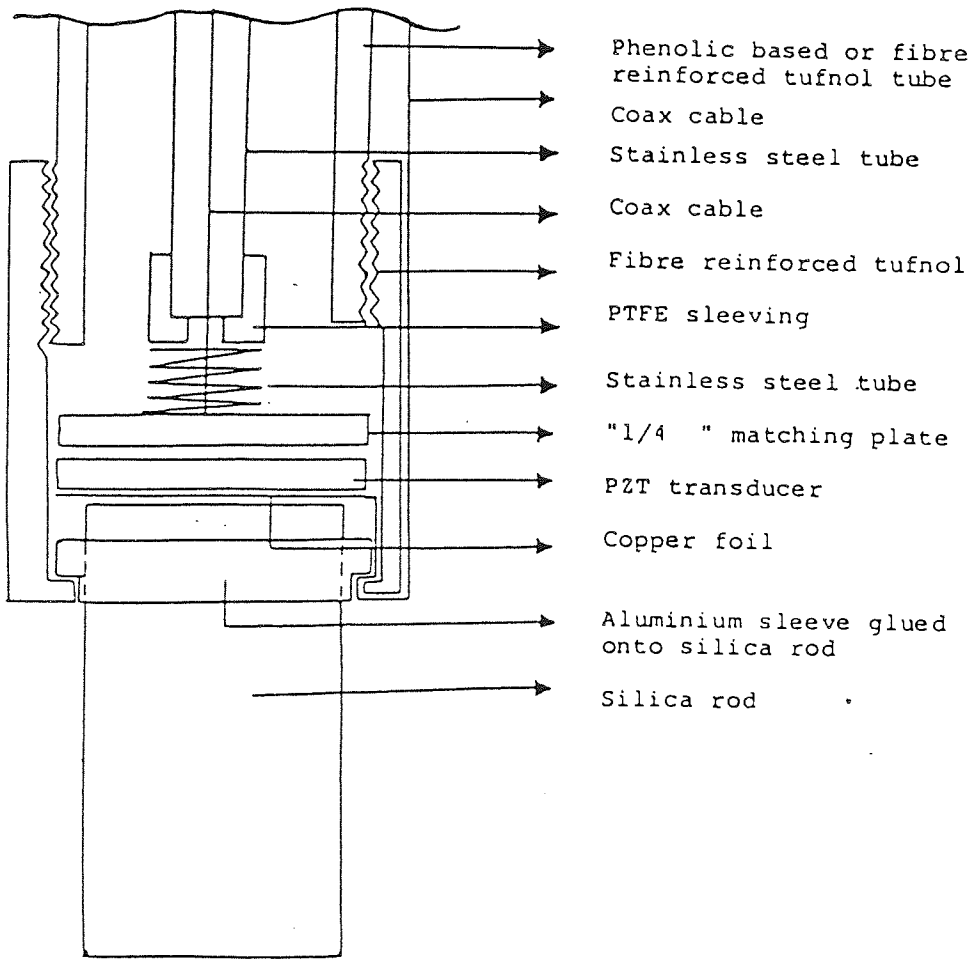

Figure 7.23: Transducer mountings constructed with fibre-reinforced tubes and a silica rod; with a compressional spring type fittings.

insulated stainless steel tube and a matching copper disc (1/4 λ). A coax cable (diameter 1.17mm) runs through the centre of the stainless tube and forms a part of the electrode and was soldered onto the matching disc.

The stainless tube also served another purpose. It allowed gas to be blown down onto the PZT transducer so as to keep it cool as well as to starve the liquid sample contained in the NMR tube of oxygen.

Figure 7.23 illustrates a slightly modified version of Figure 7.22, in that it contains a short length of silica rod (50mm) and of a smaller diameter (3mm), which is held directly beneath a PZT transducer. The silica rod was now a medium through which sound could travel and prevent any direct heating of the liquid sample as a result of the transducer getting hot.

Temperature measurements were made possible using various types of thermocouples. These thermocouples connection were embedded in adhesive in a groove made along the walls of the fibre reinforced tubes and the perforated asbestos reinforced tufnol sleeving. These thermocouples were insulated using a copper braid which was earth.

These two prototypes worked extremely well. However the heating effects across the transducer were still large and could not be minimized sufficiently in order to maintain similar properties of the transducer for a long period of time.

(ii) Transducer mountings constructed with glass tubes sealed at one end. This type of construction had two long tinned strands of electrical wire running parallel on opposite sides of the glass tube wall with the transducers soldered at the bottom. The transducers were either left floating in air or joined by adhesives to the sealed end of the glass tube. Figure 7.24 and 7.25 illustrates the two types of transducer mountings using a glass tube.

The glass tube had two small holes, (each of a diameter of 1mm). One hole had a thermocouple protruding out from inside the glass tube which allows measurement of temperature variations. The second hole allowed gas injected from

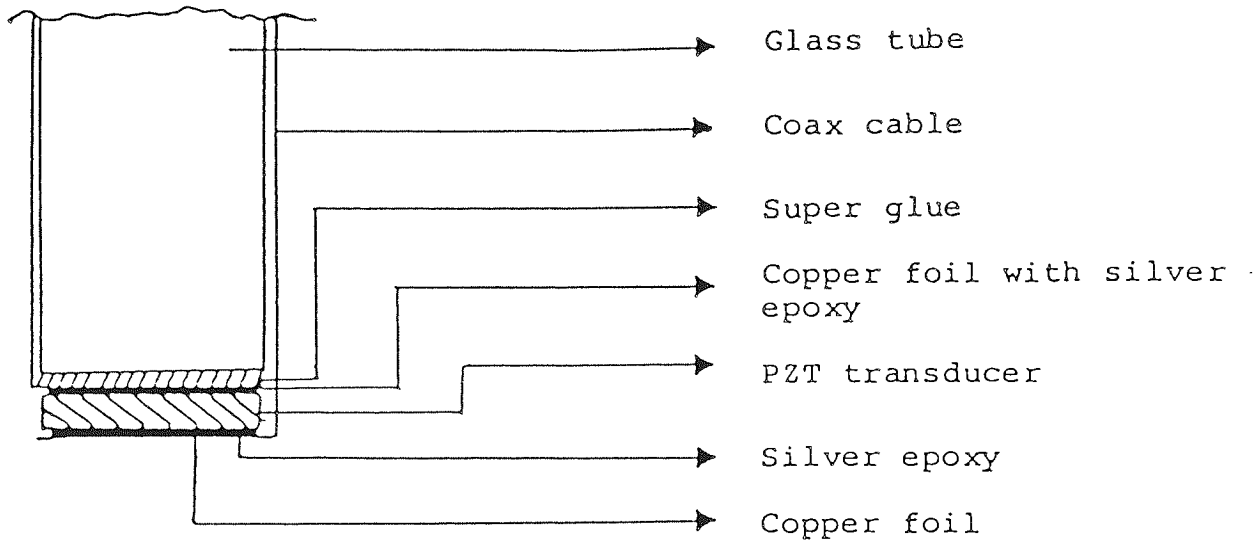

Figure 7.24: Transducer mounting constructed with glass tube sealed at one end. The transducer is joined by adhesives to the sealed flat end of the tube.

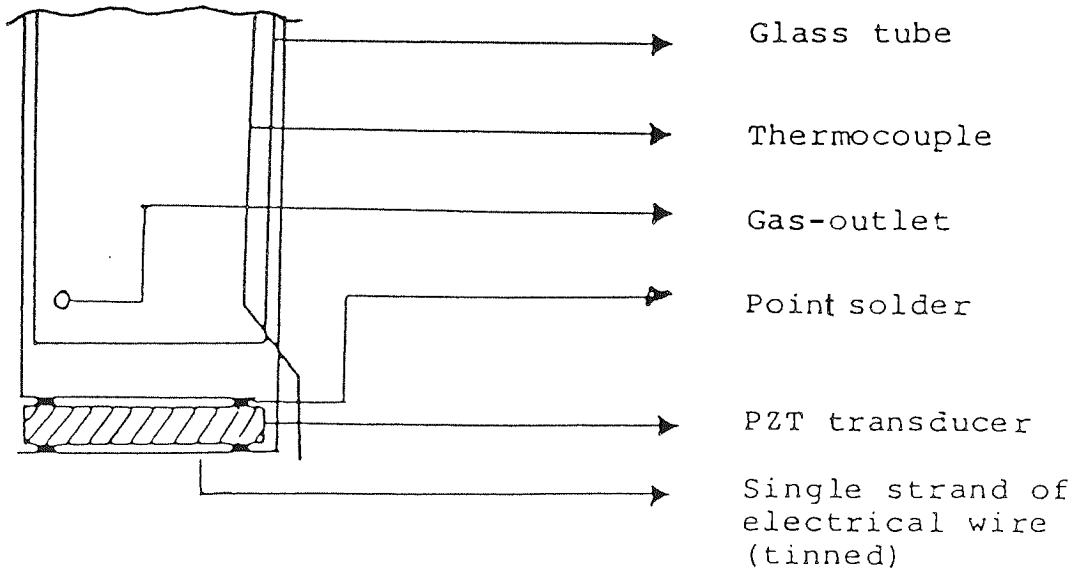

Figure 7.25: Transducer mountings constructed with a glass tube sealed at one end. The transducer is left "floating" in the air. The glass tube has two holes which allow for gas to be blown down the tube as well as having a thermocouple protruding out from one of the holes.

the top of the tube to be blown out. The thermocouple inside the glass tube is insulated using a copper braid, which was earth.

Transducer mountings on a glass tube with the transducer floating in the air proved to be the most satisfactory design as it had minimum heat losses as well as having a maximum forward power delivered into the transducer, suggesting very small electrical and acoustic impedance mismatch.

Figure 7.26 illustrates a total diagrammatic representation of the application of ultrasound to a sample in a nuclear magnetic resonance spectrometer using the apparatus design last mentioned.

7.5(e) Thermocouples

Numerous combinations of thermocouple wire exist[282-283]. The two types of thermocouple used throughout this work were of the type "T" and "J". Type T consists of a copper/constantan (60% copper with 40% nickel) wire and is suitable for a temperature range between -252°C and 320°C. Type J consists of a iron/constantan wire which is suitable for a temperature range between -200°C and 565°C.

In order to measure temperature variations to an accuracy of 0.1°C, the emf's produced by the thermocouple was monitored by means of a potentiometer connected to a galvanometer[285]. Figure 7.27 illustrates a circuit diagram for construction of such a potentiometer.

7.6 Effects of Lowering an Ultrasonic Probe into a Liquid Sample Contained in a NMR tube

As discussed in Section 7.4(b), the following experiments were performed to ensure the NMR instrument's sensitivity, resolution, electronics and the elctromagnet were not affected by the introduction of an ultrasonic probe. The experiment were performed using proton NMR studies, on a liquid mixture of bromoform and cyclohexane. The experiments were:

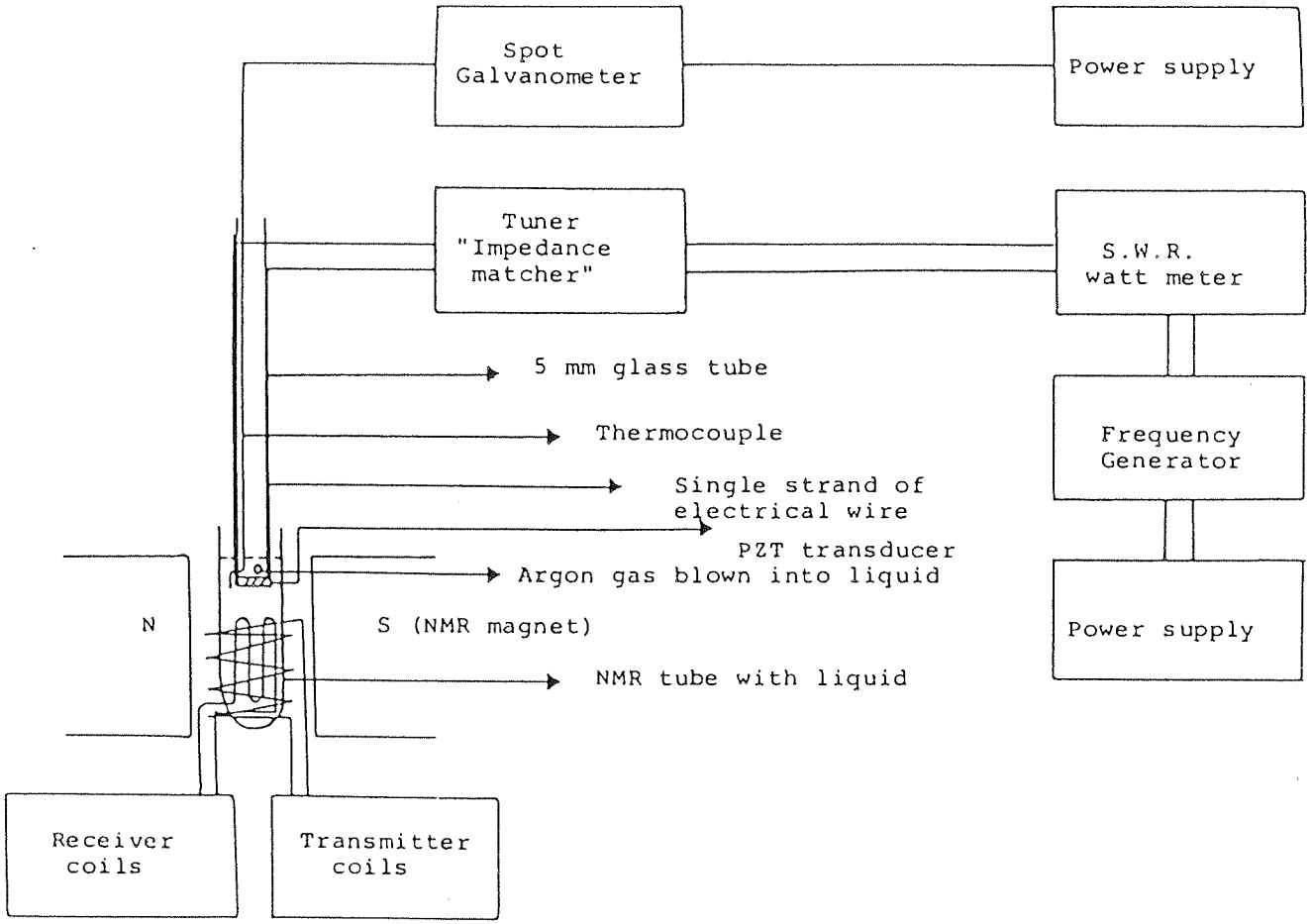

Figure 7.26: A diagrammatic representation for the application of ultrasound in a nuclear magnetic resonance spectrometer.

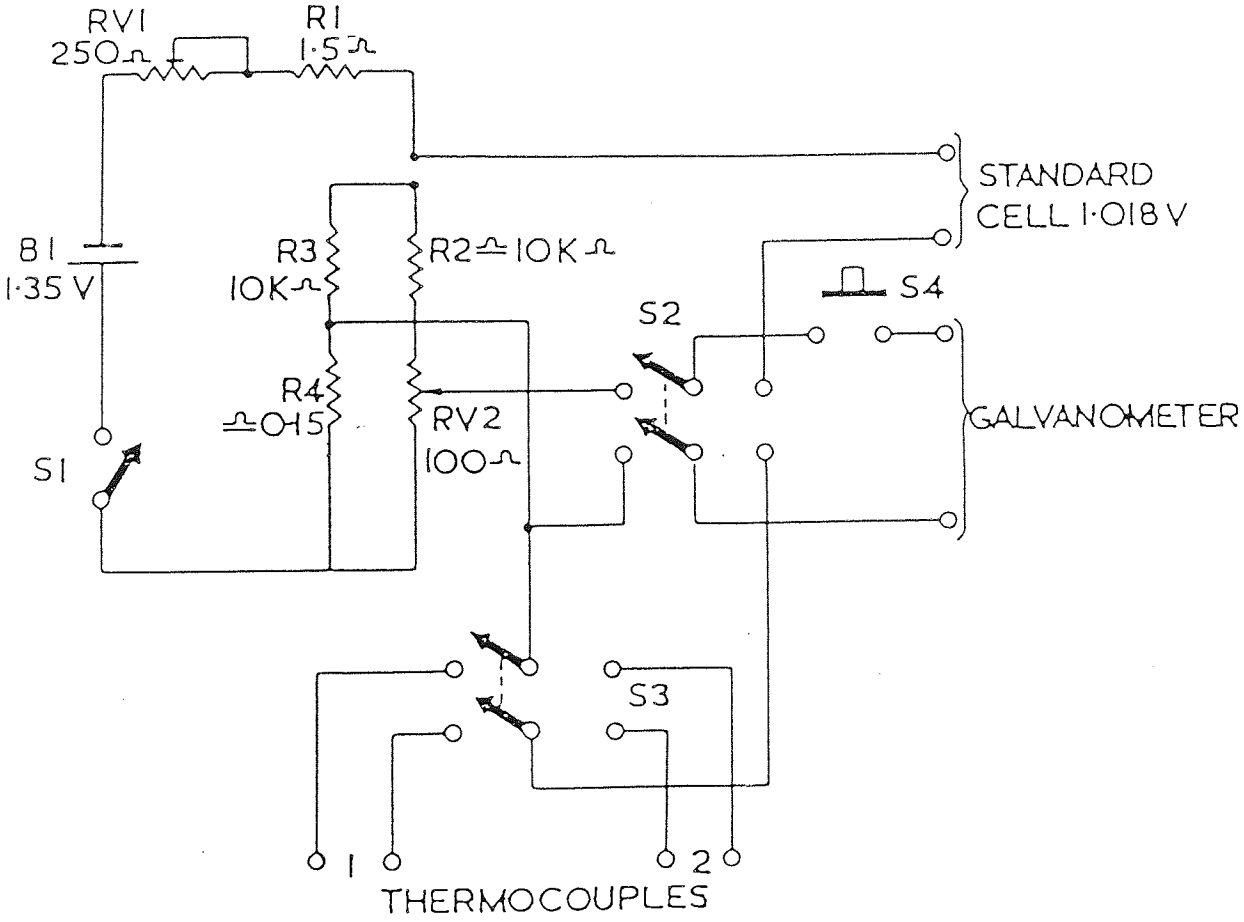

Switch Functions

S1 ON/OFF

S2 MEASURE/STANDARD

S3 +/− Thermocouple Polarity

S4 GALVO ON

FIG. 7.27 POTENTIOMETER CIRCUIT FOR VARIABLE TEMPERATURE EQUIPMENT

(i) Initial measurement of NMR linewidths with increasing pulse widths (nutation angle). These measurements were performed with neither the application of ultrasound into the liquid nor the presence of the ultrasonic probe being anywhere near the magnet. The NMR tube was allowed to spin at a constant specific speed.

(ii) Measurement of an NMR linewidth at a particular pulse width, whilst lowering the probe down into the liquid sample contained in the NMR tube and the transmission of ultrasound off.

(iii) Measurement of NMR linewidths at various pulse widths with the ultrasonic probe in the liquid sample, 1cm away from the centre of the NMR transmitter and receiver coils. The transmission of ultrasound was still off and the NMR tube allowed to spin at a constant specific speed.

(iv) The effects on the NMR instrument resolution through the effects of the ultrasonic probe on the spinning speed were measured. The ultrasonic probe was in the NMR liquid sample, and 1cm away from the centre of the NMR transmitter and receiver coils. The transmission of ultrasound was still off.

(v) Measurements of NMR linewidths at various pulse widths with the transmission of ultrasound on. The ultrasonic probe was in the NMR liquid sample and 1cm away from the centre of the NMR transmitter and the receiver coils. The NMR tube was allowed to spin at a constant speed.

Experiment (ii) was performed for the two main types of transducer mountings. The first experiment involved using a transducer mounted on the top end of the rod and the free end of silica rod was lowered into the liquid sample. The second experiment involved using a transducer mounted at the bottom end of a glass tube and lowered into the liquid sample.

The results of the experiment were as follows:

(i) In the first experiment, the effects of increasing the pulse width had negligible effects on NMR linewidths. This suggested that the NMR instrument resolution was uniform and had little affect on either B_1 or B_0 field homogeneity.

(ii) Two observations were made on the effects on the linewidth whilst lowering the ultrasonic probe into the liquid sample to approximately 1cm away from the centre of transmitter and receiver coils. The first showed no observable initial changes to the NMR tubes spinning speed as the probe was lowered down into the tube (unless the probe touched the NMR tube). However, when the probe came into contact with the liquid sample, the tube spinning speed decreased by approximately 3-5 revolutions per second. To overcome this, the tube spinning speed was physically increased. Figure 7.28 shows the effects of decreasing the spinning speed, with the ultrasonic probe in the liquid sample and 1cm away from the centre of the transmitter and receiver coils.

The second observation was concerned with the NMR instruments resolution as measured from NMR linewidths. There was no loss of resolution until and up to the point the probe came into contact with the liquid sample. As the probe was lowered further into the liquid and thus, nearer to the transmitter and receiver coils, the resolution loss could be enormous, such that, the NMR magnet resolution had to be tuned using the shim coils. Using a transducer driven silica rod had smaller (but still distinct) effects on the resolution in comparison with a probe that had a transducer mounted at the bottom end of a glass tube. Figure 7.29 illustrates the effect of the second ultrasonic probe in a liquid mixture of bromoform and cyclohexane. The probe was finally 1cm from the centre of the NMR transmitter and receiver coils. The figure also shows the use of NMR shim coils to tune and improve the instrument resolution.

(iii) Once the resolution was retuned with the presence of the ultrasonic probe in the liquid sample, effects of increasing the pulse width with the transmission of ultrasound now on, showed in comparison with the first experiment neither improvement nor losses in resolution or changes in linewidths.

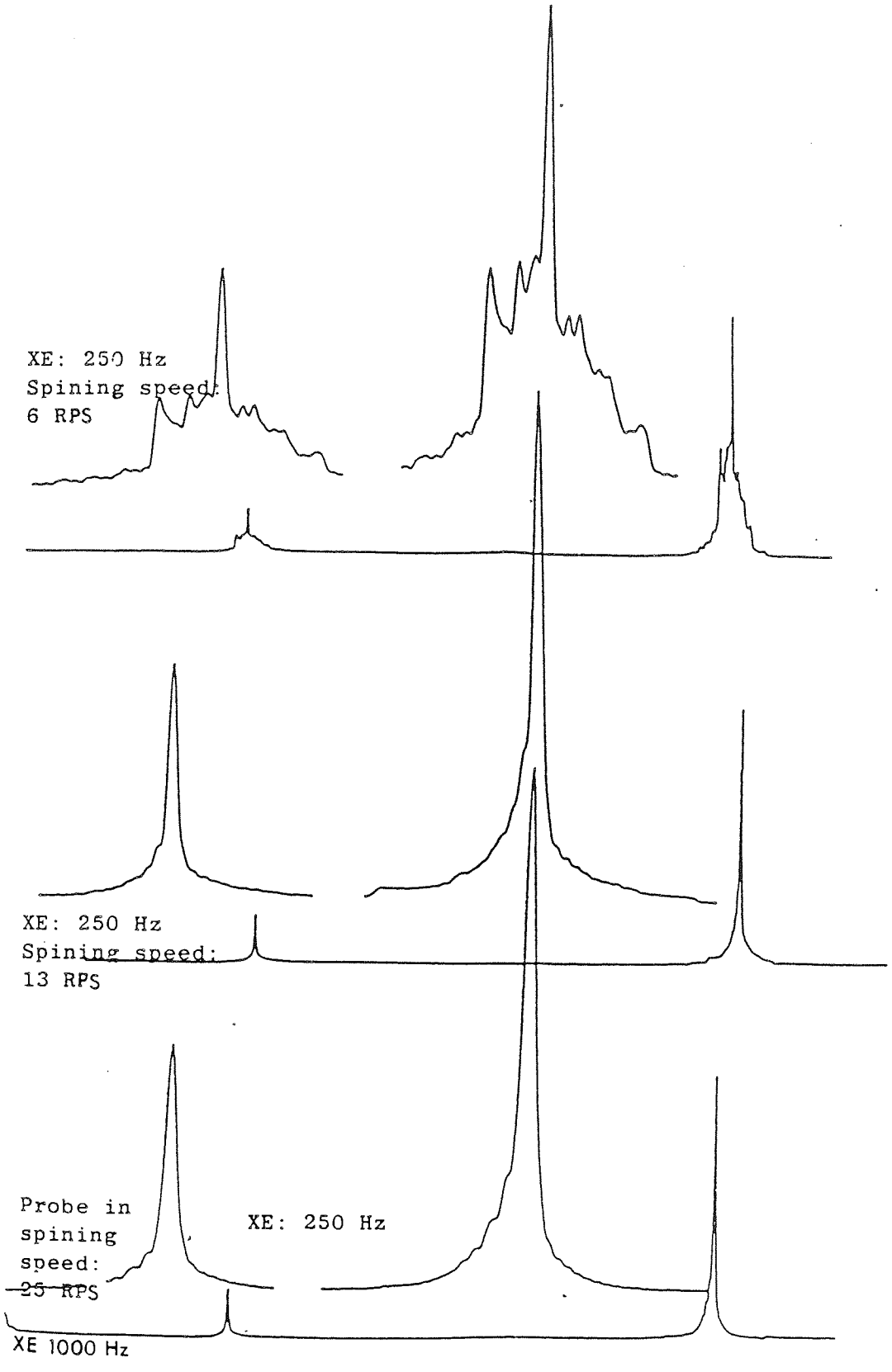

Figure 7.28: Effects of decreasing the spinning speed with the ultrasonic probe in a liquid mixture of bromoform and cyclohexane. The probe is 1cm from the centre of the transmitter and receiver coils.

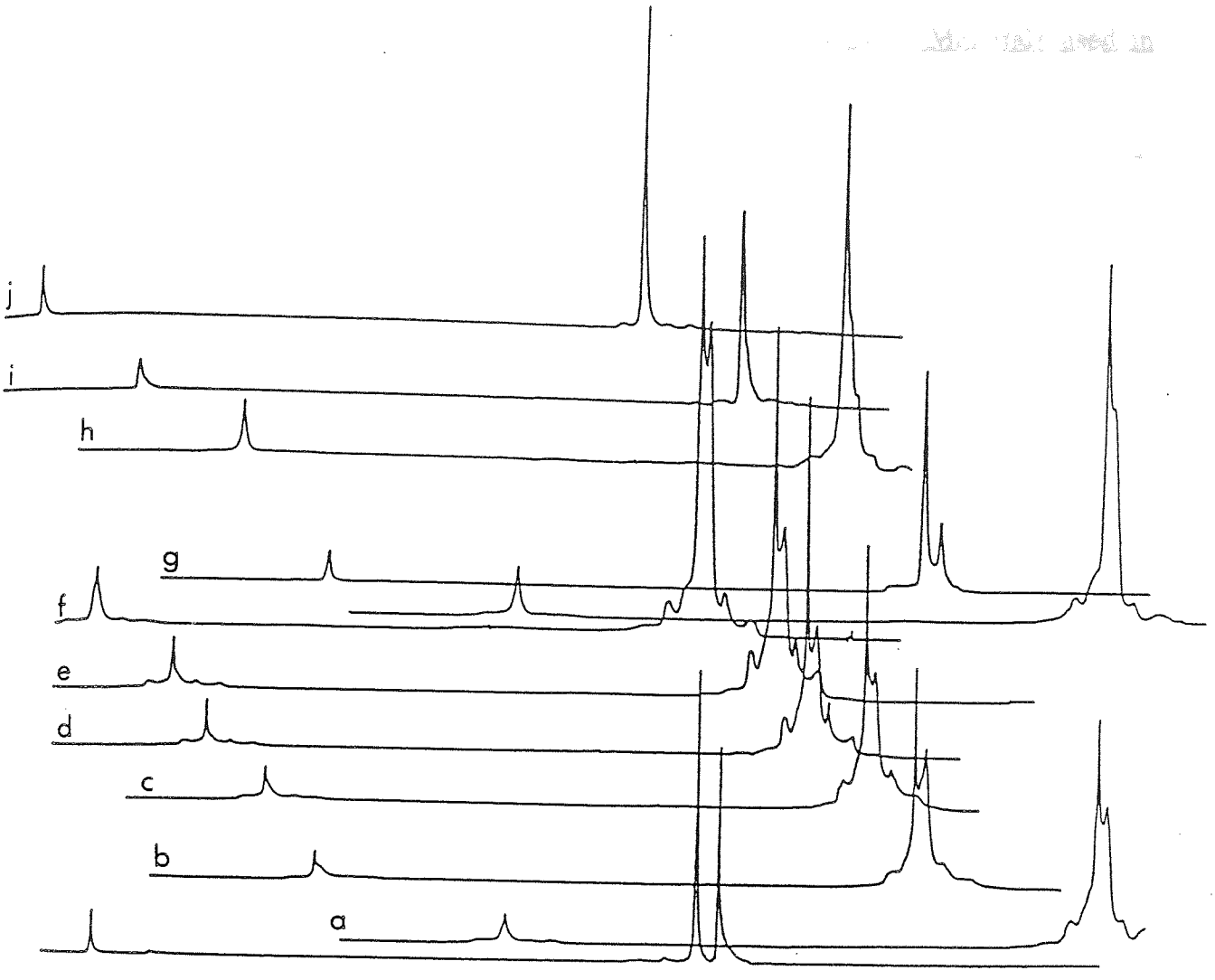

Ultrasonic probe in. Use of shim coils to tune and improve the resolution. (a - j).

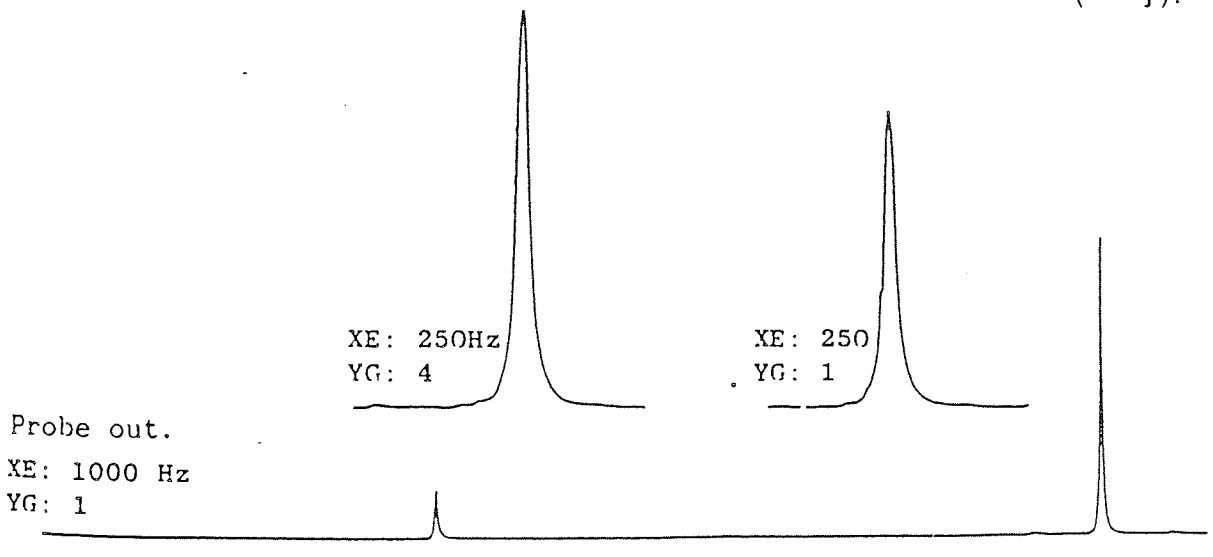

Figure 7.29: Effect of a glass ultrasonic probe in a liquid mixture of bromoform and cyclohexane. The probe is 1cm from the centre of the NMR transmitter and receiver coils. In addition, the use of the NMR shim coils to tune and improve the resolution is shown.

7.7 Effects of Sample Contamination by Various Materials used in Construction of the Ultrasonic Probes

When designing various probes with different types of transducer mountings, experiments were also performed to test whether the components used to build the probes contaminated the sample in a manner that would effect the NMR spin-lattice relaxation times. These experiments were performed by taking the appropriate material and placing it into a liquid mixture of bromoform and cyclohexane leaving it to stand for several hours (2-3 hrs). The liquid/material mixture was then filtered and the filtrate analysed by proton NMR. Table 7.4 shows the effects of different materials on the liquid mixture of bromoform and cyclohexane, in terms of their influence on the proton spin-lattice relaxation times.

The results of the experiments revealed that most materials did not effect the proton spin-lattice relaxation times. However, it appears that materials such as copper, nickel and brass drastically reduced the relaxation times. This is because these materials are paramagnetic and the species that dissolved added a relaxation mechanism to the dominant dipolar-dipolar relaxation, reducing the ^{1}H relaxation time. The paramagnetic mechanism obviously became the more dominant mechanism. Thus, extreme caution had to be exercised when building the ultrasonic probes and when interpreting the results.

Material	^{1}H NMR spin-lattice relaxation times (seconds)	
	$CH Br_3$	C_6H_{12}
Neat liquid mixture	4.63	3.41
PZT ceramic	4.57	3.36
Asbestos tufnol	4.75	3.51
Fabric tufnol	4.83	3.43
Paper tufnol	4.52	3.48
Copper/nickel constantan	0.42	1.40
Copper filings	Data unreliable	1.33
Iron filings	Data unreliable	1.28
Brass filings	Data unreliable	1.26
Solder wire (lead/tin)	4.40	3.27
Super glue	4.63	3.39
Fused silica	4.58	3.39
"Pyrex" soda glass	4.61	3.42

Table 7.4: Effects of sample contamination on proton spin-lattice relaxation times, due to the various materials used in building numerous probes and transducer mountings which were lowered into the liquid NMR sample.

7.8 Experimental: Experiments performed to test for sample contamination

The following experiments were performed to test for sample contamination, through measurement of the effects of the materials used on proton spin-lattice relaxation times.

(1) Preparation of stock solution of bromoform and cyclohexane (1:1 molar ratio)

Bromoform (75.8g, 26.2cm^3, 0.3 mol) was added to cyclohexane (25.2g, 32cm^3, 0.3 mol) and the liquid mixture shaken well.

The ^1H NMR spin-lattice relaxation times were then measured for stock solution of bromoform and cyclohexane ($2cm^3$).

(2) Test for sample contamination

The following materials were tested for sample contamination.

(a) PZT ceramic (crystal size: 1mm thick and 5mm diameter)

(b) Fine grated fibre reinforced tufnol filings (0.5g)

(c) Fine grated fabric reinforced tufnol filings (0.5g)

(d) Fine grated paper reinforced tufnol filings (0.5g)

(e) Fine Copper/Nickel Constantan filings (0.5g)

(f) Fine Copper filings (0.5g)

(g) Fine Iron filings (0.5g)

(h) Fine Brass filings (0.5)

(i) Fine solder (contains lead and tin) filings (0.5g)

(j) "Super glue" (cyanoacrylate) (4 drops)

(k) Small pieces of fused silica (0.5g)

(l) Small pieces of pyrex.

The procedure used for sample preparation and the measurement of spin-lattice relaxation times for each of the materials was as follows: To the prepared stock solution of bromoform and cyclohexane (4 cm^3), one of the above materials was added and shaken well. The liquid/material mixture was then left standing for 2 hours after which it was filtered. The filtrate ($2cm^3$) was analysed using NMR, by measurement of spin-lattice relaxation times, T_1, using the DESPOT method.

7.9 Measurement of the temperatures changes due to increasing ultrasonic power

The effects of increasing ultrasonic power causes the transducer to get warm and at times very hot. The heat generated across the transducer is as a direct

result of a large impedence mismatch between the transducer and the frequency generator amplifier, tuner and other materials used to mount the transducer, and also due to lack of coupling between the transducer and the liquid under investigation. Absorption of acoustic energy by the sample can also lead to temperature rises.

Experiments were performed to measure the extent of the heating on a pure liquid sample of cyclohexane. Table 7.5 shows the maximum temperature changes as the ultrasonic power driving the transducer is increased after the sample was allowed to reach thermal equilibrium. The results reported are for a transducer mounted at the bottom of a glass tube with the transducer floating in air (Figure 7.25).

Ultrasonic power levels (watts)	Maximum temperature rise ^{o}C (after reaching thermal equilibrium)
0.5	~0.5
1	1.5
2	3
5	7
10	12
15	16

Table 7.5: The maximum temperature rise as the ultrasonic power driving the transducer is increased.

The results revealed that if ultrasonic experiments are to be performed to observe the effects of NMR spin-lattice relaxation times, one must make sure that relaxation time measurements are carried out the system has been allowed to come to thermal equilibrium. This would then allow one to measure the effects of ultrasound. Alternatively, one must make sure that all possible precautions are taken to minimize the heating effects across the transducer. For example, by blowing nitrogen gas directly onto the transducer.

7.10 Measurement of power attenuation with increasing distance in a liquid

An experiment was performed to observe how far the ultrasonic waves travelled down in a liquid sample. This was carried out by measuring the power attenuation using a receiver transducer. The receiver transducer was initially placed directly underneath the transmitter transducer. By applying a constant power to the transmitter transducer and lowering the receiver transducer to various depths in the liquid sample, the amount of power attenuation was measured. The experiment was performed using two matching transducers operating at 1 MHz, using the electrical circuit shown in Figure 7.12.

Table 7.6 shows the voltage levels measured as various depths by the receiver transducer, whilst applying 0.8 Watts of power to the transmitter transducer. Figure 7.30 shows a graphical plot of this.

Depth of receiver transducer (in cm)	Voltage levels measured at various depths by receiver transducer (in volts)
Approximately zero depth (point contact)	0.6
0.5	0.5
1	0.35
1.5	0.285
2	0.200
2.5	0.15
3	0.1

Table 7.6: Voltage levels measured at various depths by a receiver transducer, whilst applying 0.8 Watts of power to the transmitter transducer

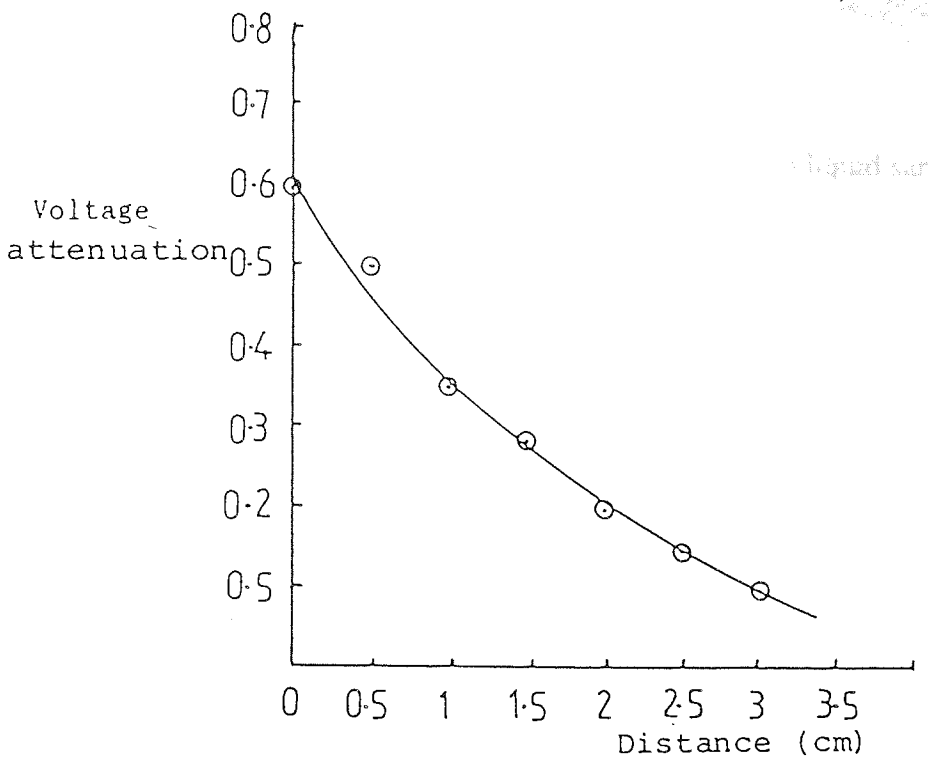

Figure 7.30: Voltage attenuation as the receiver transducer is moved further away from the transmitter transducer

The above results suggest that it is important when performing spin-lattice relaxation times, that the ultrasonic probe is lowered into the liquid NMR sample to exactly the same depth for all the experiments, otherwise, discrepancies in relaxation time measurements may occur.

7.11 Deoxygenation of Liquid Samples

The preparation of deoxygenated liquid samples for accurate measurement of spin-lattice relaxation rates has been the subject of considerable interest[67, 289-291]. The procedure selected for deoxygenating a liquid sample was to use tris (2,2-bipyridyl) cobalt (II) perchlorate in the presence of sodium borohydrate. The cobalt compound is golden brown in colour when solid. When dissolved with sodium borohydride in a suitable solvent, it removes oxygen in a reversible colour indicating reaction and when all the dissolved oxygen has been removed the solution turns deep blue.

Experiments performed using the ultrasound probe inside the liquid sample contained in the NMR tube meant that liquid samples could not be sealed and air could not be prevented from getting into the liquid. The only way to minimize the air from getting into the liquid sample was to have two immiscible liquid layers

with a deoxygenating liquid layer floating on the top of the two liquid samples.

7.12 Instruments, Experimental Methods and Conditions Developed for Sonochemical Reactions

The instrument required for studying the effects of acoustic cavitation on sonochemical reactions was commercially purchased. The instrument purchased operates via the piezoelectric effect at a constant frequency of 20 KHz and has a variable power output ranging from 1W cm^{-2} to 150W cm^{-2}. Under manufacturers specifications the instrument had been calibrated using water as a medium, with maximum probe deflection of 18 μm corresponding to a power of 118 W cm^{-2} being supplied to the transducer.

The instrument has two separate titanium probes (also referred to as acoustic horns) of length 77cm and 28cm, each having a probe tip diameter of 5mm. The longer probe was designed to perform experiments in a liquid sample contained in the NMR tube which was at the same time being investigated by NMR for chemical and structural changes. The shorter probe was designed to perform experiments on the bench.

A glass vessel was designed and built to perform experiments using the shorter probe, at known constant temperature and with an option of gas being blown into the liquid mixture. In addition, the vessel was designed so that liquid samples could be siphoned at various time intervals.

An acoustic cabinet was also constructed to perform the experiments inside the cabinet, in order to minimize the audible noise generated by the acoustic cavitation processes as well as perform the experiments in the dark. Figure 7.31 illustrates the glass vessel used with an acoustic probe connected to a frequency generator, for studying the effects of acoustic cavitation.

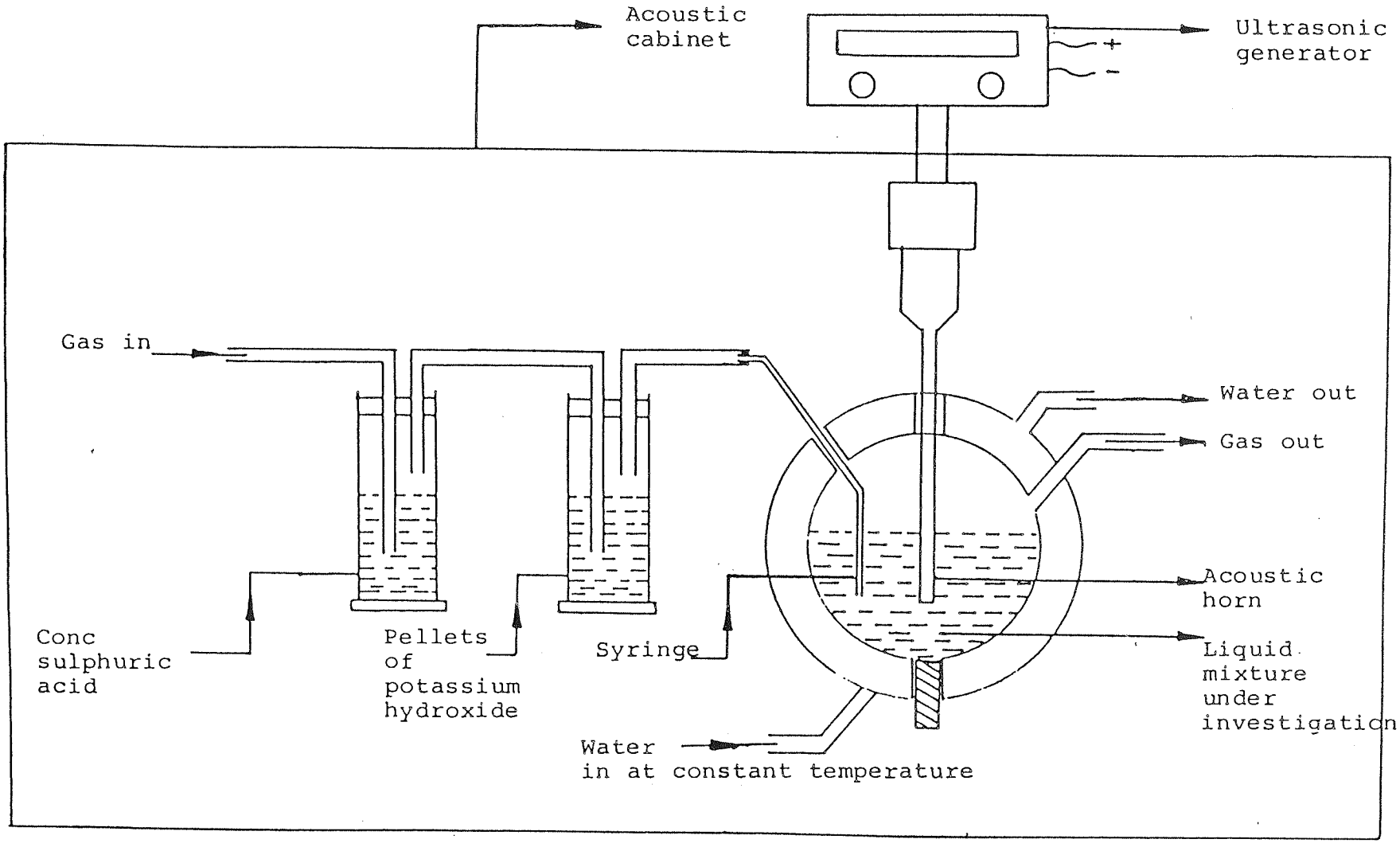

Figure 7.31 A glass vessel with acoustic horn connected to a frequency generator, for studying the effects of acoustic cavitation.

CHAPTER EIGHT

RESULTS, DISCUSSION, EXPERIMENTAL AND FUTURE WORK

8.0 Introduction

This chapter presents results, discussions, and details of the experiments performed. In addition, a final section presenting possible future work is also discussed. The results reported are for experiments which were repeated several times and include results of experiments which showed interesting features.

The chapter is divided into five sections. These describe:

1 Experiments performed at r.f. ultrasonic frequencies to observe changes in spin-lattice relaxation times or changes which affect the fine structure observed in NMR spectra. Experiments attempted in the low frequency range at 20 kHz, to observe changes in relaxation times will also be discussed in this section. The spin-lattice relaxation times were measured using DESPOT for which absorption signal heights were used rather than integrated signal intensities because, as will be seen later, the signal line widths were unaffected by ultrasound.

2 Experiments performed at low frequency, viz 20 kHz, to observe sonochemical reactions.

3&4 Experimental procedures for the experiments performed using both high and low frequencies, are discussed.

5 Recommended future work in terms of experiments and technical aspects to gain a further understanding of ultrasonic perturbation of molecular dynamics in the liquid phase: additionally the reproducibility of the experiments performed is discussed.

8.1 Effects of ultrasound frequencies in the mega-hertz region on NMR spin- lattice relaxation times

Experiments were performed at ultrasound frequencies of 1,2,6,6.42 and 10 MHz to observe their effects on spin-lattice relaxation or changes in the fine structure. Spin-lattice relaxation times were measured for ^{1}H, ^{13}C and ^{14}N nuclei. In addition, the effects of increasing ultrasonic power on NMR spin-lattice relaxation times were

investigated at each of the mentioned frequencies, with power levels ranging from 1W to 20W. These experiments were performed using various ultrasonic probes and it will be mentioned where appropriate the type of ultrasonic probe used.

Experiments were either performed on neat liquids, binary mixtures or mixtures which additionally contained deuterated chloroform. The reason for adding deuterated chloroform was essentially to provide a locking signal for the NMR studies. The liquids investigated are as follows: chloroform, bromoform, cyclohexane, 2-bromo-2-methyl propane, 2-chloro-2-methyl propane, benzene, 1,3,5-trimethylbenzene, 1-4-para-di-tertbutyl-benzene, 1,3,5-tri-tertbutyl benzene, N-methyl formamide, N,N-dimethyl formamide, N,N-dimethyl acetamide, acetonitrile, an aqueous solution of potassium chloride and a saturated solution of ammonium chloride in deuterated dimethylsulfoxide containing a trace of hydrochloric acid.

There were several criteria for selecting the compounds listed above These are:

(i) Because of symmetry in the molecules, interpretation of the NMR spectra is made easier.

(ii) By increasing the number of groups and maintaining molecular symmetry, not only is the interpretation of NMR spectra easier but also increases the overall molecular size and molecular weight.

(iii) By observing nitrogen-14 nuclei, it was possible to study the effects of ultrasound in two connections. These are:

(a) because the NMR linewidths of the Nitrogen-14 absorptions are large, it allows the observation of the effects of ultrasound on spin-spin relaxation times, T_2, in addition to its effects on spin-lattice relaxation times, T_1.

(b) because the NMR observation frequency for the nitrogen-14 nuclei on the NMR spectrometer is 6.42 MHz, this permits the investigation of the effects of ultrasound near, at the exact resonance frequency, and above the resonance frequency of the spectrometer by using the appropriate ultrasonic transducers.

Two experiments which involved the outgassing of dissolved air in liquids were performed. The first experiment involved measurement of spin-lattice relaxation times for

liquid which had just been simply purged with nitrogen gas. The second experiment involved measurement of spin-lattice relaxation times for liquid mixtures which are simultaneously being subjected to ultrasound and contained a deoxygenating agent, tris-(2,2-bipyridyl) cobalt (II) perchlorate and sodium borohydride. The experiments in both cases were performed separately on equimolar mixtures of bromoform and cyclohexane.

The significance of performing the above two types of experiments have already been discussed in Chapters Four and Seven in terms of the effects of paramagnetic impurities on relaxation mechanism. Thus, an understanding of these results should lead to a better understanding of the role of the paramagnetic relaxation mechanism when comparing and interpreting results to those obtained for liquids which owing to experimental difficulties are exposed to air and are simultaneously being subjected to ultrasound. This would then enable one to understand the real extent of ultrasonically induced molecular perturbation in the liquid phase.

Experiments involving measurement of the effects of temperature variations on spin-lattice relaxation times were also performed. The purpose of these experiments was again to compare these results with those obtained for liquid mixtures which were ultrasonically treated. Thus, through a comparison of the results it will allow one to assess the effects of ultrasonically induced temperature changes. Two sets of experiments were performed. These were on equimolar mixtures of bromoform and cyclohexane, and 1,3,5-trimethylbenzene (mesitylene) and cyclohexane.

RESULTS AND DISCUSSION

8.1(a) Measurement of the effect of ultrasound on proton (^{1}H) spin-lattice relaxation times using a silica rod as an ultrasonic probe

The results presented in Tables 8.1, 8.2, 8.3 and 8.4 were obtained using a fused silica rod as the ultrasonic probe. The operating transducer was of the type PZT-5A which was mounted on the top of the silica rod. This was then resonated at 1.94 MHz (the actual specification resonance frequency was 2 MHz ± 10% tolerance), with approximately 15-20W of power supplied to it using a home-built power amplifier.

Experiments performed in the presence of ultrasound on chloroform, bromoform and cyclohexane revealed that there were no effects on the spin-lattice relaxation times of pure liquids (Table 8.1). However, experiments performed several times, on equimolar mixtures of chloroform and cyclohexane, chloroform and 2-methyl-2-chloropropane (isopropyl-chloride), bromoform and cyclohexane, and cyclohexane and mestylene, revealed that ultrasound did in fact affect the relaxation times; in some cases, a decrease and in others, an increase in the relaxation times (Tables 8.2-8.4).

From the results presented, several separate conclusions can be deduced. Results from experiments performed with the presence of ultrasound in pure liquids showed almost no effects to the NMR relaxation times. From these results, it could be said that the effects of acoustic energy imposed onto the molecules are nil. Alternatively, it could be argued that the effects of acoustic energy are such that the relative motions of the molecules to the motion of the liquid as a whole, are negligibly small and therefore very small changes are observed in the relaxation times. By comparison, for liquid mixtures which contain unlike molecules, in terms of molecular weight or molecular size, positive and negative changes in the NMR relaxation times are observed.

In this case, either the relative amount of energy each molecule has is unequal or the same as the rest of the molecules. However, in either case, because of different molecular mass, the relative motion for each molecular species is different. Moreover, any

effects of acoustic energy in the liquid mixture will further cause the individual molecules to move at different rates. This is reflected in the changes observed in the relaxation times.

One argument which can be presented in the discussion for the observed reduction of spin-lattice relaxation times is the possibility of acoustic streaming. In this case, it is visualised that for molecules which lie in the region of the acoustic field, obtain more energy. As a result, these molecules now move out of the acoustic field and are subsequently replaced by molecules which were not previously under the effect of the acoustic field. Thus in measuring spin-lattice relaxation times of the sample, one may argue that the relaxation times measured are for molecules which are either moving at a different rate to molecules which are under the influence of the acoustic field or of molecules which are now relaxing back to thermal equilibrium following their change in the equilibrium. This argument can however be eliminated by referring to results obtained for experiments performed using ultrasound on pure liquids in which only very small changes in spin-lattice relaxation times was observed.

In a recent review by Lorimer and Mason[292], they suggest that movement of molecules is transmitted through adjoining particles before returning to equilibrium. As already discussed in Chapter Five, the addition of "impurity" molecules to pure liquids, enables collisions between unlike molecules which may be more effective in producing energy transfer than those between like molecules. In addition, it may also lead to an effective structure relaxation by way of volume changes which effects molecular packing. From Table 8.3, relating to experiments performed on cyclohexane and 1,3,5-trimethylbenzene, it is interesting to note that the relaxation times for the aromatic hydrogens, the methyl groups, and the methylene groups in the two molecules are affected by different relative amounts. The aromatic hydrogens are least affected due to the rigidity of the aromatic ring. This suggests that the acoustic energy can only affect its relaxation times through the translational and rotational motionof the molecule as a whole. In comparison with the aromatic hydrogens, the methyl groups are affected more, as a consequence of the effects of acoustic enertgy on its rotational motion (ie. rotational motion about the aromatic carbon and the methyl carbon bond axis) in addition to the

translational and rotational motion of the molecule as a whole. For the methylene group in cyclohexane, the effects of ultrasound are two fold. It will not only cause changes in the translational and rotational motion of the molecule but also in the rate at which the molecules changes its conformations as it goes from one chair conformation to the other chair conformation via the boat conformation. Thus larger changes in the relaxation times are observed in comparison to those observed for mesitylene.

The positive and negative changes in spin-lattice relaxation times will be discussed later in another section following further experimental results.

Experiments involving measurement of spin-lattice relaxation times for protons, in liquid mixtures of bromoform and cyclohexane which were degassed, revealed that the relaxation times were longer compared to those obtained for experiments in which no degassing was performed (Table 8.4a). In the experiment involving equimolar mixtures of bromoform and cyclohexane in the presence of the deoxygenating agent tris-(2,2-bipyridyl) cobalt (II) perchlorate and sodium borohydride which also removes molecular oxygen, the results revealed that spin-lattice relaxation times for liquid mixtures had increased (compare Tables 8.4(b) and 8.2(c) for "ult off"). Subsequent treatment of this liquid mixture to ultrasound revealed larger changes in the relaxation times compared to experiments which were performed without the presence of the deoxygenating agent but in the presence of ultrasound in the liquid mixture (compare Tables 8.4(b) and 8.2(c) in terms of percentage reductions in the relaxation times). Several conclusions can be deduced from such observations: As expected, the removal of paramagnetic species such as molecular oxygen increases spin-lattice relaxation times. This result suggests that in the presence of paramagnetic species in liquids, relaxation via the paramagnetic relaxation mechanism is an important mechanism in comparison to the dipole-dipole relaxation mechanism. For liquids which are deoxygenated and are subjected to ultrasound, larger reductions in spin-lattice relaxation times are observed. Thus, in experiments where molecular oxygen was not removed, relaxation via the paramagnetic relaxation mechanism is important and may even be comparable to the changes produced in liquid mixtures which have been subjected to ultrasound. In addition, three competing relaxation

mechanisms leading to spin-lattice relaxation times now exists for liquids which arenot deoxygenated and are subjected to ultrasound. These being, dipole-dipole, paramagnetic and ultrasound.

The results of the effects of temperature changes on spin-lattice relaxation times shows that as the temperature is increased, spin-lattice relaxation time become longer (Table 8.5a and b). This suggests that the correlation time, τ_c, on average, for molecules which are being investigated decreases as temperature increases. In terms of the spectral density, the molecules now have fewer Fourier components at the Larmor frequency and therefore the relaxation time has increased. This can be easily understood from Figure 2.4 (Chapter Two) which shows that if the molecular motion moves away from the motional averaging where $\tau_c\omega_o \sim 1$, then spin-lattice relaxation times increase. Increasing temperature causes faster molecular motions due to a result of an increase in thermal energy. This suggests that the translational and rotational correlation times for molecules on average, will have decreased. This further suggests, that one must be on the left side of the T_1 minimum of Figure 2.4 (Chapter Two) and that any further decreases in correlation times increases spin-lattice relaxation times. Further discussion on the effects of temperature and effects of ultrasound will be presented in a later section.

The inconsistencies in the results in the induced changes in spin-lattice relaxation times in the second and third sets of experiments, may be due to several reasons. These are:

(i) Lack of reproducibility in delivering a required amount of power/energy into the liquid system through the probe. This may have arisen from the mounted transducer not being able to maintain contact with the silica rod at all times whilst resonating.

(ii) Impedance mismatch between the transducer and the fused silica rod. This meant that the total energy was inefficiently transmitted across from the transducer to the silica rod. This inefficiency in energy coupling causes the transducer to physically get hot which further leads to changes in the characteristics of the transducer to the extent that reproducibility of the transducer becomes in question.

(iii) Multiple reflections of the acoustic wave in the silica rod. This means that the total amount of energy delivered into the liquid mixture is in effect inconsistent each time the experiment is performed.

(iv) Mismatch of impedence between the silica rod and the liquid mixture under investigation. This means that there is an inefficiency in energy coupling and energy transfer between the two media.

RESULTS OF MEASUREMENT OF THE EFFECTS OF ULTRASOUND ON PROTON (^{1}H) SPIN-LATTICE RELAXATION TIMES USING SILICA ROD AS AN ULTRASONIC PROBE (TABLES 8.1-8.5)

RELAXATION TIME MEASUREMENTS

NUCLEI UNDER INVESTIGATION: ^{1}H NMR.

NMR INSTRUMENT OBSERVATION FREQUENCY: 89.56 MHz.

SYSTEM UNDER INVESTIGATION: Pure liquids of chloroform, bromoform and cyclohexane.

90 DEGREE PULSE: 258 us.

PULSE REPETITION: 1.0 s. ACQUISITION TIME: 0.6 s. SCANS: 20.

TRANSDUCER FREQUENCY: 1.94 MHz.

TOTAL INPUT POWER: 15-20W.

METHOD OF ANALYSIS: Curve fit programme.

SPIN-LATTICE RELAXATION TIME MEASUREMENTS (T_1). IN SECONDS

	Chloroform	% change	Bromoform	% change	cyclohexane.	% change
PROBE IN. ULT. OFF	2.10		2.59		2.76	
PROBE IN. ULT. ON (1)	2.326	+10.7	2.62	+ 1.1	2.61	-2.2
(2)	1.99	- 5.2	2.34	- 9.6	2.65	-3.9

Table 8.1 : The effect of ultrasound at a frequency of 1.94MHz on proton (^{1}H) spin-lattice relaxation times (T_1) for pure liquids, using a fused silica rod as an ultrasonic probe.

RELAXATION TIME MEASUREMENTS

NUCLEI UNDER INVESTIGATION: ^{1}H NMR.

NMR INSTRUMENT OBSERVATION FREQUENCY: 89.56 MHz.

SYSTEM UNDER INVESTIGATION: Equimolar mixture of chloroform and cyclohexane.

90 DEGREE PULSE: 258 us.

PULSE REPETITION: 1.0 s. ACQUISITION TIME: 0.6 s. SCANS: 20.

TRANSDUCER FREQUENCY: 1.94 MHz.

TOTAL INPUT POWER: 15-20W

METHOD OF ANALYSIS: Curve fit programme.

SPIN-LATTICE RELAXATION TIME MEASUREMENTS (T_1). IN SECONDS

results for chloroform

EXPT. NO.	PROBE IN. ULT. OFF	PROBE IN. ULT. ON	% changes
1	1.90	2.10	+10.5
2	1.99	1.89	- 5.0
3	1.97	2.21	+12.3
4	2.51	2.81	+12.0
5	1.99	1.78	-10.3

Table 8.2 (a) : The effect of ultrasound at a frequency of 1.94MHz on proton (^{1}H) spin-lattice relaxation times (T_1) for an equimolar mixture of chloroform and cyclohexane, using a fused silica rod as an ultrasonic probe.

RELAXATION TIME MEASUREMENTS

NUCLEI UNDER INVESTIGATION: ^{1}H NMR.

NMR INSTRUMENT OBSERVATION FREQUENCY: 89.56 MHz.

SYSTEM UNDER INVESTIGATION: Equimolar mixture of chloroform and 2-chloro-2-methyl propane (isopropyl chloride).

90 DEGREE PULSE: 258 us.

PULSE REPETITION: 1.0 s. ACQUISITION TIME: 0.6 s. SCANS: 20.

TRANSDUCER FREQUENCY: 1.94 MHz.

TOTAL INPUT POWER: 15-20W

METHOD OF ANALYSIS: Curve fit programme.

SPIN-LATTICE RELAXATION TIME MEASUREMENTS (T_1). IN SECONDS

results for chloroform

EXPT. NO.	PROBE IN. ULT. OFF	PROBE IN. ULT. ON	% changes
1	1.36	1.29	-5.14
2	1.41	1.27	-10.0

Table 8.2 (b) : The effect of ultrasound at a frequency of 1.94MHz on proton (^{1}H) spin-lattice relaxation times (T_1) for an equimolar mixture of chloroform and 2-chloro-2-methyl propane (isopropyl chloride), using a fused silica rod as an ultrasonic probe.

RELAXATION TIME MEASUREMENTS

NUCLEI UNDER INVESTIGATION: ^{1}H NMR.

NMR INSTRUMENT OBSERVATION FREQUENCY: 89.56 MHz.

SYSTEM UNDER INVESTIGATION: Equimolar mixture of bromoform and cyclohexane.

90 DEGREE PULSE: 258 us.

PULSE REPETITION: 1.0 s. ACQUISITION TIME: 0.6 s. SCANS: 20.

TRANSDUCER FREQUENCY: 1.94 MHz.

TOTAL INPUT POWER: 15-20W

METHOD OF ANALYSIS: Curve fit programme.

SPIN-LATTICE RELAXATION TIME MEASUREMENTS (T_1). IN SECONDS

results for bromoform

EXPT. NO.	PROBE IN. ULT. OFF	PROBE IN. ULT. ON	% changes
1	2.54	1.92	-6.2
2	2.09	1.58	-7.5
3	3.22	2.98	-7.4
4	2.62	2.42	-8.6

Table 8.2 (c) : The effect of ultrasound at a frequency of 1.94MHz on proton (^{1}H) spin-lattice relaxation times (T_1) for an equimolar mixture of bromoform and cyclohexane, using a fused silica rod as an ultrasonic probe.

RELAXATION TIME MEASUREMENTS

NUCLEI UNDER INVESTIGATION: ^1H NMR.

NMR INSTRUMENT OBSERVATION FREQUENCY: 89.56 MHz.

SYSTEM UNDER INVESTIGATION: Equimolar mixture of 1,3,5- trimethylbenzene and cyclohexane.

90 DEGREE PULSE: 258 us.

PULSE REPETITION: 1.0 s. ACQUISITION TIME: 0.6 s. SCANS: 20.

TRANSDUCER FREQUENCY: 1.94 MHz.

TOTAL INPUT POWER: 15-20W

METHOD OF ANALYSIS: Curve fit programme.

SPIN-LATTICE RELAXATION TIME MEASUREMENTS (T_1). IN SECONDS

MOLECULAR GROUP	PROBE IN. ULT. OFF	PROBE IN. ULT. ON	% changes
Aryl hydrogen.	1.12	0.069	-30.4
	1.13	0.76	-32.5
Methyl.	0.86	0.34	-60.8
	0.89	0.49	-44.6
Methylene.	1.02	0.36	-64.5
	0.50	0.24	-51.9

Table 8.3 : The effect of ultrasound at a frequency of 1.94MHz on proton (^1H) spin-lattice relaxation times (T_1) for an equimolar mixture of 1,3,5-trimethylbenzene and cyclohexane, using a fused silica rod as an ultrasonic probe.

RELAXATION TIME MEASUREMENTS

NUCLEI UNDER INVESTIGATION: ^{1}H NMR.

NMR INSTRUMENT OBSERVATION FREQUENCY: 89.56 MHz.

SYSTEM UNDER INVESTIGATION: Equimolar mixture of bromoform and cyclohexane.

90 DEGREE PULSE: 258 us.

PULSE REPETITION: 1.0 s. ACQUISITION TIME: 0.6 s. SCANS: 20.

METHOD OF ANALYSIS: Curve fit programme.

SPIN-LATTICE RELAXATION TIME MEASUREMENTS (T_1). IN SECONDS

TYPE OF EXPERIMENTS	Bromoform.	Cyclohexane.
No degassing.	2.66	2.26
With degassing.	15.34	19.77

Table 8.4 (a) : The effect of outgassing dissolved air, by purging with nitrogen gas on proton (^{1}H) spin-lattice relaxation times (T_1) for an equimolar mixture of bromoform and cyclohexane.

RELAXATION TIME MEASUREMENTS

NUCLEI UNDER INVESTIGATION: ^1H NMR.

NMR INSTRUMENT OBSERVATION FREQUENCY: 89.56 MHz.

SYSTEM UNDER INVESTIGATION: Equimolar mixture of bromoform and cyclohexane containing tris (2,2-bipyridyl) cobalt (II) perchlorate containing sodium borohydride.

90 DEGREE PULSE: 258 us.

PULSE REPETITION: 1.0 s. ACQUISITION TIME: 0.6 s. SCANS: 20.

TRANSDUCER FREQUENCY: 1.94 MHz.

TOTAL INPUT POWER: 15-20W

METHOD OF ANALYSIS: Curve fit programme.

SPIN-LATTICE RELAXATION TIME MEASUREMENTS (T_1). IN SECONDS

	Bromoform.			Cyclohexane.		
EXPT. NO.	PROBE IN ULT. OFF	PROBE IN ULT. ON	% changes	PROBE IN ULT. OFF	PROBE IN ULT. ON	% changes
1	4.46	3.92	-12.1	3.83	3.31	-13.6
2	3.35	2.95	-11.7	3.08	2.63	-14.6
3	4.66	2.30	-50.5	3.50	1.62	-53.8

Table 8.4 (b) : The effect of ultrasound at a frequency of 1.94MHz on proton (^1H) spin-lattice relaxation times (T_1) for an equimolar mixture of bromoform and cyclohexane containing tris (2,2-bipyridyl) cobalt (II) perchlorate and sodium borohydride.The measurements were made using a fused silica rod as an ultrasonic probe.

RELAXATION TIME MEASUREMENTS

NUCLEI UNDER INVESTIGATION: ^1H NMR.

NMR INSTRUMENT OBSERVATION FREQUENCY: 89.56 MHz.

SYSTEM UNDER INVESTIGATION: Equimolar mixture of bromoform and cyclohexane.

90 DEGREE PULSE: 258 us.

PULSE REPETITION: 1.0 s. ACQUISITION TIME: 0.6 s. SCANS: 20.

METHOD OF ANALYSIS: Curve fit programme.

SPIN-LATTICE RELAXATION TIME MEASUREMENTS (T_1). IN SECONDS

TEMPERATURE °C	Bromoform.	Cyclohexane.
30	4.25	2.26
40	4.84	3.02
50	5.52	3.50
60	6.53	4.02

Table 8.5 (a) : The effect of increasing temperature on proton (^1H) spin-lattice relaxation times (T_1) for an equimolar mixture of bromoform and cyclohexane.

RELAXATION TIME MEASUREMENTS

NUCLEI UNDER INVESTIGATION: ^{1}H NMR.

NMR INSTRUMENT OBSERVATION FREQUENCY: 89.56 MHz.

SYSTEM UNDER INVESTIGATION: Equimolar mixture of 1,3,5-trimethylbenzene (mesitylene) and cyclohexane.

90 DEGREE PULSE: 258 us.

PULSE REPETITION: 1.0 s. ACQUISITION TIME: 0.6 s. SCANS: 20.

METHOD OF ANALYSIS: Curve fit programme.

SPIN-LATTICE RELAXATION TIME MEASUREMENTS (T_1). IN SECONDS

TEMPERATURE °C	1,3,5-trimethylbenzene	Cyclohexane.
34.48	3.45	3.03
39	3.97	3.45
47	4.18	3.63
53	4.79	4.74
61	5.27	5.94
72	5.82	6.98

Table 8.5 (b) : The effect of increasing temperature on proton (^{1}H) spin-lattice relaxation times (T_1) for an equimolar mixture of 1,3,5-trimethylbenzene (mesitylene) and cyclohexane.

8.1(b) Measurement of proton (^{1}H) and carbon-13 nuclei (^{13}C) NMR relaxation times using a glass tube with the transducer mounted on the bottom of the tube

The results of experiments performed on equimolar mixtures of liquid of cyclohexane and benzene, cyclohexane and 1,3,5-trimethylbenzene, cyclohexane and 1,4-para-di-tetbutylbenzene and, cyclohexane and 1,3,5-tri-tert-butylbenzene at 1.115 MHz and 6 MHz are presented in Tables 8.6 to 8.13. The experiments were performed at various ultrasonic powers ranging from 0.5W to 15W. Tables 8.7(a) and (b) and 8.11(a) and (b), shows the reproducibility of the ultrasonic experiments through experiments performed on both proton and carbon-13 spin-lattice relaxation times. The experiments were performed using an ultrasonic frequency of 1.115 MHz, in a equimolar mixture of cyclohexane and 1,3,5-trimethylbenzene (mesitylene). The results show the reproducibility in terms of the overall percentage changes in the spin-lattice relaxation times.

Results of experiments performed using an ultrasonic frequency of 10 MHz, showed inconsistencies when the ultrasonic power was increased. This was later found to be due to the irreproducibility in the performance of the 10 MHz transducer. Thus, no further results are presented for such experiments.

A preliminary inspection of the results presented in Tables 8.6 to 8.13 suggest the following:

(i) As expected the initial numerical values of the proton spin-lattice relaxation times are smaller than those for the carbon-13 relaxation times. If one accepts that the magnetic dipolar-dipolar relaxation mechanism (discussed in Chapter Three) is dominant for simple non-viscous liquids and is the sum of inter and intra molecular dipolar-dipolar interactions, then the combined effects of inter and intra molecular dipolar-dipolar contribution on proton relaxation times are larger in comparison to those for the carbon-13 nuclei. For the carbon-13 nuclei the intra molecular dipolar-dipolar relaxation mechanism is predominant. Thus, if the effects of ultrasound on liquid mixtures is largely translational (T_1 inter), then the effects on protons should be more pronounced than those on carbon-13 nuclei. This is

exactly what is observed. These results suggest that the effects of sound is more pronounced on the translational motion of molecules compared to the effects of sound on the rotational motion of molecules. This is best illustrated by Tables 8.6(a) and (b), and 8.10(a) and (b) for cyclohexane and benzene where there is a larger percentage reduction in the relaxation times for protons compared to the carbon-13 nuclei.

(ii) The relaxation times initially decrease with increase in power. However, using ultrasonic powers of 5W and above, the relaxation times start to increase. This suggests that temperature effects due to the absorption of ultrasound now also becomes important. Explanation of such behaviour will be presented later in this section.

(iii) There were no significant differences in the changes observed in the spin-lattice relaxation times in changing the ultrasonic frequency from 1.115 MHz to 6 MHz.

(iv) From the arguments presented in section 8.1(a) on the effects of ultrasound on liquid mixtures containing unlike molecules, it was visualised that by studying the effects of increasing molecular groups such as methyl and tertbutyl groups on benzene, would lead to a better understanding of how ultrasound interacts with molecular systems. However, comparison of the results obtained for the liquid mixtures containing cyclohexane and benzene, cyclohexane and 1,3,5-trimethylbenzene, and cyclohexane and 1,3,5-tri-tertbutylbenzene, (Tables 8.6 to 8.13) for both proton (^{1}H) and carbon-13 nuclei (^{13}C) spin-lattice relaxation times revealed that increasing molecular group size and in consequence molecular weight, showed that such changes could not be evaluated in terms of how ultrasound affects different molecular systems.

(v) Comparison of the NMR spectra for the carbon-13 nuclei, with and without being subjected to ultrasound, shows, in general, a sharp radio frequency beat signal at approximately 41.7 hertz from the centre of the spectral frequency. Attempts in terms of earthing the probe did not remove the radio-frequency beat signal.

(vi) Comparison of NMR linewidths for the liquid mixtures investigated with and without ultrasound, revealed that there were no effects on spin-spin relaxation times.

So far, throughout the discussion, the significance and importance relating to the increases and decreases observed in the spin-lattice relaxation times for liquids which were

subjected to ultrasound have not been explained. In order to explain such observations it is necessary to recall the effects of a wave passing through a medium as well as the effects on the spin-lattice relaxation times due to changes in the correlation times τ_c. Both issues have been discussed in Chapters Five and Two respectively.

From the discussion presented in Chapter Five on the effects of an elastic wave passing through a medium it became apparent that if the period of the wave was much longer than the relaxation time for the alteration of the position of equilibrium of the medium the latter would be disturbed. However, if the period of the wave was much shorter than the relaxation times the wave would in effect not "see" the equilibrium, which would consequently remain undisturbed. When the period of the wave is comparable to the relaxation time, changes in velocity of propagation and absorption coefficient of the elastic wave would occur. As discussed in Chapter Six and from the results of experiments performed on pure liquids in which a very small effect was observed on the spin-lattice relaxation times, this may be due to the fact that there may be an inefficient coupling of energy between the sound wave and the external mode of freedom. Thus, a poor transfer of energy from the external mode to the internal degrees of freedom occurs. In addition, a poor molecular packing gives rise to a larger free volume for the molecule to move around before it collides with another molecule. This means that the frequency of energy transfer between molecules is low. Thus, any effects of ultrasound in liquids, on the external modes of freedom of molecules will not be transferred at a high frequency. Furthermore, once the sound energy is transferred to the external modes of the molecules, energy transfer to other degrees of freedom of the molecules may not be efficient and as a result, very small changes in the spin-lattice relaxation times will be observed. On the other hand, a nil effect can still be observed if the relative motion of the molecules relative to the bulk of the liquid is zero, as discussed earlier.

If one accepts that there is an adequate coupling, it is then apparent that a compressional wave will cause a change in the translational, rotational and vibrational energies of the molecules. If the energy is passed on from molecule to molecule by collisions, then the whole molecular system will have a new energy equilibrium compared

to its initial equilibrium. In terms of its effects on spin-lattice relaxation rates, an efficient coupling of the acoustic energy to the external and internal energies of molecules may either lead to an increase or a decrease in the correlation time τ_c.

From Figure 2.4 (Chapter Two) , for molecules which lie to the far left of T_1 minima, that is, for molecules which are moving very rapidly and thus possess short correlation times τ_c, a gradual increase in the correlation time decreases the spin-lattice relaxation times up to a point where $\tau_c\omega_o \sim 1$. Further increases in the correlation time now causes the relaxation time to increase. Similarly, for molecules which lie to the far right of T_1 minimum, that is, for molecules which are moving relatively slowly, a decrease in correlation time by forcing the molecules to translate and rotate faster, will cause a decrease in the relaxation times, up to a point where again $\tau_c\omega_o \sim 1$. Further decrease in correlation times will now increase the relaxation times. In terms of spectral density in extreme narrowing, the contribution of components at the Larmor frequency is small, but increases as the molecular reorientation rate is slowed down. This means that any factors such as the effects of ultrasound being imposed on liquids may slow down molecular motion to the extent that it shortens the spin-lattice relaxation times. A minimum is reached near the condition for intermediate molecular tumbing rates and any further slowing of the motion reduces the components at the Larmor frequency and therefore increases the relaxation times. Thus, the purpose of using ultrasound in the mega-hertz region now becomes apparent, which is, to force the molecules to translate and rotate at, or near the such frequencies and thereby provide larger frequency components at the Larmor frequency. This will then lead to motional averaging where $\tau_c\omega_o \sim 1$ and thus lead to a minimum in the relaxation times. This effect has been shown mathematically in Chapter Six.

The above discussion appears to be adequate for observations made on the effects of ultrasound in liquids via changes in spin-lattice relaxation times. However, results of experiments performed to measure the effect of temperature variations on liquid mixtures revealed that spin-lattice relaxation times increases with increasing temperature. Furthermore, it was deduced that the correlation times decreased with increasing

temperature and from Figure 2.4 (Chapter Two), one must be on the left of the T_1 minimum. These results suggest that when starting experiments to observe the effects of ultrasound in liquid mixtures, via measurement of the changes observed in spin-lattice relaxation times, one must initially be on the left of T_1 minimum. Thus, imposing ultrasound on liquid mixtures with increasing ultrasonic powers shows an initial decrease in the spin-lattice relaxation times followed by an increase in spin-lattice relaxation times at higher ultrasonic powers. In terms of correlation times, at low ultrasonic powers an increase in the correlation time must occur. However, at higher ultrasonic powers, either a further increase in the correlation times or a decrease in correlation times can occur. If there is a decrease in the correlation time at higher ultrasonic powers, this suggests that all the changes observed in the spin-lattice relaxation times must have occurred on the left of T_1 minimum. To explain such observations in terms of spectral density starting from the left of T_1 minimum in Figure 2.4 (Chapter Two): an increase in the correlation times at low ultrasonic powers in liquid mixture lends to a larger contribution of the Fourier components at the Larmor frequency, thereby leading to shorter spin-lattice relaxation times. As the ultrasonic power is now increased, the correlation times start to decrease, which means there is now a smaller contribution of Fourier components at the Larmor frequency and therefore longer spin-lattice relaxation times.

Results of experiments performed to observe the effects of ultrasound on pure liquids and liquid mixtures, reveal that liquid mixtures containing molecules of different molecular weights show significant changes in the NMR spin-lattice relaxation times unlike those observed for pure liquids. The fact that molecules pass on energy from molecule to molecule during collision, and molecules having different relative molecular weights will, although possessing the same additional energy obtained from sound, will move differentially relative to one another. This is reflected in the relative changes in the spin-lattice relaxation times.

In Chapter Six, the discussion on the effects of sound absorption in liquids arising from vibrational and structural relaxation was related to the properties and behaviour of liquids, with the concept of free volume in which molecules are allowed to move freely

before encountering another molecule. Moreover, the volume changes in a liquid could either occur by forcing the molecules to move closer to one another and this would increase the efficiency and the probability of the number of collisions and the probability of energy transfer during collisions. All these changes encountered are due to the fact that each molecule now has a smaller volume to move freely as well as by changing the number of nearest neighbours. Thus, liquids containing molecular systems of different molecular weights, and different sizes and shapes will have a different order of molecular packing compared to that encountered in pure liquids. In addition, "impurity effects" discussed earlier (in section 8.3(a)) suggests that this will have pronounced effects on the relaxation times. Alternatively, if the molecular arrangements are poor (in terms of packing and energy transfer during collisions), then this will have very small effects on the relaxation times. However, it is important to realise that in order to observe a reduction in the relaxation times, the approach to motional averaging, where $\tau_c\omega_o \sim 1$, must result in larger Fourier components at the Larmor frequency and any deviations from such behaviour, will mean an increase in the relaxation times. The implication of this in relation to the results obtained in which a reduction in spin-lattice relaxation time is observed, suggests that more Fourier components exist at the Larmor frequency, for molecules which were subjected to ultrasound than in experiments where ultrasound was not applied. The increase in spin-lattice relaxation times at higher ultrasonic powers suggests that other ultrasonic absorption relaxation mechanisms now come to play. These other mechanisms will be discussed together with the effects of temperature in a later section.

In addition to the above discussion, the behaviour of sound as being a continuous and alternating pressure wave was extrapolated to the behaviour observed for static pressures in liquids. Through these discussion, it was apparent that pressure induces changes in volume, density and viscosity. The changes in volume results in changes in density. In molecular terms, increasing pressure, causes the molecular reorientation to become increasingly more hindered and anisotropic in nature, due to the closer proximity of the neighbouring molecules. This also results in enhancing the reorientational and translational coupling. Moreover, the actual nature of the reorientation which couple the

translational motion remains unaffected, thus volume rather than kinetic energy plays the decisive role in determining the degree of coupling. This analysis is consistent with the results of Artaki and Jonas[225] presented in Chapter Six which shows that increasing pressure does decrease the volume and this in turn decreases the relaxation times.

The effect of increasing pressure on viscosity, also has to be considered. If viscosity represents a measure of the forces that work against movement or flow, then, through the effects on volume and density which may result in hindered motions due to the volume changes described above, it will cause the viscosity to increase. Recalling equations 3.36 and 3.39 from Chapter Three, which define the inter and intra molecular dipole-dipole contribution to spin-lattice relaxation times and are re-expressed below, these show the effects of viscosity on relaxation times. The equation shows that increasing the viscosities η_{AB} and η_A, causes the relaxation times to decrease. This is in agreement with the results obtained elsewhere[225].

$$T^{-1}_{1\ intra} = \hbar^2 \gamma_i^2 \left[3/2\ \gamma_i^2 \sum_{j}^{i} r_{ij}^{-6} + \gamma_f^2 \sum_{f}^{*} r_{if}^{-6}\right] K_A^2\, \sigma_{AB}\, \eta_{AB}/kT \qquad \ldots\ldots\ 3.36$$

$$T^{-1}_{1\ inter} = \frac{\pi \hbar^2 \gamma_i^2 N}{kT} \left[3\ \gamma_i^2 \sum_{j}^{i} r_{ij}^{-1} + 2\ \gamma_f^2 \sum_{f}^{*} r_{if}^{-1}\right][\eta_{AB}\, \sigma_{AB}\, f_B + \eta_A\, \sigma_A\, f_A]$$

$\ldots\ldots\ 3.39$

In order to explain the results obtained for liquid mixtures in which shorter relaxation times are observed using low ultrasonic powers and longer relaxation times at higher powers it is necessary at low powers, for the molecular correlation times to be decreased. This could arise because of a net increase in microviscosity due to the Stokes force operative in the presence of ultrasound. The subsequent increase in T_1 could be due to either the dominating effect of temperature increasing with ultrasound power or due to a further increase in correlation times.

Experiments performed to observe the effects of temperature on spin-lattice relaxation have already been discussed in Section 8.1(a). The results revealed that as the

temperature is increased spin-lattice relaxation times become longer. The results of experiments performed to measure temperature effects due to increasing power supplied to a transducer immersed in cyclohexane, as discussed in Chapter Seven, Section 7.9, showed a gradual increase in temperature with increasing ultrasonic powers. Moreover, a new equilibrium temperature is obtained for a constant fixed amount of ultrasonic power supplied to a transducer. However, and more importantly, results of experiments performed to observe the effects of ultrasound in liquids showed that as the ultrasonic power is increased spin-lattice relaxation times initially become shorter and then start to get longer at higher ultrasonic powers. These results suggest that several ultrasonic relaxation mechanisms leading to absorption of sound in liquids compete with one another. At low powers, absorption of sound in liquids arising from vibrational, and structural relaxation and the addition of "impurities" are more dominant whilst at higher powers, thermal relaxation becomes the dominant mechanism. Furthermore, it can be concluded that shorter spin-lattice relaxation times for molecules can only be obtained by supplying low power to the transducer. This means that motional averaging is only achieved at lower powers which provide molecules with sufficient energies to have large Fourier components at the Larmor frequency, otherwise at higher ultrasonic powers, thermal relaxation mechanisms become dominant and lead to a situation where molecules have energies which have smaller Fourier components at the Larmor frequency. This in turn leads to longer spin-lattice relaxation times.

RESULTS OF MEASUREMENTS OF THE EFFECTS OF ULTRASOUND ON PROTON (^{1}H) SPIN-LATTICE RELAXATION TIMES USING A TRANSDUCER MOUNTED ON THE BOTTOM OF THE TUBE
(TABLES 8.6 - 8.9)

RELAXATION TIME MEASUREMENTS

NUCLEI UNDER INVESTIGATION: ^{1}H NMR.

NMR INSTRUMENT OBSERVATION FREQUENCY: 89.56 MHz.

SYSTEM UNDER INVESTIGATION: Cyclohexane + Benzene + chloroform(d).

MOLAR RATIO : 1:1:2.

90 DEGREE PULSE: 30 us. PULSE W1: 12 us. PULSE W2: 24 us.

PULSE REPETITION: 2.0 s. ACQUISITION TIME: 1.0 s. SCANS: 10.

TRANSDUCER FREQUENCY: 1.115 MHz.

METHOD OF ANALYSIS: 2pt curve fit.

	SPIN-SPIN RELAXATION TIME MEASUREMENT (T_2) LINE WIDTHS		SPIN-LATTICE RELAXATION TIME MEASUREMENTS (T_1) IN SECONDS	
	MOLECULAR GROUPS: aryl H		MOLECULAR GROUPS:	
	Hz	SECONDS	ipso H,	aryl CH
SAMPLE PROBE OUT	1.33	0.24	4.9	3.94
SAMPLE PROBE IN (ULT. OFF)	1.07	0.29	4.87 4.86	3.87 3.84
ULT. ON POWER (Watts)				
0.5			4.056	3.57
1.0			3.89	2.76
2.0			2.81 (42%)	2.15 (44%)
5.0			4.10	3.06
10	Resolution lost.			
15	resolution lost.			

Table 8.6 (a): The effect of ultrasound at a frequency of 1.115MHz on proton (^{1}H) spin-lattice relaxation times (T_1) for an equimolar mixture of cyclohexane and benzene.

RELAXATION TIME MEASUREMENTS

NUCLEI UNDER INVESTIGATION: ^1H NMR.

NMR INSTRUMENT OBSERVATION FREQUENCY: 89.56 MHz.

SYSTEM UNDER INVESTIGATION: Cyclohexane + Benzene + chloroform(d).

MOLAR RATIO : 1:1:2.

90 DEGREE PULSE: 30 us. PULSE W1: 12 us. PULSE W2: 24 us.

PULSE REPETITION: 2.5 s. ACQUISITION TIME: 1.0 s. SCANS: 10.

TRANSDUCER FREQUENCY: 6 MHz.

METHOD OF ANALYSIS: 2pt curve fit.

	SPIN-SPIN RELAXATION TIME MEASUREMENT (T_2) LINE WIDTHS		SPIN- LATTICE RELAXATION TIME MEASUREMENTS (T_1) IN SECONDS	
	MOLECULAR GROUPS: aryl H		MOLECULAR GROUPS:	
	Hz	SECONDS	ipso H,	aryl CH
SAMPLE PROBE OUT			4.9	3.76
SAMPLE PROBE IN (ULT. OFF)	0.79	0.4	4.50 4.86	3.62 3.84
ULT. ON POWER (Watts)				
0.5	0.53	0.60	4.11	3.13
1.0			3.89	2.76
2.0	0.53	0.60	2.69	2.38
5.0			2.56 (42%)	2.28 (37%)
10	0.53	0.60	3.88	2.61
15	Resolution lost.			

Table 8.6 (b): The effect of ultrasound at a frequency of 6MHz on proton (^1H) spin-lattice relaxation times (T_1) for an equimolar mixture of cyclohexane and benzene.

RELAXATION TIME MEASUREMENTS

NUCLEI UNDER INVESTIGATION: ^1H NMR.

NMR INSTRUMENT OBSERVATION FREQUENCY: 89.56 MHz.

SYSTEM UNDER INVESTIGATION: Cyclohexane + 1,3,5-trimethylbenzene + Chloroform(d).

MOLAR RATIO : 1:1:2.

90 DEGREE PULSE: 30 us. PULSE W1: 12 us. PULSE W2: 24 us.

PULSE REPETITION: 2.0 s. ACQUISITION TIME: 1.0 s. SCANS: 10.

TRANSDUCER FREQUENCY: 1.115 MHz.

METHOD OF ANALYSIS: 2pt curve fit.

	SPIN-SPIN RELAXATION TIME MEASUREMENT (T_2) LINE WIDTHS		SPIN-LATTICE RELAXATION TIME MEASUREMENTS (T_1) IN SECONDS		
	MOLECULAR GROUPS: aryl H		MOLECULAR GROUPS:		
	Hz	SECONDS	ipso H,	methyl,	methylene
SAMPLE PROBE OUT	2.66	0.12	4.17	3.76	4.4
SAMPLE PROBE IN (ULT. OFF)	3.19	0.10	3.60	2.70	3.37
ULT. ON POWER (Watts)					
0.5	3.19	0.10	3.55	2.61	3.32
1.0	3.19	0.10	3.16	2.18	2.66
2.0	3.19	0.10	2.79	1.66	2.02
5.0			2.56	2.28	2.53
10	3.19	0.10	3.48	2.42	2.69
15	No expt. done.				

Table 8.7 (a): The effect of ultrasound at a frequency of 1.115MHz on proton (^1H) spin-lattice relaxation times (T_1) for an equimolar mixture of cyclohexane and 1,3,5-trimethylbenzene (mesitylene).

RELAXATION TIME MEASUREMENTS

NUCLEI UNDER INVESTIGATION: ^1H NMR.

NMR INSTRUMENT OBSERVATION FREQUENCY: 89.56 MHz.

SYSTEM UNDER INVESTIGATION: Cyclohexane + 1,3,5-Trimethylbenzene + Chloroform(d).

MOLAR RATIO : 1:1:2.

90 DEGREE PULSE: 30 us. PULSE W1: 12 us. PULSE W2: 24 us.

PULSE REPETITION: 2.0 s. ACQUISITION TIME: 1.0 s. SCANS: 10.

TRANSDUCER FREQUENCY: 1.115 MHz.

METHOD OF ANALYSIS: 2pt curve fit.

	SPIN-SPIN RELAXATION TIME MEASUREMENT (T_2) LINE WIDTHS		SPIN-LATTICE RELAXATION TIME MEASUREMENTS (T_1) IN SECONDS		
	MOLECULAR GROUPS: aryl H		MOLECULAR GROUPS:		
	Hz	SECONDS	aryl H,	methyl,	methylene.
SAMPLE PROBE OUT	2.57	0.12	3.96	3.23	3.84
SAMPLE PROBE IN (ULT. OFF)	2.98	0.11	3.53	2.80	3.52
ULT. ON POWER (Watts)					
0.5	2.98	0.11	3.48	2.69	3.47
1.0	2.98	0.11	3.05	2.21	2.71
2.0	2.98	0.11	2.64	1.68	2.04
5.0	2.98	0.11	2.85	1.82	2.56
10	2.98	0.11	3.35	2.54	2.92
15	No expt. done.				

Table 8.7 (b): Repeated experiment on the effect of ultrasound at a frequency of 1.115MHz on proton (^1H) spin-lattice relaxation times (T_1) for an equimolar mixture of cyclohexane and 1,3,5-trimethylbenzene. (mesitylene).

RELAXATION TIME MEASUREMENTS

NUCLEI UNDER INVESTIGATION: ^1H NMR.

NMR INSTRUMENT OBSERVATION FREQUENCY: 89.56 MHz.

SYSTEM UNDER INVESTIGATION: Cyclohexane + 1,3,5-trimethylbenzene + Chloroform(d).

MOLAR RATIO : 1:1:2.

90 DEGREE PULSE: 30 us. PULSE W1: 12 us. PULSE W2: 24 us.

PULSE REPETITION: 2.0 s. ACQUISITION TIME: 1.0 s. SCANS: 10.

TRANSDUCER FREQUENCY: 6 MHz.

METHOD OF ANALYSIS: 2pt curve fit.

	SPIN-SPIN RELAXATION TIME MEASUREMENT (T_2) LINE WIDTHS		SPIN-LATTICE RELAXATION TIME MEASUREMENTS (T_1) IN SECONDS		
	MOLECULAR GROUPS: aryl H		MOLECULAR GROUPS:		
	Hz	SECONDS	ipso H,	methyl,	methylene
SAMPLE PROBE OUT	2.66	0.12	4.17	3.68	3.79
SAMPLE PROBE IN (ULT. OFF)	2.92	0.11	3.8	3.02	3.67
ULT. ON POWER (Watts)					
0.5			3.6	3.03	3.39
1.0			3.3 (13%)	2.64 (12%)	2.59 (30%)
2.0			3.54	2.42	2.65
5.0	Resolution lost.				
10	No expt. done				
15	No expt. done.				

Table 8.7 (c): The effect of ultrasound at a frequency of 6MHz on proton (^1H) spin-lattice relaxation times (T_1) for an equimolar mixture of cyclohexane and 1,3,5-trimethylbenzene (mesitylene).

RELAXATION TIME MEASUREMENTS

NUCLEI UNDER INVESTIGATION: ^1H NMR.

NMR INSTRUMENT OBSERVATION FREQUENCY: 89.56 MHz.

SYSTEM UNDER INVESTIGATION: Cyclohexane + 1,4-di-tertbutylbenzene + Chloroform(d).

MOLAR RATIO : 1:1:2.

90 DEGREE PULSE: 30 us. PULSE W1: 12 us. PULSE W2: 24 us.

PULSE REPETITION: 2.0 s. ACQUISITION TIME: 1.0 s. SCANS: 10.

TRANSDUCER FREQUENCY: 1.115 MHz.

METHOD OF ANALYSIS: 2pt curve fit.

	SPIN-SPIN RELAXATION TIME MEASUREMENT (T_2) LINE WIDTHS		SPIN- LATTICE RELAXATION TIME MEASUREMENTS (T_1) IN SECONDS		
	MOLECULAR GROUPS: aryl H		MOLECULAR GROUPS:		
	Hz	SECONDS	aryl H,	methyl,	methylene.
SAMPLE PROBE OUT	1.33	0.24	2.98	1.77	3.71
SAMPLE PROBE IN (ULT. OFF)	1.66	0.20	2.96	1.75	3.64
ULT. ON POWER (Watts)					
0.5	1.60	0.20	2.41	1.41	3.4
1.0			1.99	0.83	2.76
2.0	1.60	0.20	1.52	0.99	2.43
5.0			1.44	0.86	1.85
10	1.60	0.20	1.35 (54%)	0.77 (55.8%)	1.43 (60%)
15	No expt. done.				

Table 8.8 (a): The effect of ultrasound at a frequency of 1.115MHz on proton (^1H) spin-lattice relaxation times (T_1) for an equimolar mixture of cyclohexane and 1,4-para-di-tertbutylbenzene.

RELAXATION TIME MEASUREMENTS

NUCLEI UNDER INVESTIGATION: ^1H NMR.

NMR INSTRUMENT OBSERVATION FREQUENCY: 89.56 MHz.

SYSTEM UNDER INVESTIGATION: Cyclohexane + 1,4-di-tertbutylbenzene + Chloroform(d).

MOLAR RATIO : 1:1:2.

90 DEGREE PULSE: 30 us. PULSE W1: 12 us. PULSE W2: 24 us.

PULSE REPETITION: 2.0 s. ACQUISITION TIME: 1.0 s. SCANS: 10.

TRANSDUCER FREQUENCY: 6 MHz.

METHOD OF ANALYSIS: 2pt curve fit.

	SPIN-SPIN RELAXATION TIME MEASUREMENT (T_2) LINE WIDTHS		SPIN- LATTICE RELAXATION TIME MEASUREMENTS (T_1) IN SECONDS		
	MOLECULAR GROUPS: aryl H		MOLECULAR GROUPS:		
	Hz	SECONDS	aryl H,	methyl,	methylene.
SAMPLE PROBE OUT	1.06	0.30	2.41	1.41	3.21
SAMPLE PROBE IN (ULT. OFF)	1.06	0.30	2.49	1.48	3.21
ULT. ON POWER (Watts)					
0.5	1.06	0.30	2.15	0.98	3.04
1.0	1.06	0.30	2.13	0.87	3.02
2.0	1.06	0.30	1.20 (19%)	0.63 (57%)	2.24 (30%)
5.0	Resolution lost.				
10	Resolution lost.				
15	Resolution lost.				

Table 8.8 (b): The effect of ultrasound at a frequency of 6MHz on proton (^1H) spin-lattice relaxation times (T_1) for an equimolar mixture of cyclohexane and 1,4-para-di-tertbutylbenzene.

RELAXATION TIME MEASUREMENTS

NUCLEI UNDER INVESTIGATION: ^1H NMR.

NMR INSTRUMENT OBSERVATION FREQUENCY: 89.56 MHz.

SYSTEM UNDER INVESTIGATION: Cyclohexane + 1,3,5-tri-tertbutylbenzene + Chloroform(d).

MOLAR RATIO : 1:1:3.

90 DEGREE PULSE: 30 us. PULSE W1: 12 us. PULSE W2: 24 us.

PULSE REPETITION: 2.0 s. ACQUISITION TIME: 1.0 s. SCANS: 10.

TRANSDUCER FREQUENCY: 1.115 MHz.

METHOD OF ANALYSIS: 2pt curve fit.

	SPIN-SPIN RELAXATION TIME MEASUREMENT (T_2) LINE WIDTHS		SPIN- LATTICE RELAXATION TIME MEASUREMENTS (T_1) IN SECONDS		
	MOLECULAR GROUPS: aryl H		MOLECULAR GROUPS:		
	Hz	SECONDS	aryl H,	methyl,	methylene.
SAMPLE PROBE OUT	1.60	0.20	1.55	1.61	2.27
SAMPLE PROBE IN (ULT. OFF)	1.86	0.17	1.54	1.43	2.23
ULT. ON POWER (Watts)					
0.5	1.86	0.17	1.48	1.27	2.18
1.0	2.13	0.15	1.30	1.22	1.99
2.0	2.66	0.12	1.29 (15%)	0.93 (38%)	1.60 (28%)
5.0	2.66	0.12	1.52	0.87	1.90
10	2.66	0.12	1.37	0.76	1.90
15	3.19	0.09	1.38	0.75	1.94

Table 8.9 (a): The effect of ultrasound at a frequency of 1.115MHz on proton (^1H) spin-lattice relaxation times (T_1) for an equimolar mixture of cyclohexane and 1,3,5-tri-tertbutylbenz e.

RELAXATION TIME MEASUREMENTS

NUCLEI UNDER INVESTIGATION: ^1H NMR.

NMR INSTRUMENT OBSERVATION FREQUENCY: 89.56 MHz.

SYSTEM UNDER INVESTIGATION: Cyclohexane + 1,3,5-tri-tertbutylbenzene + Chloroform(d).

MOLAR RATIO : 1:1:3.

90 DEGREE PULSE: 30 us. PULSE W1: 12 us. PULSE W2: 24 us.

PULSE REPETITION: 2.0 s. ACQUISITION TIME: 1.0 s. SCANS: 10.

TRANSDUCER FREQUENCY: 6 MHz.

METHOD OF ANALYSIS: 2pt curve fit.

	SPIN-SPIN RELAXATION TIME MEASUREMENT (T_2) LINE WIDTHS		SPIN- LATTICE RELAXATION TIME MEASUREMENTS (T_1) IN SECONDS		
	MOLECULAR GROUPS: aryl H		MOLECULAR GROUPS:		
	Hz	SECONDS	aryl H,	methyl,	methylene.
SAMPLE PROBE OUT	1.07	0.03	1.94	1.19	2.16
SAMPLE PROBE IN (ULT. OFF)	1.33	0.24	1.93	1.20	2.06
ULT. ON POWER (Watts)					
0.5	1.33	0.24	1.89	1.07	2.06
1.0	1.33	0.24	1.20	0.93	1.65
2.0	1.33	0.24	1.23	0.98	1.00
5.0	1.86	0.17	1.09	Data unrel.	1.22
10	1.86	0.17	1.37	Data unrel.	1.21
15	No expts. done				

Table 8.9 (b): The effect of ultrasound at a frequency of 6MHz on proton (^1H) spin-lattice relaxation times (T_1) for an equimolar mixture of cyclohexane and 1,3,5-tri-tertbutylbenzene.

RESULTS OF MEASUREMENTS OF THE EFFECTS OF ULTRASOUND ON CARBON-13 NUCLEI (^{13}C) SPIN-LATTICE RELAXATION TIMES USING A TRANSDUCER MOUNTED ON THE BOTTOM OF THE TUBE (TABLES 8.10-8.13)

RELAXATION TIME MEASUREMENTS

NUCLEI UNDER INVESTIGATION: ^{13}C NMR.

NMR INSTRUMENT OBSERVATION FREQUENCY: 22.5 MHz.

SYSTEM UNDER INVESTIGATION: Cyclohexane + Benzene + Chloroform(d).

MOLAR RATIO : 1:1:2.

90 DEGREE PULSE: 22.5 us. PULSE W1: 12 us. PULSE W2: 18 us.

PULSE REPETITION: 1.0 s. ACQUISITION TIME: 0.5 s. SCANS: 50.

TRANSDUCER FREQUENCY: 1.115 MHz.

METHOD OF ANALYSIS: 2pt curve fit.

	SPIN-SPIN RELAXATION TIME MEASUREMENT (T_2) LINE WIDTHS		SPIN-LATTICE RELAXATION TIME MEASUREMENTS (T_1) IN SECONDS	
	MOLECULAR GROUPS: aryl H		MOLECULAR GROUPS:	
	Hz	SECONDS	aryl H,	methylene.
SAMPLE PROBE OUT	No measurements		12.88	10.96
SAMPLE PROBE IN (ULT. OFF)	1.33	0.24	11.99	10.11
ULT. ON POWER (Watts)				
0.5	1.33	0.24	10.62	9.86
1.0	1.33	0.24	10.79	9.80
2.0	1.33	0.24	9.80 (24%)	9.61 (12%)
5.0	1.33	0.24	10.89	9.34
10	1.33	0.24	11.64	11.17
15	No expt. done.			

Table 8.10 (a): The effect of ultrasound at a frequency of 1.115MHz on carbon-13 nuclei (^{13}C) spin-lattice relaxation times (T_1) for an equimolar mixture of cyclohexane and benzene.

RELAXATION TIME MEASUREMENTS

NUCLEI UNDER INVESTIGATION: ^{13}C NMR.

NMR INSTRUMENT OBSERVATION FREQUENCY: 22.5 MHz.

SYSTEM UNDER INVESTIGATION: Cyclohexane + Benzene + Chloroform(d).

MOLAR RATIO : 1:1:2.

90 DEGREE PULSE: 22.5 us. PULSE W1: 12 us. PULSE W2: 18 us.

PULSE REPETITION: 2.5 s. ACQUISITION TIME: 2.0 s. SCANS: 50.

TRANSDUCER FREQUENCY: 6 MHz.

METHOD OF ANALYSIS: 2pt curve fit.

	SPIN-SPIN RELAXATION TIME MEASUREMENT (T_2) LINE WIDTHS	SPIN-LATTICE RELAXATION TIME MEASUREMENTS (T_1) IN SECONDS	
	MOLECULAR GROUPS: aryl H	MOLECULAR GROUPS:	
	Hz SECONDS	aryl H,	methylene.
SAMPLE PROBE OUT	No measurements.	12.83	10.97
SAMPLE PROBE IN (ULT. OFF)	Sharp linewidths.	12.94	10.18
ULT. ON POWER (Watts)			
0.5	No measurements.	11.20	11.18
1.0		10.92	9.32
2.0		10.37 (19%)	9.32 (13%)
5.0		11.46	10.73
10		10.99	7.04
15	No expt. done.		

Table 8.10 (b): The effect of ultrasound at a frequency of 6MHz on carbon-13 nuclei (^{13}C) spin-lattice relaxation times (T_1) for an equimolar mixture of cyclohexane and benzene.

RELAXATION TIME MEASUREMENTS

NUCLEI UNDER INVESTIGATION: ^{13}C NMR.

NMR INSTRUMENT OBSERVATION FREQUENCY: 22.5 MHz.

SYSTEM UNDER INVESTIGATION: Cyclohexane + 1,3,5-Trimethylbenzene + Chloroform(d).

MOLAR RATIO : 1:1:2.

90 DEGREE PULSE: 22.5 us. PULSE W1: 9 us. PULSE W2: 18 us.

PULSE REPETITION: 1.0 s. ACQUISITION TIME: 0.6 s. SCANS: 50.

TRANSDUCER FREQUENCY: 1.115 MHz.

METHOD OF ANALYSIS: 2pt curve fit.

	SPIN-SPIN RELAXATION TIME MEASUREMENT (T_2) LINE WIDTHS		SPIN-LATTICE RELAXATION TIME MEASUREMENTS (T_1) IN SECONDS			
	MOLECULAR GROUPS: ipso C		MOLECULAR GROUPS:			
	Hz	SECONDS	ipso, -C	aryl, -CH	methyl, $-CH_3$	methylene. $-CH_2-$
SAMPLE PROBE OUT	Probe already in.					
SAMPLE PROBE IN (ULT. OFF)			7.52	4.03	4.40	8.47
ULT. ON POWER (Watts)						
0.5	1.33	0.24	7.15	3.70	4.68	7.58
1.0	1.33	0.24	6.60	3.50	4.68	6.40
2.0	1.33	0.24	6.17 (18%)	3.25 (19%)	3.90 (11%)	5.90 (30%)
5.0	1.33	0.24	7.76	3.47	3.96	6.32
10	1.33	0.24	7.52	3.10	3.84	6.33
15	No expt. done					

Table 8.11 (a):The effect of ultrasound at a frequency of 1.115MHz on the carbon-13 nuclei (^{13}C) spin-lattice relaxation times (T_1) for an equimolar mixture of cyclohexane and 1,3,5-trimethylbenzene.

RELAXATION TIME MEASUREMENTS

NUCLEI UNDER INVESTIGATION: ^{13}C NMR.

NMR INSTRUMENT OBSERVATION FREQUENCY: 22.5 MHz.

SYSTEM UNDER INVESTIGATION: Cyclohexane + 1,3,5-Trimethylbenzene + Chloroform(d).

MOLAR RATIO : 1:1:2.

90 DEGREE PULSE: 22.5 us. PULSE W1: 9 us. PULSE W2: 18 us.

PULSE REPETITION: 1.0 s. ACQUISITION TIME: 0.6 s. SCANS: 50.

TRANSDUCER FREQUENCY: 1.115 MHz.

METHOD OF ANALYSIS: 2pt curve fit.

	SPIN-SPIN RELAXATION TIME MEASUREMENT (T_2) LINE WIDTHS		SPIN-LATTICE RELAXATION TIME MEASUREMENTS (T_1) IN SECONDS			
	MOLECULAR GROUPS: ipso C		MOLECULAR GROUPS:			
	Hz	SECONDS	ipso, -C	aryl, -CH	methyl, $-CH_3$	methylene. $-CH_2-$
SAMPLE PROBE OUT	Probe already in.					
SAMPLE PROBE IN (ULT. OFF)			8.18	4.37	4.85	9.11
ULT. ON POWER (Watts)						
0.5	1.31	0.24	7.79	4.11	4.21	8.09
1.0	1.31	0.24	7.19	3.69	3.75	6.68
2.0	1.31	0.24	6.70 (18%)	3.58 (18%)	3.11 (35%)	6.22 (32%)
5.0	1.31	0.24	7.53	3.76	3.61	6.76
10	1.31	0.24	8.03	4.10	3.97	7.21
15	No expt. done					

Table 8.11 (b):Repeated experiment on the effect of ultrasound at a frequency of 1.115MHz on carbon-13 nuclei (^{13}C) spin-lattice relaxation times (T_1) for an equimolar mixture of cyclohexane and 1,3,5-trimethylbenzene.

RELAXATION TIME MEASUREMENTS

NUCLEI UNDER INVESTIGATION: ^{13}C NMR.

NMR INSTRUMENT OBSERVATION FREQUENCY: 22.5 MHz.

SYSTEM UNDER INVESTIGATION: Cyclohexane + 1,3,5-Trimethylbenzene + Chloroform(d).

MOLAR RATIO : 1:1:2.

90 DEGREE PULSE: 22.5 us. PULSE W1: 9 us. PULSE W2: 18 us.

PULSE REPETITION: 1.0 s. ACQUISITION TIME: 0.6 s. SCANS: 50.

TRANSDUCER FREQUENCY: 6 MHz.

METHOD OF ANALYSIS: 2pt curve fit.

	SPIN-SPIN RELAXATION TIME MEASUREMENT (T_2) LINE WIDTHS		SPIN-LATTICE RELAXATION TIME MEASUREMENTS (T_1) IN SECONDS			
	MOLECULAR GROUPS: ipso C		MOLECULAR GROUPS:			
	Hz	SECONDS	ipso, -C	aryl, -CH	methyl, $-CH_3$	methylene. $-CH_2-$
SAMPLE PROBE OUT	3.32	0.09	11.54	3.62	8.78	7.90
SAMPLE PROBE IN (ULT. OFF)	3.32	0.09	11.44	3.40	8.98	7.80
ULT. ON POWER (Watts)						
0.5	3.32	0.09	8.99	3.51	5.12	7.76
1.0	3.32	0.09	8.58	3.49	4.34	7.04
2.0	3.32	0.09	7.94 (31%)	3.33 (3%)	5.09 (43%)	6.99 (10%)
5.0	No expt. done					
10	3.32	0.09	12.37	4.89	5.71	8.77
15	No expt. done					

Table 8.11 (c): The effect of ultrasound at a frequency of 6MHz on carbon-13 nuclei (^{13}C) spin-lattice relaxation times (T_1) for an equimolar mixture of cyclohexane and 1,3,5-trimethylbenzene.

RELAXATION TIME MEASUREMENTS

NUCLEI UNDER INVESTIGATION: ^{13}C NMR.

NMR INSTRUMENT OBSERVATION FREQUENCY: 22.5 MHz.

SYSTEM UNDER INVESTIGATION: Cyclohexane + 1,4-di-tertbutylbenzene + Chloroform(d).

MOLAR RATIO : 1:1:2.

90 DEGREE PULSE: 22.5 us. PULSE W1: 12 us. PULSE W2: 18 us.

PULSE REPETITION: 1.0 s. ACQUISITION TIME: 0.6 s. SCANS: 50.

TRANSDUCER FREQUENCY: 1.115 MHz.

METHOD OF ANALYSIS: 2pt curve fit.

	SPIN-SPIN RELAXATION TIME MEASUREMENT (T_2) LINE WIDTHS		SPIN-LATTICE RELAXATION TIME MEASUREMENTS (T_1) IN SECONDS				
	MOLECULAR GROUPS: ipso C		MOLECULAR GROUPS:				
	Hz	SECONDS	ipso, -C	aryl, -CH	quart, -C	methyl, $-CH_3$	methylene. $-CH_2-$
SAMPLE PROBE OUT	1.33	0.24	11.15	4.32	7.03	1.98	7.77
SAMPLE PROBE IN (ULT. OFF)	1.33	0.24	10.61	4.08	6.44	1.66	7.10
ULT. ON POWER (Watts)							
0.5	1.33	0.24	9.79	3.92	5.87	1.44	6.89
1.0	1.33	0.24	8.83	3.42	5.17	1.02	6.16
2.0	1.33	0.24	8.47	2.15	4.14	0.86	5.20
5.0	1.33	0.24	7.41 (30%)	1.89 (53%)	8.64 (45%)	0.84 (49%)	4.78 (32.7%)
10	1.33	0.24	7.71	1.89	4.93	1.49	7.12
15	No expt. done.						

Table 8.12 (a): The effect of ultrasound at a frequency of 1.115MHz on carbon-13 nuclei (^{13}C) spin-lattice relaxation times (T_1) for an equimolar mixture of cyclohexane and 1,4-para-di- tertbutylbenzene.

RELAXATION TIME MEASUREMENTS

NUCLEI UNDER INVESTIGATION: ^{13}C NMR.

NMR INSTRUMENT OBSERVATION FREQUENCY: 22.5 MHz.

SYSTEM UNDER INVESTIGATION: Cyclohexane + 1,4-di-tertbutylbenzene
Chloroform(d).

MOLAR RATIO : 1:1:2.

90 DEGREE PULSE: 22.5 us. PULSE W1: 12 us. PULSE W2: 18 us.

PULSE REPETITION: 1.0 s. ACQUISITION TIME: 0.6 s. SCANS: 50.

TRANSDUCER FREQUENCY: 6 MHz.

METHOD OF ANALYSIS: 2pt curve fit.

	SPIN-SPIN RELAXATION TIME MEASUREMENT (T_2) LINE WIDTHS		SPIN-LATTICE RELAXATION TIME MEASUREMENTS (T_1) IN SECONDS				
	MOLECULAR GROUPS: ipso C		MOLECULAR GROUPS:				
	Hz	SECONDS	ipso, -C	aryl, -CH	quart, -C	methyl, $-CH_3$	methylene. $-CH_2-$
SAMPLE PROBE OUT	No	measurements.	9.41	3.38	7.13	1.43	10.32
SAMPLE PROBE IN (ULT. OFF)	No	measurements.	9.23	3.05	7.29	1.41	10.08
ULT. ON POWER (Watts)							
0.5	No	measurements.	8.42	3.37	6.72	1.41	8.46
1.0	No	measurements.	7.32 (20%)	3.15 (43%)	5.87 (18%)	1.58 (11%)	6.92 (31%)
2.0	No	measurements.	7.65	1.53	8.14	1.44	10.04
5.0	Expt. error.						
10	No	expt. done.					
15	No	expt. done.					

Table 8.12 (b): The effect of ultrasound at a frequency of 6MHz on carbon-13 nuclei (^{13}C) spin-lattice relaxation times (T_1) for an equimolar mixture of cyclohexane and 1,4-para-di- tertbutylbenzene.

RELAXATION TIME MEASUREMENTS

NUCLEI UNDER INVESTIGATION: ^{13}C NMR.

NMR INSTRUMENT OBSERVATION FREQUENCY: 22.5 MHz.

SYSTEM UNDER INVESTIGATION: Cyclohexane + 1,3,5-tri-tertbutylbenzene + Chloroform(d).

MOLAR RATIO : 1:1:2.

90 DEGREE PULSE: 22.5 us. PULSE W1: 12 us. PULSE W2: 18 us.

PULSE REPETITION: 1.0 s. ACQUISITION TIME: 0.5 s. SCANS: 50.

TRANSDUCER FREQUENCY: 1.115 MHz.

METHOD OF ANALYSIS: 2pt curve fit.

	SPIN-SPIN RELAXATION TIME MEASUREMENT (T_2) LINE WIDTHS		SPIN-LATTICE RELAXATION TIME MEASUREMENTS (T_1) IN SECONDS				
	MOLECULAR GROUPS: ipso C		MOLECULAR GROUPS:				
	Hz	SECONDS	ipso, -C	aryl, -CH	quart, -C	methyl, $-CH_3$	methylene. $-CH_2-$
SAMPLE PROBE OUT	1.33	0.24.	10.59	1.67	10.78	1.42	8.16
SAMPLE PROBE IN (ULT. OFF)	2.66	0.12	10.41	1.53	10.54	1.39	7.82
ULT. ON POWER (Watts)							
0.5	2.66	0.12	9.74	1.24	8.89	1.37	6.98
1.0	2.66	0.12	9.24	1.07	8.54	1.21	5.36
2.0	2.66	0.12	8.96	0.95	8.36	0.94	4.97
5.0	2.66	0.12	8.31 (20%)	0.89 (41%)	8.06 (23%)	0.87 (37%)	4.53 (42%)
10	2.66	0.12	9.83	1.43	9.53	1.19	5.93
15	2.66	0.12	9.69	1.35	9.90	1.25	8.16

Table 8.13 (a): The effect of ultrasound at a frequency of 1.115MHz on carbon-13 nuclei (^{13}C) spin-lattice relaxation times (T_1) for an equimolar mixture of cyclohexane and 1,3,5-tri-tertbutylbenzene.

RELAXATION TIME MEASUREMENTS

NUCLEI UNDER INVESTIGATION: ^{13}C NMR.

NMR INSTRUMENT OBSERVATION FREQUENCY: 22.5 MHz.

SYSTEM UNDER INVESTIGATION: Cyclohexane + 1,3,5-tri-tertbutylbenzene + Chloroform(d).

MOLAR RATIO : 1:1:2.

90 DEGREE PULSE: 22.5 us. PULSE W1: 12 us. PULSE W2: 18 us.

PULSE REPETITION: 1.0 s. ACQUISITION TIME: 0.5 s. SCANS: 50.

TRANSDUCER FREQUENCY: 6 MHz.

METHOD OF ANALYSIS: 2pt curve fit.

	SPIN-SPIN RELAXATION TIME MEASUREMENT (T_2) LINE WIDTHS		SPIN-LATTICE RELAXATION TIME MEASUREMENTS (T_1) IN SECONDS				
	MOLECULAR GROUPS: ipso C		MOLECULAR GROUPS:				
	Hz	SECONDS	ipso, -C	aryl, -CH	quart, -C	methyl, $-CH_3$	methylene. $-CH_2-$
SAMPLE PROBE OUT	2.0	0.16	15.02	1.21	15.23	1.02	9.65
SAMPLE PROBE IN (ULT. OFF)	2.66	0.12	14.63	1.01	15.23	0.96	9.28
ULT. ON POWER (Watts)							
0.5	2.66	0.12	14.77	0.92	14.39	0.92	8.58
1.0	2.66	0.12	14.58	0.99	14.50	0.88	8.56
2.0	2.66	0.12	13.15	1.01	11.64	0.86	7.74
5.0	2.66	0.12	13.14 (10%)	0.91 (11%)	10.67 (30%)	0.93 (3%)	7.13 (21%)
10	2.66	0.12	14.70	0.94	14.7	0.84	9.76
15	No expts. done.						

Table 8.13 (b): The effect of ultrasound at a frequency of 6MHz on carbon-13 nuclei (^{13}C) spin-lattice relaxation times (T_1) for an equimolar mixture of cyclohexane and 1,3,5-tri-tertbutylbenzene.

8.1(c) Observation of the effects of ultrasound on protons (^{1}H) carbon-13 (^{13}C) and nitrogen-14 (^{14}N) spin-lattice and spin-spin relaxation times, and on the fine structure, for nitrogen containing compounds

The experiments were performed using a glass tube with the transducer mounted at the bottom end of the tube. The following samples were used to perform the investigation:

(1) acetonitrile

(2) N-methylformamide

(3) N,N-dimethylformamide

(4) N,N-dimethylacetamide

(5) A saturated solution of ammonium chloride in a deuterated dimethyl sulfoxide containing a trace of concentrated hydrochloric acid.

Results of the effects of ultrasound on the first four samples will be discussed collectively under each of the three different nuclei investigated by NMR. Results of the effects of ultrasound on ammonium chloride will be discussed separately at the end of this section.

(A) PROTON (^{1}H) NMR RESULTS

(1) For an equimolar mixture of acetonitrile and deuterated chloroform:

Measurement of the effects of ultrasound on proton NMR spin-lattice and spin-spin relaxation times using ultrasonic frequencies of 1.115, 6, 6.42 and 10 MHz.

(i) At 1.115 MHz: The results show that increasing ultrasonic power causes spin-lattice relaxation times to initially start to decrease and then increase at higher ultrasonic powers (Table 8.14). The explanation put forward for similar observations for mixtures containing cyclohexane and substituted benzene systems in Section 8.1(a) and (b), can be used to describe such behaviour. Figure 8.1(a) shows the effects of ultrasound at 1.115 MHz on proton (^{1}H) NMR signal of acetonitrile containing deuterated chloroform.

No changes were observed to the spin-spin relaxation times.

(ii) At 6 MHz: The results again show a decrease in spin-lattice relaxation times at low powers (Table 8.14b). However at higher ultrasonic powers it leads to a loss of

instrument resolution. Furthermore, using an ultrasonic power of 2W, the NMR lineshape changes from a single line to one of triplets and a doublet (Figure 8.1(b)). The observation of this fine structure is not understood and remains to be explained. Thus, measurement of spin-spin relaxation times from the lineshape was not possible.

(iii) At 6.42: The results obtained show that the numerical data leading to the measurement of spin-lattice relaxation times is unreliable. Table 8.14(c) shows the unreliability of the results. The NMR lineshape is again no longer a single line but has fine structure (Figure 8.1(c)).

(iv) At 10 MHz: Experiments performed at 10 MHz, reveal that at very low ultrasonic powers the NMR lineshape deteriorates (Figure 8.1(c)).

(2) For Pure N-methylformamide

Measurement of the effects of ultrasound on proton spin-lattice relaxation times were not performed as the NMR signals arising from the various protons in the N-methyl formamide overlapped.

(3) For an equimolar mixture of N,N-dimethylformamide and deuterated chloroform

(i) At 1.115 MHz: The results reveal that changes in the proton spin-lattice relaxation times are very small. Furthermore, the results reveal a gradual decrease in the relaxation times at low powers followed by an increase at higher powers (Table 8.15(a)). The explanation presented for similar observations for mixtures containing cyclohexane and substituted benzene systems in Section 8.1(a) and (b) can be used to describe such behaviour.

Measurement of the linewidth for the proton attached to the carbonyl group showed there were no effects on the spin-spin relaxation times.

Figure 8.2(a) shows the effects of an ultrasonic fequency of 1.115 MHz on the NMR spectra. The spectra shows that at even as high as 10 Watts the effects on the signal is neglible.

(ii) At 6 MHz: The experiments reveal no significant changes to the lineshapes or to the signal and noise levels (Table 8.15(b)). However, performing a similar experiment at 20W, shows an improvement in the signal to noise levels as well as the lineshape of the proton NMR signal. Thus, it appears that at such high powers the NMR spectrometer resolution seems to have improved (Figure 8.2(b)).

Measurement of the lineshape for the protons attached to the carbonyl groups reveal no effects of ultrasound on the spin-spin relaxation times (Table 8.15(b)).

(iii) At 6.42 MHz: Experiments performed for the measurement of the effects of ultrasound on the spin-lattice relaxation times revealed that by using lower NMR nutation angle (at approximately 12 μs) and using an ultrasonic power of 0.5W the signal to noise levels increases by approximately by one and a half times. Performing a similar experiment at a higher nutation angle (at approximately 24 μs) reveals very little change in the signal to noise ratio and to the NMR lineshapes (Figure 8.2(c)).

Repetition of similar experiments at 1, 2 and 5W at the higher pulse angles showed the following effects:

(i) No effects or changes to the signal intensities and the NMR linewidths are observed at 1W.

(ii) A decrease in the signal intensities and no changes in the linewidths at 2W.

(iii) The instruments resolution appears to have deteriorated at 5W.

Observation of the signals intensities arising from the two methyl groups shows them to be further split into doublets.

The results of such observations are also presented in Figure 8.2(c).

Owing to such inconsistencies in the results no further measurements of spin-lattice relaxation times were performed.

(iv) At 10 MHz: The results reveal that using ultrasonic powers of 0.5W causes the NMR lineshape starts to broaden (Figure 8.2(d)). Thus, no further experiments were performed for the measurements of spin-lattice relaxation times.

(4) For an equimolar mixture of N,N-dimethylacetamide and deuterated chloroform

(i) At 1.115 MHz: The results of the experiments performed are presented in Table 8.16(a). The results reveal a similar pattern of behaviour to that encountered for the N,N-dimethylformamide. This is, an initial decrease in spin-lattice relaxation times at low powers followed by an increase at higher powers. Explanations presented for similar observations for mixtures containing cyclohexane and substituted benzene systems in Section 8.1(a) and (b) can be used to describe such behaviour.

Observation of the NMR spectra reveals no changes in the NMR lineshapes from signals arising from various groups.

(ii) At 6 MHz: The results of the experiments reveal small changes in the spin-lattice relaxation times (Table 8.16(b)). The very small changes in the relaxation times was found to be due to the performance of the PZT transducer. This revealed that the transducer was no longer performing consistently due to the heat generated and had started to burn out. Thus, it can be concluded that the results obtained at this frequency are subject to large experimental errors.

(iii) At 6.42 MHz: These results are for experiment performed using a new PZT transducer. The results now shows significant changes in the relaxation times with a similar behaviour to that observed in (i) (Table 8.16c). This is an initial decrease in the spin-lattice relaxation times at low powers followed by an increase in the relaxation times.

RESULTS OF THE EFFECTS OF ULTRASOUND ON PROTONS (^{1}H) IN NITROGEN CONTAINING COMPOUNDS (FIGURES 8.1 - 8.2)

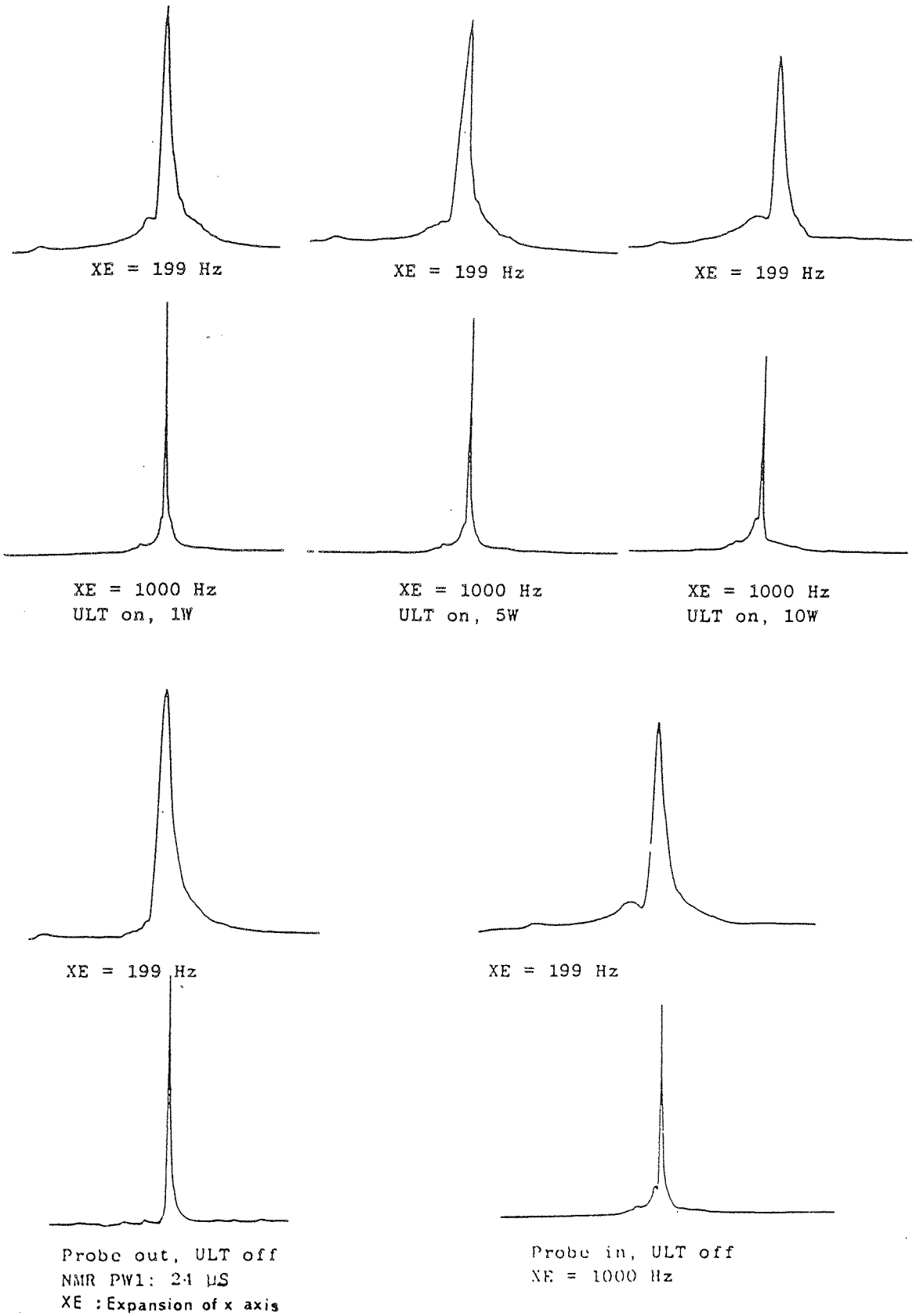

Figure 8.1 (a): The effects of ultrasound at a frequency of 1.115MHz on proton (^{1}H) NMR signal observed for an equimolar mixture of acetonitrile and deuterated chloroform. The effects shown are for applying increasing ultrasonic power from 1W to 10W across the transducer.

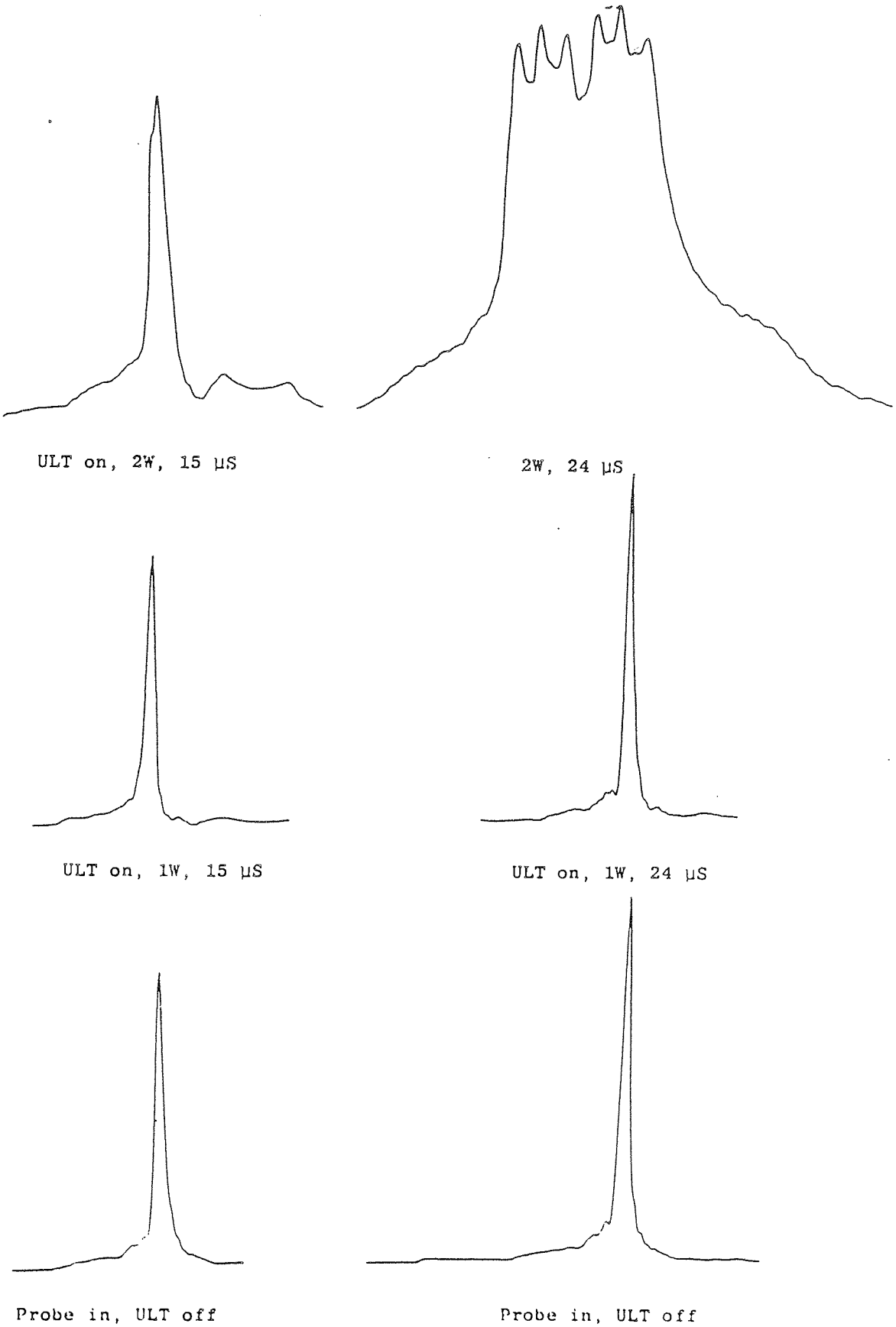

Figure 8.1 (b): The effects of ultrasound at a frequency of 6MHz on proton (^{1}H) NMR signal observed for an equimolar mixture of acetonitrile and deuterated chloroform. The effects shown are for applying ultrasonic powers of 1W and 2W across the transducer and at two different NMR pulse widths.

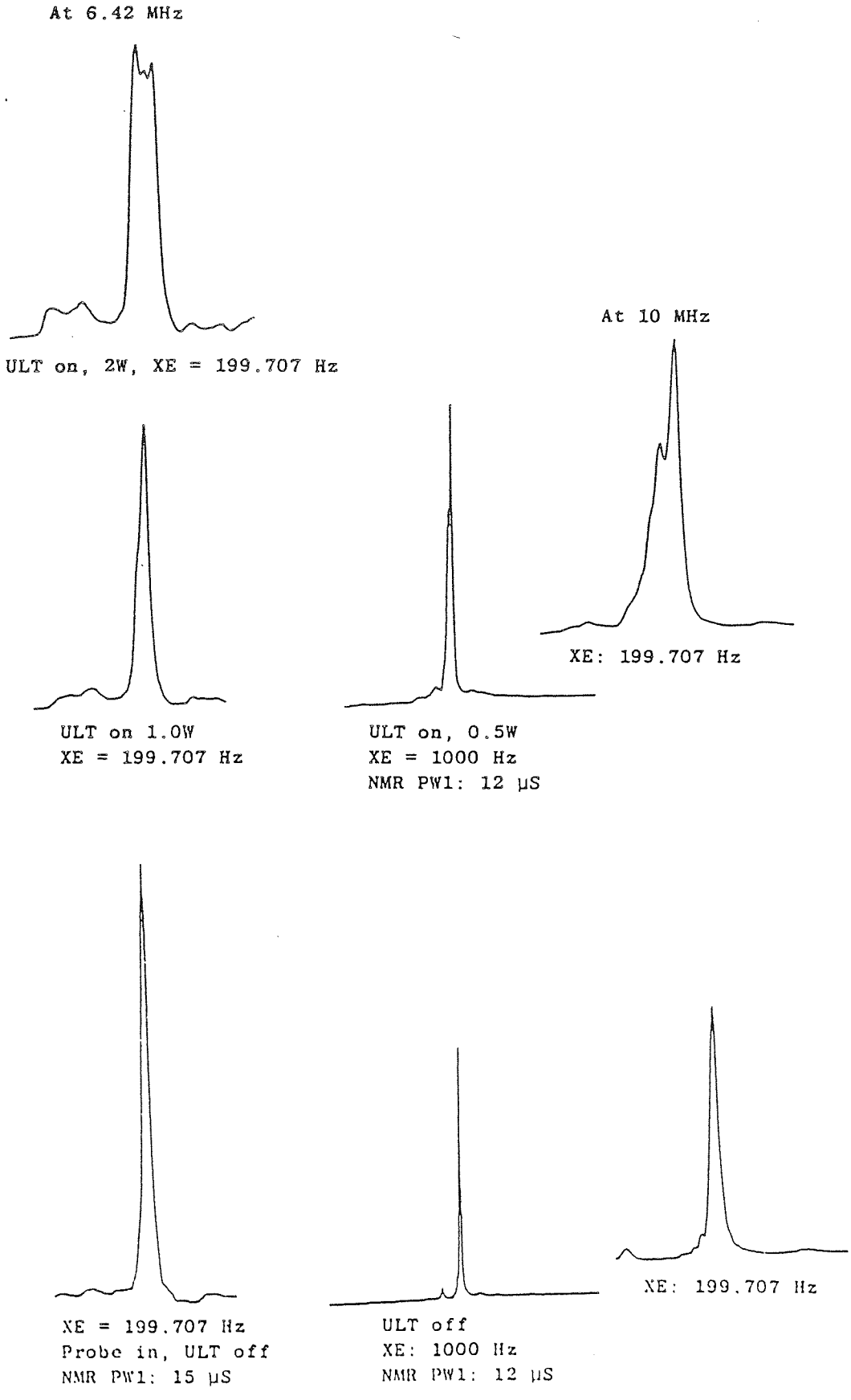

Figure 8.1 (c): The effects of ultrasound at frequencies of 6.42 and 10MHz on proton (^1H) NMR signal observed for an equimolar mixture of acetonitrile and deuterated chloroform. The effects shown are for applying increasing ultrasonic power from 0.5W to 2W across the transducer.

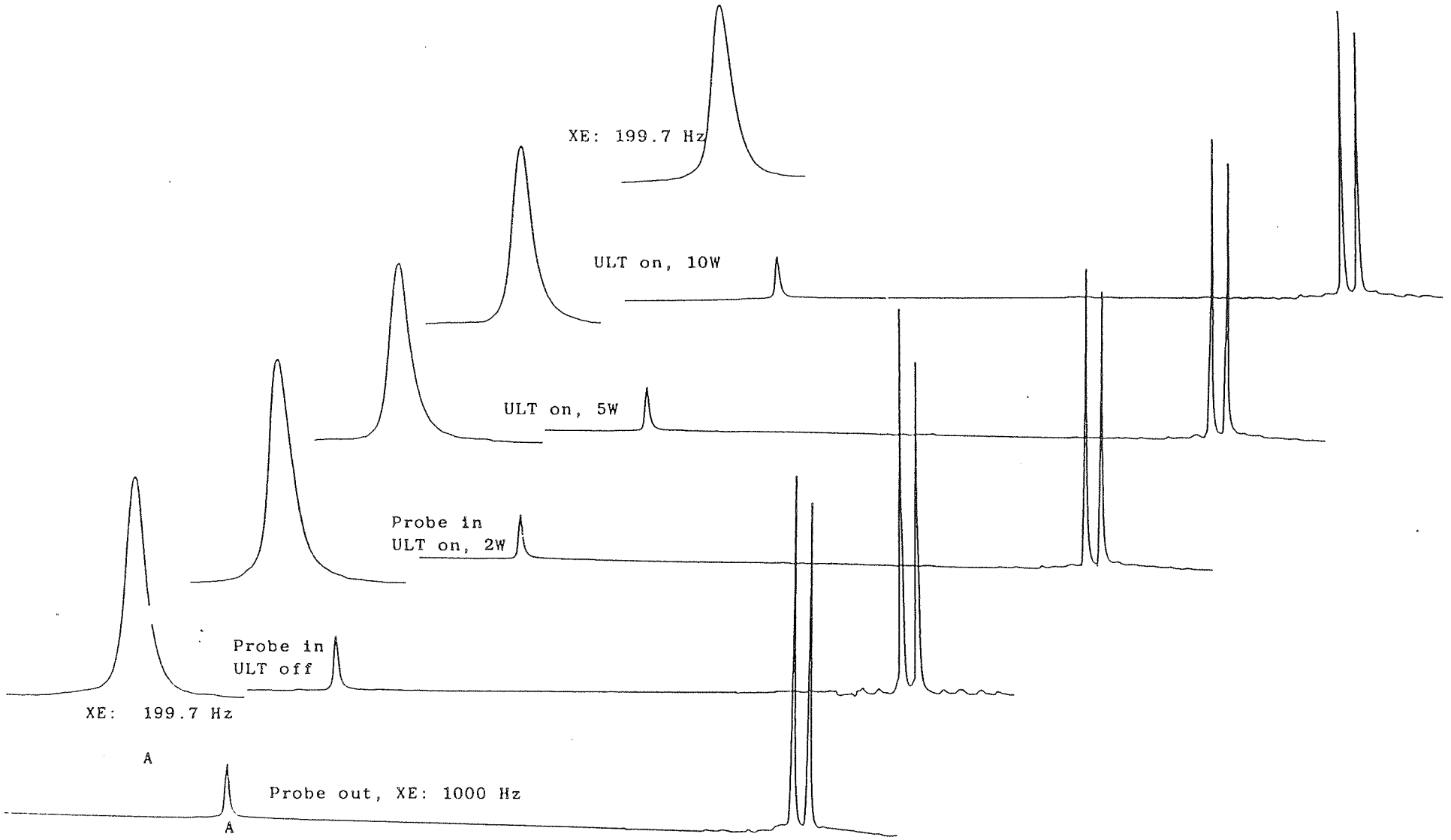

Figure 8.2 (a): The effects of ultrasound at a frequency of 1.115MHz on proton (^{1}H) NMR signals observed for an equimolar mixture of N,N-dimethylformamide and deuterated chloroform. The effects shown are for applying increasing ultrasonic power from 2W to 10W across the transducer.

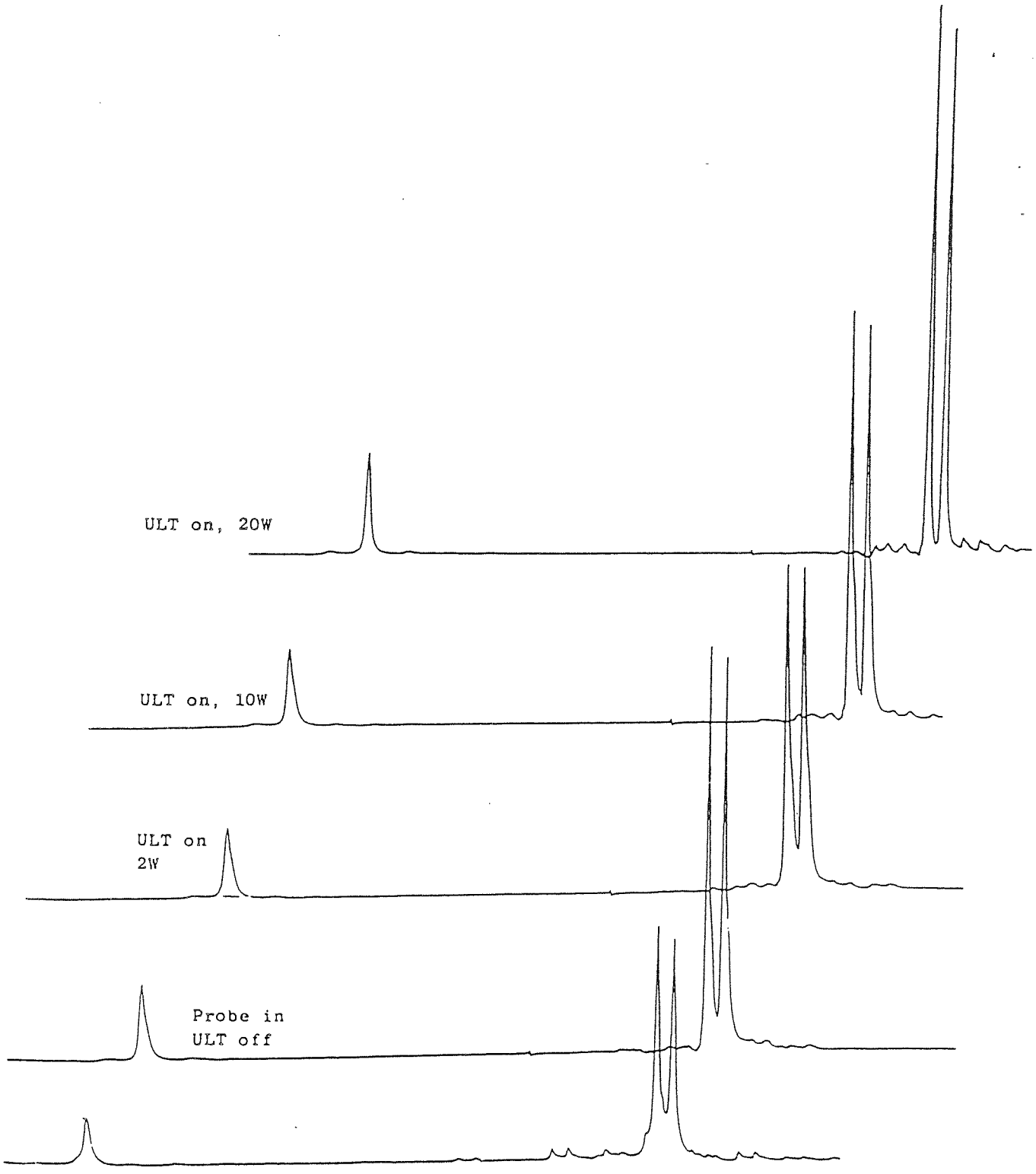

Figure 8.2 (b): The effects of ultrasound at a frequency of 6MHz on proton (^{1}H) NMR signals observed for an equimolar mixture of N,N-dimethylformamide and deuterated chloroform. The effects shown are for applying increasing ultrasonic power from 2W to 20W across the transducer.

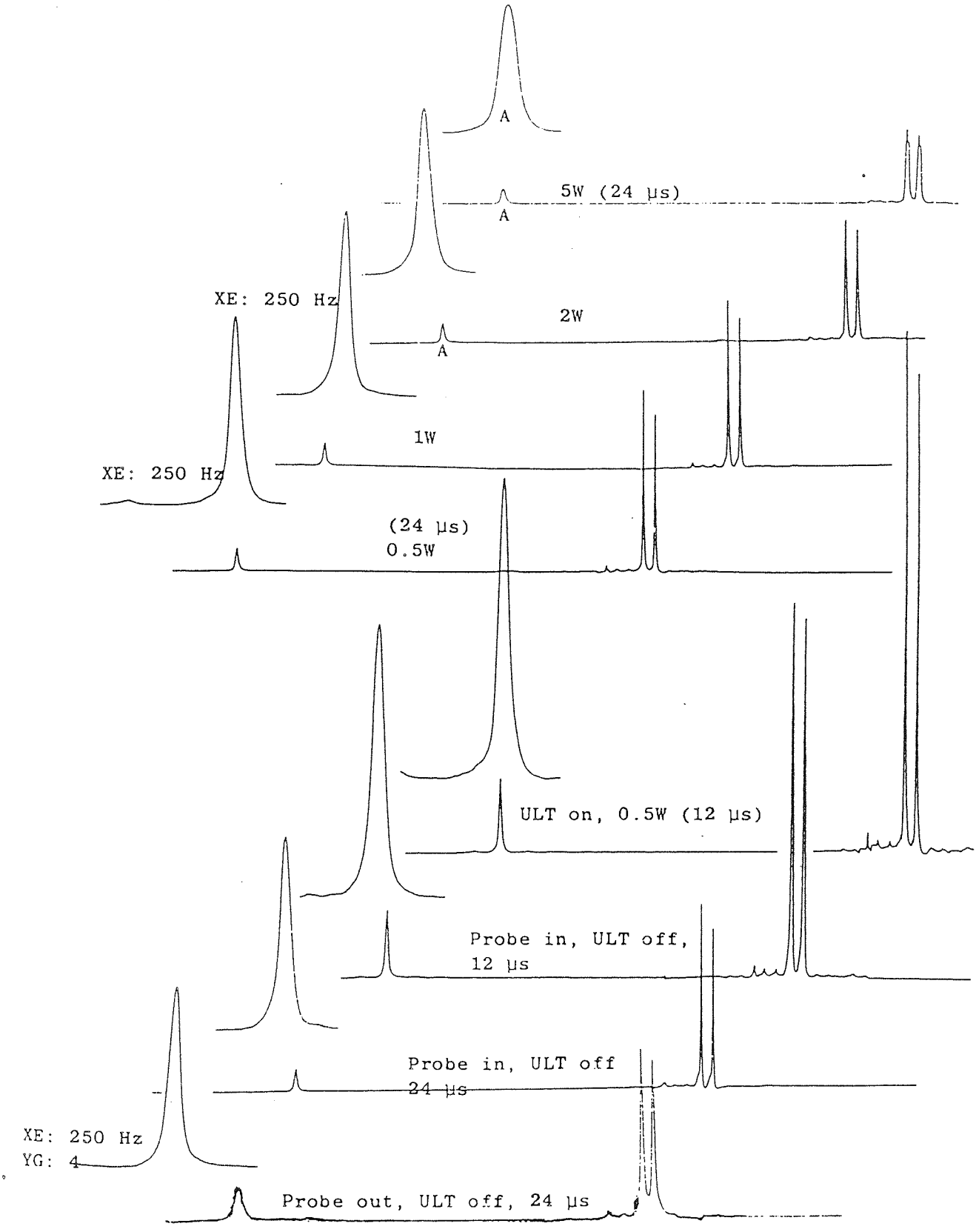

Figure 8.2 (c): The effects of ultrasound at a frequency of 6.42MHz on proton (^{1}H) NMR signals observed for an equimolar mixture of N,N-dimethylformamide and deuterated chloroform. The effects shown are for applying increasing ultrasonic power from 0.5W to 5W across the transducer.

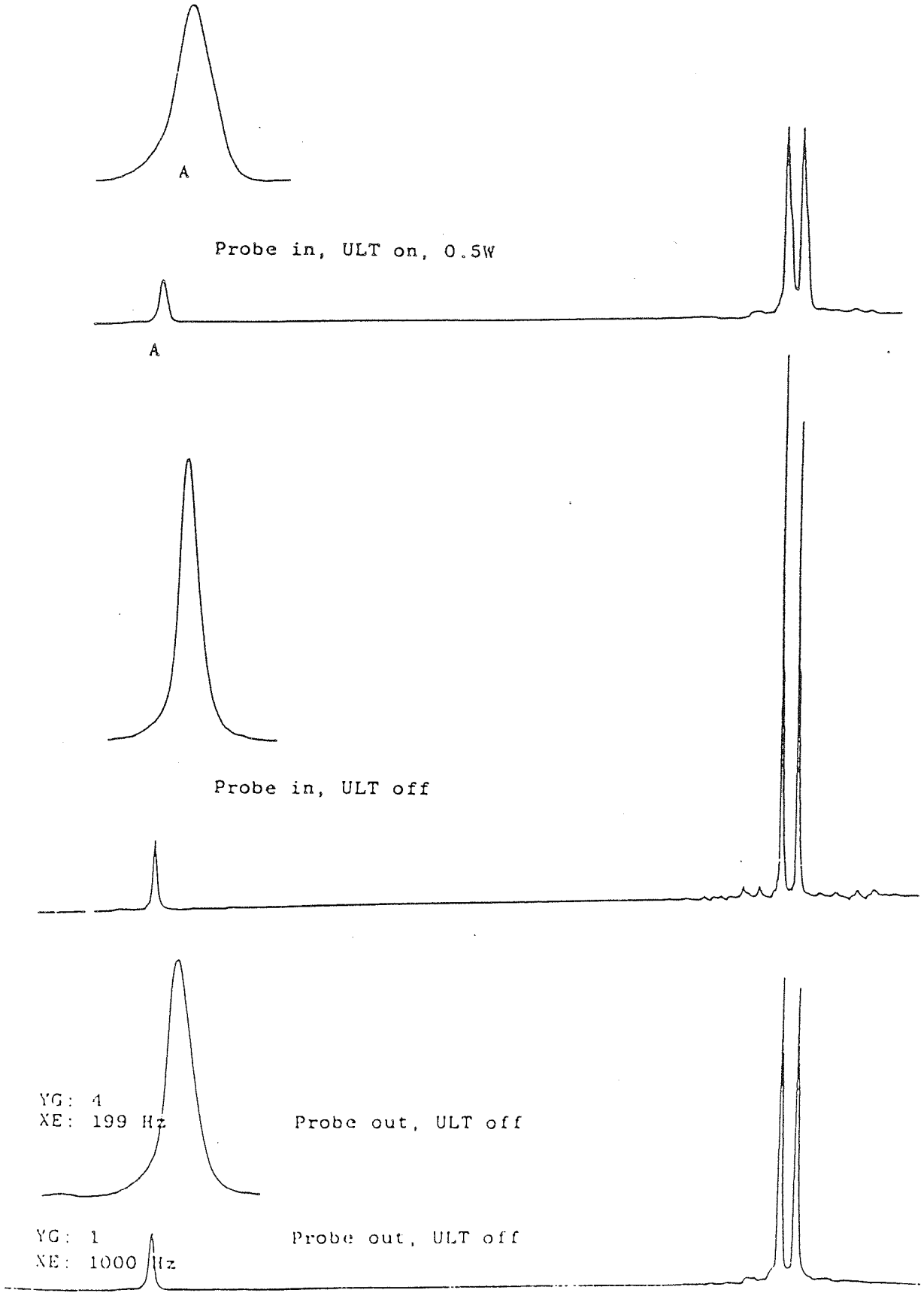

Figure 8.2 (d): The effects of ultrasound at a frequency of 10MHz on proton (^{1}H) NMR signals observed for an equimolar mixture of N,N-dimethylformamide and deuterated chloroform. The effects shown are for applying ultrasonic power of 0.5W across the transducer.

RESULTS OF MEASUREMENTS OF THE EFFECTS OF ULTRASOUND ON PROTON (^{1}H) SPIN-LATTICE AND SPIN-SPIN RELAXATION TIMES IN NITROGEN CONTAINING COMPOUNDS (TABLES 8.14 - 8.16)

RELAXATION TIME MEASUREMENTS

NUCLEI UNDER INVESTIGATION: ^1H NMR.

NMR INSTRUMENT OBSERVATION FREQUENCY: 89.56 MHz.

SYSTEM UNDER INVESTIGATION: Acetonitrile + chloroform(d).

MOLAR RATIO : 1:1.

90 DEGREE PULSE: 30 us. PULSE W1: 12 us. PULSE W2: 24 us.

PULSE REPETITION: 1.0 s. ACQUISITION TIME: 0.6 s. SCANS: 10.

TRANSDUCER FREQUENCY: 1.115 MHz

METHOD OF ANALYSIS: 2pt curve fit.

	SPIN-SPIN RELAXATION TIME MEASUREMENT (T_2) LINE WIDTHS		SPIN- LATTICE RELAXATION TIME MEASUREMENTS (T_1) IN SECONDS
	MOLECULAR GROUPS: Methyl		MOLECULAR GROUPS:
	Hz	SECONDS	Methyl.
SAMPLE PROBE OUT	2.13	0.15	1.921/2.12 (rept.)
SAMPLE PROBE IN (ULT. OFF)	2.66	0.12	1.82/1.88 (rept.)
ULT. ON POWER (Watts)			
0.5	1.59	0.20	1.49/1.45 (rept.)
1.0	1.59	0.20	1.31
2.0	1.59	0.20	1.51
5.0	1.59	0.20	1.85/1.86 (rept.)
10	No expts. done.		
15	No expts. done.		

Table 8.14 (a): The effect of ultrasound at a frequency of 1.115MHz on proton (^1H) spin-lattice relaxation times (T_1) for an equimolar mixture of acetonitrile and deuterated chloroform.

RELAXATION TIME MEASUREMENTS

NUCLEI UNDER INVESTIGATION: ^1H NMR.

NMR INSTRUMENT OBSERVATION FREQUENCY: 89.56 MHz.

SYSTEM UNDER INVESTIGATION: Acetonitrile + chloroform(d).

MOLAR RATIO : 1:1.

90 DEGREE PULSE: 30 us. PULSE W1: 12 us. PULSE W2: 24 us.

PULSE REPETITION: 2.0 s. ACQUISITION TIME: 1.0 s. SCANS: 10.

TRANSDUCER FREQUENCY: 6 MHz

METHOD OF ANALYSIS: 2pt curve fit.

	SPIN-SPIN RELAXATION TIME MEASUREMENT (T_2) LINE WIDTHS		SPIN- LATTICE RELAXATION TIME MEASUREMENTS (T_1) IN SECONDS
	MOLECULAR GROUPS: Methyl		MOLECULAR GROUPS:
	Hz	SECONDS	Methyl.
SAMPLE PROBE OUT	No measurements.		No measurements.
SAMPLE PROBE IN (ULT. OFF)	1.71	0.19	2.10
ULT. ON POWER (Watts)			
0.5	1.71	0.19	1.78
1.0	1.71	0.19	0.79
2.0	At 2W resolution degrades.		
5.0	No expts. done.		
10	No expts. done.		
15	No expts. done.		

Table 8.14 (b): The effect of ultrasound at a frequency of 6MHz of proton (^1H) spin-lattice relaxation times (T_1) for an equimolar mixture of acetonitrile and deuterated chloroform.

RELAXATION TIME MEASUREMENTS

NUCLEI UNDER INVESTIGATION: ^1H NMR.

NMR INSTRUMENT OBSERVATION FREQUENCY: 89.56 MHz.

SYSTEM UNDER INVESTIGATION: Acetonitrile + chloroform(d).

MOLAR RATIO : 1:1.

90 DEGREE PULSE: 30 us. PULSE W1: 15 us. PULSE W2: 25 us.

PULSE REPETITION: 2.0 s. ACQUISITION TIME: 1.0 s. SCANS: 10.

TRANSDUCER FREQUENCY: 6.42 MHz

METHOD OF ANALYSIS: 2pt curve fit.

	SPIN-SPIN RELAXATION TIME MEASUREMENT (T_2) LINE WIDTHS		SPIN- LATTICE RELAXATION TIME MEASUREMENTS (T_1) IN SECONDS
	MOLECULAR GROUPS: Methyl		MOLECULAR GROUPS:
	Hz	SECONDS	Methyl.
SAMPLE PROBE OUT	No measurements.		No measurements.
SAMPLE PROBE IN (ULT. OFF)	1.14	0.28	1.45
ULT. ON POWER (Watts)			
0.5	2.0	0.16	1.40
1.0	At 1W resolution degrades. Line shape splits into two.		
2.0	No expts. done.		
5.0	No expts. done.		
10	No expts. done.		
15	No expts. done.		

Table 8.14 (c): The effect of ultrasound at a frequency of 6.42MHz on proton (^1H) spin-lattice relaxation times (T_1) for an equimolar mixture of acetonitrile and deuterated chloroform.

RELAXATION TIME MEASUREMENTS

NUCLEI UNDER INVESTIGATION: ^1H NMR.

NMR INSTRUMENT OBSERVATION FREQUENCY: 89.56 MHz.

SYSTEM UNDER INVESTIGATION: N,N-dimethylformamide + Chloroform(d).

MOLAR RATIO : 1:1.

90 DEGREE PULSE: 30 us. PULSE W1: 12 us. PULSE W2: 24 us.

PULSE REPETITION: 2.0 s. ACQUISITION TIME: 1.0 s. SCANS: 10.

TRANSDUCER FREQUENCY: 1.115 MHz.

METHOD OF ANALYSIS: 2pt curve fit.

	SPIN-SPIN RELAXATION TIME MEASUREMENT (T_2) LINE WIDTHS		SPIN-LATTICE RELAXATION TIME MEASUREMENTS (T_1) IN SECONDS		
	MOLECULAR GROUPS: Carbonyl (COH)		MOLECULAR GROUPS:		
	Hz	SECONDS	Carbonyl, (COH)	N,N-methyl,	N,N-methyl
SAMPLE PROBE OUT	3.72	0.08	3.67	2.88	3.39
SAMPLE PROBE IN (ULT. OFF)	3.46	0.09	3.11	2.52	2.78
ULT. ON POWER (Watts)					
0.5	3.46	0.09	3.03	2.27	2.68
1.0	3.46	0.09	2.83	2.12	2.56
2.0	3.46	0.09	2.66	2.03	2.46
5.0	3.72	0.085	3.05	2.42	2.82
			rept. 3.17	2.70	3.00
10	3.46	0.09	3.66	2.97	3.14
15	No expt. done.				

Table 8.15 (a): The effect of ultrasound at a frequency of 1.115MHz on proton (^1H) spin-lattice (T_1) and spin-spin relaxation times (T_2) for an equimolar mixture of N,N-dimethylformamide and deuterated chloroform.

RELAXATION TIME MEASUREMENTS

NUCLEI UNDER INVESTIGATION: ^1H NMR.

NMR INSTRUMENT OBSERVATION FREQUENCY: 89.56 MHz.

SYSTEM UNDER INVESTIGATION: N,N-dimethylformamide + Chloroform(d).

MOLAR RATIO : 1:1.

90 DEGREE PULSE: 30 us. PULSE W1: 12 us. PULSE W2: 24 us.

PULSE REPETITION: 2.0 s. ACQUISITION TIME: 1.0 s. SCANS: 10.

TRANSDUCER FREQUENCY: 6 MHz.

METHOD OF ANALYSIS: 2pt curve fit.

	SPIN-SPIN RELAXATION TIME MEASUREMENT (T_2) LINE WIDTHS		SPIN-LATTICE RELAXATION TIME MEASUREMENTS (T_1) IN SECONDS		
	MOLECULAR GROUPS: Carbonyl (COH)		MOLECULAR GROUPS:		
	Hz	SECONDS	Carbonyl, (COH)	N,N-methyl,	N,N-methyl
SAMPLE PROBE OUT	5.30	0.06	2.90	2.41	2.79
SAMPLE PROBE IN (ULT. OFF)	5.30	0.06	2.59	2.58	2.79
ULT. ON POWER (Watts)					
0.5			2.18	1.63	1.84
1.0			2.15	1.62	1.83
2.0	5.30	0.06	2.09	1.44	1.67
5.0			2.31	1.50	1.91
10	No expt. done.				
15	No expt. done.				

Table 8.15 (b): The effect of ultrasound at a frequency of 6MHz on proton (^1H) spin-lattice (T_1) and spin-spin relaxation times (T_2) for an equimolar mixture of N,N-dimethylformamide and deuterated chloroform.

RELAXATION TIME MEASUREMENTS

NUCLEI UNDER INVESTIGATION: ^1H NMR.

NMR INSTRUMENT OBSERVATION FREQUENCY: 89.56 MHz.

SYSTEM UNDER INVESTIGATION: N,N-dimethylacetamide + Chloroform(d).

MOLAR RATIO : 1:1.

90 DEGREE PULSE: 30 us. PULSE W1: 12 us. PULSE W2: 24 us.

PULSE REPETITION: 2.0 s. ACQUISITION TIME: 1.0 s. SCANS: 10.

TRANSDUCER FREQUENCY: 1.115 MHz.

METHOD OF ANALYSIS: 2pt curve fit.

	SPIN-SPIN RELAXATION TIME MEASUREMENT (T_2) LINE WIDTHS		SPIN-LATTICE RELAXATION TIME MEASUREMENTS (T_1) IN SECONDS		
	MOLECULAR GROUPS:		MOLECULAR GROUPS:		
	Hz	SECONDS	Methyl,	N,N-methyl,	N,N-methyl
SAMPLE PROBE OUT	No measurements.		1.72	1.65	1.64
SAMPLE PROBE IN (ULT. OFF)	No measurements.		1.59	1.59	1.54
ULT. ON POWER (Watts)					
0.5	No measurements.		1.48	1.48	1.39
1.0			1.43	1.47	1.43
2.0			1.29 (18%)	1.39 (13%)	1.29 (16%)
5.0	NO expt. done.				
10			1.34	1.41	1.34
15			1.76	1.59	1.53

Table 8.16 (a): The effect of ultrasound at a frequency of 1.115MHz on proton (^1H) spin-lattice (T_1) and spin-spin relaxation times (T_2) for an equimolar mixture of N,N-dimethylacetamide and deuterated chloroform.

RELAXATION TIME MEASUREMENTS

NUCLEI UNDER INVESTIGATION: ^1H NMR.

NMR INSTRUMENT OBSERVATION FREQUENCY: 89.56 MHz.

SYSTEM UNDER INVESTIGATION: N,N-dimethylacetamide + Chloroform(d).

MOLAR RATIO : 1:1.

90 DEGREE PULSE: 30 us. PULSE W1: 12 us. PULSE W2: 24 us.

PULSE REPETITION: 2.0 s. ACQUISITION TIME: 1.0 s. SCANS: 10.

TRANSDUCER FREQUENCY: 6 MHz.

METHOD OF ANALYSIS: 2pt curve fit.

	SPIN-SPIN RELAXATION TIME MEASUREMENT (T_2) LINE WIDTHS	SPIN-LATTICE RELAXATION TIME MEASUREMENTS (T_1) IN SECONDS		
	MOLECULAR GROUPS:	MOLECULAR GROUPS:		
	Hz SECONDS	Methyl,	N,N-methyl,	N,N-methyl
SAMPLE PROBE OUT	(1) T_2 not measured.	0.72	0.81	0.73
SAMPLE PROBE IN (ULT. OFF)	(2) No effects.	0.73	0.81	0.73
ULT. ON POWER (Watts)				
0.5	(3) No line broadening.	0.71	0.84	0.84
1.0	(4) Expt. failed.	0.68	0.90	0.70
2.0	(5) Transducer burned out.	0.89	0.91	0.85
5.0		0.89	0.98	0.93
10	No expt. done.			
15	No expt. done.			

Table 8.16 (b): The effect of ultrasound at a frequency of 6MHz on proton (^1H) spin-lattice (T_1) and spin-spin relaxation times (T_2) for an equimolar mixture of N,N-dimethylacetamide and deuterated chloroform.

RELAXATION TIME MEASUREMENTS

NUCLEI UNDER INVESTIGATION: ^1H NMR.

NMR INSTRUMENT OBSERVATION FREQUENCY: 89.56 MHz.

SYSTEM UNDER INVESTIGATION: N,N-dimethylacetamide + Chloroform(d).

MOLAR RATIO : 1:1.

90 DEGREE PULSE: 30 us. PULSE W1: 12 us. PULSE W2: 24 us.

PULSE REPETITION: 2.0 s. ACQUISITION TIME: 1.0 s. SCANS: 10.

TRANSDUCER FREQUENCY: 6.42 MHz.

METHOD OF ANALYSIS: 2pt curve fit.

	SPIN-SPIN RELAXATION TIME MEASUREMENT (T_2) LINE WIDTHS	SPIN-LATTICE RELAXATION TIME MEASUREMENTS (T_1) IN SECONDS		
	MOLECULAR GROUPS:	MOLECULAR GROUPS:		
	Hz SECONDS	Methyl,	N,N-methyl,	N,N-methyl
SAMPLE PROBE OUT	T_2 not measured.	1.16	1.11	1.05
SAMPLE PROBE IN (ULT. OFF)		1.14	1.04	1.13
ULT. ON POWER (Watts)				
0.5		0.97	1.09	1.02
1.0		0.50	0.71	0.60
2.0		0.98	0.93	0.85
5.0		1.05	1.04	1.01
10	No expt. done.			
15	No expt. done.			

Table 8.16 (c): The effect of ultrasound at a frequency of 6.42MHz on proton (^1H) spin-lattice (T_1) and spin-spin relaxation times (T_2) for an equimolar mixture of N,N-dimethylacetamide and deuterated chloroform.

(B) CARBON (^{13}C) NMR RESULTS

Measurement of the effects of ultrasound on carbon-13 NMR spin-lattice relaxation times, using ultrasonic frequencies of 1.115, 6, 6.42 and 10 MHz.

(1) For an equimolar mixture of acetonitrile and deuterated chloroform

The results of experiments revealed that the relaxation time data obtained were inconsistent and unreliable, that is, in some experiments either a large reduction or a large increase or no change in the spin-lattice relaxation times. This is partially due to the fact that in order to observe the carbon-13 signals arising from the methyl and nitrile groups an adequate signal to noise ratio is required. Thus, large number of signal accumulation needs to be performed. This meant that the transducer had to be kept oscillating for a long period of time. As a result the heat generated within the transducer due to a small impedance mismatch between the transducer and materials used to mount it and between these and the liquid medium being investigated gave results which showed both the effects of ultrasound as well as heating effects. Moreover, the heat generated within the transducer further changes characteristics to an extent that results become further unreliable.

Comparison of the NMR spectra for the liquid mixture subjected to and without ultrasound, shows, in general, a sharp radio-frequency beat signal in the base line at approximately 41.7 Hz from the centre of the spectral frequency (Figure 8.3).

(2) For Pure N-methylformamide

Measurement of the effects of ultrasound on carbon-13 spin-lattice relaxation times were also not performed. This was again due to the fact that in order to observe a sufficiently intense signal a large number of NMR signal accumulations was required. This meant that the effects of ultrasound absorption in liquids and the heat generated due to the prolonged length of time for the transducer being left resonating could not be discriminated. These observations are similar to those observed for acetonitrile.

(3) For an equimolar mixture of N,N-dimethylformamide and Deuterated Chloroform

(i) At 1.115 MHz: Experiments performed at the mentioned ultrasonic frequency showed that spin-lattice relaxation times initially decrease at low powers and then increase at higher powers (Table 8.17(a)).

Observation of the NMR spectra also shows a radio-frequency beat signal in the base line at approximately 41.7 Hz from the centre of the spectral frequency.

(ii) At 6 and 6.42 MHz: Experiments were performed in the same manner as in (i). The results again reveal similar behaviour to that described in (i) Table 8.17(b) and (c)).

Observation of the NMR spectra for both experiments, show a radio-frequency pick-up beat in the base line. This again appears at approximately 41.7 Hz from the centre of the spectral frequency.

Figure 8.4 shows the carbon-13 NMR spectra for N,N-methylformamide using ultrasonic frequencies of 1.115, 6 and 6.42 MHz.

(iii) No experiments were performed using an ultrasonic frequency of 10 MHz.

(4) For an equimolar mixture of N,N-dimethylacetamide and deuterated chloroform

(i) At 1.115, 6 and 6.42 MHz: The results of experiments performed are presented in Table 8.18(a), (b) and (c), respectively. The results reveal similar patterns at all frequencies. This is an initial decrease in the spin-lattice relaxation times at low powers, followed by an increase at higher powers. This behaviour has already been described in Section 8.1(a) and (b) for similar results obtained for mixtures of cyclohexane and substituted benzene systems.

Observation of the NMR spectra at the different ultrasonic frequencies shows a radio-frequency beat signal at approximately 41.7 Hz from the centre of the spectral frequency (Figure 8.5).

RESULTS OF THE EFFECTS OF ULTRASOUND ON CARBON-13 (^{13}C) IN NITROGEN CONTAINING COMPOUNDS (FIGURES 8.3 - 8.5)

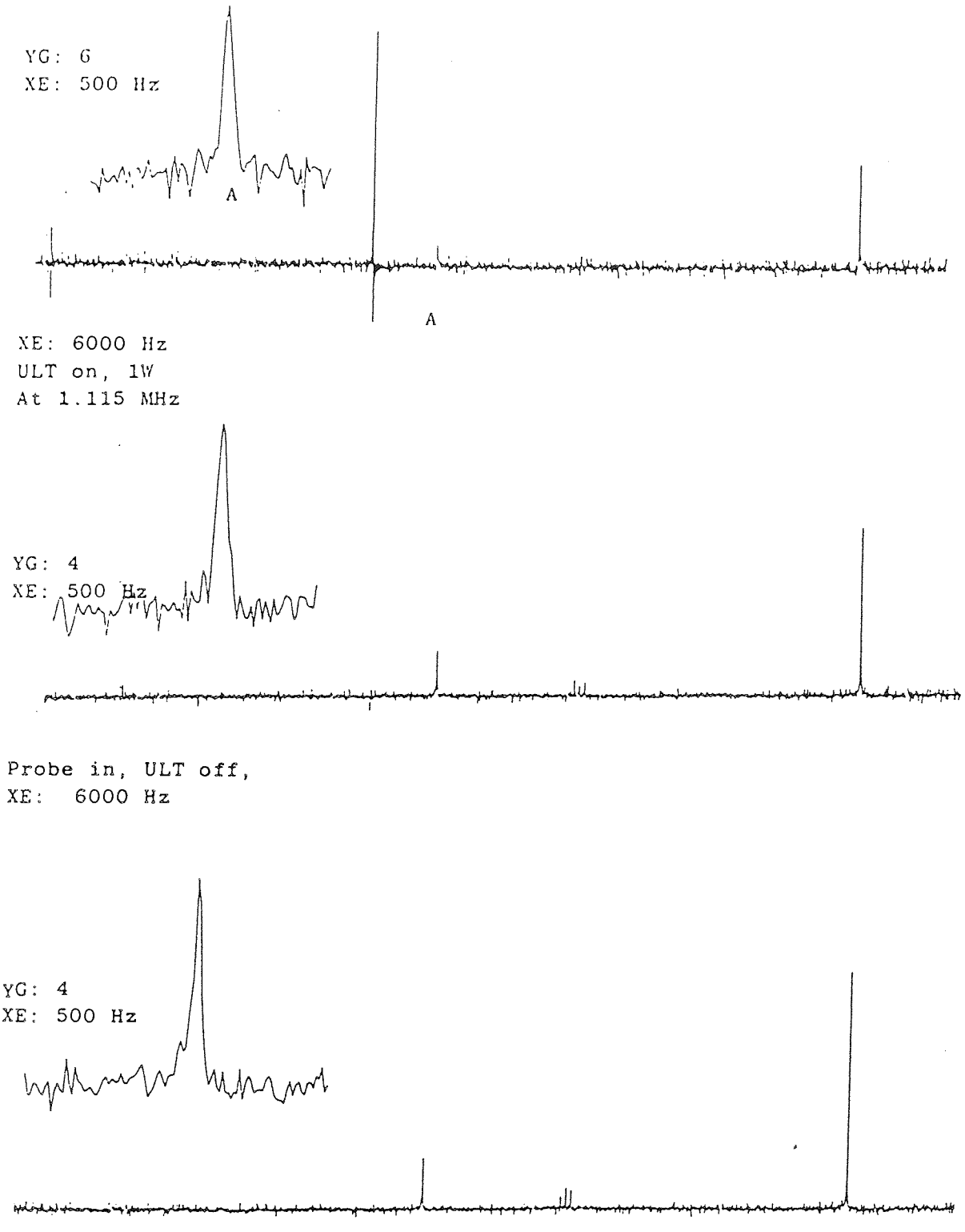

Figure 8.3: The effects of ultrasound at a frequency of 1.115MHz on carbon-13 NMR signals observed for an equimolar mixture of acetonitrile and deuterated chloroform. The effects shown are for applying ultrasonic power of 1W across the transducer. A radio-frequency beat signal is observed at 41.7Hz from the centre of the spectral frequency.

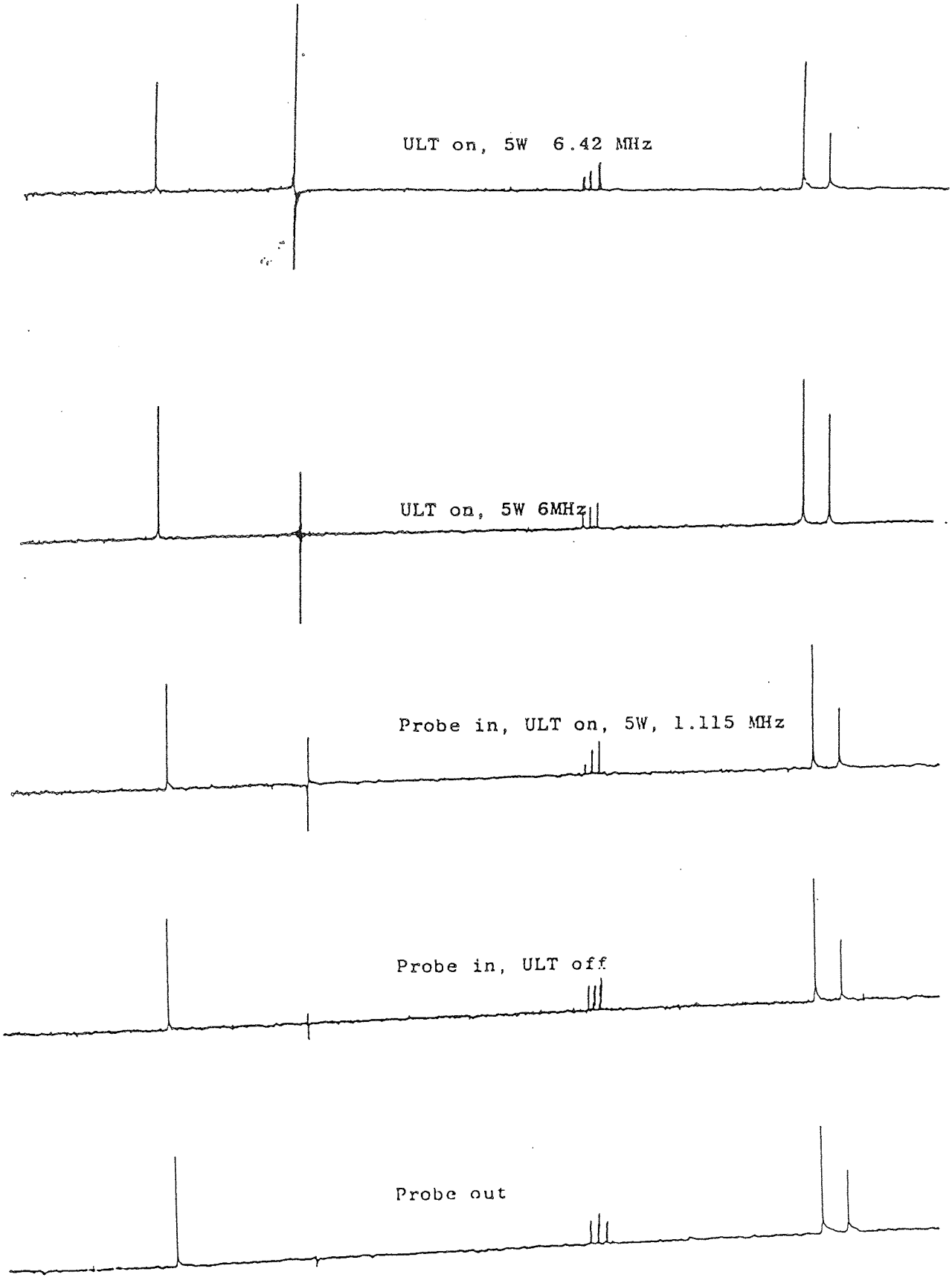

Figure 8.4: The effects of ultrasound at frequencies of 1.115, 6, and 6.42 on carbon-13 NMR signals observed for an equimolar mixture of N,N-dimethylformamide and deuterated chloroform. The effects shown are for applying ultrasonic power of 5W across the transducer.

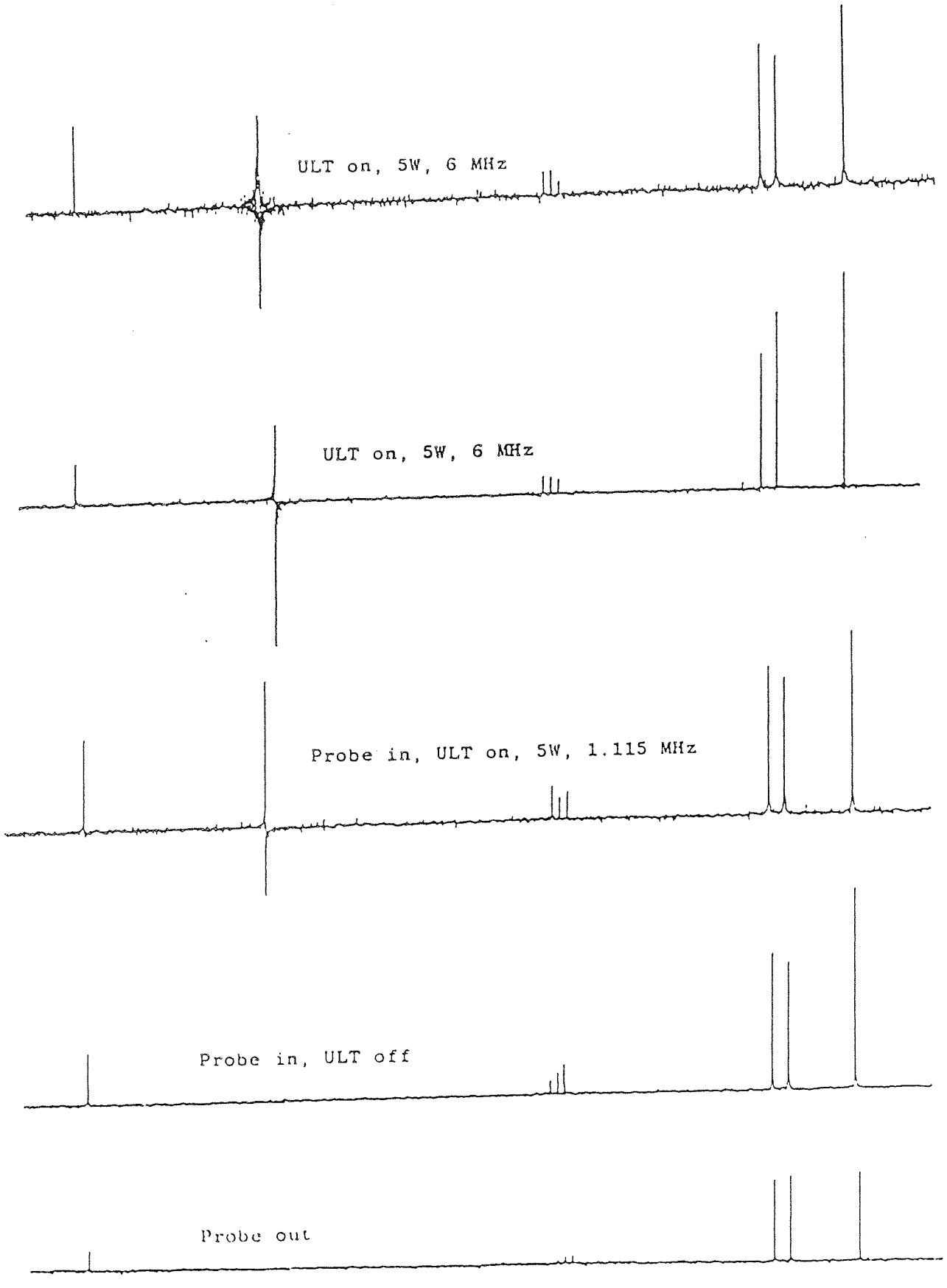

Figure 8.5: The effects of ultrasound at frequencies of 1.115, 6, and 6.42 on carbon-13 NMR signals observed for an equimolar mixture of N,N-dimethylacetamide and deuterated chloroform. The effects shown are for an ultrasonic power of 5W across the transducer.

RESULTS OF MEASUREMENT OF THE EFFECTS OF ULTRASOUND ON CARBON-13 NUCLEI (^{13}C) SPIN-LATTICE AND SPIN-SPIN RELAXATION TIMES IN NITROGEN CONTAINING COMPOUNDS (TABLES 8.17 - 8.18)

RELAXATION TIME MEASUREMENTS

NUCLEI UNDER INVESTIGATION: ^{13}C NMR.

NMR INSTRUMENT OBSERVATION FREQUENCY: 22.5 MHz.

SYSTEM UNDER INVESTIGATION: N,N-dimethylformamide + Chloroform(d).

MOLAR RATIO : 1:1.

90 DEGREE PULSE: 22.5 us. PULSE W1: 9 us. PULSE W2: 18 us.

PULSE REPETITION: 2.0 s. ACQUISITION TIME: 1.0 s. SCANS: 50.

TRANSDUCER FREQUENCY: 1.115 MHz.

METHOD OF ANALYSIS: 2pt curve fit.

	SPIN-SPIN RELAXATION TIME MEASUREMENT (T_2) LINE WIDTHS	SPIN-LATTICE RELAXATION TIME MEASUREMENTS (T_1) IN SECONDS		
	MOLECULAR GROUPS: Carbonyl	MOLECULAR GROUPS:		
	Hz SECONDS	Carbonyl,	N,N-methyl,	N,N-methyl
SAMPLE PROBE OUT	No measurements.	No measurements.		
SAMPLE PROBE IN (ULT. OFF)	No measurements.	15.82	13.82	18.09
ULT. ON POWER (Watts)				
0.5	No measurements.	14.05	10.33	17.35
1.0		13.99	9.17	17.16
2.0		13.56	9.62	17.46
5.0		13.84	10.22	17.46
10		15.64	10.42	18.96
15	No expt. done.			

Table 8.17 (a): The effect of ultrasound at a frequency of 1.115MHz on carbon-13 nuclei (^{13}C) spin-lattice relaxation times (T_1) for an equimolar mixture of N,N-dimethylformamide and deuterated chloroform.

RELAXATION TIME MEASUREMENTS

NUCLEI UNDER INVESTIGATION: ^{13}C NMR.

NMR INSTRUMENT OBSERVATION FREQUENCY: 22.5 MHz.

SYSTEM UNDER INVESTIGATION: N,N-dimethylformamide + Chloroform(d).

MOLAR RATIO : 1:1.

90 DEGREE PULSE: 22.5 us. PULSE W1: 9 us. PULSE W2: 18 us.

PULSE REPETITION: 2.0 s. ACQUISITION TIME: 1.0 s. SCANS: 50.

TRANSDUCER FREQUENCY: 6 MHz.

METHOD OF ANALYSIS: 2pt curve fit.

	SPIN-SPIN RELAXATION TIME MEASUREMENT (T_2) LINE WIDTHS	SPIN-LATTICE RELAXATION TIME MEASUREMENTS (T_1) IN SECONDS		
	MOLECULAR GROUPS: Carbonyl	MOLECULAR GROUPS:		
	Hz SECONDS	Carbonyl,	N,N-methyl,	N,N-methyl
SAMPLE PROBE OUT	No measurements.	15.13	13.88	14.46
SAMPLE PROBE IN (ULT. OFF)	No measurements.	14.94	13.67	14.29
ULT. ON POWER (Watts)				
0.5	No measurements.	14.70	10.03	13.90
1.0		13.69	9.38	11.32
2.0		10.32 (30%)	9.39 (46%)	9.28 (35%)
5.0		15.46	8.65	10.71
10	No expt. done.			
15	No expt. done.			

Table 8.17 (b): The effect of ultrasound at a frequency of 6MHz on carbon-13 nuclei (^{13}C) spin-lattice relaxation times (T_1) for an equimolar mixture of N,N-dimethylformamide and deuterated chloroform.

RELAXATION TIME MEASUREMENTS

NUCLEI UNDER INVESTIGATION: ^{13}C NMR.

NMR INSTRUMENT OBSERVATION FREQUENCY: 22.5 MHz.

SYSTEM UNDER INVESTIGATION: N,N-dimethylformamide + Chloroform(d).

MOLAR RATIO : 1:1.

90 DEGREE PULSE: 22.5 us. PULSE W1: 9 us. PULSE W2: 18 us.

PULSE REPETITION: 2.0 s. ACQUISITION TIME: 1.0 s. SCANS: 50.

TRANSDUCER FREQUENCY: 6.42 MHz.

METHOD OF ANALYSIS: 2pt curve fit.

	SPIN-SPIN RELAXATION TIME MEASUREMENT (T_2) LINE WIDTHS	SPIN-LATTICE RELAXATION TIME MEASUREMENTS (T_1) IN SECONDS		
	MOLECULAR GROUPS: Carbonyl	MOLECULAR GROUPS:		
	Hz SECONDS	Carbonyl,	N,N-methyl,	N,N-methyl
SAMPLE PROBE OUT	No measurements.	15.13	13.88	14.46
SAMPLE PROBE IN (ULT. OFF)	No measurements.	14.94	13.67	14.29
ULT. ON POWER (Watts)				
0.5	No measurements.	13.91	10.29	13.02
1.0		11.57	9.39	10.54
2.0		11.29	9.09	9.15
5.0		15.53	10.61	14.28
		rept. 13.57	9.86	18.78
10	No expt. done.			
15	No expt. done.			

Table 8.17 (c): The effect of ultrasound at a frequency of 6.42MHz on carbon-13 nuclei (^{13}C) spin-lattice relaxation times (T_1) for an equimolar mixture of N,N-dimethylformamide and deuterated chloroform.

RELAXATION TIME MEASUREMENTS

NUCLEI UNDER INVESTIGATION: ^{13}C NMR.

NMR INSTRUMENT OBSERVATION FREQUENCY: 22.5 MHz.

SYSTEM UNDER INVESTIGATION: N,N-dimethylacetamide + Chloroform(d).

MOLAR RATIO : 1:1.

90 DEGREE PULSE: 22.5 us. PULSE W1: 9 us. PULSE W2: 18 us.

PULSE REPETITION: 1.0 s. ACQUISITION TIME: 0.6 s. SCANS: 50.

TRANSDUCER FREQUENCY: 1.115 MHz.

METHOD OF ANALYSIS: 2pt curve fit.

	SPIN-SPIN RELAXATION TIME MEASUREMENT (T_2) LINE WIDTHS	SPIN-LATTICE RELAXATION TIME MEASUREMENTS (T_1) IN SECONDS			
	MOLECULAR GROUPS:	MOLECULAR GROUPS:			
	Hz SECONDS	carbonyl,	N,N-methyl,	N,N-methyl,	methyl.
SAMPLE PROBE OUT	No measurements.				
SAMPLE PROBE IN (ULT. OFF)	No measurements.	11.29	6.62	5.58	5.14
ULT. ON POWER (Watts)					
0.5	No measurements.	10.08	6.37	5.69	5.03
1.0		9.95	5.77	5.49	4.85
2.0		8.93	4.88	3.72	4.67
5.0		9.21	5.50	4.54	4.56
10		11.04	5.61	4.59	5.18
15	No expt. done				

Table 8.18 (a): The effect of ultrasound at a frequency of 1.115MHz on carbon-13 nuclei (^{13}C) spin-lattice relaxation times (T_1) for an equimolar mixture of N,N-dimethylacetamide and deuterated chloroform.

RELAXATION TIME MEASUREMENTS

NUCLEI UNDER INVESTIGATION: ^{13}C NMR.

NMR INSTRUMENT OBSERVATION FREQUENCY: 22.5 MHz.

SYSTEM UNDER INVESTIGATION: N,N-dimethylacetamide + Chloroform(d).

MOLAR RATIO : 1:1.

90 DEGREE PULSE: 22.5 us. PULSE W1: 9 us. PULSE W2: 18 us.

PULSE REPETITION: 1.0 s. ACQUISITION TIME: 0.6 s. SCANS: 50.

TRANSDUCER FREQUENCY: 6 MHz.

METHOD OF ANALYSIS: 2pt curve fit.

	SPIN-SPIN RELAXATION TIME MEASUREMENT (T_2) LINE WIDTHS		SPIN-LATTICE RELAXATION TIME MEASUREMENTS (T_1) IN SECONDS			
	MOLECULAR GROUPS:		MOLECULAR GROUPS:			
	Hz	SECONDS	carbonyl,	N,N-methyl,	N,N-methyl,	methyl.
SAMPLE PROBE OUT	No measurements.					
SAMPLE PROBE IN (ULT. OFF)	1.95	0.16	10.69	6.92	6.73	8.52
ULT. ON POWER (Watts)						
0.5	2.60	0.12	7.71	5.47	5.16	6.34
1.0			6.68	4.16	4.17	4.93
2.0	1.33	0.24	5.57	3.34	3.58	8.49
5.0	4.0	0.079	10.56	10.96	8.93	10.64
10	No expt. done.					
15	No expt. done.					

Table 8.18 (b): The effect of ultrasound at a frequency of 6MHz on carbon-13 nuclei (^{13}C) spin-lattice relaxation times (T_1) for an equimolar mixture of N,N-dimethylacetamide and deuterated chloroform.

RELAXATION TIME MEASUREMENTS

NUCLEI UNDER INVESTIGATION: ^{13}C NMR.

NMR INSTRUMENT OBSERVATION FREQUENCY: 22.5 MHz.

SYSTEM UNDER INVESTIGATION: N,N-dimethylacetamide + Chloroform(d).

MOLAR RATIO : 1:1.

90 DEGREE PULSE: 22.5 us. PULSE W1: 9 us. PULSE W2: 18 us.

PULSE REPETITION: 1.0 s. ACQUISITION TIME: 0.6 s. SCANS: 50.

TRANSDUCER FREQUENCY: 6.42 MHz.

METHOD OF ANALYSIS: 2pt curve fit.

	SPIN-SPIN RELAXATION TIME MEASUREMENT (T_2) LINE WIDTHS		SPIN-LATTICE RELAXATION TIME MEASUREMENTS (T_1) IN SECONDS			
	MOLECULAR GROUPS:		MOLECULAR GROUPS:			
	Hz	SECONDS	carbonyl,	N,N-methyl	N,N-methyl	methyl.
SAMPLE PROBE OUT	2.0	0.16	12.49	6.94	6.27	9.75
SAMPLE PROBE IN (ULT. OFF)	2.93	0.11	12.65	6.37	6.24	9.33
ULT. ON POWER (Watts)						
0.5	2.66	0.12	10.16	5.75	5.85	7.22
1.0	2.66	0.12	9.33	4.41	4.64	6.59
2.0	2.66	0.12	7.92	3.83	3.57	5.31
5.0	2.66	0.12	14.10	7.25	7.39	9.39
10	No expt. done.					
15	No expt. done.					

Table 8.18 (c): The effect of ultrasound at a frequency of 6.42MHz on carbon-13 nuclei (^{13}C) spin-lattice relaxation times (T_1) for an equimolar mixture of N,N-dimethylacetamide and deuterated chloroform.

(C) NITROGEN (^{14}N) NMR RESULTS

Measurement of the effects of ultrasound on nitrogen-14 NMR spin-lattice and spin-spin relaxation times using ultrasonic frequencies of 1.115, 6, 6.42 and 10 MHz.

(1) For an equimolar mixture of acetonitrile and deuterated chloroform

(i) At 1.115 MHz: The results show that spin-lattice relaxation times are very short (Table 8.19). Furthermore, the effects of increasing the ultrasonic power show no changes in the spin-lattice or spin-spin relaxation times. Comparison of the NMR spectra for the liquid mixture with and without ultrasound revealed no significant changes in the lineshapes or to the noise level (Figure 8.6).

(ii) At 6 MHz: The results show the numerical data obtained leading to the measurements of spin-lattice relaxation times are unreliable. However, observation of the NMR spectra, shows a decrease in the signal to noise ratio with a larger noise level on the base line. Measurement of the linewidth at an ultrasonic power level of 0.5W further reveals that spin-spin relaxation times had decreased (Figure 8.6).

(iii) At 6.42 MHz: The experiment are now performed at the exact NMR observation frequency of the spectrometer. The results reveal that at even at an ultrasonic power as low as 0.5W, only a very small NMR signal arising from the nitrogen nuclei is observed. Furthermore, there exists two large radio-frequency beat signals on the baseline (Figure 8.6).

(iv) At 10 MHz: The experiment now performed above the NMR observation frequency on the spectrometer shows that the signal to noise ratio has decreased by one third using ultrasonic power of 0.5W.

In summary, the results of experiments performed at various ultrasonic frequencies for the nitrogen-14 nuclei reveal that as the ultrasonic frequency is near, at the exact resonance and above the nitrogen NMR observation frequency, the NMR signal arising from the sample under investigation in the respective cases starts from being uneffected, followed by a small decrease in the signal to almost a complete signal saturation and finally is again unaffected. These results suggests the following two possibilities. These being:

The NMR electronic signal induced in the receiver coils as a result of energy emission from the nuclear spins returning to thermal equilibrium (following the absorption of energy during the excitation of nuclear spins from the ground states), loses its phase coherence due to an electronic signal interaction from the ultrasonic wave. This either results in a partial decrease or a total disappearance in the NMR signal intensities. This also explains why no NMR signal is observed when an exact ultrasonic frequency is used corresponding to that of the nitrogen-14 NMR spectrometer resonance frequency. In this case, there is a total loss of phase coherence of the induced NMR signal frequency. Furthermore, for ultrasonic frequency below and above the NMR spectrometer resonant frequency, small NMR signals are observed. In these cases there must only be a partial loss of phase coherence of the induced NMR signal.

The second possibility which exists is nuclear spin saturation, a process similar to nuclear acoustic resonance: Following the excitation of nuclear spins to higher energy levels due to the NMR absorption, the nuclear spins now relax back to their ground states. However, as these nuclear spins tend to relax to their ground states, they immediately gain energy but this time with their interaction with the ultrasonic wave. This either results in a partial or a total saturation of the spin energy levels which therefore either results in a decrease in signal intensities or the disappearance of the signal being observed. This explanation can also be used to explain the behaviour of signal intensities at the various ultrasonic frequencies, with the largest effect on the signal intensities when using an ultrasonic frequency corresponding to that of the NMR spectrometer resonant frequency.

(2) For Pure N-methylformamide

Measurement of the effects of ultrasound on nitrogen-14 NMR spin-lattice and spin-spin relaxation times were only performed at ultrasound frequencies of 6 and 6.42 MHz.

(i) At 6 MHz: The results of the experiment reveal that application of ultrasonic power of as little as 0.5W causes the signal to be almost saturated. This is shown in Figure 8.7.

(ii) At 6.42 MHz: Performing experiments at the exact NMR observation frequency causes the signals to disappear. In addition, there exists two radio-frequency pick-up signals in the base line (Figure 8.7). Explanations presented for similar observations in acetonitrile can be used to describe such behaviour.

(3) <u>For an equimolar mixture of N,N-dimethylformamide and deuterated chloroform</u>

(i) At 1.115 MHz: The results for the measurement of spin-lattice relaxation times for the nitrogen nuclei reveals that the nuclei have very short relaxation times. This is due to the quadrupolar relaxation being present in addition to the dipolar-dipolar relaxation which provides an efficient means of energy exchange between the spin system and the lattice. The results show the initial short relaxation times (Table 8.20). Thus, the effects of ultrasound cannot be discriminated and the results of its influence on spin-lattice relaxation times is unreliable. However, observation of the NMR spectra shows a reduction in signal intensities with increasing ultrasonic power.

Measurement of the linewidths revealed that ultrasound does not effect the spin-spin relaxation times. Figure 8.8(a) shows the effects of increasing the ultrasonic power at 1.115 MHz on the nitrogen nuclei.

(ii) At 6 MHz: The results show that with increasing ultrasonic powers the signal intensity decreases (Figure 8.8(b)).

Measurement of spin-spin relaxation times were not performed owing to the small signal intensities.

(iii) At 6.42 MHz: The results of the experiment reveals that performing experiments at the exact NMR observation frequency causes almost a total signal saturation with a large radio-frequency beat (Figure 8.8(c)).

(iv) At 10 MHz: The results of the experiment reveals that performing experiments above the NMR observation frequency now allows the observation of the nitrogen signal. Furthermore, the NMR signal appears to be dependent on the ultrasonic power, which decreases with increasing power (Figure 8.8(d)).

An explanation presented for similar observation in acetonitrile at various ultrasonic frequencies can be used to describe such behaviour.

(4) For an equimolar mixture of N,N-dimethylacetamide and deuterated chloroform

(c) Measurement of the effects of ultrasound on nitrogen-14 spin-lattice and spin-spin relaxation times were only performed using ultrasonic frequencies of 1.115, 6 and 6.42 MHz.

(i) At 1.115 MHz: The results show the nitrogen spin-lattice relaxation times are very small (Table 8.21). The effects of ultrasound although appears to show a reduction in the relaxation times with increasing power, however, one must remain sceptical of the accuracy of the results owing to short relaxation times.

Measurement of linewidth for the nitrogen signal shows spin-spin relaxation times to be uneffected by ultrasound. However, observation of the NMR spectra shows the increase in the noise level although the signal itself appears not to have changed (Figure 8.9(a)).

(ii) At 6 MHz: Measurement of spin-lattice relaxation times were not performed as the signal intensities decreased enormously with the application of ultrasound. The NMR spectra shows that at even as low as 1W the signal intensities are very small (Figure 8.9(b)).

(iii) At 6.42 MHz: The nitrogen NMR spectra results shows that the application of ultrasound at the exact resonant NMR observation frequency using an ultrasonic power of 0.5W causes the signal to become almost saturated with the appearance of two radio-frequency signals in the baseline. Application of ultrasound at 2W now causes the

nitrogen signal to disappear altogether and the appearance of one large radio-frequency signal (Figure 8.9(c)). Explanations presented for similar observations in acetonitrile at various ultrasonic frequencies can be used to describe such behaviour.

RESULTS OF THE EFFECTS OF ULTRASOUND ON NITROGEN-14 NUCLEI (^{14}N) IN NITROGEN CONTAINING COMPOUNDS (FIGURES 8.6 - 8.8)

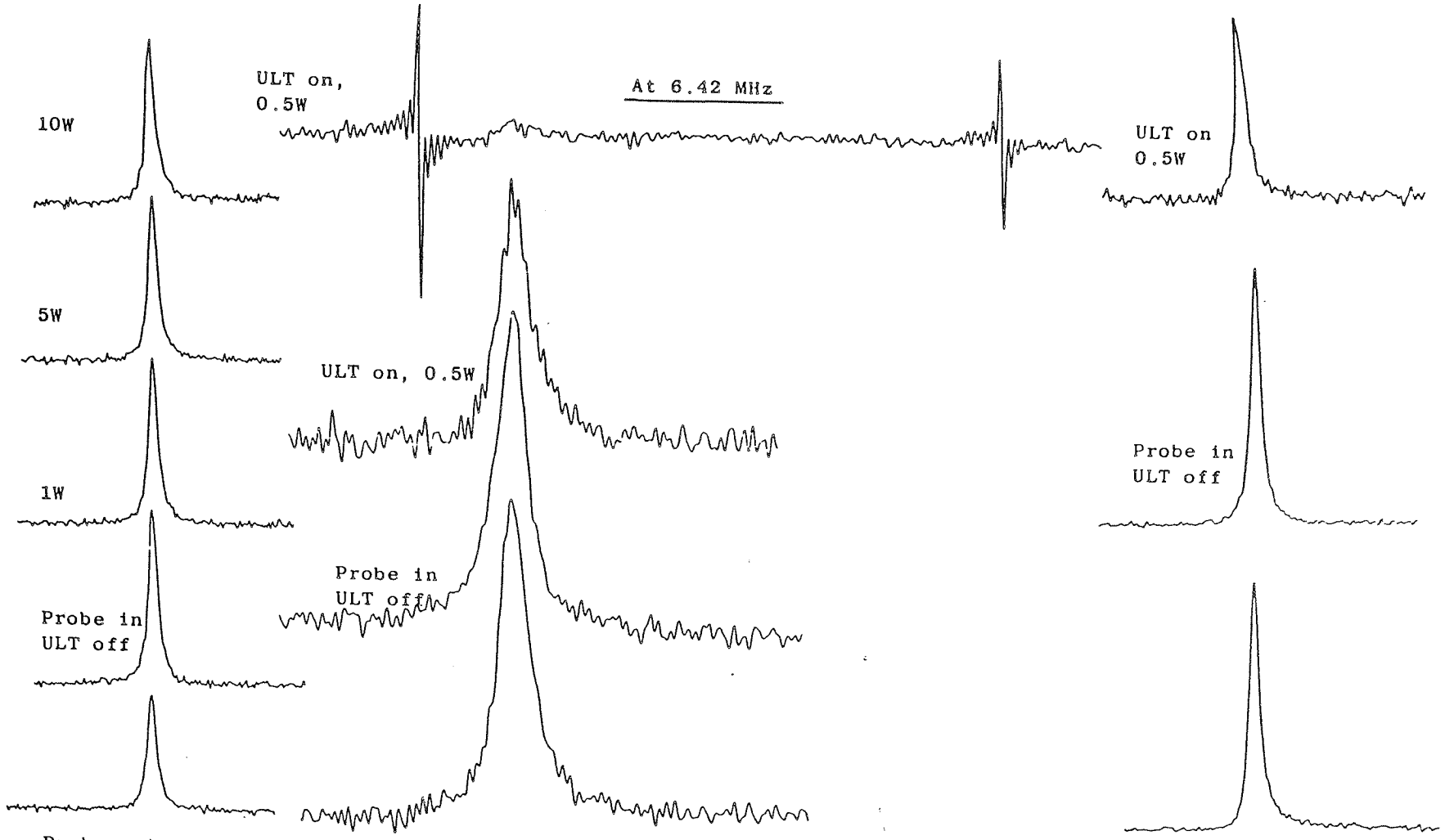

Figure 8.6: The effects of ultrasound at frequencies of 1.115, 6, 6.42 and 10MHz on nitrogen-14 NMR signals observed for an equimolar mixture of acetonitrile and deuterated chloroform. The effects shown are for applying increasing ultrasonic power from 0.5W to 10W across the transducer.

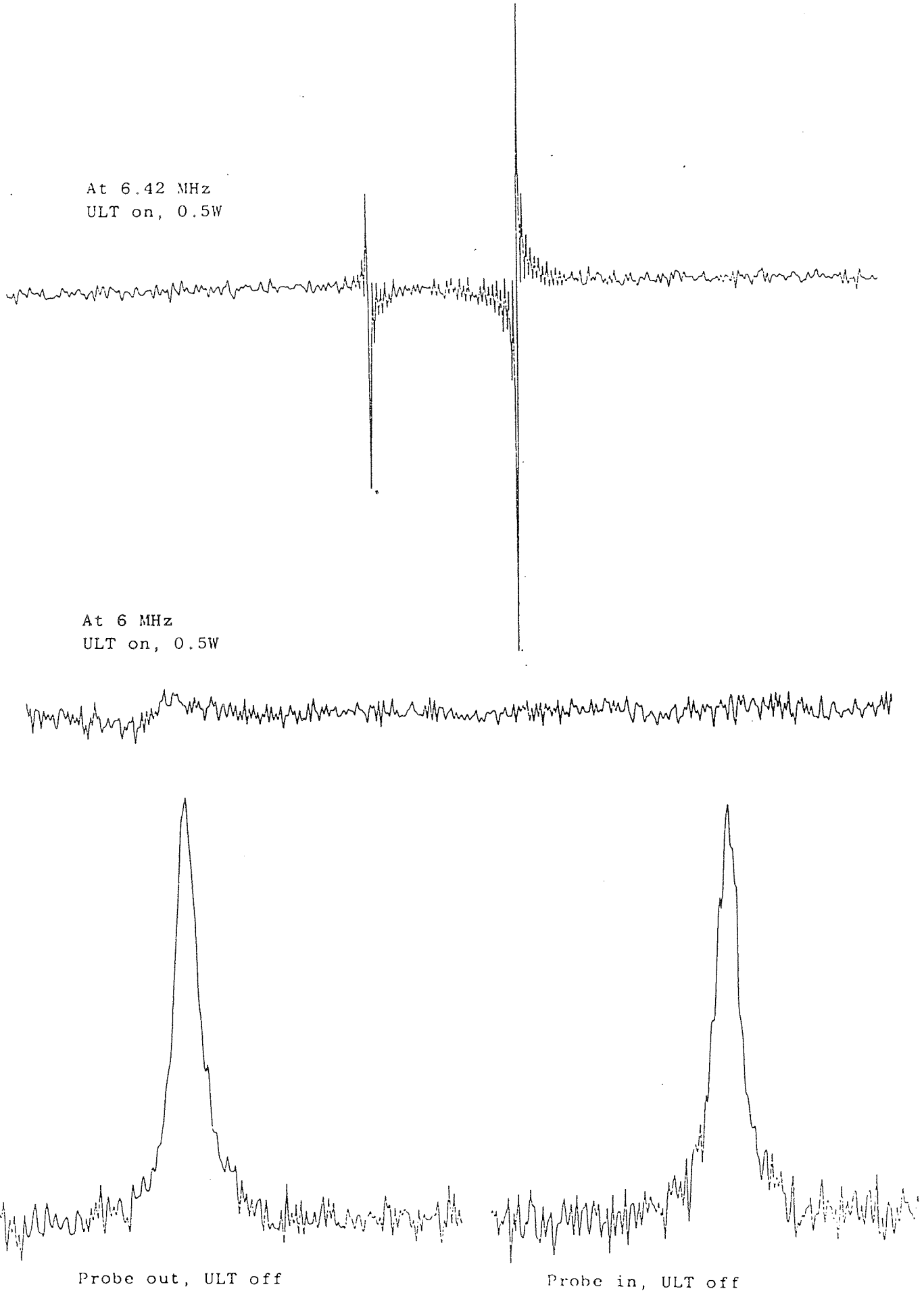

Figure 8.7: The effects of ultrasound at frequencies of 6, and 6.42MHz on nitrogen-14NMR signals observed for pure N-methylformamide. The effects shown are for applying ultrasonic power of 0.5W across the transducer.

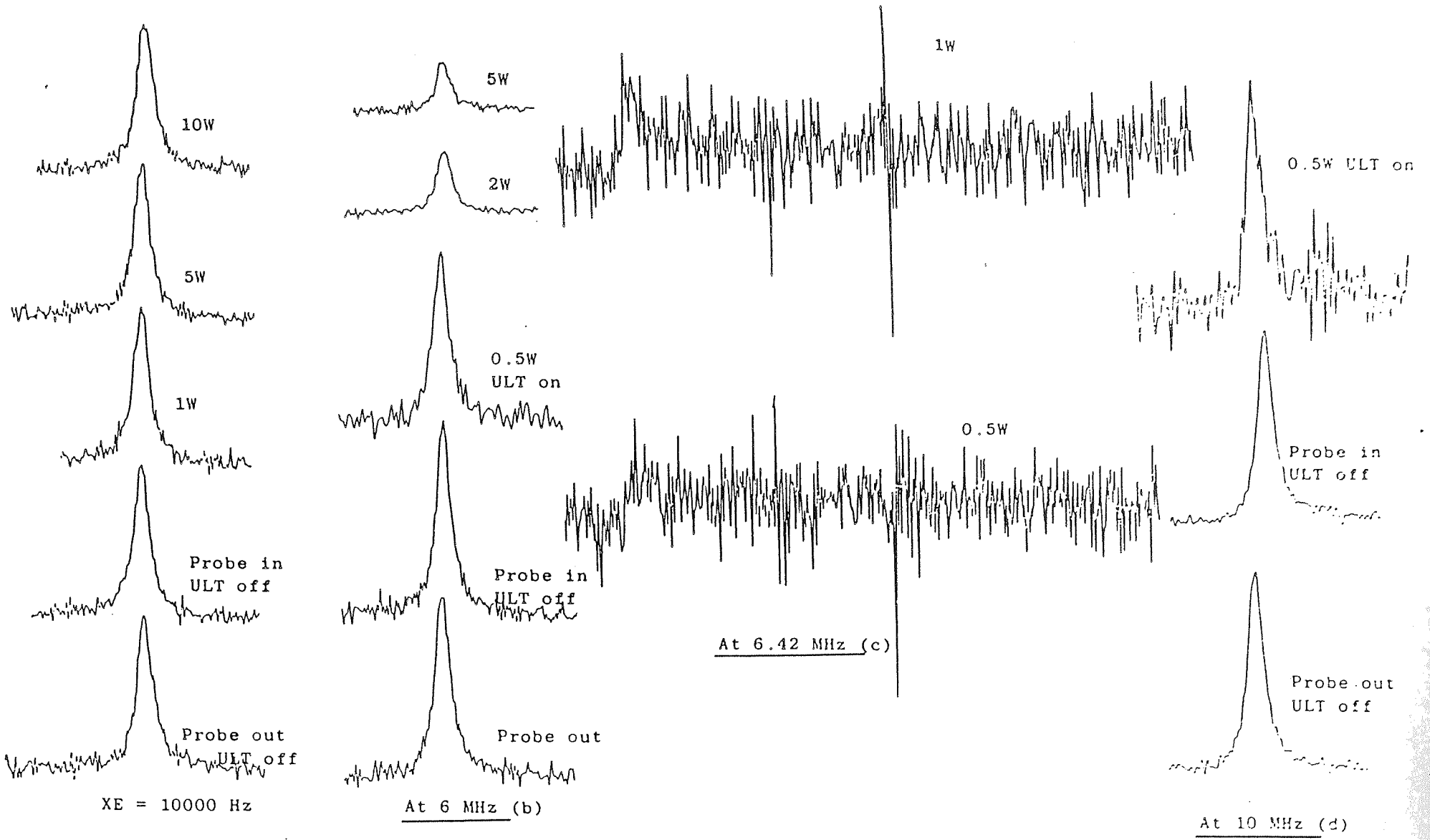

Figure 8.8 (a)-(d): The effects of ultrasound at frequencies of 1.115, 6, 6.42 and 10MHz on nitrogen-14 NMR signals observed for an equimolar mixture of N,N-dimethylformamide and deuterated chloroform. The effects shown are for ultrasonic power ranging from 0.5W to 10W across the transducer.

RESULTS OF MEASUREMENT OF THE EFFECTS OF ULTRASOUND ON NITROGEN-14 (^{14}N) SPIN-LATTICE AND SPIN-SPIN RELAXATION TIMES IN NITROGEN CONTAINING COMPOUNDS
(TABLES 8.19 - 8.21)

RELAXATION TIME MEASUREMENTS

NUCLEI UNDER INVESTIGATION: ^{14}N NMR.

NMR INSTRUMENT OBSERVATION FREQUENCY: 6.42 MHz.

SYSTEM UNDER INVESTIGATION: Acetonitrile + Chloroform(d).

MOLAR RATIO : 1:1.

90 DEGREE PULSE: 39 us. PULSE W1: 13 us. PULSE W2: 30 us.

PULSE REPETITION: 0.05 s. ACQUISITION TIME: 0.03 s. SCANS: 200.

TRANSDUCER FREQUENCY: 1.115 MHz.

METHOD OF ANALYSIS: 2pt curve fit.

	SPIN-SPIN RELAXATION TIME MEASUREMENT (T_2) LINE WIDTHS		SPIN-LATTICE RELAXATION TIME MEASUREMENTS (T_1) IN SECONDS
	MOLECULAR GROUPS: nitrogen		MOLECULAR GROUPS:
	Hz	SECONDS	nitrogen
SAMPLE PROBE OUT	106.6	2.98×10^{-3}	0.024/0.024 (rept.)
SAMPLE PROBE IN (ULT. OFF)	106.6	2.98×10^{-3}	0.023/0.024 (rept.)
ULT. ON POWER (Watts)			
0.5	106.6	2.98×10^{-3}	0.022/0.023 (rept.)
1.0	106.6	2.98×10^{-3}	0.022/0.023
2.0	106.6	2.98×10^{-3}	0.023/0.023
5.0	106.6	2.98×10^{-3}	0.023/0.025
10	106.6	2.98×10^{-3}	0.021/0.024
15	No expt. done.		

Table 8.19 : The effect of ultrasound at a frequency of 1.115MHz on nitrogen-14 nuclei (^{14}N) spin-lattice (T_1) and spin-spin relaxation times (T_2) for an equimolar mixture of acetonitrile and deuterated chloroform.

RELAXATION TIME MEASUREMENTS

NUCLEI UNDER INVESTIGATION: ^{14}N NMR.

NMR INSTRUMENT OBSERVATION FREQUENCY: 6.42 MHz.

SYSTEM UNDER INVESTIGATION: N,N-dimethylformamide + Chloroform(d).

MOLAR RATIO : 1:1.

90 DEGREE PULSE: 39 us. PULSE W1: 13 us. PULSE W2: 30 us.

PULSE REPETITION: 0.05 s. ACQUISITION TIME: 0.03 s. SCANS: 1000.

TRANSDUCER FREQUENCY: 1.115 MHz.

METHOD OF ANALYSIS: 2pt curve fit.

	SPIN-SPIN RELAXATION TIME MEASUREMENT (T_2) LINE WIDTHS	SPIN-LATTICE RELAXATION TIME MEASUREMENTS (T_1) IN SECONDS
	MOLECULAR GROUPS: nitrogen	MOLECULAR GROUPS:
	Hz SECONDS	nitrogen
SAMPLE PROBE OUT	No measurements.	No measurements.
SAMPLE PROBE IN (ULT. OFF)	No measurements.	(1) 0.157 (2) Data unreliable.
ULT. ON POWER (Watts)		
0.5	No measurements	(1) 0.028 (2) 0.013
1.0		(1) Data unreliable. (2) 0.018
2.0		(1) 0.015 (2) 0.012
5.0		(1) Data unreliable. (2) Data unreliable.
10	No expt. done.	
15	No expt. done.	

Table 8.20 : The effect of ultrasound at a frequency of 1.115MHz on nitrogen-14 nuclei (^{14}N) spin-lattice (T_1) and spin-spin relaxation times (T_2) for an equimolar mixture of N,N-dimethylformamide and deuterated chloroform.

RELAXATION TIME MEASUREMENTS

NUCLEI UNDER INVESTIGATION: ^{14}N NMR.

NMR INSTRUMENT OBSERVATION FREQUENCY: 6.42 MHz.

SYSTEM UNDER INVESTIGATION: N,N-dimethylacetamide + Chloroform(d).

MOLAR RATIO : 1:1.

90 DEGREE PULSE: 39 us. PULSE W1: 13 us. PULSE W2: 30 us.

PULSE REPETITION: 0.05 s. ACQUISITION TIME: 0.03 s. SCANS: 1000.

TRANSDUCER FREQUENCY: 1.115 MHz.

METHOD OF ANALYSIS: 2pt curve fit.

	SPIN-SPIN RELAXATION TIME MEASUREMENT (T_2) LINE WIDTHS		SPIN-LATTICE RELAXATION TIME MEASUREMENTS (T_1) IN SECONDS
	MOLECULAR GROUPS: nitrogen		MOLECULAR GROUPS:
	Hz	SECONDS	nitrogen
SAMPLE PROBE OUT	346	9.18×10^{-4}	No measurements.
SAMPLE PROBE IN (ULT. OFF)	346	9.18×10^{-4}	0.051
ULT. ON POWER (Watts)			
0.5	346	9.18×10^{-4}	0.044/ Data unreliable.
1.0	346	9.18×10^{-3}	0.027/0.028
2.0	346	9.18×10^{-3}	0.018/0.024
5.0	346	9.18×10^{-3}	0.019/0.024
10	346	9.18×10^{-3}	0.019/0.016
15	No expt. done.		

Table 8.21 : The effect of ultrasound at a frequency of 1.115MHz on nitrogen-14 nuclei (^{14}N) spin-lattice (T_1) and spin-spin relaxation times (T_2) for an equimolar mixture of N,N-dimethylacetamide and deuterated chloroform.

(5) A saturated solution of ammonium chloride in deuterated dimethyl-sulfoxide containing a trace of (concentrated) hydrochloric acid

Measurement of the effects of ultrasound NMR spin-lattice or spin-spin relaxation times for the protons and the nitrogen nuclei were not performed as this resulted in changes to the observed fine structure. However, the changes observed in the fine structure are of particular interest and therefore need to be discussed.

These experiments are of particular interest for several reasons, which are:

(i) The nitrogen observation frequency in the NMR spectrometer is 6.42 MHz. Thus, this allows the investigation of the effects of ultrasound near, at the exact resonance, and above the resonant frequency.

(ii) Due to the tetrahedral symmetry of the ammonium ion there exists a spherical charge distribution and therefore the species has a zero electric field gradient. This therefore allows the observation of sharp NMR lines and the observation of the nitrogen-hydrogen 'J' coupling (N-H) which is in the order of 50 Hz. Thus, it allows the investigation of effects of ultrasound on the nitrogen-hydrogen coupling.

(1) Proton (^{1}H) NMR Results

Observation of the effects of ultrasound on the proton nuclei using ultrasonic frequencies of 6, 6.42 and 10 MHz.

Figure 8.10(a) shows a large broad NMR signal arising from the protons in the ammonium chloride, without the application of ultrasound. The large broad signal is due to the fact that the rate of transitions among the spin-states of the nitrogen molecules is similar to the time required for proton spin transitions. Furthermore, the life time of the spin-states in this case, is similar to the NMR timescale, such that an averaging of spins occur. Figure 8.10(b) and (c) shows the effects of adding a trace of concentrated hydrochloric acid. The addition of acid now affects the proton exchange between that of a proton from the ammonium ion and that of a proton from the hydrochloric acid. If this exchange rate is slow, such that the rate of transitions among the spin-states of the nitrogen molecules is now slow compared to the time required for a proton transition, then

a coupling between the nitrogen nuclei and the proton is observed. Thus three spectral lines arising from the three different spin states of the nitrogen nuclei.

Figure 8.10(d) shows the effects of the presence of an ultrasonic probe in an NMR tube containing the above liquid mixture.

(i) At 6 MHz: Using a large ultrasonic power of 15W causes the initially observed fine structure to change to some other new fine structure (Figure 8.10(e)). Observation of this new fine structure is not understood and remains to be explained. However, two entirely separate views have been visualised: The first is that the observed fine structure is thought to arise from some form of nuclear spin transitions, of the form observed in nuclear acoustic resonance. Further explanation of this view will be presented following more experimental results.

Secondly, if one measures the total width of N-H spectral lines at half-height with all the fine structure, for both experiments with ultrasound "on" and "off", it shows that the total width of the N-H spectral lines has approximately doubled. In addition, it appears that for the ultrasound "on" experiment, each of the three N-H couplings again couple with the nitrogen giving rise to more NMR signals which appear to overlap. This overlap is shown diagrammatically in Figure 8.10(f). Furthermore, the nature for observation of the fine structure for the acid/water peak (for the ultrasound "on" experiment) is not understood and cannot be explained in the NMR terms. Thus, this leads to the conclusion that the observed effects of ultrasound on the protons of ammonium chloride may be as a direct result of electronic, ultrasound and NMR coupling.

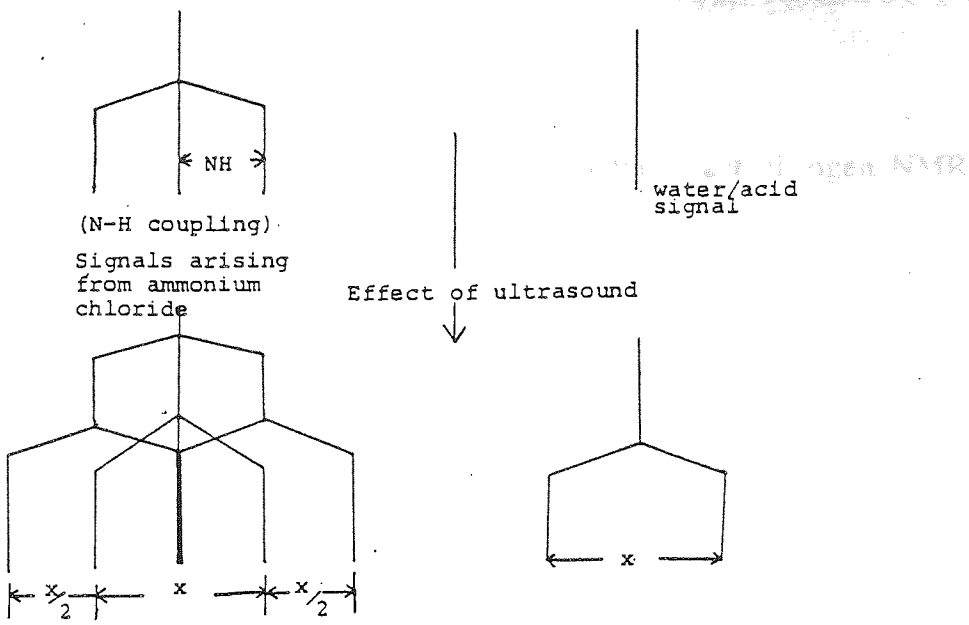

Figure 8.10(f): Effects of ultrasound using an ultrasonic frequency of 6 MHz and power of 15W

Repetition of a similar experiment was performed with increasing ultrasonic power for a new sample. The results are shown in Figure 8.10(g)-(h). These results show that operating at low ultrasonic powers and using small NMR nutation angles (12 μs) does not show any effect on the N-H coupling, but does show a decrease in the signal intensities. Performing the same experiments but using larger nutation angles (24 μs) with the application of 10W of power, now destroys the previously observed fine structure. The results emphasise that the observed signals are genuine NMR signals. However, the tiny splittings on each of the spectral lines of the N-H couplings and the water/acid peak, which are approximately 6 Hz apart, may be due to some electronic ultrasonic and NMR coupling. In addition, the fact that the N-H coupling does not appear to have changed provides further proofthat there is some of electronic ultrasound and NMR coupling. Alternatively, it was suggested that the fine structure was observed due to nuclear acoustic resonance. The proton and nitrogen nuclei have a NMR spectrometer resonance frequency of 89.99 MHz and 6.42 MHz respectively. The use of an ultrasonic frequency of 6 MHz which is close to the nitrogen resonant frequency, may have caused some changes to the nitrogen spin-transitions. The actual spin transition selection rules cannot be changed, but the probability and the rate of spin transitions occur may have been influenced by the presence of ultrasound. This explanation was later ruled out by performing experiments

using an ultrasonic frequency of 6.42 MHz, which is nowthe exact nitrogen NMR spectrometer resonant frequency.

(ii) At 6.42 MHz: Performing similar experiments to those described in (i) again shows similar behaviour to that observed for (i). This is, using ultrasonic powers from 2W to 8W the NMR signals start to deteriorate (Figure 8.11a). At higher ultrasonic powers the initially observed fine structure disappears with the appearance of a new fine structure which shows a dependance on the ultrasonic power. The results show that with increasing ultrasonic power the number of fine splittings increases (Figure 8.11(b) - 8.11(d)).

It was initially visualised that at a frequency of 6.42 MHz the N-H couplings would have totally disappeared and give rise to a single line similar to that observed in decoupling experiments. These results also suggest that saturation of the nuclear spins via nuclear acoustic resonance had not taken place.

(iii) At 10 MHz: Repetition of the same experiment as in (i) using 5W of ultrasound power showed a total loss of fine structure and the appearance of two broad signals, one arising from the protons in the ammonium ion and the other from the acid/water (Figure 8.12(a) and (b)). The explanation for such behaviour is not understood.

(2) NITROGEN (^{14}N) NMR RESULTS

Observation of the effects of ultrasound on the nitrogen-14 nuclei, using ultrasonic frequencies of 1.115 MHz, 6.42 and 10 MHz.

Figure 8.13(a), (b) and (c) shows the nitrogen-14 spectra without the ultrasonic probe inside the solution, with the ultrasonic probe in the solution with the same number of scans, and with increasing the scans from 100 to 1000 for the same systems. The results show that by placing an ultrasonic probe inside the ammonium chloride solution had increased the noise levels enormously relative to the noise level for experiments without the ultrasonic probe in the solution. Furthermore, by increasing the number of

scans from 100 to 1000 did not improve the signal to noise levels a great deal and still appeared to be worse. Thus, no further experiments were performed.

(i) At 1.115 MHz: Figure 8.14(a), (b) and (c) shows the effects of using a 1.115 MHz, ultrasonic probe. Figure 8.14(a) shows the NMR spectrum without the ultrasonic probe. Figure 8.14(b) and (c) now shows the effects of placing the ultrasonic probe into the liquid and performing the experiment using 10W, respectively. The results shows slight changes in intensities but none to the effects of N-H coupling constants.

(ii) At 6.42 MHz: Performing experiment at this frequency shows a total signal saturation with the appearance of two radio frequency beat patterns. This may be either due to a direct saturation of the nuclear spins such that all the transition energy levels are equally populated. However, this experiment gives results which are contrary to results obtained from experiments previously performed on proton NMR using ultrasonic frequency of 6.42 MHz, which showed no effects on the N-H coupling (for which it was visualised that a form of decoupling experiment using ultrasound should have proceeded). Alternatively, it could be due to electronic signal saturation by ultrasound in the NMR transmitter and receiver coils (Figure 8.15).

(iii) Attempting to perform the same experiment using a 10 MHz ultrasonic probe shows that by just placing the probe into the NMR tube containing the solution, decreases the signal to noise ratio enormously such that, the experiment was abandoned (Figure 8.16(a) and (b)).

The results of experiments performed for the proton and nitrogen NMR shows that the effects of nuclear acoustic resonance,though unlikely, cannot be easily discarded as one of the possible mechanisms for the observation of the fine splittings. In addition, in ionic solvents the problem of radio frequency beat signals and large signal loss needs to be eliminated before further definite conclusions can be elucidated.

RESULTS OF THE EFFECTS OF ULTRASOUND ON PROTON (^{1}H) ON AMMONIUM CHLORIDE (FIGURES 8.9 - 8.12)

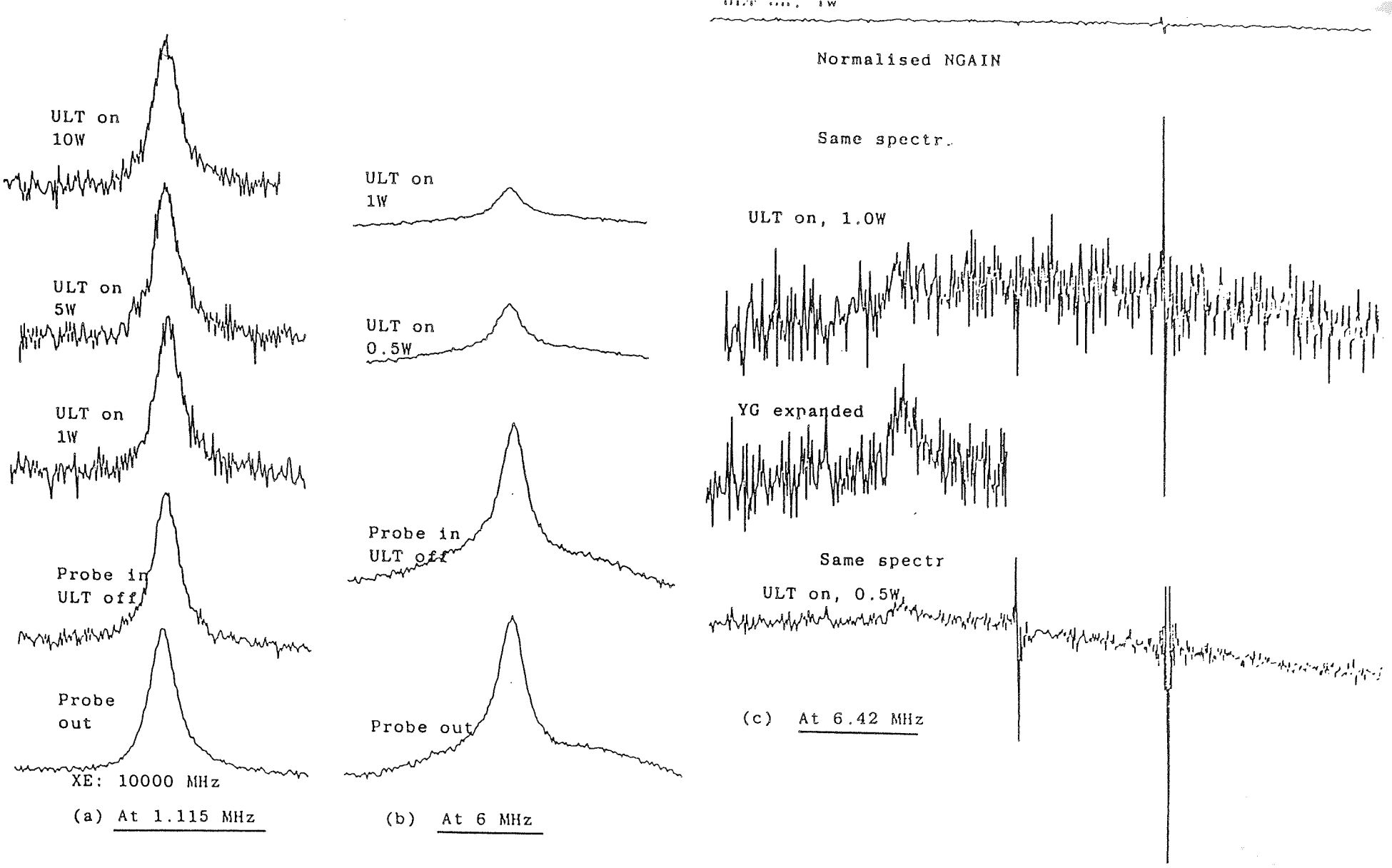

Figure 8.9 (a)-(c): The effects of ultrasound at frequencies of 1.115, 6 and 6.42MHz on nitrogen-14 NMR signals observed for an equimolar mixture of N,N-dimethylacetamide and deuterated chloroform. The effects shown are for applying ultrasonic power ranging from 0.5W to 10W across the transducer.

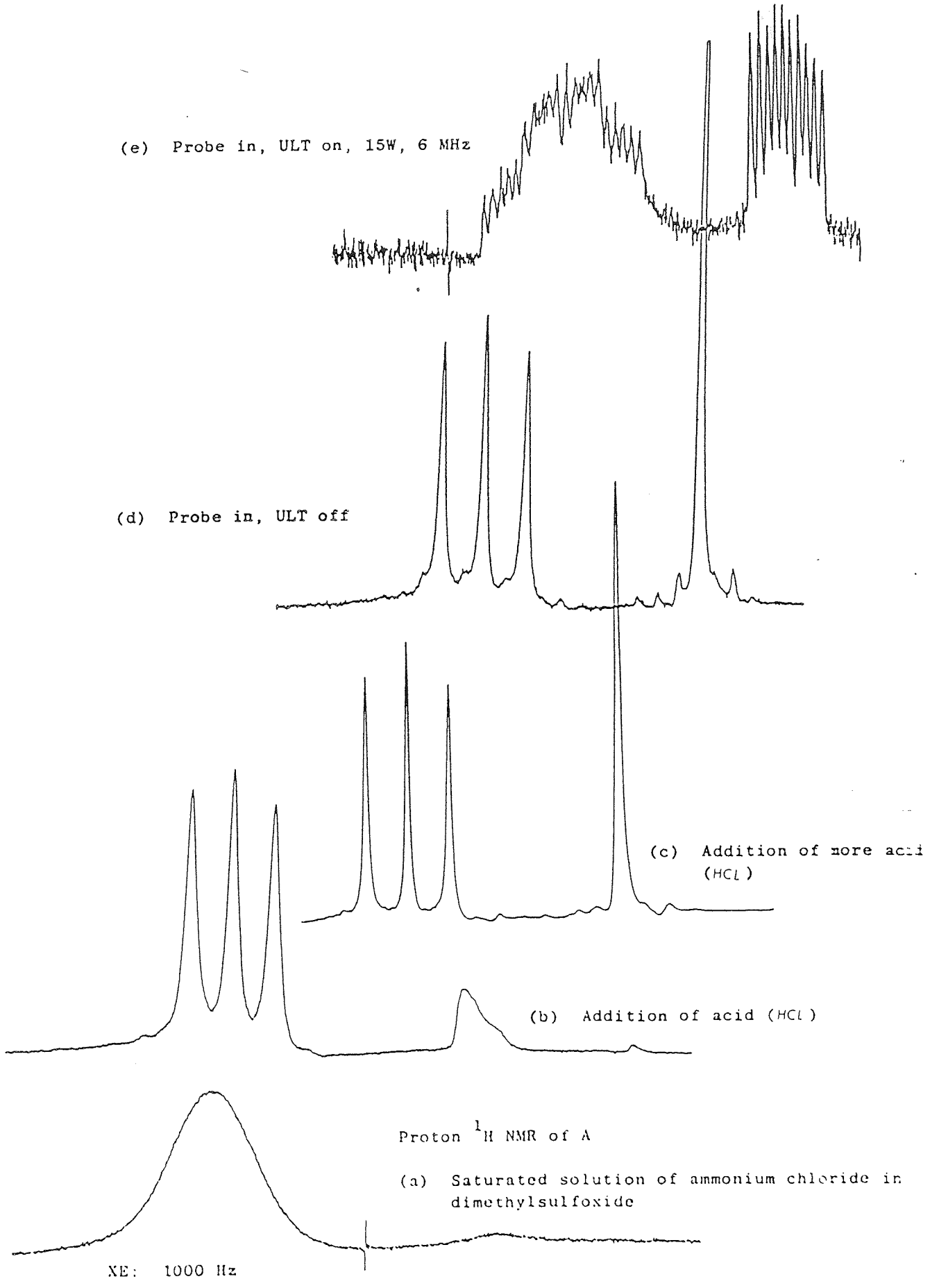

Figure 8.10 (a)-(e): ^{1}H NMR signals arising from a saturated solution of ammonium chloride in deuterated dimethylsulfoxide containing a trace of hydrochloric acid. Figure 8.10(e) shows the effects of ultrasound at a frequency of 6MHz and applying 15W across the transducer.

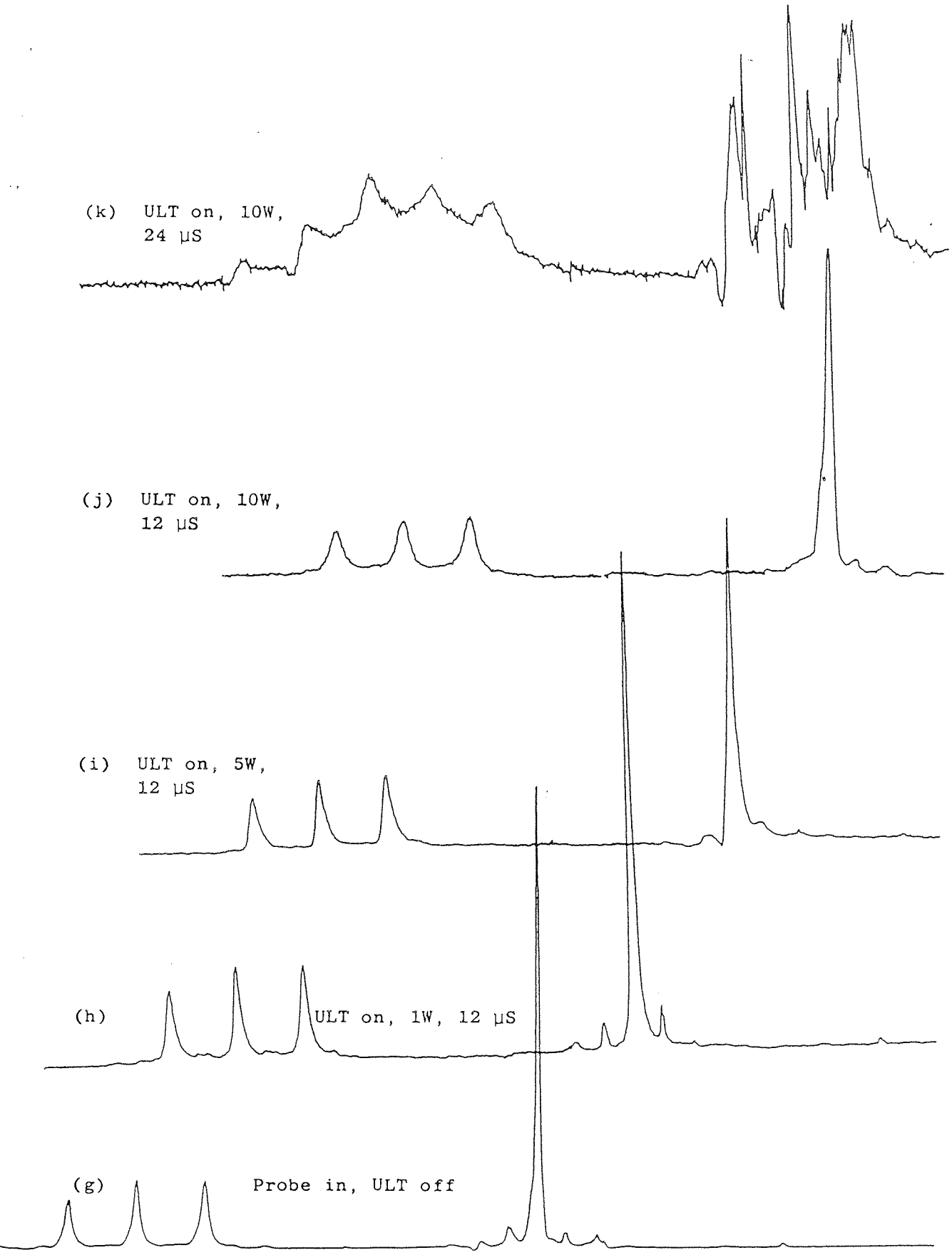

Figure 8.10 (g)-(h): The effects of ultrasound at a frequency of 6MHz on proton NMR signals observed for a saturated solution ammonium chloride in deuterated dimethylsulfoxide containing a trace of hydrochloric acid. The effects shown are for applying increasing power ranging from 1W to 10W across the transducer and changing the NMR pulse width (us).

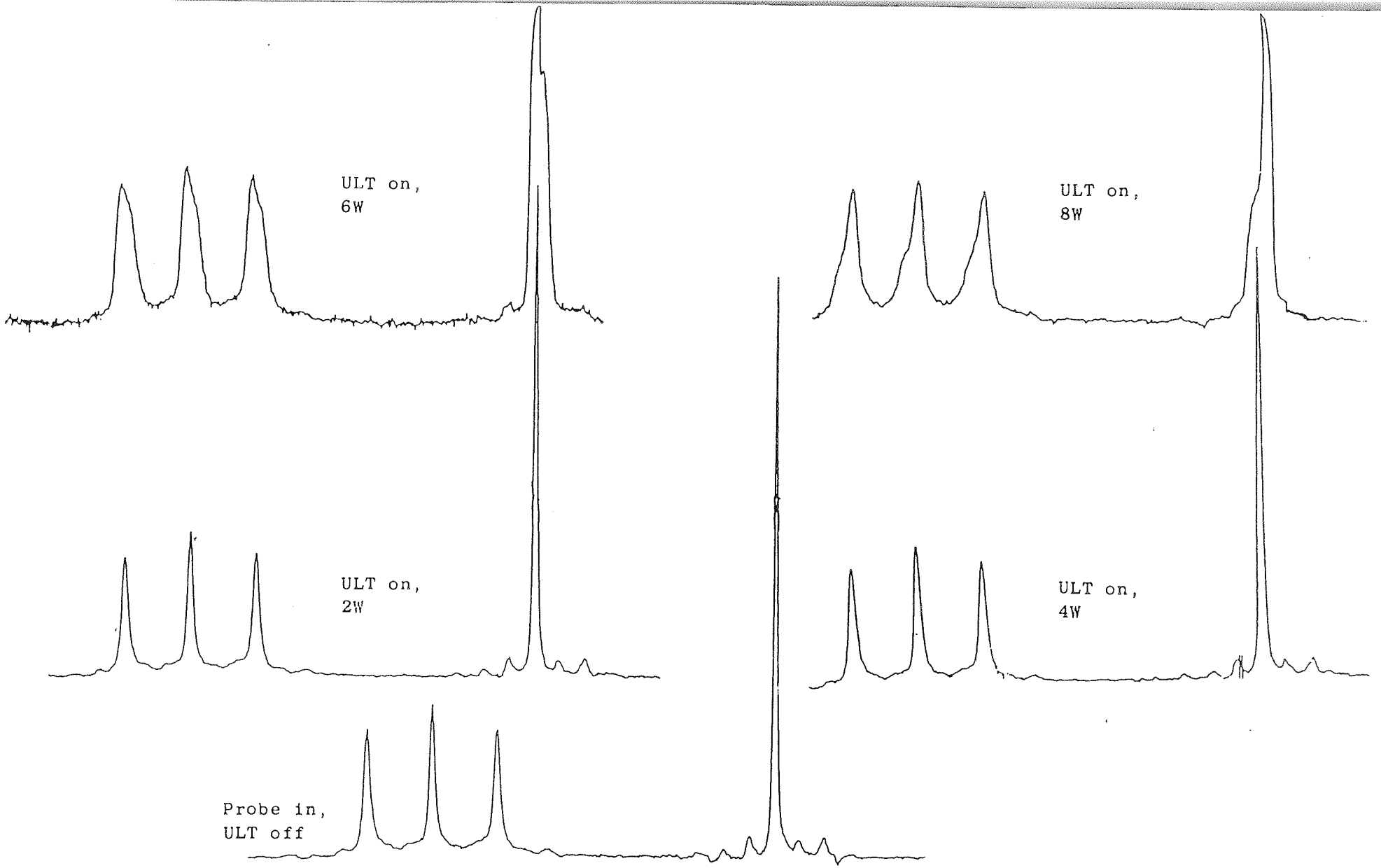

Figure 8.11(a): The effects of ultrasound at a frequency of 6.42MHz on proton NMR signals observed for a saturated solution ammonium chloride in deuterated dimethylsulfoxide containing a trace of hydrochloric acid. The effects shown are for applying increasing power ranging from 2W to 8W across the transducer.

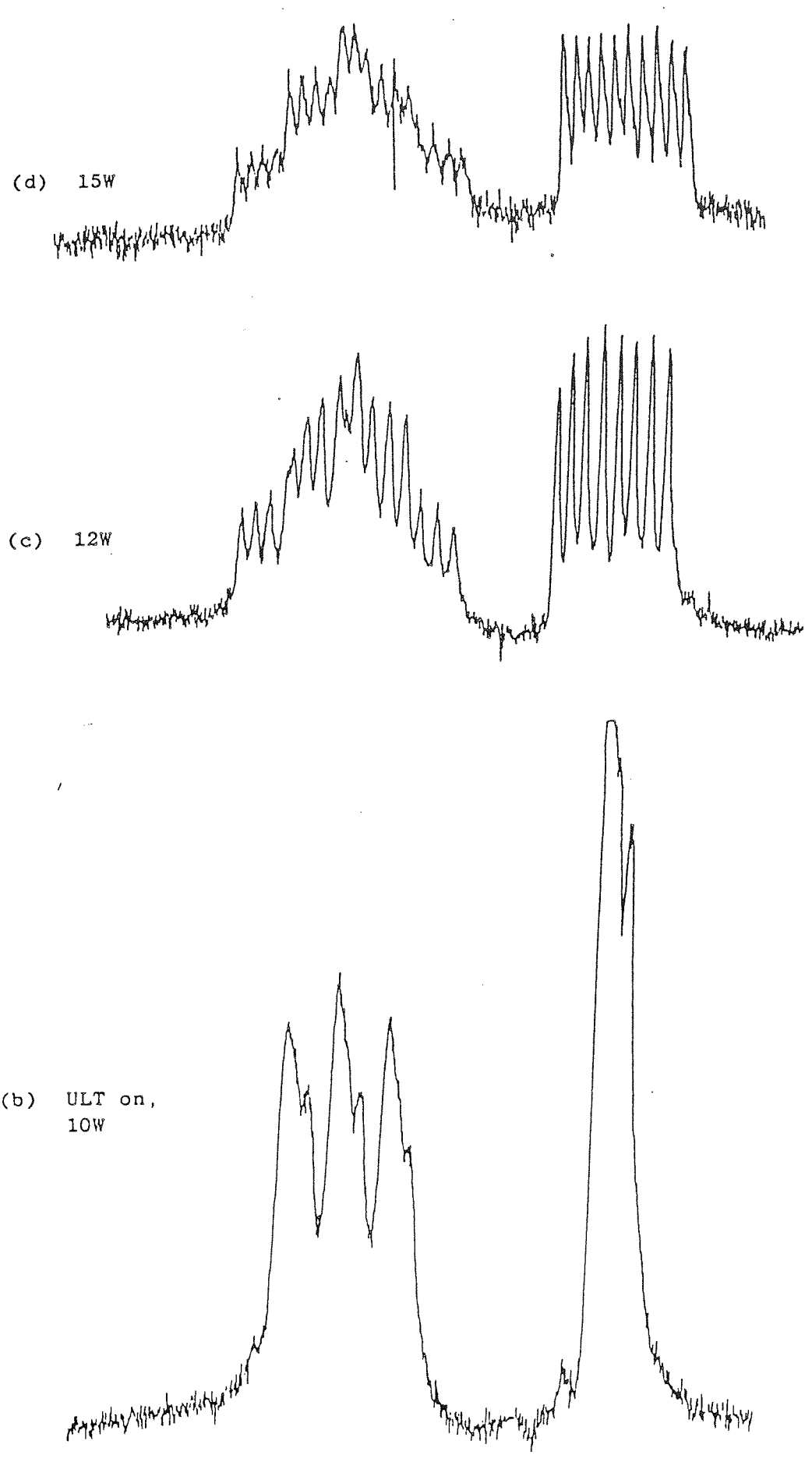

Figure 8.11(b)-(d) contd...: The effects of ultrasound at a frequency of 6.42MHz on proton NMR signals observed for a saturated solution ammonium chloride in deuterated dimethylsulfoxide containing a trace of hydrochloric acid. The effects shown are for applying increasing power ranging from 10W to 15W across the transducer.

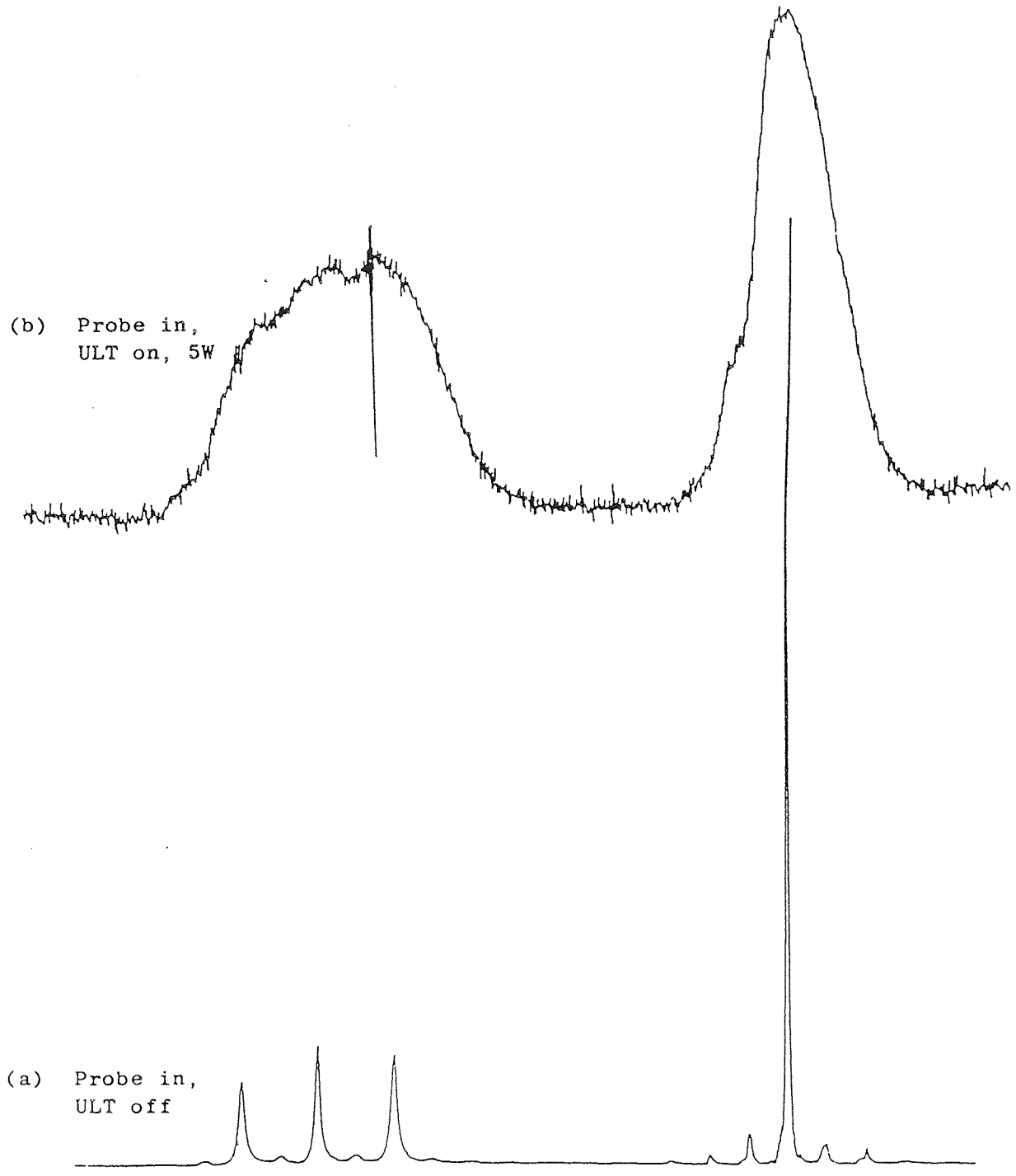

Figure 8.12(a) & (b) : The effects of ultrasound at a frequency of 10MHz on proton NMR signals observed for a saturated solution ammonium chloride in deuterated dimethylsulfoxide containing a trace of hydrochloric acid. The effects shown are for applying 5W across the transducer.

RESULTS OF THE EFFECTS OF ULTRASOUND ON NITROGEN-14 NUCLEI (^{14}) IN AMMONIUM CHLORIDE (FIGURES 8.13 - 8.16)

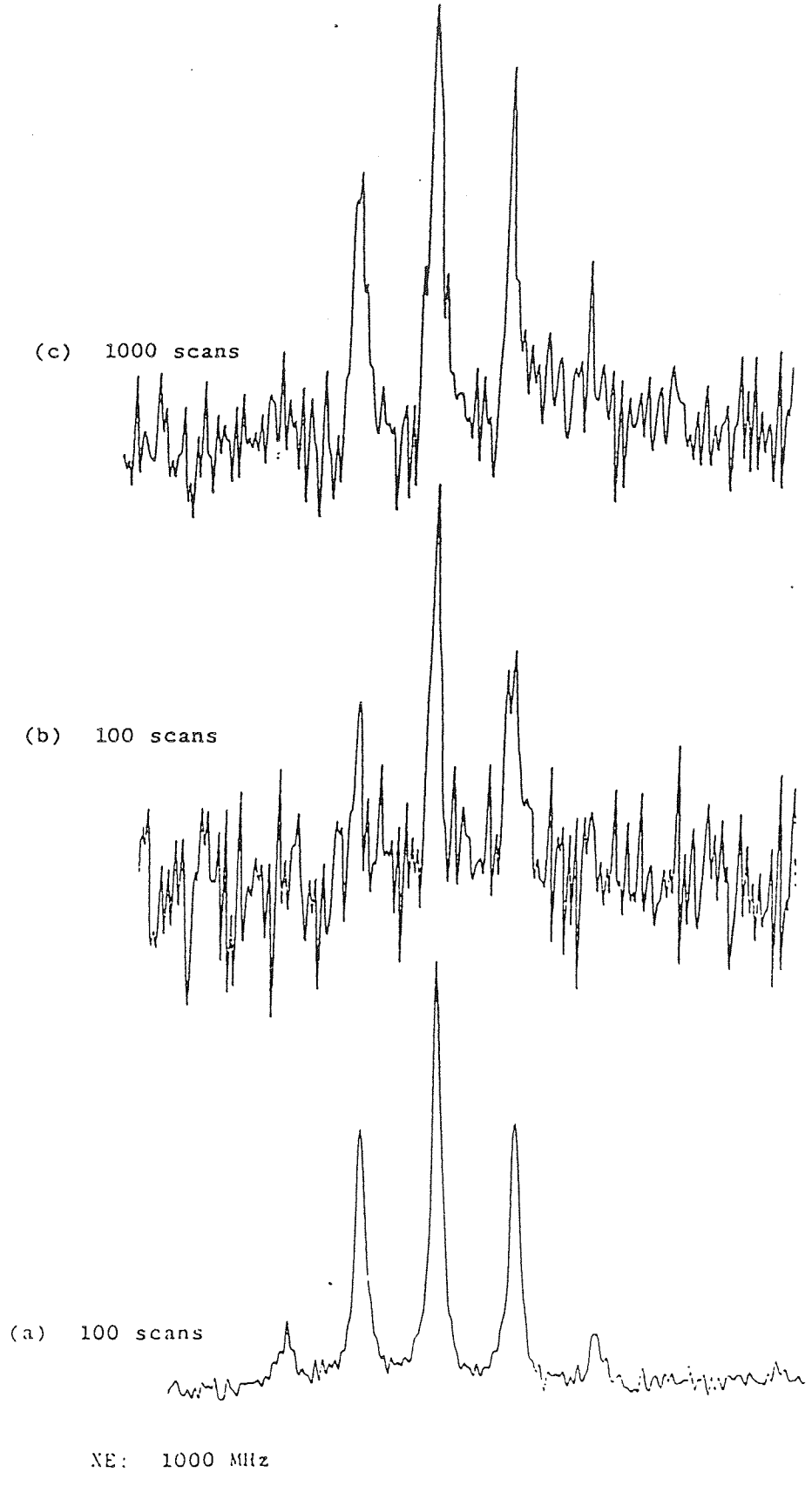

Figure 8.13(a),(b) and (c) : Nitrogen-14 NMR spectra, without and with an ultrasonic probe in a saturated solution ammonium chloride in deuterated dimethylsulfoxide containing a trace of hydrochloric acid with the same number of scans, (a) and (b), and with increasing the number of scans from 100 to 1000.

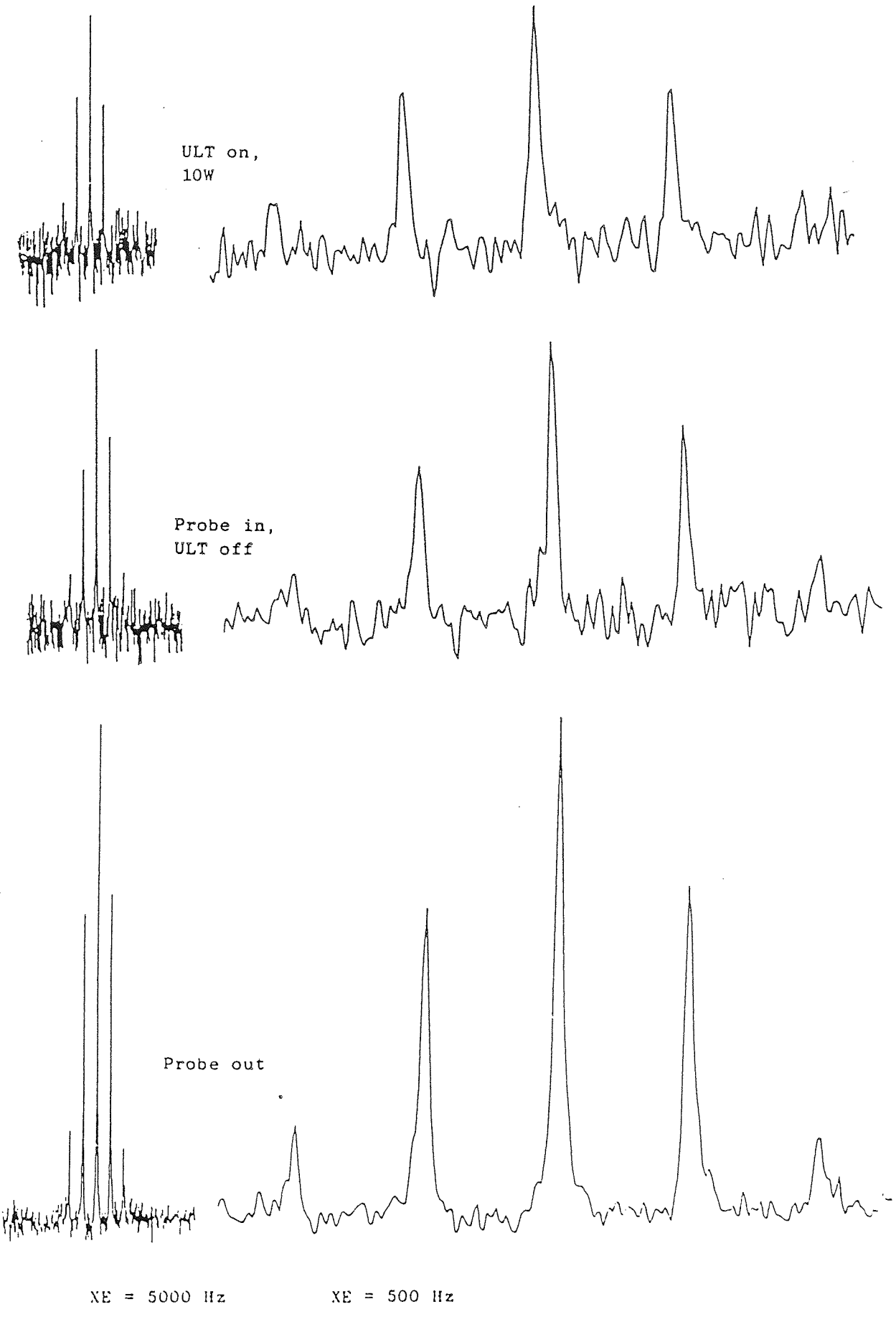

Figure 8.14(a), (b) & (c) : The effects of ultrasound at a frequency of 1.115MHz on nitrogen-14 NMR signals observed for a saturated solution ammonium chloride in deuterated dimethylsulfoxide containing a trace of hydrochloric acid. The effects shown are for applying 10W across the transducer.

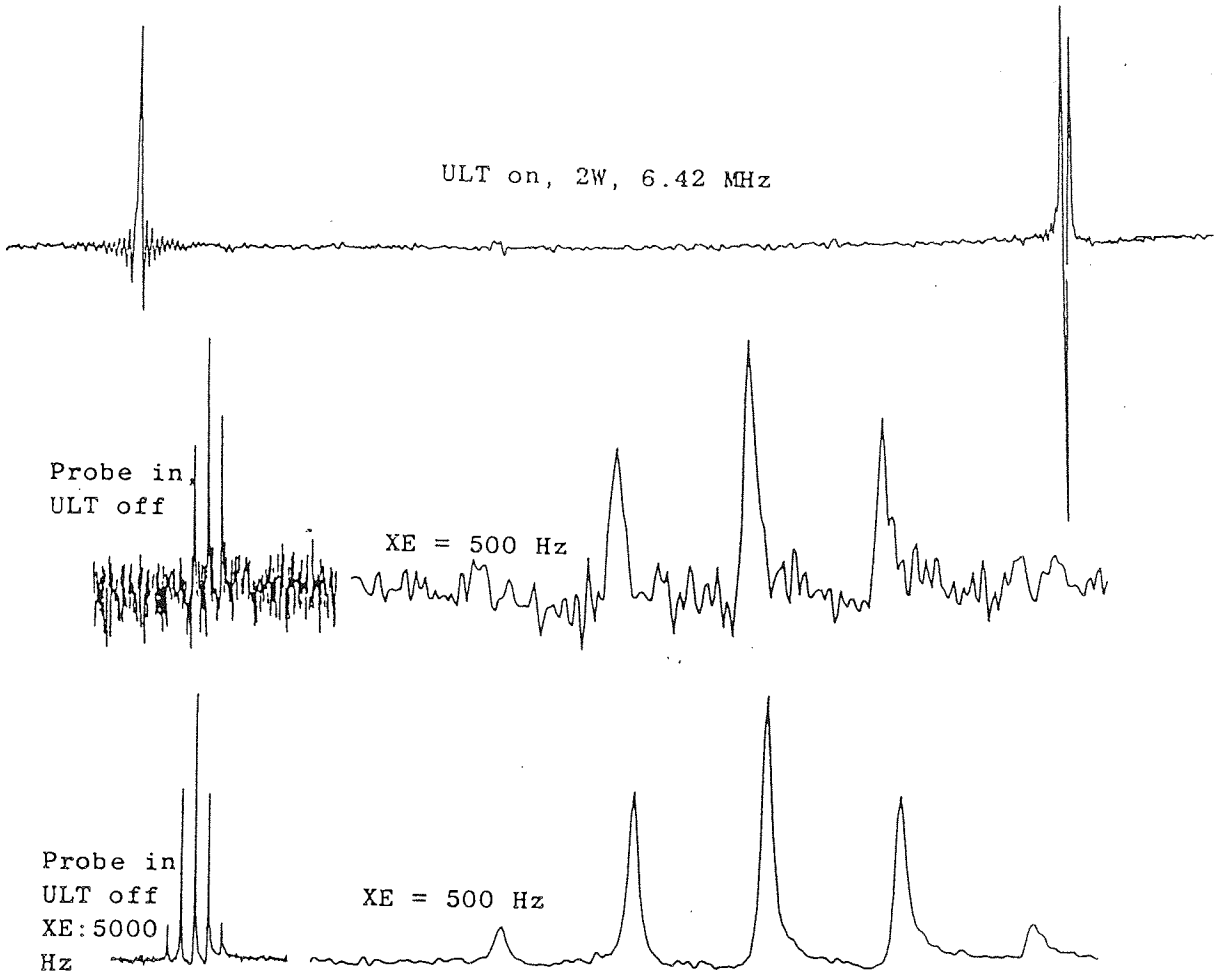

Figure 8.15: The effects of ultrasound at a frequency of 6.42MHz on nitrogen-14 NMR signals observed for a saturated solution ammonium chloride in deuterated dimethylsulfoxide containing a trace of hydrochloric acid. The effects shown are for applying 2W across the transducer.

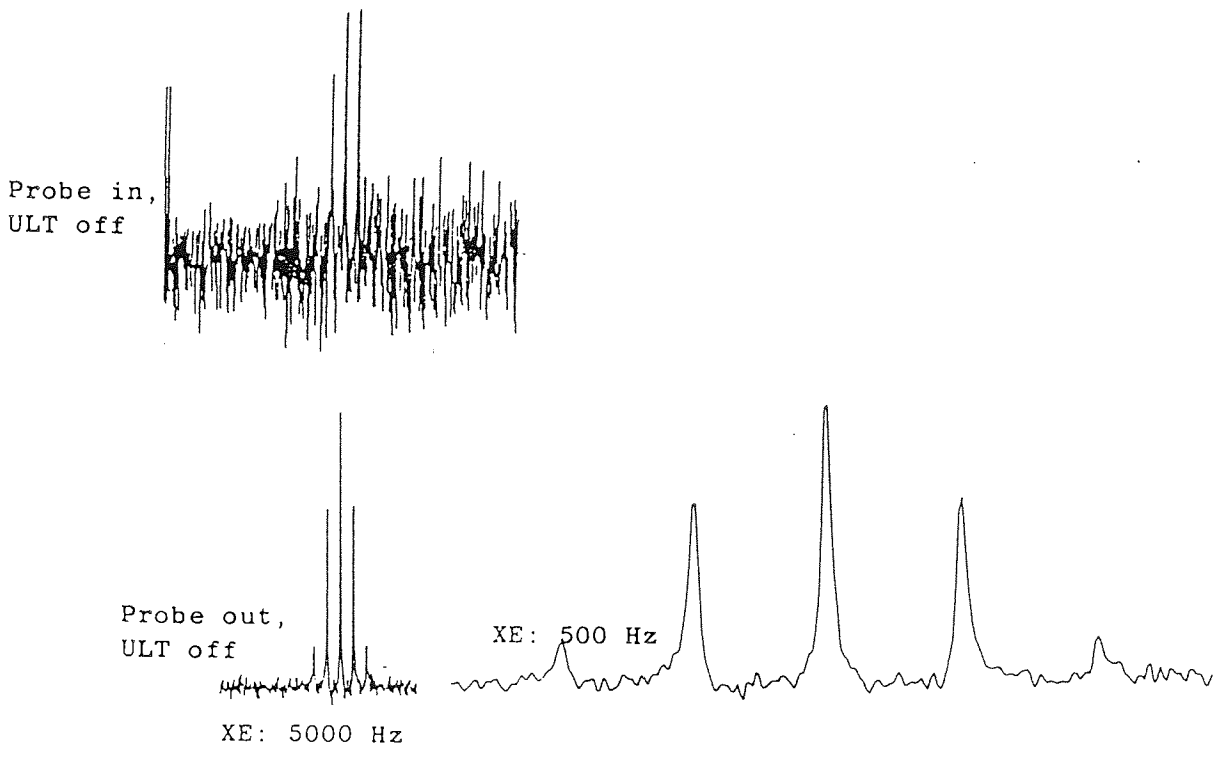

Figure 8.16: The effects of introducing a 10MHz ultrasonic probe into a NMR tube containing a saturated solution of ammonium chloride in deuterated dimethylsulfoxide and a trace of hydrochloric acid.

8.1(d) Experiments performed to observe the effects of using ultrasonic frequency of 20 KHz on molecular motion

Chapter Six presents theories and ideas which suggest that the effects of ultrasound on spin-lattice and spin-spin relaxation times would ideally be observed using ultrasonic frequencies in the mega-hertz region. This section deflects attention from using ultrasonic frequencies in the mega-hertz region to observing the effects of 20 KHz on molecular motion and other phenomena. The effects of acoustic cavitation will not be discussed in this section.

There were principally three types of experiments performed. These were:

(a) To observe the effects of ultrasound at 20 KHz on proton and nitrogen NMR spin-lattice and spin-spin relaxation times, and on the NMR lineshapes. The experiments were performed on N,N-dimethylformamide, N,N-dimethylacetamide and pyridine.

The choice for performing experiments on these samples were two-fold, being:

(i) It is well known that the effects of acoustic cavitation produces large heating effects. Thus, effects due to absorption of ultrasound in liquids and heat generated would become indistinguishable. However, through experiments using the mentioned chemical samples, the effects of temperature can easily be shown by changes to their NMR lineshapes.

(ii) By observing the nitrogen-14 using NMR, one can observe the effects of ultrasound at 20 KHz, on the nitrogen-14 NMR lineshapes which are directly related to spin-spin relaxation times.

(b) To observe the effects of ultrasound at 20 kHz on aluminium phosphate suspended in silicone oil.

(c) To observe the effects of ultrasound at 20 kHz on ionic solvents such as potassium chloride dissolved in water.

8.1(e) Effects of ultrasound at 20 KHz, on proton and nitrogen NMR, in terms of its effects on spin-lattice and spin-spin relaxation times

(a) (i) The results of performing ultrasonic experiments on the proton NMR of all the three chemical samples specified show that as the ultrasonic power is increased, changes in the fine structure are observed. The results presented in Figure 8.17(a) are for N,N-dimethylacetamide. In addition, these results also represent a typical behaviour observed for all the three samples investigated.

Experiments to observe the effects of temperature changes were also performed on the same three chemical samples. Figure 8.17(b) presents results of raising the temperature electrically via a variable temperature control unit in the spectrometer, on a sample of N,N-dimethylacetamide.

Comparison of Figure 8.17(a) to 8.17(b), the results show similar changes in the fine structure of N,N-dimethylacetamide. The collapse of the two methyl signals into a single line is due to the fact that the rate of rotational motion of the methyl groups about the nitrogen nuclei has increased, such that, on the NMR time scale, the two different conformations are indistinguishable. Thus, the rotational energy barrier for the two conformations has been overcome. In the first part of the experiment, the rotational energy barrier has been overcome by the energy absorbed from the ultrasound. This may be due to a direct influence on the rotational energy barrier as discussed in Chapter Five, and also as a result of acoustic cavitation which shows that as the ultrasonic power is raised, the temperature of the system investigated also increases. This latter conclusion also explains why similar changes are observed for the systems investigated for which the temperature was raised electrically.

(ii) Experiments performed similarly to that in (i) on the nitrogen nuclei on the three samples showed that with increasing ultrasonic power the nitrogen NMR linewidth decreases. Performing a temperature experiment on the same three samples, shows that as

the temperature is increased the NMR linewidth decreases. These results suggest that spin-spin relaxation times increase with increasing ultrasonic power. This again is as a direct result of acoustic cavitation which generates large heating effects. Figures 8.18(a) and (b), again represent a typical example of the effects of increasing ultrasound power using an ultrasonic frequency of 20 kHz, and the temperature effects, respectively, on the nitrogen NMR linewidths, for a neat sample of N,N-dimethylacetamide. Furthermore, the NMR spectra reveals that the noise level had increased.

RESULTS OF THE EFFECTS OF ULTRASOUND AT 20 KHz ON PROTON (^{1}H) AND NITROGEN-14 (^{14}N) IN NITROGEN CONTAINING COMPOUNDS (FIGURES 8.17 - 8.18)

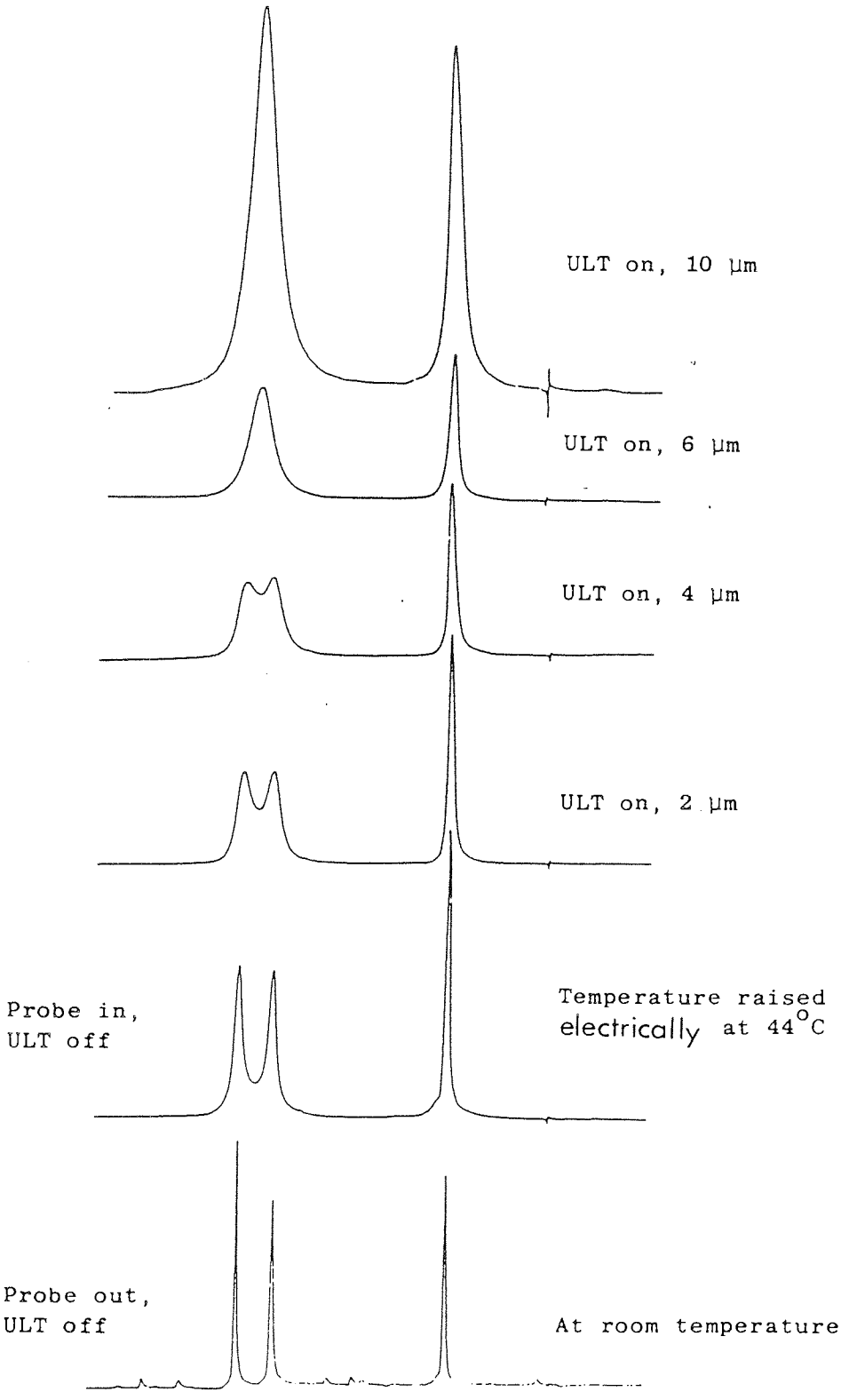

Figure 8.17 (a): The effects of ultrasound at a frequency of 20KHz with increasing ultrasonic power on proton NMR signals observed for N,N-dimethylacetamide.

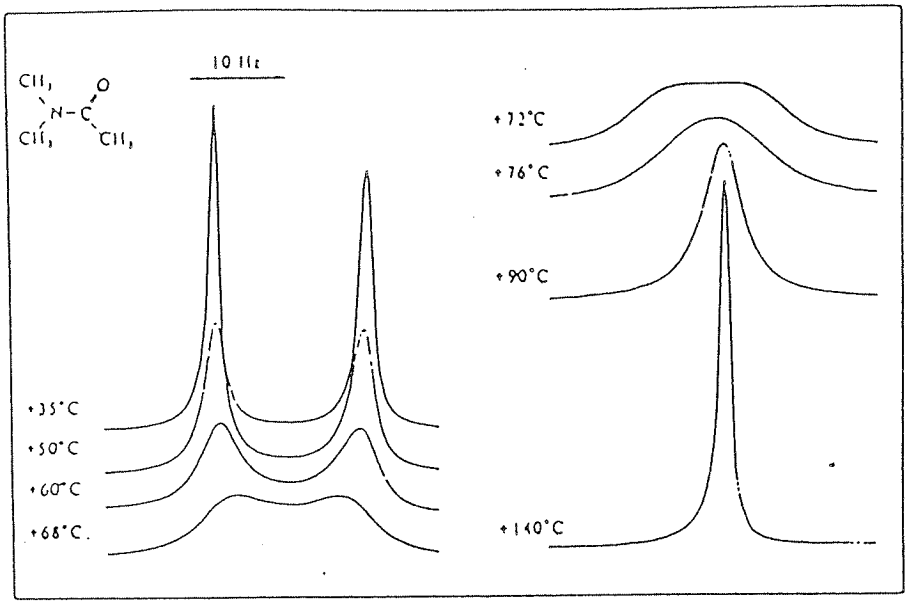

Figure 8.17 (b): The effects of temperature on the proton NMR signals observed for N,N-dimethylacetamide.

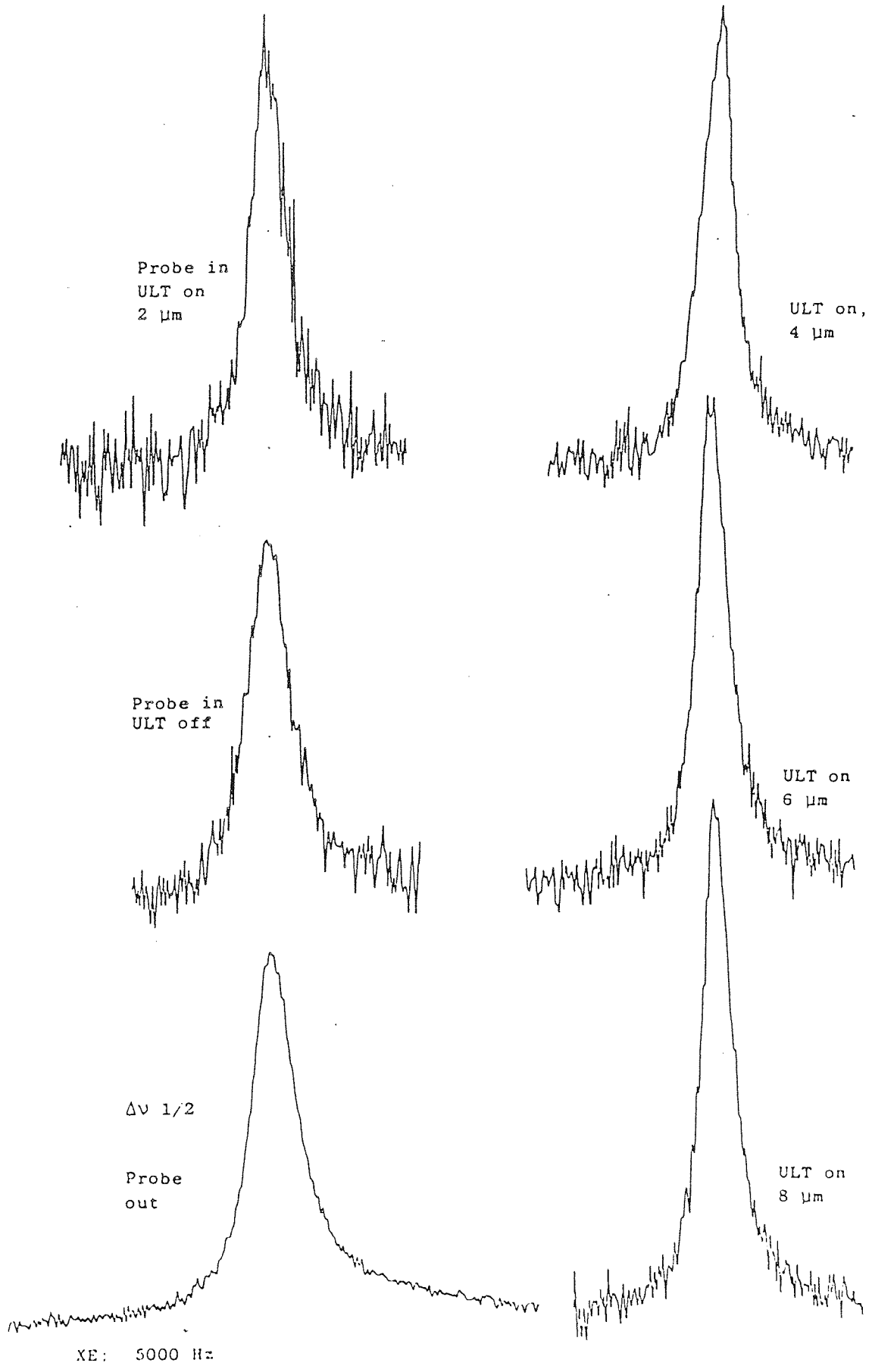

Figure 8.18 (a): The effects of ultrasound at a frequency of 20KHz with increasing ultrasonic power on nitrogen-14 NMR signals observed for N,N-dimethylacetamide.

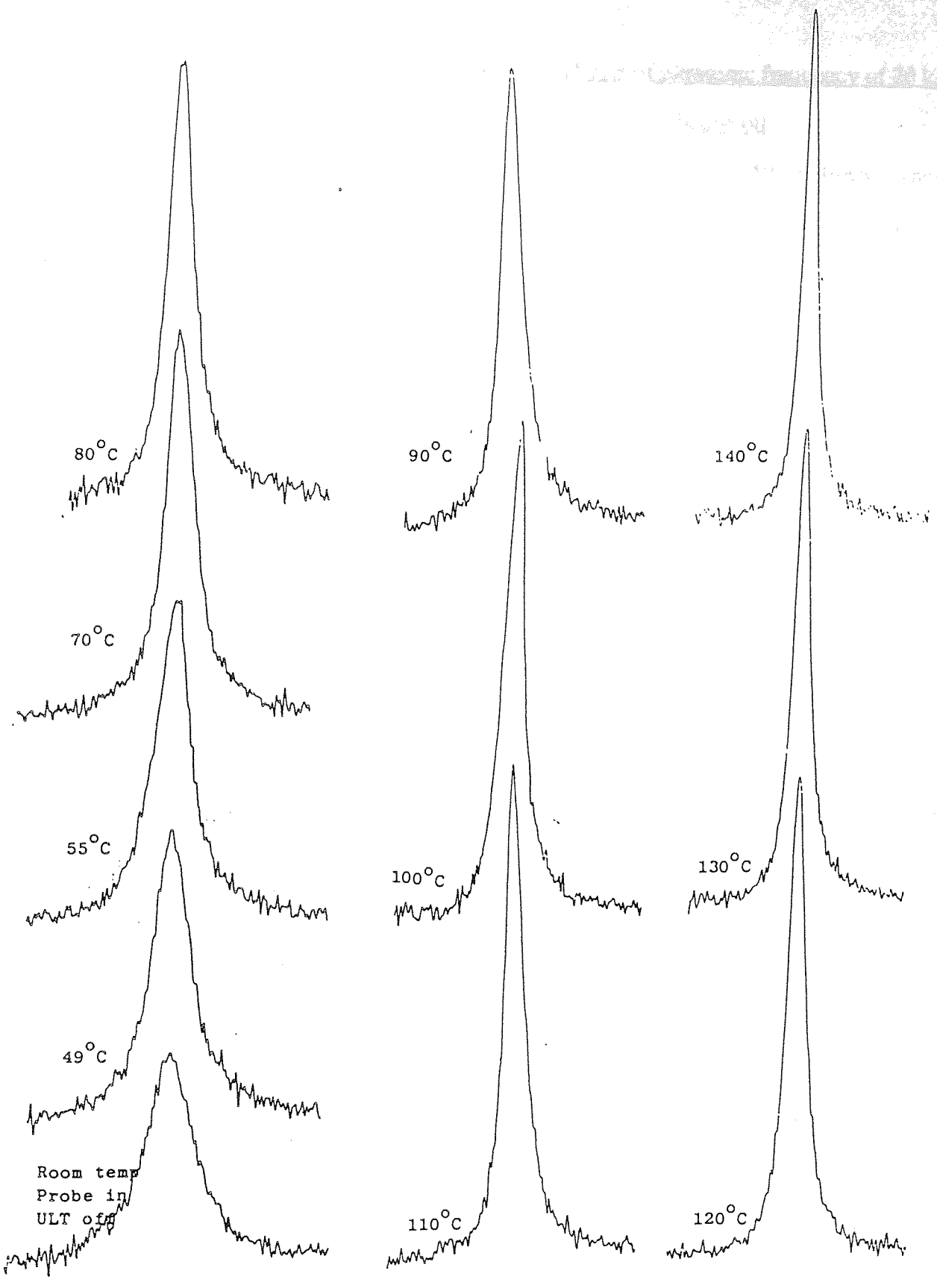

Figure 8.18 (b): The effects of increasing temperature on the nitrogen-14 NMR signals observed for N,N-dimethylacetamide.

8.1(f) Experiments performed to observe the effects of ultrasonic frequency of 20 kHz on a suspension of aluminium phosphate powder in silicone oil

(b) The experiments were performed for phosphorous-31-NMR to observe whether it was possible to induce motion on the macroscopic solid particles suspended in silicone oil. The experiments were performed in the following manner:

(i) Observation of the phosphorous NMR signal for a suspension of aluminium phosphate powder in silicone oil.

(ii) Effects of ultrasound on the suspended mixture via the observation of the effects on the phosphorous nuclei.

(iii) Observation of the effects of experiment (ii) with time after switching off the ultrasonic power.

(iv) Repeat experiment (ii) again.

(v) Change the NMR offset frequency and observe the effects of experiment (iv) with time, after the ultrasonic power has been switched off. This experiment is designed to check whether the NMR signal was genuine.

(vi) Repeat experiment (i) for solid aluminium phosphate powder packed in a NMR tube. This experiment is designed to check whether a NMR phosphrous signal could be observed from the solid particles.

The results of the experiments are as follows:

(i) A small signal is observed in the phosphorous NMR spectra (Figure 8.19(a)). This shows that either the silicone oil was initially contaminated with trace water which now allows small quantities of aluminium phosphate to dissolve and therefore give rise to a phosphorous signal in the NMR spectra or the phosphorous NMR signal appears directly from the solid aluminium phosphate itself. In addition, the spectrum shows the signal to noise ratio to be very poor.

(ii) Observation of the NMR spectra for the ultrasonically treated suspended mixture now shows that the signal to noise ratio had significantly improved (Figure 8.19(b)).

(iii) Observation of the effects of the ultrasonic experiments with time, without the presence of ultrasound showed that the phosphorous NMR signal to noise ratio decreased with time (Figure 8.19(c) and (d)).

(iv) Repetition of the same experiment on the same liquid suspension with the ultrasound switched on (Figure 8.19(e)).

(v) Observation of the effects of the ultrasonic experiment number (iv) with a change of an NMR offset frequency shows the phosphorous NMR signal to have shifted relative to the change in the offset frequency (Figure 8.19(f)). This experiment illustrates that the observed phosphorous signal was genuine.

(iv) Observation of the phosphorous NMR spectra (Figure 8.19(g)) for a solid powder of aluminium phosphate packed in a NMR tube reveals a very noisy spectrum with no real apparent phosphorous signal arising from aluminium phosphate.

From the results of experiments several conclusions can be drawn. These are; if the phosphrous NMR signal observed is purely from a suspension of aluminium phosphate and not due to small quantities of it actually being dissolved in silicone oil due to the oil being contaminated with traces of water then the results reveal that sound can be used to perturb motion of the particles such that motional averaging now produces a sharp NMR signal. However, if the NMR signal observed is due to the latter case, then the results reveal that solubility in such mineral oils can be increased profoundly by sound.

RESULTS OF THE EFFECTS OF ULTRASOUND AT 20 KHz ON PHOSPHOROUS-31 NUCLEI (^{31}P) IN ALUMINIUM PHOSPHATE (FIGURE 8.19)

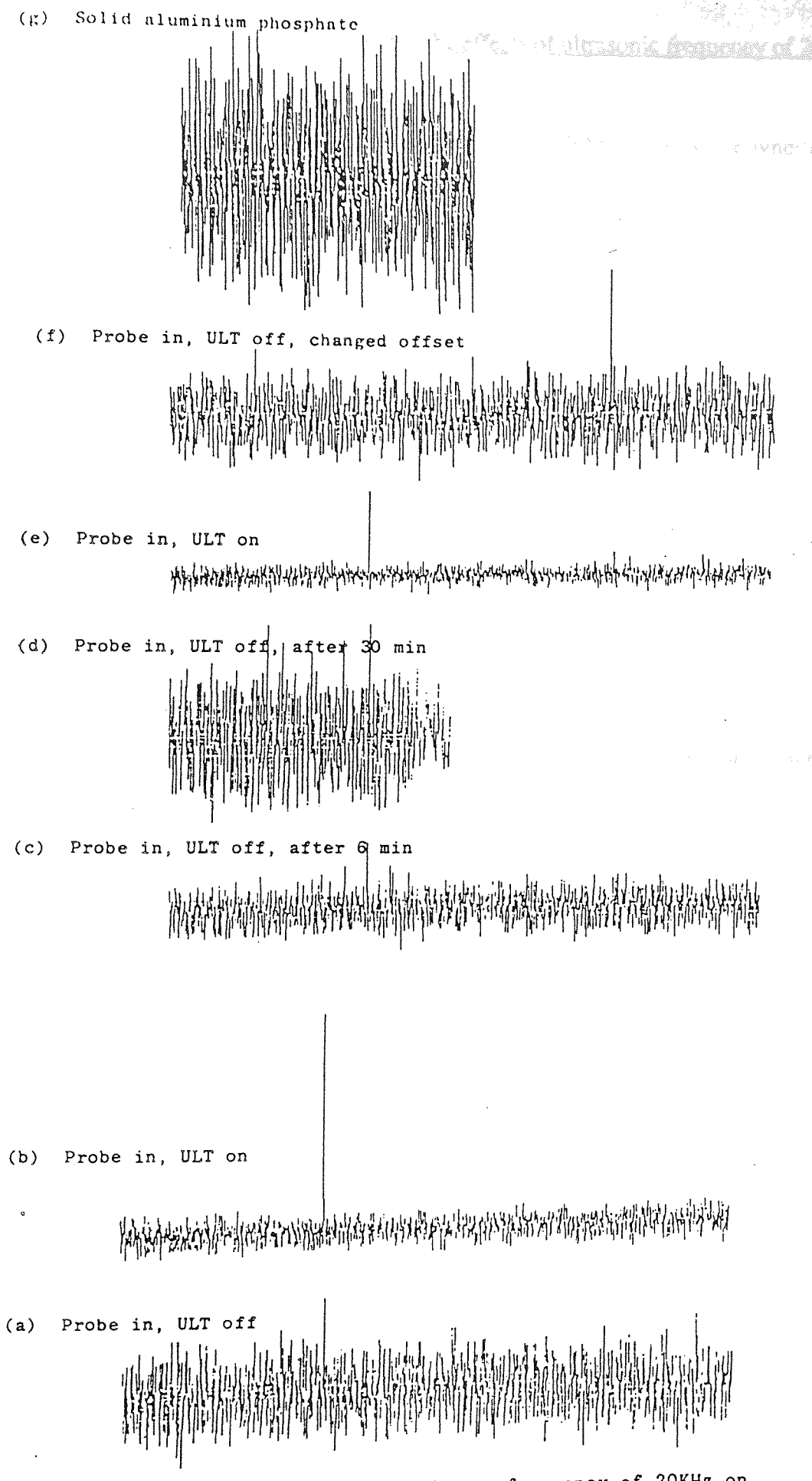

Figure 8.19 (a)- (g): The effects of ultrasound at a frequency of 20KHz on phosphorous-31 NMR signals observed for a suspension of aluminium phosphate in silicone oil.

8.1(g) Experiments performed to observe the effects of ultrasonic frequency of 20 kHz on an aqueous solution of potassium chloride

(c) The experiment was performed for chlorine-35 NMR, to observe whether it was possible to induce ionic motions.

The results of the experiments performed revealed that by placing a 20 kHz ultrasonic probe into a NMR tube containing an aqueous solution of potassium chloride radio frequency caused pick-up signals to be observed in the NMR spectra in addition to the appearance of a very small NMR chlorine signal. Earthing the ultrasonic probe appears to have removed the radio-frequency pick-up signals and improve the signal to noise ratio. However, application of ultrasound to the liquid mixture appears to have no effect on the chlorine signal but shows large radio-frequency beat signals (Figure 8.20(a)-(d) illustrates all the mentioned effects). Measurement of the separation of the radio frequency pick-up signals shows this to be approximately 50 Hz, which exactly coincides with the electrical mains frequency. Thus, no further experiments were performed.

Repetition of the same experiment in the mega-hertz region proved to be unsuccessful as introducing the ultrasonic probe into the aqueous solution of potassium chloride not only destroyed the original chloride-35 NMR signal but also introduced some type of radio-frequency beat signals. Application of ultrasound into the aqueous sample at 6 MHz and 6.42 MHz, respectively, at various ultrasonic powers did not improve the appearance of the chlorine-35 NMR signal (Figure 8.20(e)-(i)).

The results of both low and high frequencies suggests that observation of the effects of ultrasound on electrolytes presents difficulty owing to the large radio-frequency pick-up and earthing problems.

RESULTS OF THE EFFECTS OF ULTRASOUND IN THE KILO- AND MEGAHERTZ FREQUENCIES ON CHLORINE-35 NUCLEI (^{35}Cl) IN POTASSIUM CHLORIDE (FIGURE 8.20)

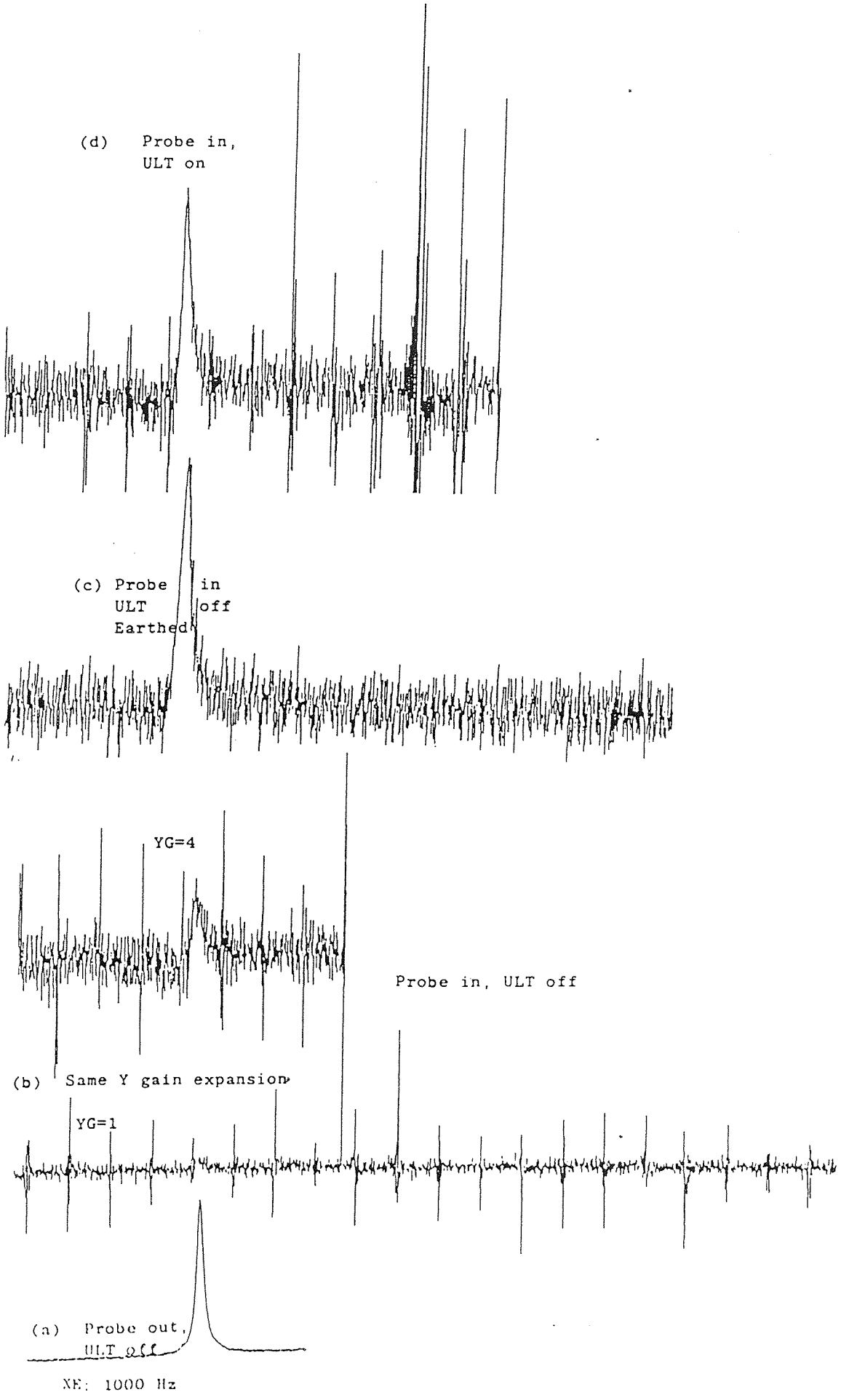

Figure 8.20 (a)- (d): The effects of ultrasound at a frequency of 20KHz on chlorine-35 NMR signals observed for an aqueous solution of potassium chloride.

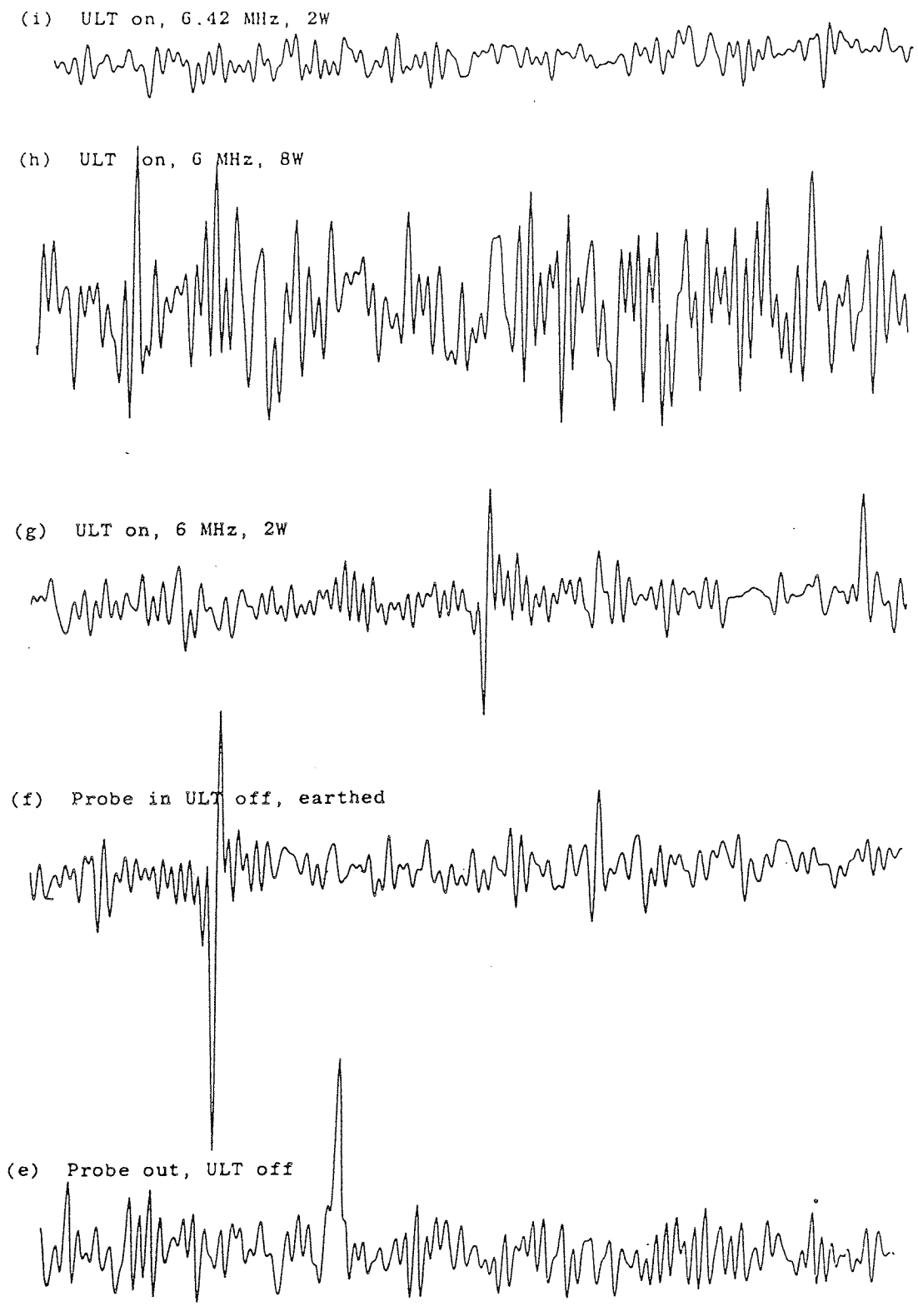

Figure 8.20 (e)- (i): The effects of ultrasound at frequencies of 6 and 6.42MHz on chlorine-35 NMR signals observed for an aqueous solution of potassium chloride.

8.2 Acoustic Cavitation: Results and Discussion

This section discusses the results of experiments performed on neat ethyliodide, benzene, bromobenzene, styrene, polystyrene, methylmethacrylate, polymethylmethacrylate and reactions performed using spin-trapping agents.

Indications in the literature suggest that the action of ultrasound causes bond scission via the weakest bond. This bond scission is facilitated at either the liquid and gas/vapour bubble interfaces or in the gas/vapour bubbles. When the bubble collapses it results in very large pressure and temperature changes being produced locally which further promotes the chemical reactions.

For monomers and polymers, bond scission is thought to result in the formation of radicals which subsequently react further to produce new polymers. There also exists another possibility, that, if radicals were actually produced they may be used to form new products, via the use of spin-trapping agents. The type of experiments performed on the above mentioned samples were designed so that the results of acoustic cavitation generated radicals or products which showed that a reaction had taken place via the generation of radicals.

Experiments performed on neat samples of ethyiodide, benzene and bromobenzene were disappointing. During the experiments performed on ethyliodide and bromobenzene, the result of acoustic cavitation produced a dark brown colouring in both samples. For benzene no physical changes were observed. Examination of all the three samples, by NMR, UV, IR and ESR, revealed only the starting materials.

It was viewed that the presence of a dark brown colouring in the samples was as a result of bond cleavage between the carbon-iodine bond and the carbon-bromine bond for ethyliodide and bromobenzene, respectively. The bond energies per mole for a C-I bond, C-Br bond, C-H bond, C-C bond and C---C bond (for benzene) are 57 kCal, 66 KCal, 99 KCal, 83 KCal and 124 KCal, respectively, it can then be clearly seen that, the C-I bond and the C-Br bond are the weakest. Thus, the brown colouring of the samples must be due to the formation of iodine and bromine from ethyliodide and bromobenzene, respectively. This suggests that ethyl and a iodide radical are generated from ethyl iodide

and, phenyl and bromide radicals are produced from bromobenzene. If the two sets of radicals are unstable and have a short life time, the results of acoustic cavitation on ethyl iodide would either lead to the formation of iodine, butane or ethyl iodide by recombination. For bromobenzene, bromine, biphenyl or bromobenzene would be the most likely products of acoustic cavitation. The fact that ESR experiments showed no presence of radicals suggests that these radicals may be very short lived. Failure to detect the formation of new products by NMR and other techniques suggests that the concentration of these products are in very small quantities such that their structure could not be elucidated. Kruus[202] has already pointed out that the results of acoustic cavitation of bromobenzene would produce phenyl and bromide radicals. However, detection of such radicals or its products proved to be impossible.

In the case of benzene, bond clearage of either the aromatic C --- C bond, or C-H bond, would result in a disruption of the Kekule structure. This form of disruption cannot take place as this would not result in the formation of stable intermediates which would subsequently produce new products.

The next experiment to be conducted was for cis-polyisoprene, (Figure 8.21(a)).

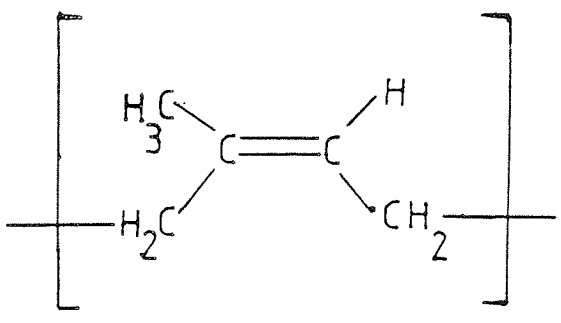

Figure 8.21(a): The structure of cis-polyisoprene

The idea of this experiment was to capture radicals which may be produced as a result of acoustic cavitation. These radicals would be trapped by the alkene and give rise to further polymerisation. The formation of new polymers could then be detected using

^{1}H and ^{13}C NMR by the disappearance of the olefinic hydrogen and the appearance of new spectral lines.

The most likely bonds that may be broken are the C-H bonds as a result of there being the weakest bond. This bond cleavage could occur either at the methyl group the olefinic group or the methylene group (Figure 8.22).

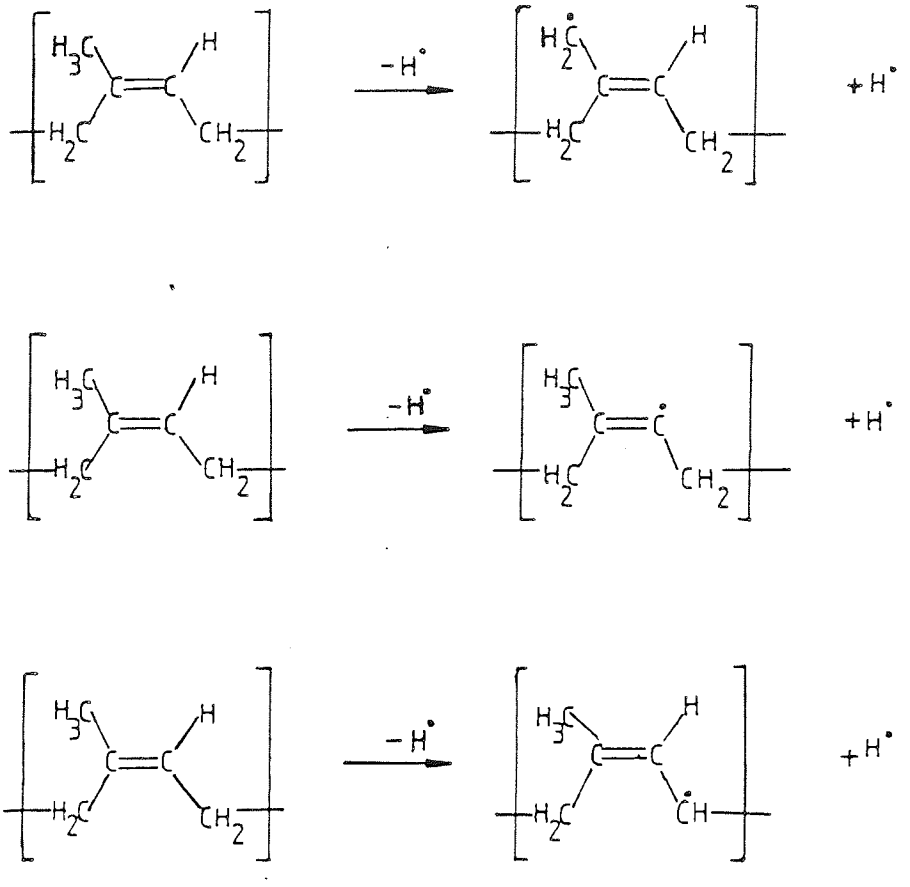

Figure 8.22: Possible place of bond cleavage occurring in cis-polyisoprene with the radicals generated

The polymer was left dissolved in toluene overnight followed by treatment of ultrasound using a ultrasonic generator, for eight hours. Physical examination of the treated solution revealed a reduction in viscosity. It was visualised that the large polymer length of polyisoprene had been broken into smaller units either as a result of molecular shearing or by acoustic cavitation. Examination of the treated material by NMR, ESR, UV and IR, revealed only the starting materials. The failure to detect any chemical changes by NMR, UV and IR suggests that the concentration of the new products may be very low.

Failure to detect the presence of radicals by ESR methods may be due to the very short life-time of the probable radicals produced.

So far, the effects of ultrasound on the solvent toluene has been neglected. Toluene, under the action of ultrasound may give rise to benzyl and methylene radicals. These radicals too can interact with the polymer radicals or the polymer itself. However, presence of these radicals could not be detected by ESR methods.

At this stage, several changes were made to the methodology of experiments, in order to observe the chemical effects of ultrasound. These were as follows:

(i) Use simpler molecules such as styrene and methylmethacrylate.

(ii) Purify the samples before treating the sample so that effects of impurities such as residual polymer, may be removed.

(iii) Gas the sample with argon gas so that cavitation may occur more readily.

(iv) Owing to exposure to light and due to the audible noise generated by the ultrasonic generator, the experiments must be performed in a closed environment with total darkness.

Using a specially designed glass vessel (discussed in Chapter Seven), ultrasonic experiments were performed on distilled styrene at a constant temperature of 30°C with argon gas blown into the liquid. Examination of the reaction mixture taken using UV at hourly intervals by spectroscopic methods using UV, IR, NMR & ESR revealed only the starting material. Repetition and examination of similar experiments performed at various ultrasonic powers showed that the end reaction mixture was still styrene.

Similar experiments were performed on distilled methylmethacrylate. Examination of the test samples again revealed the starting material.

Kruus[202,204,293] showed theoretically and experimentally the types of new products and the radicals generated from cavitation of neat styrene and methylmethacrylate. He showed that the rate of production of its radicals was of the order of 13 μ moles hr^{-1}. El'piner[118] on the other hand showed that polymerisation of

monomers does not take place in the presence of an ultrasonic field for monomers which were thoroughly dried and distilled.

Following these observations, and a further literature search, it remained unclear whether or not the literature experiments were performed in conditions where the samples were exposed to normal sunlight. Two experiments to test this hypothesis were performed using UV light and ultrasound on both styrene and methylmethacrylate. Samples were initially treated with UV light for 1 hour followed by treatment with ultrasound for six hours. Examination of the treated sample by UV IR, NMR and ESR revealed the end reaction mixture to be just the starting material. Alternatively failure to detect new products may also be due to their very low concentration. The low concentration of products may be due to the fact that if the system is considered as a collection of molecules all colliding and breaking up thus generating radicals then the probability of these radicals recombining with other radicals would be very small owing to the initial large concentration of the starting material. Thus, it was decided, it would be more suitable to perform experiments on polystyrene and polymethyl-methacrylate owing to the large number of unsaturated olefinic groups which would increase the probability of trapping the radicals.

Polystyrene dissolved in carbon tetrachloride and polymethylmethacrylate, dissolved in benzene were separately treated by ultrasound. Physical examination of the treated reaction mixture showed that the viscosity had been reduced. Examination of treated samples by UV, IR, NMR and ESR revealed only the starting material. Similar conclusions were drawn to those used to describe the physical changes in viscosity observed for cis-polyisoprene.

Viscosity changes observed in cis-polyisoprene, polystyrene and polymethacrylate are thought to be as a result of bond breaking. If these bond breakages produce radicals then it would be possible to trap these radicals. It has already been shown that it is possible to trap various radicals using spin-trapping agents[217,294-297]. These spin-trapping agents increase the lifetime of radicals, which may then be possible to observe using ESR.

Tabata et al[212] have shown that radicals produced by ultrasonic cavitation of polymethylmethacrylate could be trapped using pentamethylnitrosobenzene (PMNB). In this investigation 2,2,6,6-tetramethyl piperidol (TMP) (Figure 8.23) was used as the spin-trapping agent.

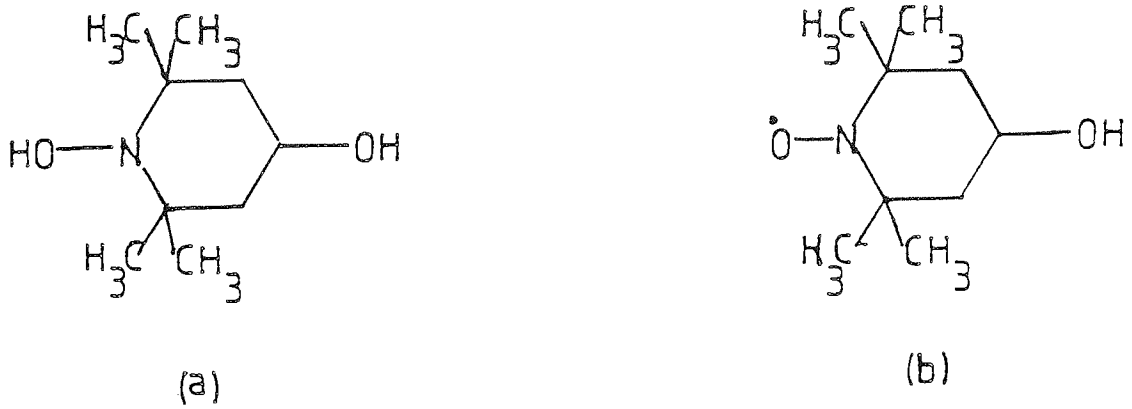

Figure 8.23: Structure of 2,2,6,6-tetramethylpiperidol (TMP) (a) and 2,2,6,6-tetramethyl-piperidnoxyl (TMPOXYL) (b).

TMP was chosen rather than TMPOXYL due to the fact that if ultrasonic cavitation does cause bond breakages then this would of course result in bond breakage at the O-H bond thus producing TMPOXYL which could subsequently trap any other radicals produced or present in the reaction mixture. These spin-trapped radicals could then be observed by ESR.

Experiments were separately performed using polymethylmethacrylate and polystyrene with TMP and TMPOXYL. Evaluation of the treated reaction mixture by NMR and ESR revealed only the starting materials. In conclusion, it was thought neither TMP nor TMPOXYL were efficient spin-trapping agents and these required to be changed.

In conclusion further new experimental ideas needs to be implemented which in effect would enable the detection of radicals being generated.

8.3 Experimental

The following samples were prepared to investigate the effects of sound on NMR spin-lattice and spin-spin relaxation rates. The experiments were performed using a JEOL FX 90Q broadband NMR spectrometer which was used to observe the ^{1}H, ^{13}C, ^{14}N, ^{35}Cl and ^{31}P spectra at nominal frequencies of 89.56, 22.53, 6.42, 8.72 and 22.50 MHz, respectively and at 30°C; the precise irradiation conditions were kept constant for each set of spectra.

The effects of temperature and degassing liquid mixtures on spin-lattice relaxation times were only performed for ^{1}H nuclei.

Sound frequencies at approximately 1, 2, 6, 6.42 and 10 MHz were used to perform the experiments. In addition, the effects of increasing power on NMR spin-lattice relaxation times were performed at each of the mentioned frequencies, with power levels ranging from 1W to 20W.

Numerous types of probe were designed and constructed. It will be mentioned where appropriate, the type of probe used and the results obtained.

The samples, unless stated otherwise, are of spectroscopic grade (gold label) supplied from Aldrich Chemicals. Following the preparation of the liquid samples, as described below, pure liquids (2 cm^3) and the liquid mixtures (2 cm^3) were then used for NMR and ultrasound investigation.

(1) (a) Pure chloroform (2 cm^3) was used.

(b) Pure bromoform (2 cm^3) was used.

(c) Pure cyclohexane (2 cm^3) was used.

(2) Chloroform:cyclohexane mixture (1:1 molar ratio). Chloroform (47.752g, 32.069 cm^3, 0.4 mol) was added to cyclohexane (33.664g, 43.214 cm^3, 0.4 mol) and the liquid mixture well shaken.

(3) Chloroform:2-chloro-2-methylpropane (1:1 molar ratio). Chloroform (11.938g, 8 cm^3, 0.1mol) was added to 2-chloro-2-methylpropane (9.257, 10.88 cm^3, 0.1 mol) and the liquid mixture well shaken.

(4) Bromoform:cyclohexane mixture (1:1 molar ratio). Bromoform (50.54g, 31.63 cm^3, 0.2 mol) was added to cyclohexane (16.83g, 21.60 cm^3, 0.2 mol) and the liquid mixture well shaken.

(5) Cyclohexane:1,3,5-trimethylbenzene (mesitylene) 1:1 molar ratio. Cyclohexane (8.416g, 10.8 cm^3, 0.1 mol) was added to mesitylene (12.0g, 13.89 cm^3, 0.1 mol) and the liquid mixture well shaken.

(6) Bromoform:2-bromo-methylpropane (1:1 molar ratio). Bromoform (12.639g, 4.39 cm^3, 0.05 mol) was added to 2-bromo-2-methylpropane (6.851g, 5.76 cm^3, 0.05 mol) and the liquid mixture well shaken. Due to partial immiscibilities of the two liquids, experiments using ultrasound proved to be difficult to perform.

(7) Cyclohexane:2-chloro-2-methylpropane (1:1 molar ratio). Cyclohexane (8.416g, 10.8 cm^3, 0.1 mol) was added to 2-chloro-2-methylpropane (9.25g, 10.87 cm^3, 0.1 mol) and the mixture well shaken. Observation of the NMR spectra showed that the two NMR signals overlapped. Thus no further experiments were performed using ultrasound.

(8) Cyclohexane:benzene:deuterated chloroform (1:1:2 molar ratio). Cyclohexane (8.416g, 10.8 cm^3, 0.1 mol), benzene (7.81g, 8.93cm^3, 0.1m) and deuterated chloroform (24.08g, 16.05 cm^3, 0.2 mol) were all added together and the liquid mixture well shaken.

(9) Cyclohexane:mesitylene:deuterated chloroform, (1:1:2 molar ratio). Cyclohexane (8.416g, 10.8 cm^3, 0.1 mol), mesitylene (12.0g, 13.89cm^3, 0.1 mol) and deuterated

chloroform (24.08g, 16.05cm^3, 0.2 mol) were all added together and the liquid mixture well shaken.

(10) Cyclohexane:1,4-di-tert-butylbenzene:deuterated chloroform (1:1:2 molar ratio). Cyclohexane (1.68g, 2.2 cm^3, 0.02 mol), 1,4-di-tert-butylbenzene (3.81g, 0.02 mol) and deuterated chloroform , (4.82g, 3.2cm^3, 0.4 mol) were all added together and the liquid mixture well shaken.

(11) Cyclohexane:1,3,5-tri-tert-butylbenzene:deuterated chloroform (1:1:3 molar ratio). Cyclohexane (1.68g, 2.2 cm^3, 0.02 mol), 1,3,5-tri-tert-butylbenzene (4.92g, 0.02 mol) and deuterated chloroform were all added together and the liquid mixture well shaken.

(12) Acetonitrile:deuterated chloroform (1:1 molar ratio). Acetonitrile (4.1g, 5.3 cm^3, 0.1 mol) was added to deuterated chloroform (12.0g, 8 cm^3, 0.1 mol) and the liquid mixture well shaken.

(13) N-methylformamide:deuterated chloroform (1:1 molar ratio). N-methyl-formamide (2.96g, 3 cm^3, 0.05 mol) was added to deuterated chloroform and the liquid mixture well shaken.

(14) N-N-dimethylformamide:deuterated chloroform (1:1 molar ratio). N-N-Dimethylformamide (3.65g, 3.9 cm^3, 0.05 mol) was added to deuterated chloroform (6.02g, 4.0cm^3, 0.05 mol) and the liquid mixture well shaken.

(15) N-N-dimethylacetamide:deuterated chloroform (1:1 molar ratio). N-N-dimethylacetamide (4.36g, 4.7 cm^3, 0.05 mol) was added to deuterated chloroform (6.02g, 4.0 cm^3, 0.05 mol) and the liquid mixture well shaken.

(16) Saturated solution of ammonium chloride in dimethyl sulphoxide. A saturated solution of ammonium chloride in dimethylsulphoxide (10 cm^3) was prepared. The solution was filtered and the filtrate (2 cm^3) used.

(17) Saturated solution of ammonium chloride in dimethylsulphoxide with hydrochloric acid. A solution of ammonium chloride in dimethylsulphoxide (10 cm^3) was prepared. The solution was filtered and hydrochloric acid (1 cm^3, 4M) was added to the filtrate. The filtrate mixture (2 cm^3) was then used.

(18) Saturated solution of potassium chloride in dimethylsulphoxide. A saturated solution of potassium chloride in dimethylsulphoxide (10 cm^3) was prepared. The solution was filtered and the filtrate (2 cm^3) used.

(19) Synthesis of tris-(2,2-bipyridyl) cobalt (II) perchlorate. Preparation of tris-(2,2-bipyridyl) cobalt (II) perchlorate was prepared as described in the literature[289-291]. Hydrated cobalt (II) perchlorate (3.67g, 10 mole) was dissolved in ethanol (50 cm^3). To this a solution of 2,2'-bipyridyl (4.69g, 30 mol) in ethanol (20 cm^3) was added. The dark brown crystals obtained were filtered and washed with ice-cold ethanol/water and dried over phosphorous pentoxide ($P_2 O_5$) under vacuum.

(20) Preparation of dexoygenating mixture with sodium borohydride. Sodium borohydride (20g) was dissolved in water (10 cm^3). To this, tris-(2,2-bipyridyl) cobalt (II) perchlorate (4mg) was added and the mixture well shaken. The cobalt complex is brown/yellow in colour when solid. When dissolved with sodium borohydride, in a suitable solvent, it removes oxygen in a reversible colour indicating reaction and when all dissolved oxygen has been removed the solution turns blue.

(21) Preparation of 1:1 molar ratio of bromoform:cyclohexane in the presence of deoxygenating agent. Chloroform (11.938g, 8 cm^3, 0.1 mol) was mixed with

cyclohexane (8.41g, 10 cm^3, 0.1 mol) and flushed with argon gas. The liquid mixture (2 cm^3) was then added to a prepared deoxygenating agent (2 cm^3) (prepared using the above method) in an NMR tube and whole mixture well shaken. Following the separation of the two phases the deoxygenating agent (1.5 cm^3) was siphoned out whilst taking care not to expose the bromoform/cyclohexane mixture to air. A fresh amount of the deoxygenating agent was introduced (1.5 cm^3) into the bromoform/cyclohexane/deoxygenating agent mixture and the mixture was again well shaken. This process was repeated at least three times before placing the NMR tube containing the mixture of bromoform, cyclohexane and deoxygenating agent into the NMR instrument for NMR and ultrasound investigation.

(22) Removal of dissolved air from liquid NMR samples via purging with nitrogen gas. Degassing of dissolved air was performed by purging the liquid samples with argon gas. The experiment was performed in a mixture of bromoform and cyclohexane mixture (2 cm^3), 1:1 molar ratio, contained within the NMR tube. Gas was blown through a pyrex glass tube immersed directly into the bromoform/cyclohexane mixture. Measurement of ^1H NMR spin-lattice relaxation times were performed immediately after.

(23) Effects of temperature.

(i) The effects of temperature changes on ^1H NMR spin-lattice relaxation times were observed using a mixture of bromoform and cyclohexane (1:1 molar ratio). Preparation of bromoform and cylohexane, mixture was carried out as described earlier. Measurements of ^1H NMR spin-lattice relaxation times were performed at 30°C, 40°C, 50°C and 60°C.

(ii) The effects of temperature changes on ^1H NMR spin-lattice relaxation times were observed using a mixture of cyclohexane and 1,3,5-trimethylbenzene (mesitylene) mixture (1:1 molar ratio). Preparation of cyclohexane and mesitylene was carried out as described earlier. Measurement of ^1H NMR spin-lattice relaxation times were performed at temperatures 35, 39, 47, 53, 61 and 72°C.

8.4 Sonochemical Experiments

These experiments were performed using a commercially purchased 20 KHz ultrasonic instrument which has variable power levels ranging from 1W to 150W.

Under the manufacturers specifications, the instrument had been calibrated using water, with the corresponding power levels measured in microns. This represented the maximum ultrasonic probe deflection during the irradiation of sound at the appropriate power level. A maximum probe deflection of 18 μm was recorded which corresponded to delivering 118Wcm^{-2} into the water.

The sonochemical reactions were performed in a specially designed glass vessel which allows reactions to be performed at constant temperature, inject or remove samples at time intervals and blow gas into the reaction mixture. These experiments can also be performed if desired in the dark (see Figure 7.40 for instrument design).

(a) Neat ethyliodide (20 cm^3) was placed in the specially designed ultrasonic vessel and maintained at a constant temperature of 35^{o}C. The experiment was performed for 2 hours in the open at 20 KHz and at a power level of 8 μm (~ 50 W). Examination of the resulting brown solution, were performed using NMR, IR and ESR.

(b) Neat benzene (20 cm^3). The experiment was performed using similar experimental conditions to those applied to ethyliodide. Examination of the resulting solution (with no apparent colour change) performed using NMR, IR and ESR.

(c) Neat bromobenzene (20 cm^3). The experiment was performed under similar experimental conditions to those applied to ethyliodide. Examination of the resulting dark brown solution was performed using NMR, IR, ESR and UV.

(d) Cis-poly-isoprene (5% (W/V)) was dissolved in toluene overnight and placed in the ultrasonic vessel. The experiment was performed under similar conditions to those

applied for ethyliodide. Samples of the reaction mixture were taken at hourly intervals for 8 hours and examined. Inspection of the reaction mixture was performed using NMR, UV and ESR.

(e) Purification of monomers. The monomers were purified before performing any ultrasonic experiment. The following procedure was used:

The monomers were purified by successive washing in dilute sodium hydroxide solution, several times with water. The two layers were separated and dried overnight using anhydrous magnesium sulphate. The monomers were then vacuum distilled.

High boiling point monomers which polymerise at or below normal boiling point or at atmospheric pressure were generally distilled at lower temperatures, under reduced pressure, using a vacuum pump. For low boiling point monomers, such as methylmethacrylate (MMA) a water pump was used.

(f) Distilled styrene (25 cm^3) was placed in the ultrasonic vessel and maintained at a constant temperature of 35°C. Argon gas was blow continuously through the solution, and ultrasound, set at a power level of 8 μm (~ 50W), was applied. Samples of the reaction mixture wre taken at hourly intervals for 8 hours and examined. Inspection of the reaction mixture was performed using NMR, IR, UV and ESR.

(g) Distilled methyl-methacrylate (25 cm^3). The experiment was performed under similar conditions to those applied to styrene. Examination of the reaction mixture was performed using NMR, IR, UV and ESR.

(h) Similar experiments were performed for (f) and (g). However, the purified monomers were first exposed to UV light for 1 hour before performing the experiment with ultrasound. Examination of UV irradiated and ultrasonically treated samples of styrene and methylmethacrylate, respectively, was performed by UV, NMR, IR and ESR.

(i) Polystyrene (20% W/V) (25 cm^3) was dissolved in carbontetrachloride. The experiment was performed using similar procedures to that of (f). Examination of the resulting ultrasonically treated reaction mixture was performed using NMR, IR, ESR and UV.

(j) Polymethylmethacrylate (20% W/V) (25 cm^3) was dissolved in benzene. The experiment was performed using similar procedures to that of (f). Examination of the resulting ultrasonically treated reaction mixture was performed using NMR, IR, ESR and UV.

(k) Polymethylmethacrylate (20% W/V) was dissolved in benzene overnight. A solution of 2,2,6,6-tetramethylpiperidnol (4g, 0.023 moles) in benzene (10 cm^3) was added to the polymethylmethacrylate solution (25 cm^3). The experiment was performed using similar procedures to that of (f). Examination of the resulting ultrasonically treated reaction mixture, was performed using NMR, UV and ESR.

(l) Polystyrene (20% W/V) was dissolved in carbon-tetrachloride overnight. A solution of 2,2,6,6-tetramethyl piperidnol (4g, 0.023 mol) in carbon tetrachloride (10 cm^3) was added to the polystyrene solution (25 cm^3). The experiment was performed using similar procedures to that of (f). Examination of the resulting ultrasonically treated reaction mixture was performed using NMR, UV and ESR.

(m) Polymethylmethacrylate (20% W/V) dissolved in benzene. A solution of 2,2,6,6-tetramethylpiperidnoxyl (TMPOXYL), (4g, 0.023 mol) in benzene (10cm^3) was added to the polymethylmethacrylate solution (25 cm^3). The experiment was performed using similar procedures to that of (f). Examination of the resulting ultrasonically treated reaction mixture was performed using NMR, ESR and UV.

(n) Polystyrene (20% W/V) was dissolved in carbontetrachloride. A solution of 2,2,6,6-tetramethylpiperidnoxyl (4g, 0.023 mol) in carbon tetrachloride (10 cm^3) was

added to the polystyrene solution (25 cm^3). The experiment was performed using similar procedures to that of (f). Examination of the resulting ultrasonically treated reaction mixture by NMR, ESR and UV revealed only the starting material.

8.5 Conclusions and Suggestions for Future Work

Results from the experiments performed and through the discussion revealed that spin-lattice relaxation times are affected through the ultrasonic perturbation of the molecular dynamics in the liquid phase. Comparison of proton and carbon-13 ultrasonically effected relaxation times further reveals intermolecular nuclear dipolar-dipolar relaxation mechanism to be effected to a greater extent than intra-molecular nuclear dipolar-dipolar relaxation mechanism. The exact details regarding the mode of coupling between acoustic energy and the external and internal degrees of freedom needs to be elucidated. Furthermore, it would be appropriate to extend the investigation to establish if the effect of ultrasound has characteristic effects on the T_1's from different functional groups with a view to develop a technique for the elucidation of molecular structure.

Several mechanisms have been invoked to explain the observed changes in the spin-lattice relaxation times with increasing ultrasonic power. The results showed that as the ultrasonic power applied to the transducer is progressively increased, T_1 decreases to a minimum and then increases. One of the explanations put forward was that as the ultrasonic power is increased, molecular correlation times are initially increased. This could arise because of a net increase in microviscosity due to the Stokes force operative in the presence of ultrasound. The subsequent increase in T_1 could be due to either the dominating effect of temperature increasing with ultrasonic power or to a further increase in correlation times. Another though less likely explanation is that the ultrasound causes the addition of a discrete relation rate to those classically associated with nuclear relaxation. The various possibilities can be examined by $T_{1\rho}$ measurements; If the temperature effect is important, the trend described above will be repeated, but if correlation times are continually increased $T_{1\rho}$ will only show a decrease with increasing

ultrasonic power. If a unique mechanism operates, the value of $T_{1\rho}$ in the presence of ultrasound will be lower than those in its absence.

Results of experiments involving the observation of the effects of ultrasound on spin-spin relaxation times via the effects on nitrogen containing samples reveals that initial spin-spin relaxation times are too short to be effected further. In addition, observation of the effects below, at the resonance, and above resonance frequency of the nuclei being observed revealed results which needs to be explained. Attempted experiments via nuclear acoustic resonance reveal saturation of the NMR signals. This may either be due to an electronic saturation of the NMR signals or due to saturation of the nuclear spins. This observation needs to be resolved.

Observation of the effects of ultrasound on electrolytes such as ammonium chloride and potassium chloride reveals large earthing problems which needs to be resolved if the effects of ultrasound on ionic solutions is to be investigated.

Sonochemical experiments performed to detect radical generation failed although it has been shown through various literature data to exhibit great promise. Furture experimental investigation in a more suitable form would be to perform the ultrasonic experiments within a electron-spin resonance (ESR) spectrometer.

The research performed, although successful, highlighted significant difficulties in reproducibility. These difficulties can be attributed to predominantly three factors. These are:

(i) Poor coupling of ultrasonic energy with different energies of a liquid state can be understood from the use of various ultrasonic frequencies. Discussions from previous chapters reveal that translational, rotational and vibrational frequencies of molecular motions occur at high frequencies. Thus, an ideal coupling between the ultrasonic energy with the various energies of the liquid state would occur at high frequenices in the giga-hertz region. Thus, the effects on molecular motions and molecular structure of using different ultrasonic frequencies should be investigated.

(ii) The irreproducibility in the performance of the instruments used is two fold. These are:

(a) non-ideal coupling of the piezo-electric transducer and the liquid.

(b) Performance of the transducer assembly. Various designs have been tried and tested. The results reveal that impedance mismatch between the frequency generator, amplifier, and the tuner with the PZT transducer and its assembly leads to large heating effects with again results in an electrical impedance mismatch.

(c) Sample purity. Results of experiments performed with impurities such as molecular oxygen reveals paramagnetic relaxation mechanisms to play a large role in determining spin-lattice relaxation times. Thus, any experiments which are to be performed to show the importance of the influence of ultrasound on relaxation times, T_1 and T_2, must be performed on pure samples.

In conclusion, in as much as creating a novel technique in the modification of NMR relaxation times by ultrasound, much work yet needs to be done if the long term interest is to use ultrasound as a directional "torch" in magnetic resonance imaging.

REFERENCES

1 Pauli, W. Naturwiss., 12, 741, 1924

2 Stern, D. & Gerlach, W., Ann. Physik., 74, 673, 1924

3 Ramsay, N.F., "Molecular Beams", Oxfo d Univ Press, Oxford, 1956

4 Purcell, E.M., Torrey, H.C. & Pound, R.V., Phys. Rev., 69, 37, 1946

5 Bloch, F., Hansen, W.W. & Packard, M.E., Phys. Rev. 69, 127, 1946

6 Goldstein, H., "Classical Mechanics". Addison-Wesley, Reading, Massachusetts (USA), 1950

7 Corio, P.L.,"Structure of High Resolution NMR Spectra". Academic Press, New York, 1966, pp60-63

8 Abragam, A., "The Principles of Nuclear Magnetism", Oxford University Press, Great Britain, 1961

9 Pauling, L. & Wilson, E., "Introduction to Quantum Mechanics", Mcgraw Hill Cook Co., New York, 1935

10 Emsley, J.W., Feeney J., & Sutcliffe, L.H., "High Resolution Nuclear Magnetic Resonance Spectroscopy", Pergamon Press, Oxford, 1965

11 Einstein, A., Phys. Rev., Z, 18, 121, 1917

12 Buckingham, A. D & Pople, J., Discuss Faraday Soc., 22, 14, 1956

13 Lamb,W.E., Phys. Rev., 60, 817, 1941

14 Saika, A. & Slichter, C.P., J. Chem. Phys., 22, 26, 1954

15 Homer, J., App. Spect. Rev., 9(1), 1-132, 1975

16 Bloch, F. Phys. Rev., 70, 104, 1946

17 Bloch, F., Phys. Rev., 70, 104, 1946

18 Bloch, F., Hansen, W.W. & Packard, M., Phys Rev., 7, 974, 1946

19 Tiers, G.V.D., J. Phys. Chem., 65, 1916, 1961

20 Harris, R.K., "Nuclear Magnetic Resonance Spectroscopy". Pitman Books Ltd, London, 1983

21 Hahn, E.L., Phys. Rev., 80, 580, 1950

22 Pake, G.E., J. Chem. Phys., 16, 327, 1948

23 Van Vleck, J.H., Phys. Rev., 116B, 74, 1168, 1948

24 Carrington, A. & McLachlan, A.D., "Introduction to Magnetic Resonance", Harper & Row Publishers, Inc., New York, 1967

25 Endrew, E.R., "Nuclear Magnetic Resonance", University Press, Cambridge, England, 1955, pp114

26 Bloembergen, N., Purcell, E.M. & Pound, R.V., Phys. Rev., 73, 679, 1948

27 Doob, J.L., An. Math Statistics, 15, 229, 1944

28 Reif, F. "Fundamentals of Statistical and Thermal Physics". McGraw Hill Co., 1965

29 Farrach, T.C. & Becker, E.D., "Pulse and Fourier Transform NMR", Academic Press, New York, (1971), 2nd Ed, 1980

30 Fukushima, E. & Roeder, S.B.W., "A Nuts and Bolts Approach", Addison-Wesley Publishing Co, 1981

31 Kubo, R. & Tomita, K., J. Phys. Soc. Japan., 9, 888, 1954

32 Aleksandrov, I.V. "The Theory of Nuclear Magnetic Resonance", Academic Press, New York, 1966

33 Solomon, I., Phys. Rev., 99, 559, 1955

34 Debye, P. "Polar Molecules", Dover Publications, New York, 1945

35 Stokes, G.G. "Tran Cambridge Philos. Soc." 60, 4354, 1974

36 Einstein, A. in "Investigation on the theory of the Brownian movement", Dover Publications, New York, 1956, pp19-34

37 Huntress, W.T., "Adv. Mag. Res.", Vol 4, Academic Press, New York, 1970

38 Boere, R.T. & Kidd, R.G., Ann. Rep. NMR, 5, 1-79, 1980

39 Gutowsky, H.S. & Woessner, D.E., "Phys. Rev.", 104, 843, 1956

40 Hubbard, P.S., Phys. Rev., 109, 1153, 1958

41 Mitchell R.W. & Eisner, M.J., J. Chem. Phys., 34, 651, 1961

42 Redfield, A.G., IBM J. Res. Develop., 1, 19, 1957

43 Kattawar, G.W. & Eisner, M., Phys. Rev., 126, 1054, 1961

44 Powles, J.G., Proc. Phys. Soc., 78, 377, 1961

45 Torrey, H.C., Phys. Rev., 107, 962, 1953

46 Zeidler, M.D., Mol. Phys., 30, 1441, 1975

47 Hubbard, P.S., Phys. Rev., 131, 275, 1963

48 Inlow, R.O., Juestan, M. & Vanwazer, J.R., J. Phys. Chem., 79, 21, 1975

49 Hertz, H.G., "Program in NMR Spectroscopy". 3, 159, 1967

50 Woessner, D.E., J. Chem. Phys., 37, 642, 1962, 42, 1855, 1965

51 Gierer, A. &Wirtz, K., Zeit Naturforsch. A8, 532, 1953

52 Moniz, W.B., Steele, W.A. & Dixon, J.D., J. Chem. Phys., 38, 2418, 1963

53 Steele, W.A., J. Chemical Phys., 38, 2404, 1963. 38, 2411, 1963

54 Hu, C.M. & Wanzig, R., J. Chem. Phys., 60, 4354, 1974

55 Youngren, G.K. & Acrivos, A., J. Chem. Phys., 63, 3846, 1975

56 Bauer, D.R., Brauman, J.I. & Pecora, R., J. Amer. Chem. Soc., 96, 6840, 1974

57 Alms, G.R., Grerke, T.D. & Patterson, G.D., J. Chem. Phys., 67, 5779, 1977

58 Alms, G.R. & Patterson, G.D., J. Chem. Phys., 71, 563, 1979

59 Harris, R.K. & Newman, R.H., Mol. Phys., 38, 1315, 1979

60 Hill, N.E., Proc. Phys. Soc. (London), 67B, 149, 1954. 68B, 209, 1955

61 Andrade, D.A.C., E:N., 17, 497, 1934. 17, 698, 1934

62 Hill, N.E., Vaughan, W., Price, A.H. & Davies, M. "Dielectric properties and molecular behaviour", Van Nastrand Reinhold London, 1969, Chapter 1

63 Pitt, D.A. & Smith, C.P., J. Amer. Chem. Soc., 81, 783, 1959

64 Mohammadi, M.S. & Homer, J., Unpublished results. University of Aston, Birmingham, 1986

65 Kivelsosn, D. & Tsay, S.J., Mol. Phys., 29, 29, 1975

66 Alms, G.R., Bauer, D.R., Brauman, J.I. & Pecora, R., J. Chem. Phys., 58, 5570, 1973., 61, 2255, 1974

67 Valdivieso, C.E.R., PhD thesis, University of Aston, Birmingham, (pg 244), 1984

68 Slichter, C.P., "Principles of magnetic resonance". Harper & Row Publishers, Inc, 1963

69 Tsang, T. & Farrach, T.C., J. Chem. Phys., 50, 3498, 1969

70 Pound, R.V., Phys. Rev., 79, 675, 1950

71 Abraham R.J. & Loftus, P. "Proton and Carbon 13 NMR Spectroscopy", Heyden & Sons Ltd., London, 1980

72 Shaw, D., "Fourier Transform NMR Spectroscopy", Elsevier, London, 1984

73 McConnell, H.M. & Holm, C.H., J. Chem. Phys., 25, 1289, 1956

74 Haeberlen, U., "Advances in magnetic resonance", Academic Press, New York, 1976

75 Allerhand, A. & Gutowsky, H.S., J. Chem. Phys., 41, 21115, 1964. 42, 1587, 1965

76 Allerhand, A., Rev. Sci. Instrum., 41, 269, 1970

77 Lyerla, J.R. & Grant, D.M., J. Phys. Chem., 75, 3967, 1971

78 Powles, J.G., Bev. Bunsenges Physik. Chem., 67, 328, 1963

79 Hubbard, P.S., Phys. Rev., 131, 1155, 1963

80 Matheson, A.J., "Molecular acoustics", Wiley-Interscience, England, 1974

81 Stumpf, F.B., "Analytical Acoustics", Ann. Abor. Science Publishers Inc Michigan, USA, 1980

82 Kinsler, L.E. & Frey, A.R., "Fundamentals of Acoustics", John Wiley & Sons Inc., New York, 1962

83 Beyer, R.T. & Letcher, S.V., "Physical Ultrasonics", Academic Press, New York, 1969

84 Lindsay, R., "Mechanical Radiation", McGraw-Hill Book Co., New York, 1960

85 Herzfeld, K.F. & Litovitz, T., "Absorption and Dispersion of Ultrasonic Waves", Academic Press Inc., New York, 1959

86 Moorse, P.M. & Ingard, K.U., "Theoretical Acoustics". McGraw-Hill Book Co., New York, 1968

87 Stephens, R.W.B. & Bates, A.E., "Acoustics and Vibrational Physics", Edward Arnold Ltd, London, 1966

88 Mason, W.P., "Physical Acoustics", Academic Press, New York, VI, pt 1, and VII pt. A, 1964

89 Krass, P., "Liquids and solutions". Marcel Dekker Inc., New York, 1977

90 Temperley, H.N.V. & Trevena, D.H., "Liquids and their properties". Ellis Horwood Ltd, Chichester, England, 1978

91 Moelwyn-Hughes, C.A., "Chemical statics and kinematics of solutions", Academic Press, New York, 1971

92 Homer, J. & Mohamadi, M.S. J. Chem. Soc., Faraday Trans. 83(11), 1957-1974, 1987

93 Tabor, D., "Gases, liquids and solids", Cambridge University Press, England, 1979

94 Barker, J.A., "Lattice theories of the liquid state", Pergamon Press England 1963

95 Barker, J.A. & Henderson, D. Rev Modern Phys 48(4), 587-671, 1976

96 Hirschfelder, J.O., "Intermolecular Forces", Adv. Chem. Phys., Vol XII, John Wiley & Sons Inc., London, 1967

97 Murrell, J.N. & Boucher, E.A., "Properties of Liquids and Solutions", John Wiley & Sons Inc., London, 1982

98 Marcus, Y., "Introduction to Liquid State Chemistry", John Wiley & Sons Inc., London, 1977

99 Lennard-Jones, J.E. & Devonshire, A.F., Proc. Roy. Soc. Ser. A, A163, 53, 1937

100 Lennard-Jones, J.E. & Devonshire, A.F., Proc. Roy. Soc. Ser. A, A165, 1, 1938

101 Lennard-Jones, J.E. & Devonshire, A.F., Proc. Roy. Soc. Ser. A, A170, 317, 1939

102 Lennard-Jones, J.E. & Devonshire, A.F., Proc. Roy. Soc. Ser. A, A170, 464, 1939

103 Eyring, H., J. Chem. Phys., 4, 283, 1936

104 Cernuschi, F. & Eyring., J. Chem. Phys., 7, 547, 1939

105 Eyring, H., Ree, T. & Hirai, H., Proc. Nat. Acad. Sci. (USA), 44, 683, 1958

106 Eyring, H. & Jhon, M.S., "Significant Liquid Structures", John Wiley & Sons Inc., London, England, 1969

107 Peck, H.M. & Hill, T.L., J. Chem. Phys., 18, 1252, 1950

108 Henderson, D., J. Chem. Phys., 37, 631, 1962

109 Rowlinson, J.S. & Curtiss, C.F., J. Chem. Phys., 19, 1519, 1951

110 Barker, J.A., J. Australian Chem., 13, 187, 1960

111 Bretsznajder, S. "Prediction of Transport and Other Physical Properties of Fluids", Pergamon Press, Oxford, 1971

112 Moelwyn-Hughes, E.A., "States of Matter", Oliver & Boyd Ltd., Edinburgh, 1961

113 Ensminger, D. "Ultrasonics", Marcel Dekker Inc., New York, 1973

114 Pethrick, R.A., Sci. Prog. Oxf., 58, 563-584, 1970

115 Markam, J.J., Beyer, R.J. & Lindsay, R.B., Rev. Modern Phys., 23(4), 353-389, 1951

116 Litovitz, T.A., J. Acoust. Soc. Am., 31(6), 681, 1959

117 Pethrick, R.A., Prog. Polym. Sci., 9, 197-295, 1983

118 El'piner, I.E., "Ultrasound", Consultant Bureau Enterprises Inc., New York, 1963

119 Moore, W.J., "Physical Chemistry", Lowe & Brydone Ltd., London, 1972

120 Soczkiewicz, E., Archives of Acoustics, 2(4), 325, 1977

121 Kuczeva, F., Archives of Acoustics, 3(1), 49, 1978

122 Eyring, H. & Hirschfelder, J., Trans. Faraday Soc., 249, 1936

123 Vigoureux, P., "Ultrasonics", Jarrold & Sons Ltd., Norwich, England, 1950

124 Kleszczewski, Z., Archives of Acoustics, 1(1), 43-50, 1976

125 Khabibullaer, P.K., & Shakhparonov, M.I., Sov. Phys. Acoust., 18(2), 251-256, 1972

126 Davidovich, L.A., Ivanov, A.A., Makhkamov, S., Pulatova, L., Khabibullaer, P.K., Khaliulin, M.G. & Sharipov, S.H., Sov. Phys. Acoust., 19(1), 18-21, 1973

127 Eyring, H. & Hirschfelder, J., J. Phys. Chem., 4, 249-257, 1937

128 Jacobson, B., Acta. Chem. Scand., 5, 1214-1217, 1951

129 Jacobson, B., Acta. Chem. Scand., 6, 1485-1498, 1952

130 Jacobson, B., J. Chem. Phys., 20, 929, 1952

131 Ramanjappa, T., Sivakumar, K.V. & Rajagopal, E., Acoustica, 57, 35-37, 1985

132 Sivakumar, K.V., Rajagopal, E. & Manohara Murthy, N., Acoustica, 59, 287-289, 1986

133 Ernst, S. & Glinski, J., Acoustica, 48, 109-119, 1981

134 Litovitz, T.A., J. Chem. Phys., 26, 469, 1957

135 Karpovich, J., J. Chem. Phys., 22, 1767-1773, 1954

136 Richards, W.T., Revs., Modern Phys., 11, 36, 1939

137 Hall, L., Phys. Rev., 73, 772, 1948

138 Mikhailov, I.G. & Polunin, V.M., Sov. Phys. Acoust., 18(2), 236-240, 1972

139 Litovitz, T.A. & Carnevale, E.H., J. App. Phys., 26, 816, 1955

140 Setta, D., Nuovo Cimento, 7, 318, 1950

141 Storey, W., Proc. Phys. Soc. (London), 13, 65, 943, 1957

142 DeGroot, M.S., PhD thesis, Imperial College, England, 1958

143 Slichter, C.P., "Principles of Magnetic Resonance", Harper, New York, 1963

144 Truell, R., Elbaum, C. & Chick, B.B., "Ultrasonic Methods in Solid State Physics", Academic Press, London, 1969

145 Shutilov, V.A., Sov. Phys. Acoust., 8(4), 303-318, 1963

146 Bolef, D.I., Science, 136 (3514), 359-369, 1962

147 Kessel, A.R., Sov. Phys. Acoust., 16(4), 425-435, 1971

148 Emsley, J.W., "Progress in NMR Spectroscopy", 4, 424-444, 1969

149 Orbach, R., Proc. Phys. Soc., A264, 458, 1961

150 Finn, C.B.P., Orback, R. & Wolf, W.P., Proc. Phys. Soc., A77, 261, 1961

151 Kastler, A., Experimenta., 8, 1-9, 1952

152 Altshulter, S.A., Zhur Eksptl. i. Theoret. Fiz., 24, 681, 1953. 28, 49, 1954. Translation in Soviet Phys. JETP., 1, 9 (1955), 1, 37, 1955

153 Altshulter, S.A., Kochelaev, B.I. & Leuslin, A.M., Usp. Fiz. Nank (USSR), 75, 459, 1961. Translated in Soviet Phys. Uspekhi., 4, 880, 1962

154 Bolef, D.I. & Sundfords, R.K., Proc. IEEE., 53, 1574, 1965

155 Schiff, L.I., "Quantum Mechanics", p65, McGraw-Hill, New York, 1949, pg65, (1st Edn.)

156 Bolef, D.I. & Menes, M., Phys. Rev., 114, 1441, 1959

157 Proctor, W.G. & Tanttila, W.H., Phys. Rev., 98(6), 1854, 1955

158 Proctor, W.G. & Robinson, W.A., Phys. Rev., 104(5), 1344-1352, 1956

159 Brugger, K. & Mason, W.P., Phys. Rev. Lett., 7(7), 270-273, 1961

160 Silverstein, S.D., Phys. Rev., 132(3), 997-1003, 1963

161 Buishvili, L.L., Sov. Phys. Solid State. 5(4), 748-750, 1963

162 Muller, V., Phys. Lett., 60A(3), 240-242, 1977

163 Kessel, A.R. "Nuclear Acoustic Resonance", (in Russian), Nauke, Moscow, USSR, 1969

164 Bowen, L.O., Brit. J. App. Phys., 15, 1451-1452, 1964

165 Bowen, L.O., Proc. Phys. Soc. 87, 717-720, 1966

166 Iolin, E.M., J. Phys. C. Solid State Phys., 6, 3469-3477, 1973

167 Iolin, E.M., Sov. Phys. Dokl., 18, 527-528, 1974

168 Iolin, E.M. & Kozlov, V.V., Mol. Phys., 35(2), 419-425, 1978

169 Alekseev, A.V. & Kopvillem, U.Kh., Ultrasonics, 76-80, 1980

170 Sundfors, R.K., Bolef, D.I. & Fedders, P.A., Hyperfine Int., 14, 271-313, 1983

171 Antokol'skii, G.L., Baranov, V.S. & Iolin, E.M., JETP LETT 23, 629-633, 1976

172 Unterhorst, E.J., Miller, V. & Schanz, G., Phys. Stat. Sol., (b), 84, K53-K56, 1977

173 Rousseu, J., Vermeersch, G. & Marcharidise, X., Group d'etude sur la RMN Biomédicale. Université de Lille II, 1 Place der Verdun, 59045, Lille Cedex, France, Private communication

174 Myers, K.J., Hirsch, T.J. & Barrett, H.H., SPIE Vol 626, Medicine XIV/PACS IV, 2-6, 1986

175 Flynn, H.G. "Physics of acoustic cavitation in liquids", in "Physical acoustics", Vol IB, Ed: Mason, W.P., Aacdemic Press, New York, 1964, pp57-172

176 Apfel, R.E. "Ultrasonics", Ed: Edmonds, P.D., Academic Press, New York, Vol 19, 1981, pp355-411

177 Coakley, W.T. & Nyborg, W.L., "Ultrasound", its applications in medicine and biology, Ed: Fry, F.J., Elsevier, New York, 1978, pp77-159

178 Noltingk, B.E. & Neppiras, E.A., Proc. Phys. Soc. B. (London), 63B, 674, 1950, 64B, 1032, 1951.

179 Neppiras, E.A., Ultrasonics, pp25-29, Jan, 1984
Prosperetti, A., Ultrasonics, pp69-77, March 1984
Prosperetti, A., Ultrasonics, pp115-124, May 1984
Apfel, R.E., Ultrasonics, pp167-173, July 1984
Crum, L.A., Ultrasonics, pp215-223, Sept 1984
Miller, D.L., Ultrasonics, pp261-269, Nov 1984

180 Riesz, P., Derdahl, D. & Christman, C.L., "Environmental health perspective". 64, 233-255, 1985

181 Cruum, L.A., Papers IEEE group on Sonics and Ultrasonics, 1982 Ultrasonic Symposium proceedings, USA. 27-29 Oct 1982, New York, USA. Vol 1, 1-11, 1982

182 Saksena, T.K., J. Acoust. Soc. India. Vol VIII (I), 12-19, 1980

183 Apfel, R.E., IEEE Trans. Ultrasonics, Ferroelectrics and Frequency Control. Vol UFFC 33 (2), 139-142, 1986

184 Niemczewski, B., Ultrasonics. 107-110, May 1980

185 Apfel, R.E., Sci. American, 227(6), 58-71, 1972

186 Greenspan, M. & Tschiegg, C.E., J. Res. Natl. Bur. Stand., 71C, 299-312, 1967

187 Crum, L.A., J. Acoust. Soc. Am., 68, 203-211, 1980

188 Fitzgerald, M.E., Griffing, V. & Sullivan, J., J. Chem., Phys., 25(5), 926-933, 1956

189 Lauterborn, W., Acoustica, 22, 48-54, 1969/1970

190 Flynn, H.G., J. Acoust. Soc. Amer., 72, 1926-1932, 1982

191 Suslick, K.S. & Hammerton, D.A., IEEE Transactions on ultrasonics, ferroelectrics, and frequency control. Vol UFFC-33(2), 143-146, 1986

192 Fujikawa, S. & Akamatsu, T., J. Fluid Mech., 97, 418-512, 1980

193 Margulis, M.A., & Dmitrieva, A.F., Zli. Fiz. Khim., 56, 323-327, 1982

194 Alliger, H., Amer. Lab., Oct 1975

195 Esche, R., Acoustica. 2, AB 208, 1952

196 Apfel, R.E., J. Acoust. Soc. Amer., 69, 1624-1633, 1981

197 Doulah, M.S., J. Appl. Polym. Sci., 22, 1735, 1978

198 Mark, H., J. Acoust. Soc. Amer., 16(3), 183-187

199 Casale, A. & Porter, R.S., "Polymer stress reactions". Academic Press, New York, Vol 1&2, 1979

200 Luche, J.L., & Damiano, J.C., J. Acoust. Soc. Amer., 102, 7926-7927, 1980

201 Han, B.H., & Boudjouk, P. Tet. Lett., 22, 2757-2756, 1981, 22, 3813-3814, 1981, 23, 1643-1646, 1982

202 Kruus, P., Ultrasonics. 201-204, Sept 1983

203 Dupont, L.A., Kruus, P. & Prataboy, T.J., Ultrasonics International 83, 14th Conf. Proc., Healifax, Canada, 1983, pp502-506

204 Kruus, P., & Patraboy, T.J., J. Phys. Chem., 89, 3379-3384, 1985

205 Porter, R.S. & Casale, A., Poly. Eng. & Sci., 25, 129, 1985

206 Kruus, P., Kiedrich, G.K. & Rachlis, L.M., Can. J. Chem., 50, 1743, 1972

207 Mason, T.J., Ultrasonics, 24, 245-253, 1986.
Mason, T.J., Henglein, A., Astier, R.C., Kruus, P., Lorimer, J.P., Verall, R.E., Reisz, P., Luctie, J.L., Lindley, J., Pugin, B., & Suslick, K.S., Ultrasonics, 25(1), 5-59, 1987

208 Carmichael, A.J., Mossoba, M.M., Riesz, P. & Christman, C.L., IEEE Trans Ultrasonics, ferroelectrics, and frequency control, Vol UFFC-33(2), 148-154, 1986

209 Makino, K., Mossoba, M.M. & Reisz, P., J. Am. Chem. Soc., 104, 3537-3539, 1982

210 Janzen, E.G., "Free Radicals in Biology", Vol IV, 116-154, Ed: W.A. Pryor. Academic Press, New York, 1980

211 Aurich, H.G. "The Chemistry of Amino, Nitroso and Nitro Compounds and their Derivatives", Suppl. F., Part I, Ed: S. Patai, John Wiley & Sons, New York, 1982

212 Tabata, M., Miyazaw, T., Kobayashi, O. & Soma, J,. Chem. Phys. Lett., 73, 198, 1980

213 Rosenthal, I., Mossoba, M.M., Riesz, P., J. Magn. Res., 45, 359-361, 1981

214 Riesz, P. & Rosenthal, I., Can. J. Chem., 60, 1474, 1982

215 Schultz, R. & Henglein, A., Z. Naturforch., 86, 160, 1953

216 Weissler, A., Pecht, I. & Anbar, M. Science. 150, 1288, 1965

217 Tabata, M. & Sohma, J., Eur. Polym. J., 16, 589, 1980

218 Sehgal, C., Yu, T.J., Sutherland, R.G. & Verrall, R.E., Amer. Chem. Soc., 2982-2986, 1982

219 Encina, M.V., Luin, E., Sarama, M., Chyargallo, L. & Radic, D., J. Polym. Sci. Polym. Lett. 18, 757, 1980

220 Fogler, S. & Barnes, D., Ind. Eng. Chem. Fundam., 7, 222, 1968

221 Chou, J.W. & Kalback, W.M., Ind. Eng., Chem. Fundam., 6, 175, 1967

222 Couppis, E.C. & Klinzing, G.E., AIChE. J., 20, 485, 1974

223 Davidson, R.S., Patel, A.M., Safder, A.F. & Thornthwaite, D., Tett. Lett., 24, 5907-5910, 1983

224 Ando, T., Shumi, S., Kawate, T., Ichihara, J. & Hanafusa, T., J. Chem. Soc. Chem. Commun., 439, 1984

225 Artaki, I. & Jones, J., J. Chem. Phys., 82(7), 3360-3370, 1985

226 Jefrey, K. & Armstrong, R., Rev. Sci-Instr., 38, 639, 1967

227 Levy, G.C. & Peat, I.R., J. Mag. Res., 18, 500, 1975

228 Ellet, J.D., Gibby, M.G., Haeberlen, U., Huber, L.M., Mehring, M., Pines, A. & Wangh, J.S., "Advances in Magnetic Resonance", Vol 5, p117, Ed: Wangh, J.S., Academic Press, New York, 1971

229 JEOL FT NMR Spectrometer, JNM, FX 90Q, Instruction manual

230 Derome, A.E., "Modern NMR techniques for chemistry research", Pergamon Press Ltd., Oxford, England, 1987

231 Kemp, W. "NMR in Chemistry". Macmillan Education Ltd, London, England, 1986

232 Bretmaier, E., Spotin, K.H., & Berger, S., Angew Chem. Internat. Edit., 14(3), 144-159, 1975

233 Baun, R. & Gunther, H., Angew Chem. Internat. Edit. Engl., 22, 350-380, 1983

234 Brevard, C. & Granger, P., "Handbook of High Resolution Multinuclear NMR", John Wiley & Sons Inc., 1981

235 Martin, M.L., Delpueeh, J.J. & Martin, G.J., "Practical NMR Spectroscopy", Heyden, 1980

236 Vold, R., Waugh, J., Klein, M.P. & Phelps, D.E., J. Chem. Phys., 48, 3831, 1968

237 Freeman, R. & Hill, H.D.W., J. Chem. Phys., 51, 3140, 1969

238 Demco, D.E., Van Hecke, P. & Waugh, J.S., J. Magn. Reson., 16, 467, 1974

239 Cutnell, J.D., Bleich, H.E. & Glasel, J.A., J. Magn. Reson., 21, 43, 1976

240 Kowalewski, J., Levy, G.C., Johnson, L.F. & Palmer, L., J. Magn. Reson., 26, 533, 1977

241 Gupta, R.K., Ferretti, J.A., Becker, E.D. & Weiss, G.H., J. Magn., Reson., 38, 447, 1980

242 Rabenstein, D.L., Nakashima, T. & Bigam, G., J. Magn. Reson., 34, 669, 1979

243 Markley, J.L., Horsley, W.J. & Klein, P.M., J. Chem. Phys., 55, 3604, 1971

244 McDonald, G.G. & Leigh, J.S., J. Magn. Reson. 9, 358, 1973

245 Freeman, R. & Hill, H.D., J. Chem. Phys., 54, 3367, 1971

246 Bangerter, B.W., J. Magn. Reson., 13, 87, 1974

247 Homer, J. & Beevers, M.S., J. Magn. Reson., 63, 287-297, 1985

248 Homer, J. & Roberts, J.K., J. Magn. Reson., 74, 424-432, 1987, 80, 116-118, 1988

249 Armitage, I.M., Huber, H., Live, D., Pearson, H. & Roberts, J., J. Magn. Reson., 15, 142, 1974

250 Freeman, R., "A Handbook of Nuclear Magnetic Resonance". Longman Group, UK Ltd., England, 1988

251 Homer, J. & Coupland, A., Analyst., 100, 865, 1976

252 Simon, H.E. & Vold, R.L., J. Magn. Reson., 24, 399, 1976

253 Led, J.J. & Petersen, S.B., J. Magn. Reson., 32, 1, 1978

254 Wilkins, Ch.L., Brunner, T.R., & Thoennes D., J. Magn. Reson., 17, 373, 1972

255 Shields, J.P., "Basic Piezoelectricity". W. Foulsham and Co. Ltd., Slough, Berks, England, 1966

256 Gooberman, G.L., Ultrasonics. The English University Press Ltd., London, England, 1968

257 Blitz, J., "Fundamentals of Ultrasonics", Butterworths, England, 1963

258 Carlin, B., Ultrasonics. McGraw-Hill Book Co. Ltd., USA, 1960

259 Hykes, D.L., Hedrick, W.R. & Starchman, D.E., "Ultrasound Physics and Instrumentation", Churchill Livingstone Inc., New York, USA, 1985

260 Pierce, A.D., "Acoustics", McGraw-Hill, Inc, USA, 1981

261 Duran, P. & Moure, C., Mater. Chem. and Phys., 15, 193-211, 1986

262 Jen, C.K., Cielo, P., Maldague, X., Alder, E.L. & Shapiro, G., Ultrasonics. 24(3), 133, 1986

263 Kepler, R.G. & Anderson, R.A., CRC. Crit. Rev. Solid State and Matter Sci. (USA), 9(4), 399-446, 1980

264 Ohigashi, H., Jpn. J. App. Phys. Suppl. (Japan), 24, Suppl. 24-2, 23-7, 1985

265 Multhaupt, R.G., Ferroelectrics (GB), 75(3), 385-96, 1987

266 Jen, C.K., Cielo, P., Maldagne, X., Alder, E.L. & Shapiro, G., "Ultrasonics", 24(3), 133, 1986

267 Cellerame, J., Tancell, R.H. & Wilson, D.T., Ultrasonic Symposium Proceedings, Cherry Hill, New Jersey, USA, 25-27, Sept 1978, (NJ, USA: IEEE 1978, pp117-121

268 Ralton, J., Aust. Electron. Bull. (Australia), 22-26, 1981

269 Sydenham, P.H., Aust. Electron. Bull. (Australia), 15-20, 1981

270 Broomfield, G.H., Report AERE-R 11942, UKAEA, Harwell, Oxon, England, 37pp, Dec, 1985

271 Hill, R. & El-Dardiry, S.M.A., Ultrasonics, 19(1), 9-16, 1981

272 Smith, W.M.R., & Awojobi, A.O., Ultrasonics, 20-26, Jan 1979

273 Pearson, H.W. & Hertz, C.H., Ultrasonics. 23(2), 83, March 1985

274 Desilets, C.S., Fraser, J.D. & Kino, G.S., IEEE Trans Sonics and Ultrasonics, Vol Su-25, No 3, 115-125, 1978

275 Silk, M.G., Ultrasonics. 27-33, Jan 1983

276 Bainton, K.F. & Silk, M.G., Brit. J. NDT., 15-20, Jan 1980

277 Sylivestrowicz, W.D., IEEE Trans on Sonics and Ultrasonics, 50-59, June , 1964

278 The MECLEC Company, 5/6 Towerfield Close, Shoeburyness, Essex, E.igland, Private communications.

279 Richter, K.P., Ultrasonics (GB), 25(4), 229-36, July 1987

280 Christofferson, B.K. & Light, T.R., Ultrasonics International, 161-70, 1977

281 Vernitron Ltd., Thornhill, Southampton, England, SO9 5QF, Private communications

282 McDonald, N.H., Control and Instrum. (GB), 10(8), 31-37, 1978

283 Jansen, P., Control and Instrum. (GB), 10(8), 39, 1978

284 Eng. Mater & Des. (GB), Vol 22(8), 25-30, 1978 (no author)

285 Huck, P.J., PhD thesis, University of Aston, 1968, pg 38

286 Acton, W.I., Ultrasonics. 124-128, May 1974

287 Bamber, J.C., Ultrasonics. 187-188, July 1981

288 Kirsten, E.B. & Zinsser, H.H., IEE Trans. Ultrasonics Eng., 112-116, 1963

289 Burstall, F.H. & Nyholm, R.S., J. Chem. Soc., 3570, 1952

290 Buayat, I. PhD thesis, University of Aston in Birmingham, 1972

291 Coupland, A. PhD thesis, University of Aston in Birmingham, 1978

292 Lorimer, J.P. & Mason, T.J., Chem. Soc. Rev., 16, 239-274, 1987, 16, 275-311, 1987

293 Kruus, P. & Patraboy, T.J., "Ultrasonic International", E02, 1985

294 Osenthal, R., Massoba, M.M. & Riesz, P., J. Magn. Res., 45, 359, 1981

295 Carmichael, A.J., Makine, M.M. & Riesz, P., Radiat. Res., 100, 222, 1984

296 Makino, K., Massoba, M.M. & Riesz, P., J. Am. Chem. Soc., 104, 3537, 1982

297 Makino, K, Massoba, M.M. & Riesz, P., J. Phys. Chem., 87, 1369, 1983